Modeling and Analysis of Single and Two-phase MHD Blood Flow in a Stenosed Artery with Heat and Mass Transfer

THESIS

Submitted in partial fulfilment

of the requirements for the degree of

DOCTOR OF PHILOSOPHY

BY

BHAVYA TRIPATHI

Under the Supervision of

Prof. BHUPENDRA KUMAR SHARMA

BIRLA INSTITUTE OF TECHNOLOGY AND SCIENCE, PILANI

2018

To My Parents and Teachers

BIRLA INSTITUTE OF TECHNOLOGY AND SCIENCE, PILANI

CERTIFICATE

This is to certify that the thesis entitled **"Modeling and Analysis of Single and Two-phase MHD Blood Flow in a Stenosed Artery with Heat and Mass Transfer"** and submitted by **Bhavya Tripathi**, **ID No.2013PHXF0435P** for award of Ph.D. Degree of the institute embodies original work done by her under my supervision.

_____

Signature of the Supervisor

Name : **Bhupendra Kumar Sharma**

Designation : **Associate Professor**

Department : **Mathematics**

Date :

Acknowledgments

Firstly, I would like to thank my supervisor Prof. Bhupendra Kumar Sharma for his support and constant encouragement during the tenure of my Ph.D. work. He always motivated me to learn new techniques, knowledge of which really helped in my Ph.D.. Under his supervision I improved my presentations skills as well as my writing skills, his personal generosity helped my time at BITS Pilani enjoyable.

I would like to extend my gratitude towards my DAC committee members Dr. Ashish Tiwari and Dr. Sangita Yadav. Their valuable comments and suggestions during various progress seminars have significantly enhanced the quality of my research work. Whenever I contacted them, they were very kind, patient and were always available to clarify my doubts despite their busy schedules.

I owe a debt of gratitude to former HODs of Mathematics department Prof. P. H. Keskar, Prof. Dilip Kumar Maiti, Prof. Chandra Shekhar and Prof. Balram Dubey for providing me with requisite facilities to carry out my research. I also gratefully acknowledge all the faculty members of the Department of Mathematics, BITS Pilani for paying their attention and genuine interest during my end semester seminars and non-teaching staff of the Mathematics Department for their help. I express my special gratitude to Vice Chancellor, Director, Deputy Directors, Deans, BITS Pilani, Pilani Campus for providing me the opportunity to pursue my doctoral studies. I extend my thanks to SRCD and AGSRD staff for their helpful support.

I would like to thank Prof. Sangeeta Sharma, Department of Humanities and Social Sciences, BITS Pilani, Dr. Amit Kumar Verma former faculty at BITS Pilani-Pilani campus (currently he is faculty in IIT Patna) and Prof. Suresh Kumar, Department

of Mathematics, BITS Pilani, Pilani Campus, they guided me during my coursework at BITS Pilani, Pilani Campus. They inspired me by their teaching skills and their in-depth knowledge of subjects.

I take this opportunity to thank Prof. Alfio Quarteroni, Professor of Mathematics, EPFL, Lausanne, Switzerland who recommended and sent me some good books related to my research field which really helped me of doing my work. His humble nature towards students inspired me in many ways.

A special thanks to my master's advisor Prof. Shiv Prasad Yadav, Department of Mathematics, IIT Roorkee who motivated me to pursue doctoral studies. I am really thankful to all the professors of the mathematics department at IIT Roorkee who taught me various courses during my master degree.

I sincerely acknowledge the financial support provided by UGC(BSR) and DST New Delhi, India during the tenure of my doctoral research work.

I also extend my heartfelt thanks to my all friends at BITS Pilani as well as at IIT Roorkee, who have been a part of this long journey. I enjoyed the evening with my badminton teams, It was one reason I never felt down at any moment at BITS Pilani. I will cherish all the fun-filled moments during my entire stay at BITS Pilani, Pilani Campus.

Word would not be adequate to express how much I am thankful to my parents Saroj Tripathi and Ved Prakash Tripathi and to my brother Manas Tripathi and to my sisters Kavita Mishra, Bhumika Shukla and brother-in-law, Vaibhav Mishra, Vishwas Shukla for their love, encouragement and support, without that it could not be possible to complete this long journey.

Lastly, I am very grateful to God for all the blessings in my life.

Bhavya Tripathi

Abstract

This thesis presents a mathematical analysis of the phenomenon of blood flow through a stenosed artery under the influence of the magnetic field with heat and mass transfer. Study on the narrow artery considering the two-phase flow behavior of blood flow is also a part of the thesis work. The major part of the thesis work includes variable viscosity of blood flow which depends upon hematocrit, temperature or pressure of the artery as occurs in real situations. The thesis is divided into eight chapters and the chapter wise summary is as follows:

The first chapter of this thesis provides a brief background of the biomechanics and describes the aim and objectives of the thesis as well as gaps in existing research followed by the literature survey.

In the second chapter, the effects of heat transfer on MHD blood flow through a stenosed inclined porous artery with heat source have been analyzed. The viscosity of the blood is assumed to be varying radially with hematocrit throughout the region of the artery. The governing equations have been solved using Homotopy perturbation method (HPM). Variation of flow rate and shear stress for different values of inclination angle and hematocrit parameter along the diseased part of the artery have been discussed.

In the third chapter, a mathematical study of heat and mass transfer effects on the arterial blood flow under the influence of an applied magnetic field with chemical reaction has been done. The variable viscosity of the blood is considered varying with the hematocrit ratio. For having an adequate insight of blood flow behavior through a stenosed artery, an analysis has been done to study the behaviour of wall shear stress, velocity, temperature and concentration profiles with varying values of the applied magnetic field, chemical reaction parameter and porosity parameter.

Effects of heat and mass transfer on two-phase pulsatile blood flow through a narrowed stenosed artery with radiation and the chemical reaction have been investigated in chapter 4. Exact solutions have been found for momentum, energy and concentration equations of the blood flow. In order to validate our result, a comparative study has been presented between the single-phase and two-phase model of the blood flow and it is observed that the two-phase model fits more accurately with the experimental data than the single phase model data.

The study of heat and mass transfer effects on the two-phase model of the blood flow through a stenosed artery with radiation has been presented in chapter 5. The major characteristics of the blood flow such as flow resistance, total flow rate and wall shear stress are calculated for different values of the magnetic field and radiation parameter.

In the presence of variable magnetic field, effects of both heat and mass transfer on an unsteady two-phase blood flow through a stenosed artery with simultaneous effects of viscous dissipation and Joule heating have been investigated in chapter 6. The viscosity of the cell-free plasma layer is assumed to be constant while the viscosity of the core region is considered as a function of the hematocrit level. To understand the flow pattern in the diseased narrowed artery, velocity contours have been plotted which alters significantly in the downstream of the stenosis under the influence of the magnetic field.

Further, in chapter 7, the MHD mixed convection problem of two-phase blood flow through a stenosed inclined artery having viscous dissipation and Joule heat effect with k^{th} order homogeneous chemical reaction and radiation effect has been discussed. The viscosity of the core layer is considered as temperature dependent, while, the viscosity of the plasma layer is assumed as constant. In both core and plasma regions geometry of the stenosed artery is considered as elliptic shaped. Graphs have been plotted to examine the effects of different physical quantities of interest on flow rate, wall shear stress and impedance profile of blood flow.

In chapter 8, we summarized the main findings of the thesis and propose future scopes of the thesis.

Contents

List of Figures

List of Tables

Chapter 1

Introduction

"Biomechanics has been defined as the study of the movement of living things using the science of mechanics."

- Hatze,

In science, mechanics is a branch of physics which is concerned about the description of motion and how forces create motion. Biomechanics is the scientific study of the motion of living structure as in living things how muscles, bones, tendons, and ligaments work together to produce movement. To improve human movement, biomechanics provides major information on the most effective and safest equipment, movement patterns and relevant exercises (Knudson, 2007). On the other hand, biofluid mechanics explains the mechanism of biological fluids and their interrelationship with physiological processes, in health and in diseases/disorder with the use of liquids, gases. As the human body is composed of approximately 65% water and each cell of the body is dipped within an extracellular water compartment, these cells feel some forces that are distributed and transmitted through this water layer. Under non-pathological conditions, some nonadherent cells as red blood cells, white blood cells and platelets through the body blood stream experience many types of fluidic force such as shear and pressure forces which directly change their functions. Hence, biofluid mechanics also focuses on the study of the circulatory system as well as respiratory systems such as animal flight, fish swimming and blood flow in arteries. Biofluid dynamics is so critical to study as the report presented by the American Heart

Association in 2014, declare that in the United States approximately 16 million people had suffered from some coronary heart disease (Rubenstein et al., 2015). All over the world cardiovascular disease is a major cause of death of the people. Therefore, nowadays the area of biofluid mechanics has gained serious attention by many researchers and physiologists person due to its vast applications in the field of diagnosing, treating the certain surgical procedures related to the disorders/diseases which originate in the body relating to cardiovascular, synovial, pulmonary systems etc. (Chandran et al., 2006; Mazumdar, 2015; Schneck, 2013).

1.1 Aim and Objective

The cardiovascular disease refers to situations that include narrowed or blocked blood vessels which can cause heart attack, stroke or chest pain (angina). To fully understand this behavior many theoretical as well as experimental studies on blood flow through narrowed, blocked blood vessel have been the subject of scientific research (Vlachopoulos et al., 2011). We have proposed and analyzed some mathematical model which describes the heat and mass transfer effects on blood flow through a constricted region for inclined, horizontal and vertical vessels considering variable viscosity of blood flow. Effects of different physical parameters such as magnetic field, radiation, chemical reaction, Joule heating and viscous dissipation which directly affects the flow of blood have been discussed through our study. Some important objectives which are addressed to develop blood flow models in this thesis are:

- To analyze the effect of heat transfer on blood flow having hematocrit dependent viscosity through the inclined stenosed porous artery in the presence of an external magnetic field.
- To study both heat and mass transfer effects on blood flow through an inclined arterial segment with chemical reaction.
- To investigate the heat and mass transfer effects on the two-layered model of pulsatile blood flow (consists central core region of suspended erythrocytes and cell-free

plasma region) through a narrowed stenosed vertical artery with radiation and the chemical reaction.

- To examine the effects of heat and mass transfer on two-phase blood flow through a stenosed horizontal artery with radiation in the presence of an external magnetic field.

- To analyze the influence of heat and mass transfer with Joule heating and viscous dissipation effect on two-phase blood flow having variable viscosity in the presence of radially variable magnetic field.

- To examine the mathematical model of a mixed convection problem of heat and mass transfer on magnetohydrodynamics two-phase blood flow having temperature dependent viscosity considering the geometry of an elliptically shaped stenosis.

The system that operates in a medium of fluid is analyzed using the fluid mechanics principles. Therefore, to understand the modeling of blood flow dynamics, it is necessary to have a clear idea about fluid dynamics. Basic definitions which help to do mathematical modeling on blood flow are discussed in the following section.

1.2 Fundamental Concept of Fluid Dynamics

A fluid is a substance that deforms constantly under the action of shearing stress, even if the tension is small. The fluid dynamics which is a sub-discipline of fluid mechanics describes the flow of fluids such as liquids and gases. In fluid dynamics, liquids are fluid which contain the molecule of mean free paths of order 10^{-7} to 10^{-8} cm and do random motion under an adequate resistance to compression. While gases consist of molecules having mean free paths of order 10^{-3} which move over much larger distances and are readily compressed. As a result, material properties of matter are directly related to its molecular structure and intermolecular forces. These forces not only depend on the structure of the molecules but also their intermolecular distances. Although in this case the molecules always undergo random motion/vibration, the bulk material exhibits

a stable behavior at the macroscopic level. Therefore, fundamentally the deformation behavior of matter can be analyzed in two ways:

1. **Statistical mechanics**: In statistical mechanics, molecules are treated as discrete particles.

2. **Continuum mechanics**: In continuum mechanics, the bulk material is treated as a continuous medium and the time function is defined with continuous space function with the matter.

The concept of a continuum is the basis of classical fluid mechanics. Under the assumptions of the continuum hypothesis, we assume the fluid to be continuously distributed in a given space by considering the macroscopic behavior of the fluid. The given hypothesis directly allows us to identify with each point a "fluid parcel", or "fluid particle" or "fluid element" and then consider the volume of fluid as a whole to be a continuous aggregation of these particles by subdividing them indefinitely.

1.2.1 Velocity Field

A very important property described by field is the velocity field, given by

$$\overrightarrow{V} = \overrightarrow{V}(x, y, z, t).$$

The velocity field is a vector field which requires magnitude and direction for complete description as similar to the velocity. It can be written in terms of its three scalar components u, v, and w (in the directions of x, y and z, respectively) as

$$\overrightarrow{V} = u\widehat{i} + v\widehat{j} + w\widehat{k},$$

where each component u, v, and w are the function of x, y, z and t. In Eulerian sense, here $\overrightarrow{V}(x, y, z, t)$ measures the velocity of fluid particle passing through the point x, y, z at a time t.

The flow is termed as steady flow if all fluid properties at every point in a flow field do not change with time. Mathematically, we define a steady flow as

$$\frac{\partial \eta}{\partial t} = 0,$$

where η represents any fluid property. So for a steady flow, all the fluid properties vary from point to point but they remain constant with time at every point in the field.

1.2.2 Timelines, Pathlines, Streamlines and Streaklines

In fluid, flow field can be visualized by using timelines, streaklines, pathlines or streamlines. In flow field, a timeline pattern is generated when at a given instant a number of adjacent fluid particles are marked and form a line in a fluid at that instant.

A pathline is a trajectory traced by a moving fluid particle. These trajectories are used to visualize the path of contaminant leaving smokestack.

In flow field, streamlines are lines for a given instant of time which are tangent to the direction of flow at every point of the flow field. Furthermore, there is no flow across the streamlines because these lines are tangent to the velocity vector at every point in the flow field. These trajectories are the most commonly used visualization technique. For steady flow, streamline shape do not vary with time as the velocity at each point in the flow field remains constant from one instant to the next.

On the other hand in Streakline, we focus our attention on a fixed location in space and identify all fluid particles passing through this point. As time passes, we have a number of identifiable fluid particles in the flow, all of which at some time had passed through one fixed location in space. The line drawn through those fluid particles is defined as a streakline. For steady flow, all steaklines, pathlines and streamlines are identical. On the other hand all these lines show different shapes for unsteady flow.

Velocity field is used to derive the shapes of pathlines, streaklines and streamlines. Streamlines for two dimensional flow by using velocity field can be derived as

$$\left(\frac{dy}{dt}\right)_{\text{streamline}} = \frac{v(x,y)}{u(x,y)},$$

where $\bar{V} = u\widehat{i} + v\widehat{j}$. As streamlines are obtained at an instant in time, for unsteady flow time t is treated as constant.

In two dimensional flow to derive the expression for pathlines, we assume $x = x_p(t)$ and $y = y_p(t)$ which represent the instantaneous coordinates of a specific particle. We then

get

$$\left(\frac{dx}{dt}\right)_{\text{particle}} = u(x,y,t), \quad \left(\frac{dy}{dt}\right)_{\text{particle}} = v(x,y,t). \tag{1.2.1}$$

Solution of the eq.(1.2.1) provides the path of a particle in parametric form $x_p(t)$, $y_p(t)$. To compute the streakline, first we compute the pathline of a particle that releases from the streak source point at time t_0 of coordinate(x_0, y_0), in the form $x_{\text{particle}}(t) = x(t, x_0, y_0, t_0)$ and $y_{\text{particle}}(t) = y(t, x_0, y_0, t_0)$. Now, we write the equations for streaklines as

$$x_{\text{streakline}}(t_0) = x(t, x_0, y_0, t_0), \quad y_{\text{streakline}}(t_0) = y(t, x_0, y_0, t_0). \tag{1.2.2}$$

At point (x_0, y_0), the eq.(1.2.2) gives the line originated from a streak source. In this equation to show the instantaneous positions of all particles t_0 varies from 0 to t.

1.2.3 Stress Field and Viscosity

In fluid mechanics, there is a different kind of forces act on fluid particles such as surface forces (pressure, friction) which are produced by interaction with other fluid particles or solid surface, and body forces (electromagnetic and gravity) which act on all over the particles. A stress field is defined by the distribution of internal forces in a body that balance a given set of external forces.

Viscosity is the property of the fluid which is manifested only if the fluid is in motion. The concept of the viscosity is realized through the motion of the fluid and it is nothing to do when fluid is at rest. The velocity profile as shown in fig.1.1 displays the one-dimensional parallel flow. In the fluid in between two adjacent fluid layers, upper layer tries to drag the lower layer in the direction of flow with a force F. By Newton's third law of motion, the upper layer due to high velocity tries to accelerate the lower layer while the lower layer tries to decelerate the upper layer in the opposite direction. Therefore, shear stress develops between the layers. Newton found that in these types of fluid, shear stress depends upon the velocity gradient as

$$\tau \propto \frac{du}{dy}, \tag{1.2.3}$$

and direction of shear stress depends upon $\left(\frac{du}{dy}\right)$. Relation as given in eq.(1.2.3) results that if the value of the gradient $\left(\frac{du}{dy}\right)$ is going to be less then the shear stress will go to a very low value and the curves as shown in fig.1.1 becomes flat. Therefore, from eq.(1.2.3)

$$\tau = \mu \left(\frac{du}{dy}\right). \tag{1.2.4}$$

In eq.(1.2.4), μ represents the coefficient of viscosity or viscosity.

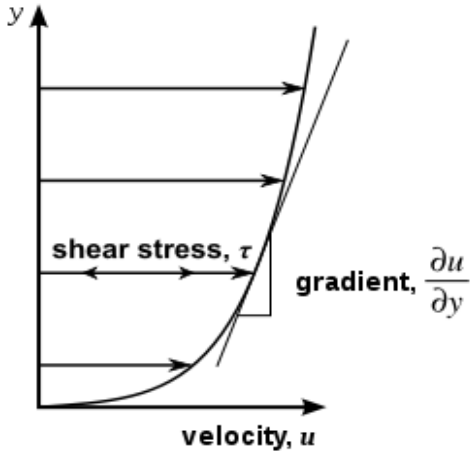

Figure 1.1: One dimensional parallel flow (source: Biswas (2003))

1.2.4 Classes of fluids

The constitutive equations of the fluid are the functional relations between the shear stress τ and the shear strain $\left(\frac{du}{dy}\right)$, which depend upon the fluid under consideration. Therefore, fluids are categorized in the following two classes which are given as:

Newtonian Fluids

In continuum mechanics, a Newtonian fluid is a fluid in which at every point the viscous stresses arising from its flow and which are linearly proportional to the local strain rate (Panton, 2006). By Newton's law of viscosity

$$\frac{\tau}{\left(\frac{du}{dy}\right)} = \text{Constant}. \tag{1.2.5}$$

In the physical sense, the factor $\left(\frac{du}{dy}\right)$ is treated as the rate of the shear strain. The fluid which follows this linearity law between shear stress and velocity gradient are Newtonian fluids. All gases and most liquids such as water, benzene, ethyl alcohol, hexane and most solutions of simple molecules which have a simpler molecular formula and low molecular weight are Newtonian fluids.

Non-Newtonian Fluids

In fluid mechanics, non-Newtonian fluids are those which do not follow Newton's law of viscosity and for which the constitutive relationship between the shear stress and the velocity gradient is non-linear through the origin. In non-Newtonian fluids, viscosity μ is the property of the fluid and treated as apparent viscosity. A non-newtonian fluid is classified into two different time-independent and time-dependent behaviours. The relation between τ and $\frac{du}{dy}$ for time-independent fluids can be represented by the power law model for one-dimensional flow as

$$\frac{\tau}{\left(\frac{du}{dy}\right)} = m\left(\frac{du}{dy}\right)^{n-1}. \tag{1.2.6}$$

In eq.(1.2.6), n is the flow consistency index and m is the flow behaviour index. A fluid in which apparent viscosity decreases as values of deformation rate increases,$(n \leq 1)$ is called as pseudoplastic fluid. The fluid is termed as dilatant if deformation rate increases with increasing values of the apparent viscosity deformation. Subsequentially, Bingham plastic is the limiting case of a plastic which requires finite yield stress before it starts to flow as shown in fig.1.2. There is a growing importance of non-Newtonian fluids in geophysical fluid dynamics, chemical technology and the petroleum industry.

1.2.5 Types of Flow

Fluid mechanics is subdivided in terms of whether or not viscous effects and comprehensibility effects are present as well as it is classified in terms of whether a flow is laminar or turbulent and internal or external. Now we discuss each of these sequentially:

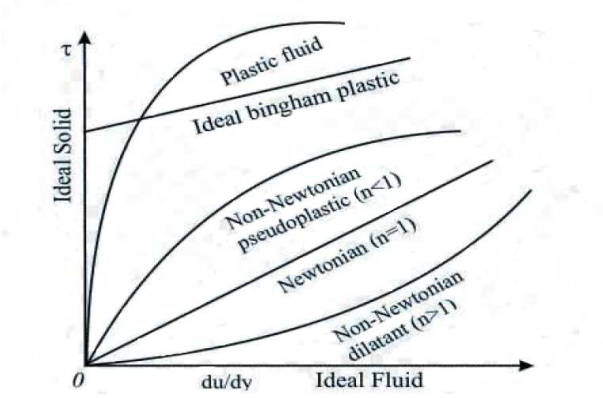

Figure 1.2: Shear stress and deformation rate relationship of different fluids (source: Pinto and Meo (2017))

Viscous and Inviscid Flows

Flows in which flow patterns are dominated by the viscous properties of the fluid are viscous flows. This occurs in the fluid where the velocity gradients are large. On the other hand, flow in which viscous properties are not dominant or viscosity of the fluid is zero is called as an inviscid flow. In these types of fluids, the Reynolds number approaches infinity as the viscosity approaches zero.

Laminar and Turbulent Flows

In fluid mechanics, Laminar are those flows in which each fluid particle traces out and a definite curve and the curves traced out by any two different fluid particles do not intersect. While turbulent flows are those in which each fluid particle does not trace out a definite curve and the curves traced out by fluid particles intersect.

Compressible and Incompressible Flows

Incompressible flows are those in which variations in density are negligible. On the other hand, incompressible flows density variations within the flow are not negligible. Gases are the example of compressible flows and their density changes readily with temperature and pressure. Generally, liquids are treated as incompressible flows, which are rather difficult to compress. Only some exceptions such as sound propagation in liquids do one need to

consider their compressibility.

1.2.6 Governing Equations of Fluid Dynamics

Fluid flows obey the laws of conservation of mass, momentum, energy and mass flux.

Equations of Continuity or Conservation of Mass

According to the law of conservation of mass, fluid mass can neither be created nor destroyed. In a mathematical form, the law of conservation of mass is expressed with the help of the equation of continuity. This law states that the increase in the mass of fluid within any closed surface in any time interval must be equal to the excess of mass that flows in over the mass that flows out. This law gives rise to the equation of continuity and when expressed in vector notation, it can be written as

$$\frac{\partial \rho}{\partial t} + \bigtriangledown.(\rho \overrightarrow{q}) = 0, \tag{1.2.7}$$

where ρ is the density of the fluid, $\overrightarrow{q}$ is the velocity vector and $\bigtriangledown$ is the vector differential operator defined as.

$$\bigtriangledown = \frac{\partial}{\partial x}\overrightarrow{i} + \frac{\partial}{\partial y}\overrightarrow{j} + \frac{\partial}{\partial z}\overrightarrow{k}.$$

The eq.(1.2.7) is known as the equation of continuity or the conservation of mass. The equation holds at all points of fluid free from sources and sinks.
The equation of continuity can be written in three different forms as
1st form:

$$\frac{\partial \rho}{\partial t} + \rho \bigtriangledown . \overrightarrow{q} + \bigtriangledown \rho . \overrightarrow{q} = 0, \tag{1.2.8}$$

since $\bigtriangledown.(\rho \overrightarrow{q}) = \rho \bigtriangledown . \overrightarrow{q} + \bigtriangledown \rho . \overrightarrow{q}$.
2nd form:

$$\frac{D\rho}{Dt} + \rho \bigtriangledown . \overrightarrow{q} = 0, \tag{1.2.9}$$

3rd form:

$$\frac{D(log\rho)}{Dt} + \bigtriangledown . D\overrightarrow{q} = 0. \tag{1.2.10}$$

If the density of any fluid particle is invariable with time, the fluid is considered as incompressible and heterogeneous and for that fluid the term $\frac{D\rho}{Dt} = 0$, where D is the material derivative. Then eq.(1.2.9) is termed in to

$$\bigtriangledown . \overrightarrow{q} = 0, \qquad \text{i.e.} \qquad div\, \overrightarrow{q} = 0. \tag{1.2.11}$$

For homogeneous and incompressible fluid as ρ is constant. Therefore, eq.(1.2.7) is changed into the form

$$\bigtriangledown .(\rho \overrightarrow{q}) = 0, \qquad \text{i.e.} \qquad \bigtriangledown . \overrightarrow{q} = 0. \tag{1.2.12}$$

Conservation of Momentum

The flow behavior is governed by the Navier-Stokes equations of motion which are obtained from the second law of motion, which states that the total forces acting on a fluid mass enclosed in an arbitrary volume fixed in space is equal to the time rate of change of linear momentum. This law gives rise to the equation of motion and when it is expressed in vector notation it can be written as

$$\rho \left(\frac{\partial \overrightarrow{q}}{\partial t} + (\overrightarrow{q} . \bigtriangledown) \overrightarrow{q} \right) = - \bigtriangledown p + \rho g + \mu \bigtriangledown^2 \overrightarrow{q}, \tag{1.2.13}$$

where $\bigtriangledown p$ is the pressure gradient due to normal stress, ρg is the buoyancy force and $\mu \bigtriangledown^2 \overrightarrow{q}$ is the viscous force due to tangential force.

The gradient is the vector operator which is operated on the scalar quantity. The gradient of the pressure, physically is the negative of the surface force, per unit volume due to pressure. Here, $(- \bigtriangledown p)$ is the pressure magnitude which is not related to the net pressure force while it counts the rate of change of pressure with distance.

Eq.(1.2.13) is known as the Navier-Stokes equation. This equation was first set up by Navier and Sur (1827) on the basis of consideration on the action of the inter-molecular forces. Later the same equations were derived without such hypotheses by Stokes (1966), using a basis that the normal and shear stresses are linear functions of the rate of deformation which had already been introduced via Newton's law of viscosity.

Conservation of Energy

This law states that the rate of increase of energy of the fluid in the volume V is equal to the negative of the outward flux of the energy plus the energy generated due to the work. if present. This law gives rise to the equation of energy and when expressed in vector notation for an incompressible fluid it can be written as

$$\rho c_p \left(\frac{\partial T}{\partial t} + (\overrightarrow{q} . \bigtriangledown) T \right) = k \bigtriangledown^2 T + \frac{\partial Q}{\partial t}, \tag{1.2.14}$$

where T is the temperature, k is the thermal conductivity of the fluid, c_p is the specific heat at constant volume and Q is the heat due to external source or sink.

Conservation of Concentrated Species

In the case of conservation of mass (or continuity through) of a fluid of density ρ, fluid might very well have been a mixture of two or more fluids and the principle of mass conservation is applied to each component of the constituent in the mixture. Mass transfer is the net movement of mass from one place to another place. The statement for this law is

$$\frac{DC}{Dt} = - \bigtriangledown . \overrightarrow{J} + R, \tag{1.2.15}$$

where $\frac{D}{Dt} = \frac{\partial}{\partial t} + (\overrightarrow{q} . \bigtriangledown)$ is the material derivative, C is the concentration of the components in the mixture and $\overrightarrow{J}$ is the diffusion flux vector and R is the volumetric rate of constituent generation. This term must be taken into account in reactive flows which generate constituent as a product of the reaction. If the constituent is consumed by the reaction, the species generation rate R is negative. The diffusion flux vector $\overrightarrow{J}$ driven by the concentration gradient $\bigtriangledown C$ in the same manner that the conduction heat flux is driven by the local temperature gradient. This idea was put forth by the German Physiologist Fick [34]. It is responsible for the analytical development of the fluid of mass transfer in the same way that Fourier's idea on heat conduction in the thermal boundary layer. Fick's law of mass diffusion is

$$\overrightarrow{J} = -D_f \bigtriangledown C. \tag{1.2.16}$$

The mass diffusivity D_f, is a transport property whose numerical value depends, in general on the mixture pressure, temperature and composition. Substituting eq.(1.2.16) in the mass conservation statement (eq.(1.2.15)), we get

$$\frac{DC}{Dt} = D\bigtriangledown^2 C + R. \tag{1.2.17}$$

1.2.7 Dimensionless parameter

In dimensional analysis, dimensionless parameters are those to which no dimension is assigned and these quantities are very much useful in characterizing many types of engineering systems. In fluid dynamics, dimensionless parameters tend to be very useful for either scaling fluid properties or connecting important parameters that govern fluid flows. In fluid dynamics, use of dimensionless parameters does not change any of the fluid properties or the analysis of the problem while under these conditions it becomes easier to report the data or analyze the problem. There are numbers of dimensionless parameters which help us to rescale the problem as needed. Description of some of them are as follows:

Reynolds Number(Re)

In biofluid dynamics, the Reynolds number (Re) is the very important dimensionless quantity to study. It connects both the viscous forces that impede the flow to the overall inertial forces that govern the flow. It helps to determine the flow characteristics as well. For the low value of Reynolds number, flow is considered as laminar flow and on the other hand, one can notice the turbulent behavior of flow for higher values of Reynolds number. The Reynolds number basically, gives a measurement in which the force dominates the change in fluid velocity (Rott, 1990). The Reynolds number is defined as

$$Re = \frac{\text{inertial forces}}{\text{viscous forces}} = \frac{\rho v d}{\mu}, \tag{1.2.18}$$

where v is some characteristic velocity, d is a characteristic length of the flow, ρ is the density of the fluid, μ is fluid viscosity.

Schmidt Number(Sc)

Schmidt number is defined as a dimensionless number which is the ratio of momentum and mass diffusivity. Schmidt number helps to characterize the flow of those fluids in which momentum and mass diffusion-convection process take place. It was named after the German engineer Ernst Heinrich Wilhelm Schmidt. The formula for the Schmidt number is expressed as

$$Sc = \frac{\text{viscous diffusion rate}}{\text{molecular or mass diffusion rate}} = \frac{\nu}{D_f},$$

$$= \frac{\mu}{\rho D_f}, \tag{1.2.19}$$

where D_f is the mass diffusivity, ν is the kinematic viscosity, μ is the dynamic viscosity and ρ is the density of the fluid.

Eckert Number (Ec)

In continuum mechanics, the Eckert number is the dimensionless number which is used to characterize heat dissipation. It is named after Ernst R. G. Eckert. Eckert number basically shows the relationship between the boundary layer enthalpy difference and kinetic energy of the flow. The formula for Eckert number is defined as

$$Ec = \frac{\text{Heat dissipation potential}}{\text{Adective transport}} = \frac{u^2}{c_p \Delta T}, \tag{1.2.20}$$

where u is the fluid velocity, ΔT is the difference between wall temperature and local temperature and c_p is the specific heat at constant pressure.

Prandtl Number (Pr)

The Prandtl number is the ratio of viscous force to the thermal force and defined as

$$Pr = \frac{\mu c_p}{\kappa}. \tag{1.2.21}$$

Peclet Number

The peclet number plays a significant role when as compared to inertia force the thermal force is large and the viscous force is small. It is defined as

$$Pe = PrRe. \tag{1.2.22}$$

Grashof Number

In fluid dynamics, Grashof number is the dimensionless number which is used frequently for the case involving natural convection. Value of Grashof number is equal to the ratio of the buoyancy force to viscous force acting on fluid. It is named after the Franz Grashof.

Thermal Grashof Number (Gr)

Thermal Grashof number is the form of Grashof number which is used when in fluid, free convection is produced by a change in density of the fluid due to a temperature gradient and given by

$$Gr = \frac{g\beta(T_s - T_\infty)L^3}{\nu^3}. \tag{1.2.23}$$

Solutal Grashof Number (Gm)

Solutal Grashof number takes in to the place when natural convection is caused due to a concentration gradient.

$$Gm = \frac{g\beta^*(C_{a,s} - C_{a,a})L^3}{\nu^2}. \tag{1.2.24}$$

In eq.(1.2.23) and eq.(1.2.24), g is acceleration due to Earth's gravity, ν is the kinematic viscosity, L is the length, and β is the coefficient of thermal expansion, T_s is the surface temperature, T_∞ is the bulk temperature, $C_{a,s}$ is the concentration of surface and $C_{a,a}$ is the concentration of species a in ambient medium. In eq.(1.2.24), β^* is defined as

$$\beta^* = -\frac{1}{\rho}\left(\frac{\partial \rho}{\partial C_a}\right)_{T,p},$$

where C_a is the concentration of species a.

Brinkmann Number

Brinkmann shows the relationship between heat transported by molecular conduction to heat produced by viscous dissipation (Khonsari and Booser, 2017). It holds in such a way that with high value of Brinkmann number the heat generation due to viscous dissipation reduces and influence of which directly increases the temperature of the fluid.

$$Br = \frac{\mu u^2}{\kappa(T_w - T_0)} = Pr\, Ec, \tag{1.2.25}$$

where κ is the thermal conductivity, T_0 is the bulk temperature of the fluid, T_w is the wall temperature, Pr is the Prandtl number, Ec is the Eckert number, u and μ are the velocity and viscosity of the fluid, respectively.

Nusselt number (Heat transfer coefficient)

For the case of heat transfer at a boundary (surface) within a fluid, the Nusselt number, which is known as heat transfer coefficient is the ratio of convective to conductive heat transfer across the boundary (Cengel et al., 2004).

$$Nu = \frac{\text{Convective heat transfer}}{\text{Conductive heat tranfer}} = \frac{h'}{\frac{k}{l}} = -\left(\frac{\partial \theta}{\partial y}\right)_{y=0}, \tag{1.2.26}$$

where L is the characteristic length, κ is the thermal conductivity of the fluid and h' is the convective heat transfer coefficient of the flow.

Sherwood number(Mass transfer coefficient)

The dimensionless Sherwood number (Sh) is calculated with the ratio of the convective mass transfer to the rate of diffusive mass transport (Welty et al., 2009). It is named in honor of Thomas Kilgore Sherwood.

$$Sh = \frac{\text{Convective mass transfer rate}}{\text{Diffusion rate}} = \frac{h}{\frac{D_f}{L}} = -\left(\frac{\partial \sigma}{\partial y}\right)_{y=0}, \tag{1.2.27}$$

where D_f is mass diffusivity, L is a characteristic length and h is the convective mass transfer film coefficient.

1.3 The Cardiovascular System

In the circulatory system of our body, heart, blood and blood vessels make up the cardiovascular component. The system that operates in a medium of fluid is analyzed using fluid mechanics principles. Blood is a bodily fluid in humans and other animals and it has great importance in physio-pathology. In components of blood, plasma is an aqueous solution for the suspension of cells. There are about $5 * 10^9$ cells in a milliliter of human blood. About 5% of these are "platelets" which perform a function related to blood clotting. About 0.2% of the cells are 'white cells' which play a role in the resistance of the body to infection. Most of the cells in the blood are 'red cells' the erythrocytes. The red cells make up about 45% of the blood volume in the average man. The volume fraction of red cells is known as the 'hematocrit' (Desjardins and Duling, 1987). Plasma is composed of 90% water and about 7% protein. Among the major protein constituents of plasma are albumins and globulins which maintain osmotic balance and thereby control the movement of water between blood and various tissues. The arterial blood flow provides a way for glucose, oxygen and hormones to reach various organs around the body. Blood leaves the heart from the left ventricle into the biggest artery called the aorta. It is important that fresh blood from the aorta goes directly to the brain because the brain needs oxygen constantly to avoid irreversible damage to its (Faber, 1995; Fung, 1993).

Blood Vessel

Blood flows in blood vessels which include arteries, capillaries and veins. These vessels are the part of our circulatory system and by forming the closed network of tubes they transport blood throughout the body. Different types of blood vessel which are found in our body are as follows

Arteries and Arterioles

Arteries are the most strong, flexible, and resilient blood vessels of our body. They carry blood away from the heart and bear the highest blood pressures as the blood they carry being pushed from the heart by applying a great force. As they are elastic in nature they

help to maintain the blood pressure by narrowing passively between the beats when the heart is relaxing. The arteries branch into a very small vessel called arterioles. Arteries and arterioles have muscular walls and they can increase or decrease blood flow to a particular part of the body by adjusting their diameter.

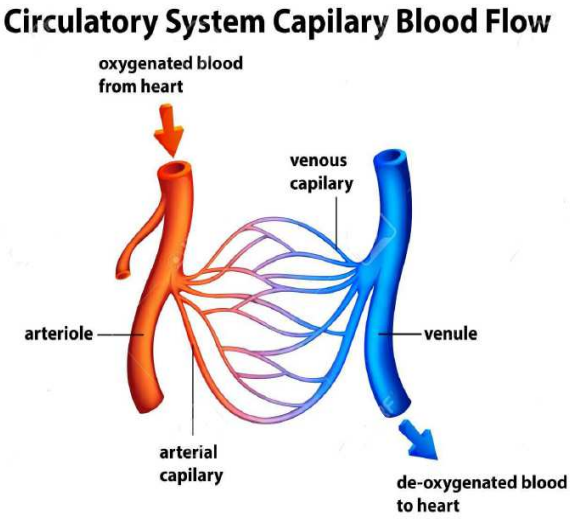

Figure 1.3: Circulatory system of the body (source: Gabryś et al. (2006))

Venules and Veins

In our body, blood flows from the capillaries into very small veins called venules, then into the veins which bring back blood to the heart. Veins act as the blood return counterparts of arteries and are the large return vessels of the body. Veins and venules feel very low blood pressures as compared to arteries, arterioles, and capillaries because they absorb most of the force of the heart's contractions. Therefore, walls of veins are much thinner, less elastic, and less muscular as compared to arteries.

Capillaries

Capillaries connect both arteries (which carry blood away from the heart) and veins (which carry blood back to the heart) and those have tiny, extremely thin-walled vessels. They almost work in every tissue of our body and keep the limit on the edges of the body's unwanted tissues. Their thin walls composed of only a thin layer of endothelium and

hence they allow waste products to pass from tissues into the blood and simultaneously allow oxygen and nutrients to pass from the blood into tissues.

The circulatory system is a vast network of organ and vessels in which the significant part of the blood functioning is to circulate through our body and transport essential nutrients and oxygen to the body's cell as well as remove metabolic products and carbon dioxides from the body as shown in fig.1.3. Human life majorly depends on the ability of the blood to carry oxygen. Any kind of obstruction, blockage, or diseases can affect the proper functioning of the blood vessels and in that situation, it would be impossible to preserve life. These types of situations can appear due to the different type of factors from genetics to lifestyle. We will discuss here one of the diseases named as atherosclerosis and how it is manifested within the arterial system.

1.4 Review of Literature

Mathematical modeling is an application of mathematics to explain and predict real-world behavior. The mathematical model, which describes the dynamics of blood flow, has been playing an important role in a better understanding of the behaviour of blood flow when it flows through a diseased artery. These are really useful in decision-making policies for public health.

The flow of blood through arteries is an important physiological problem and is of considerable interest for biomedical researchers, physiologists, and clinicians. In this regard, Olufsen et al. (2000) with the help of one-dimensional Navier-Stokes equations, modeled the phenomenon of blood flow in the large systemic arteries. They numerically solved the model and validate the results with the experimental data.

1.4.1 Atherosclerosis or Stenosis

Atherosclerosis disease which is also known as stenosis is characterized by the thickening, narrowing and stiffening of an arterial wall. The disease grows inside the artery when the endothelium is damaged by causing harmful cholesterol inside an arterial wall. Thrombosis also is known as clotting, is the medical term in which a blood clot is formed inside the

blood vessel, which inhibits the flow of blood through the circulatory system (Ross Jr and Braunwald, 1968). All steps of stenosis formulation are shown in fig.1.4. In the context of the heart the accumulated material which restricts the path of the blood flow mainly consists of debris or macrophage cells containing lipids, calcium and a variable amount of fibrous connective tissue, is known as plaque. Stenosis is a common occurrence in human

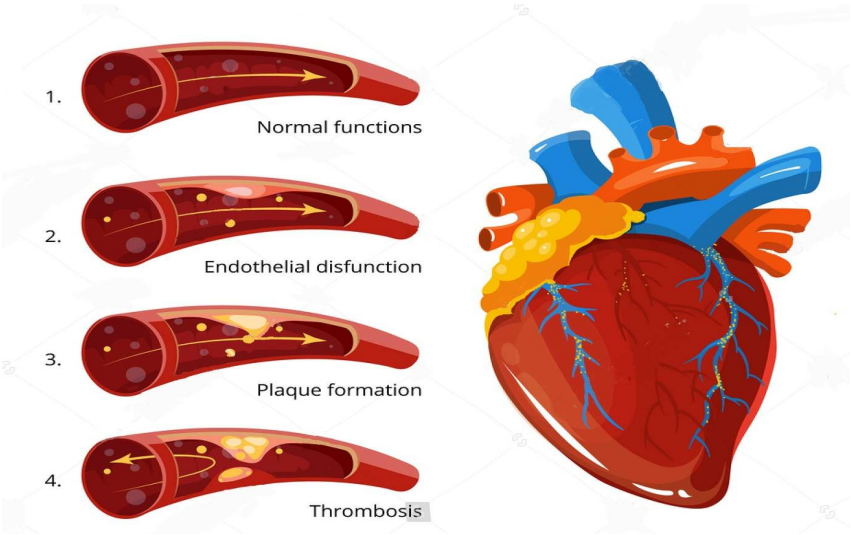

Figure 1.4: Stenosis growth inside conronart artery (source: Marcus et al. (1982))

arteries in which hemodynamic factors play an important role in the formation and dissemination of this disease. Due to abnormal intravascular growths, stenosis can develop at various locations in the arterial system. Presence of stenosis inside an arterial wall can have multiple effects in the body. Inside the blood vessel, flow is increased around the constriction part of the artery which affects the shear stress or pressure gradient by increasing their values within the fluid. A diet with high cholesterol, high blood pressure, cigarette smoking, diabetes create more risk factors for arteriosclerosis (Frank et al., 1973).

The mechanical hydrodynamic factors like turbulence, wall shear stress and lateral wall pressure affect the growth of the stenosis. Once stenosis is formed inside an artery, due to gradual deposition of the pearly substance such as cholesterol, lipid and other substance at the same place, it may advance further. As fatty substance continuously deposits at the stenotic place it undergoes many different forms such as mild stenosis,

moderate or serves stenosis. The high growth of stenosis inside an artery creates high chances of the heart stroke inside the body (Wren et al., 1990).

As the presence of stenosis inside an arterial wall causes serious consequences such as cerebral strokes and myocardial infarction leading to heart failure, hence it is believed to be one of the most serious physiological problems. The flow behavior in the stenosed artery is different from the normal artery and resistance and stresses to flow are also much higher in the stenosed artery as compared to the normal artery. For a proper treatment (surgery) of such disease, it is very important for the medical personnel to have a clear and proper idea about the flow parameters in the stenosed artery such as stress, flow rates and velocity patterns. Many mathematical models have been developed which describes the case of single and multiple stenosis. Young (1968) presented a mathematical analysis for axially symmetric, time-dependent stenosis which grows inside the lumen of a tube of the constant cross-section through which a Newtonian fluid is steadily flowing. With the help of his analysis, he suggested that by neglecting time-dependent boundary condition as for quasi-steady flow, growth of the stenosis plays no role in the fluid mechanics analysis while the rate at which variables such as shear stress and pressure are altering play an important role in certain cellular processes. Chakravarty and Mandal (1994) define the time-dependent geometry for overlapped stenosis. Further, considering the Newtonian behavior of blood flow, Misra et al. (2011b) developed a mathematical model which describes the case of double stenosis having the same size.

1.4.2 Variable Viscosity of Blood Flow

We have already discussed the viscosity of fluids, further in this section we explain the factors which affect the viscosity of blood. It is observed that blood viscosity is not constant in real physiological systems. It alters either with the hematocrit ratio or with temperature or pressure. The function of viscosity variation with hematocrit ratio is defined as

$$\mu(\bar{r}) = \mu_0(1 + \lambda\hbar(\bar{r})), \tag{1.4.1}$$

where

$$\hbar(\bar{r}) = H\left[1 - \left(\frac{\bar{r}}{d_0}\right)^m\right],$$

and $H_r = \lambda H$, in which λ is a constant having the value 2.5 and H is the maximum hematocrit at the center of an artery. Where m is the parameter that determines the exact shape of the velocity profile of blood and H_r is the hematocrit parameter (Shit and Majee, 2015; Sinha and Misra, 2014).

The temperature dependent viscosity of the blood is given by

$$\mu_c(\bar{T}) = \bar{\mu_p}\exp\left[\lambda_i\left(\frac{1}{2} - \frac{\bar{T} - \bar{T_f}}{\bar{T_w} - \bar{T_0}}\right)\right],$$

where T_f is the temperature of the fluid and T_w is the temperature of the wall and the λ_i is the variable viscosity parameter (Siddiqa et al., 2017a, 2018). Many scientific studies have been done considering variable viscosity of blood. Bali and Awasthi (2007) investigated the effect of an external magnetic field on blood flow through a stenosed artery considering radial co-ordinate dependent blood viscosity. Layek et al. (2009) studied the effects of variable viscosity on unsteady viscous fluid flow through a vascular tube with overlapping stenosis. In a typical situation when a large temperature difference exists, most of the fluids have temperature dependent viscosity and this property varies significantly (Çinar et al., 2001). Nadeem and Akbar (2010a) presented the mathematical model to analyze the effects of variable viscosity of blood on the peristaltic flow of a Jeffrey-six constant fluid by defining the viscosity parameter. They solved the model using the homotopy analysis method and resulted that as values of the viscosity parameter increase, the temperature of flow also increases. Recently Siddiqa et al. (2017b) studied the effects of strong temperature-dependent viscosity on bio-magnetic fluid flow under the action of the localized magnetic field with viscous dissipation. In their study, they explained that variable viscosity of blood greatly influence the flow field and creates a lot of vortices within the vicinity of the walls.

1.4.3 Magnetic Effects on Blood

Nowadays, it has gained serious attention to study the magnetohydrodynamics (MHD) behavior of blood flow through the blood vessel due to its wide application in the area

of medical science. Magnetohydrodynamics includes studying the magnetic properties of an electrically conducting fluid. Fluid in the living creature which is affected by the presence of an external magnetic field is known as Bio-magnetic fluid. Blood behaves as bio-magnetic fluid due to red blood cells, in which iron oxides are present at a uniquely high concentration in the mature red blood cells in the form of hemoglobin molecules. Therefore, the principle of the magnetic field is applied when the human body undergoes in the high static magnetic field such as during radiology technique named as Magnetic Resonance Imaging (MRI). The high strength of an applied magnetic field reduces the rate of blood flow in the human arterial system and the given result is very much applicable to treat many types of cardiovascular diseases. In this field Chen and Sana (1985) in the theoretical analysis investigated the effect of magnetic field on blood flow considering blood as an electrically conducting fluid. Habibi et al. (2012) presented a mathematical model to numerically investigate the flow of blood through a channel under the influence of the magnetic field. With the help of their result they found that as values of the magnetic field increase, the velocity of blood flow also increases as attaining maximum value at the center of the artery and zero at the arterial wall. Further, Misra et al. (2011a) presented a mathematical model for second-grade viscoelastic electrically conducting blood flow through a channel having oscillatory stretching walls under the influence of the magnetic field. Bhatti et al. (2017a) developed a mathematical model to study the effects of the blood clot on non-Newtonian Jeffrey fluid through an annulus under the influence of an external radially variable magnetic field. With the help of their study, they resulted that under the effect of magnetic field velocity profile significantly reduce for $r < 0.6$ while it shows converse attitude for $r > 0.6$.

1.4.4 Chemical Reaction

In the chemical reaction, two or more chemicals interact and generate one or more new chemical compound. Heat and accelerator work as a catalyst for the processing of any chemical reaction. The chemical reaction is of two types (Misra and Adhikary, 2016)

- **Homogeneous catalytic reaction:** These are the chemical reactions in which reactant and catalyst are in the same state of matter (i.e. in the same phase).

- **Heterogeneous catalytic reactions:** In these types of chemical reactions reactant and catalyst are not in the same phase.

The chemical reaction with heat and mass transfer effect has many applications in engineering as well as in industrial processes. Many industrial processes which involve heat and mass transfer over the flow surface by producing/absorbing the diffusing species, exists due to the chemical reaction with the ambient fluid. This event which happens within the fluid directly influence the heat and mass characteristics of the flow. A chemical reaction is known as a first-order reaction if its reaction rate is directly proportional to the concentration. On the other hand, if consumption caused by the reaction rate is directly proportional to the k^{th} order concentration difference is known as k^{th} order chemical reaction, where k is any natural number (Mythili et al., 2015). Effects of first-order homogeneous chemical reaction on the fluid flowing through a vertical plate are discussed by Muthucumaraswamy and Ganesan (2001). Further, considering the reaction entirely in the stream, Muthucumaraswamy (2002) analyzed the effects of first order homogeneous chemical reaction on the viscous fluid flowing through a vertically moving surface. With the help of their study, they concluded that the concentration profile of fluid decreases with increasing values of the chemical reaction parameter. Recently, Kandasamy et al. (2005) presented the model to show the effects of heat and mass transfer with heat source under the influence of the chemical reaction of the first order. In their study Singel and Stamler (2005) discussed chemical physiology of blood flow regulation by red blood cells. Influence of reaction rate on the transfer of chemically reactive species in a laminar, non-Newtonian fluid immersed in a porous medium over a stretching has been studied by Prasad et al. (2003). Koriko et al. (2018) described the effects of heat and mass transfer on viscoelastic fluid through a vertical surface with thermophoresis and variable fluid properties considering the influence of n^{th} order of chemical reaction in the fluid. They resulted that taking positive values of chemical reaction parameter, concentration boundary layer thickness decreases with an increase in shear stress for both cases of $n = 1, 2$.

1.4.5 Porosity

It is more physically realizable to consider the porous nature of the medium during the flow. The model related to porosity nature of the pulmonary system and blood vessels comes into the picture for the case of arterial blockage when fatty substance deposits on the arterial wall. Presence of porous media cooled or heated the fluids and enhance the thermal conductivity of fluids. Normally, to model the flow through a porous medium under high-pressure gradients a Darcy model is used while for the case where inertial effects dominate the viscous effects such as in highly porous regime this model is insufficient. To analyze the porosity effect, Khaled and Vafai (2003) gave a rigorous review of heat and fluid dynamics applications in porous (biological) media. Further, Ogulu and Amos (2007) presented a study to analyze the effects of temporally varying wall mass flux on hydromagnetic pulsatile Newtonian blood flow in a Darcian porous model of the cardiovascular system, solving it by applying a regular perturbation technique. The popular approach to simulate drag forces experienced at higher velocities employs the Forchheimer extension to Darcian model and thus known as Darcy-Forchheimer drag model. Using the approach of this model, various researches have been presented in the context of porous media heat transfer, as described by Pop and Ingham (2001). Significant works include those by Preziosi and Farina (2002) who investigated mass exchange using an extended Darcy model. Recently, Ozgumus and Mobedi (2015) studied the effects of porous media on the Newtonian fluid flowing through in between the inline array of rectangular rods and calculated the effects of the pore to throat size ratio on heat transfer coefficient. Krishna et al. (2018) in their study discussed the heat and mass transfer effects on unsteady MHD oscillatory blood flow through porous arteriole.

1.4.6 Inclined Artery

There are so many mathematical models that have been developed to show the effects of an inclined artery on blood flow. Considering the case of an accelerated body, Srivastava (2014b) analyzed the effect of an inclined tapered artery on Casson fluid in the presence of an external magnetic field. Further, Srivastava (2014a) investigated the flow character-

istics of blood flow through an inclined tapered porous artery under the influence of an external inclined applied magnetic field and resulted that as values of an inclined angle (made by artery from the horizontal axis) increase from 0 to $\frac{\pi}{3}$, velocity profile of the blood flow decreases, respectively. Chakraborty et al. (2011) analyzed the effects of an inclined artery on blood flow considering a case of axially non-symmetrical but radially symmetrical mild stenosis inside an artery and noticed that impedance decreases with increased angle of inclination of the artery. Garcia and Riahi (2014) presented a study on two-phase blood flow through an inclined stenosed artery with or without a catheter. Sharma et al. (2014) studied the effects of the inclined catheterized stenosed artery on pulsatile MHD flow with slip on the wall. Slip effects on unsteady non-Newtonian blood hydro-magnetic flow through an inclined catheterized overlapping stenotic artery have been done by Zaman et al. (2016b). With the help of their study, they concluded that the flow rate increases with an increase in the magnitude of an inclination angle.

1.4.7 Viscous dissipation and Joule Heating

In capillary circulation where associated Reynolds number has a value less than 0.01, viscous dissipation in the blood is of considerable importance (JW, 1962). Brinkman (1951) presented an analysis of heat transfer with viscous dissipation and explained the viscous heating in Newtonian fluids. Effect of viscous dissipation on thermal entrance heat transfer region in the laminar pipe flow with convective boundary has been discussed by Lin et al. (1983). Effect of viscous dissipation on magnetohydrodynamics incompressible viscous fluid over the porous stretching surfaces has been presented by Devi and Ganga (2009). Hussain et al. (2017) presented a computational analysis to show the effects of viscous dissipation and temperature dependent thermal conductivity on magnetohydrodynamics Sisko fluid flow over a stretching cylinder. With the help of their study, they resulted that enhancement in the values of Eckert number increases the advective transportation i.e. kinetic energy, in resultant fluid particles collide more frequently and this trend directly transforms the kinetic energy into thermal energy and hence the temperature of fluid increases.

It is well observed that Joule heating is generated when an external electric field

is applied to conductive fluids. The produced Joule heating not only cause an increase in the temperature distribution but also create the temperature gradient. Joule heating effect control temperature rises in the flow and characterizes the thermomechanical/thermophysical properties of an electro-osmotic flow (Horiuchi and Dutta, 2004; Shit et al., 2016). There have been lots of scientific studies which show Joule heating effect on fluid flow (Bhatti and Rashidi, 2017; Pal and Talukdar, 2011). In this regard, Abbasi et al. (2015) presented a study to explain the effect of Joule heating and inclined magnetic field on non-Newtonian fluid for the problem of mixed convective peristaltic transport. Asghar et al. (2014) investigated the effects of Hall and ion slip with Joule heating on peristaltic flow. Simultaneous effects of slip and wall properties on peristaltic transport of nanofluid with Joule heating have been done by Hayat et al. (2015). Further, Abbasi et al. (2016) studied the Joule heating effects with slip-on Carreau–Yasuda Nanofluid through an asymmetric channel. They solved the model numerically and with the help of the result concluded that due to the Joule heating effect as the strengths of an external applied magnetic field increase, the temperature of flow also increases.

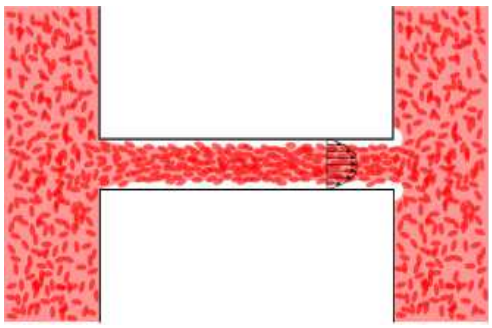

Figure 1.5: Fåhræus effect (source: Minasyan (2016))

1.4.8 Two-phase Blood Flow

Blood flow shows various features. Its one of the basic characteristics is its volume content of erythrocytes (hematocrit level). Depending upon that various rheological properties of the blood flow have been observed through *in vivo* and *in vitro* analysis and those are as follows:

1. **Fåhræus effect** The effect explains that as blood flows from a wide diameter of a blood vessel to a smaller diameter of blood vessel level of hematocrit decreases.

2. **Fåhræus– Lindqvist effect** The effect gives the idea about the blood viscosity when it flows through the narrow blood vessel. According to this effect of blood viscosity also decreases as vessel diameter decreases in size as shown in fig.1.4.7.

Two-phase behavior of blood flow through a small diameter blood vessel can be clearly understood by the Haynes' marginal theory (Haynes, 1960), which explains that in the two-layer model of blood flow RBC collects towards the center of the blood vessels while RBC free plasma collects at the outer region of the vessel. Many mathematical models have been developed which discuss the two-phase behavior of blood flow. Medvedev and Fomin (2011) presented their study for both large and small blood vessels by taking the varying diameter of the blood vessel from 4.5 to 1000 μm. In their study, they explained the known characteristics of the blood flow such as viscosity of blood which depends upon the hematocrit level and blood vessel diameter. Chebbi (2015) in his study extends the work of Haynes' marginal theory. He presented a mathematical model for two-layered blood flow and compared his result with the experimental data of Haynes' marginal theory without using any fitting parameter for computation. With the help of his study, he resulted that the decrease in apparent viscosity decreases the microvascular resistance to blood flow and results in lower blood pressures. Further,Ponalagusamy (2016) presented a mathematical model to study the combined effects of plasma layer thickness, heat transfer and magnetic field on the two-phase flow of blood through a stenosed artery considering Newtonian characteristics of the fluid in both core and plasma regions. With the help of their study, they resulted that the shear stress and flow resistance both decrease in the stenosed artery as the thickness of the plasma layer increases.

1.4.9 Heat Source

There are so many studies in the literature which describe the effect of an external heat source on blood flow. Presence of heat source leads to affect the heat transfer rate of the flow by changing the temperature distribution over the region. In this regard, Petrofsky

et al. (2009) investigated the effect of the moisture content of the heat source on the skin blood flow response and concluded that the total rise in skin temperature is matched with moist and heat sources. In their study, Hayat et al. (2016) analyzed the effects of the heat source with homogeneous-heterogeneous reactions and the influence of Newtonian heating on MHD peristaltic flow of micropolar fluid through a curved channel. They described that enhanced values of heat source parameter increase the temperature profile of the blood flow. Fetecau et al. (2017) presented a general study of magnetohydrodynamic (MHD) natural convection flow with the heat source, radiative effects and shear stress on the boundary. In their study, they discussed different cases for heat absorption and heat generation and resulted that for the case of heat absorption temperature decreases for increasing values of heat source parameter and for the case of heat generation it shows the opposite effect.

1.4.10 Heat Transfer

In the physical system, heat transfer includes the transport as conversion and exchange of thermal energy due to the level of temperature difference. The laws of thermodynamics process the heat transfer although a separate science is required to quantify the process of heat transfer. The reason for this is that the heat transfer falls in a non-equilibrium state while on the other hand classical thermodynamics concerns itself with an equilibrium state. The heat can be transferred by one, or by a combination of three separate mechanisms as thermal conduction, convection and radiation.

Thermal Conduction

Thermal conduction takes place in a stationary medium. Heat conduction is the movement of heat by the microscopic collisions of the particle and motion of electrons within the body. Heat conduction is governed by Fourier's law and states that "the rate of conduction is proportional to the area measured normal to the direction of the heat flow and the temperature gradient in the direction of the heat flow". Mathematically we express the

Fourier's law for the x direction as

$$q = -\kappa \Delta T, \tag{1.4.2}$$

where q is the local heat flux density, κ thermal conductivity and ΔT is the temperature gradient.

Thermal Convection

As opposed molecular motion within the fluid, thermal convection occurs in a moving fluid. When a solid surface is encountered by a moving fluid heat is convected either to it or from it. It depends upon the sign of the surface-to-fluid temperature difference. A mathematical expression for convective heat flux in convective heat transfer is written as

$$q = h'(T_s - T_f), \tag{1.4.3}$$

where h' convective heat transfer coefficient, T_s is the temperature of solid and T_f is fluid temperature.

Thermal Radiation

Radiation does not need any medium to occur and it is the transmission of energy in the form of waves or particles through space or through the material medium. Anything having the temperature above than the absolute zero (-273.15^0C) emits some kind of energy as thermal radiation by experiencing molecular and atomic vibration. The part of thermal radiation on flow and heat transfer processes puts a major importance in the design of many advanced energy conversion systems which operate at high temperature. In a unit volume, the equation of conservation of radiative transfer (which consider the radiative energy incident from all directions) for all wavelength is defined as

$$\nabla.\bar{q}_{ra} = \int_0^\infty K_\lambda(\bar{T})(4e_{\lambda h}(\bar{T}) - G_\lambda)d\lambda, \tag{1.4.4}$$

where $\nabla.\bar{q}_{ra}$ is the radiative flux divergence, G_λ is the incident radiation and $e_{\lambda h}$ is the Plank's function, which is expressed as,

$$G_\lambda = \frac{1}{\pi} \int_{4\pi} e_\lambda(\Omega) d\Omega, \tag{1.4.5}$$

where Ω is the solid angle and the injection parameter λ is determined as bySharma et al. (2007)

$$\lambda = \frac{u_0 R_0}{\mu}.$$

Now, for an optically thin fluid which exchanges the radiation with an isothermal flat plate at temperature T_0 and by applying the Kirchhoff's law, the conserved radiative heat transfer from eq.(1.4.4) for an incident radiation $G_\lambda = 4e_{\lambda h}(T_0)$, converts into the given form

$$\nabla.\bar{q}_c = 4\int_0^\infty K_\lambda(\bar{T})(e_{\lambda h}(\bar{T}) - e_{\lambda h}(\bar{T_0}))d\lambda. \tag{1.4.6}$$

We apply the Taylor series expansion for $K_\lambda(\bar{T})$ and $e_{\lambda h}(T_0)$ around T_0 for small $(T^* - T_0)$ which transform the given eq.(1.4.6) in the form

$$\nabla.\bar{q}_c = 4(\bar{T} - \bar{T_0})\int_0^\infty K_{\lambda_0}\left(\frac{\partial e_{\lambda h}}{\partial T}\right)_0 d\lambda, \tag{1.4.7}$$

where $K_{\lambda_0} = K_\lambda(\bar{T_0})$. Further, assuming ${\alpha_c}^2 = \int_0^\infty K_{\lambda_0}\left(\frac{\partial e_{\lambda h}}{\partial T}\right)_0 d\lambda$, eq.(1.4.7) changes in to

$$\nabla.\bar{q}_{ra} = 4(\bar{T} - \bar{T_0}){\alpha_{ra}}^2,$$

where α_{ra} is the mean radiation absorption coefficients.

In radiation therapy, as radiation waves are widely used to treat cancer and tumor, it is an important subject of research to study the radiation effect on blood flow. Timmerman et al. (2003) and Alongi et al. (2012) explained stereotactic body radiation therapy as a system in which a high dose of radiation is delivered to the tumor by affecting less to the surrounding critical tissues. Effect of body temperature on blood flow is very much important to study as it is noticed that during heat muscle treatment body temperature can cause radiative heat transfer on the blood flow. Craciunescu and Clegg (2001) discussed the influence of blood velocity pulsation on bioheat transfer by having Newtonian characteristics of blood flow. Effects of radiation parameter on wall shear stress and temperature distribution have been investigated by Ogulu and Abbey (2005). Infrared radiation is very much used for heat treatment to different parts of the human body. In this regard, several experimental investigations have been done by Kobu (1999), and

Nishimoto et al. (2006) to analyze the effects of infrared radiation/ultrasonic radiation on blood flow. It is preferred to use in heat therapy because with its help it is possible to directly heat the blood capillaries of the affected areas of the body.

1.4.11 Mass Transfer

In a mixture due to concentration gradients, mass transfer particularly refers to the relative motion of species. In terms of dimensionless numbers, the mass transfer coefficients are typically published including Peclet numbers, Reynolds numbers, Sherwood numbers and Schmidt numbers (Welty et al., 2009). Rashidi et al. (2014) presented a study to show the effects of both heat and mass transfer on MHD fluid flow over a permeable vertical stretching sheet in the presence of the radiation and buoyancy effects. In their study, they compared the effects of Biot number and magnetic parameter on heat and mass transfer rate. Ellahi et al. (2014a) presented a model to study the influence of heat and mass transfer on peristaltic flow in a non-uniform rectangular duct under the consideration of long wavelength ($0 \ll\rightarrow \infty$) and low Reynolds number ($Re \rightarrow 0$). Bhatti and Zeeshan (2017) examined the heat and mass transfer effects on particle-fluid suspension with the help of slip effects considering Casson fluid model in both fluid phase and particulate phase. Further, heat and mass transfer effects on two-phase flow with Electric double layer effects induced due to peristaltic propulsion in the presence of transverse magnetic field have been analyzed by Bhatti et al. (2017b).

1.5 Gaps in Existing Research

In above-mentioned studies, the fluid viscosity is assumed to be constant. This assumption is not valid everywhere. Whole blood viscosity is mainly determined by hematocrit and temperature, whereas plasma viscosity mainly depends on the concentration of high molecular weight proteins (Koppensteiner, 1996). In general, the coefficient of viscosity for real fluids depends upon the temperature and pressure of the fluid. For many liquids, such as water, oils and blood, the variation in viscosity due to temperature change is more dominant than other effects. In fact, in many thermal transport processes, the tem-

perature distribution within the flow field is never uniform, i.e. the fluid viscosity may change noticeably if a large temperature difference exists in the system. For instance, the fluid viscosity of water decreases by 240% when the temperature increases from 100^0C to 500^0C. To accurately predict the flow behavior, it is necessary to take the function of the variation of viscosity with temperature or hematocrit. Therefore, it is highly desirable to include the effect of temperature-dependent viscosity and variable hematocrit in momentum and thermal transport processes.

The idea of electromagnetic fields in medical research was firstly given by Kolin (1936), and later Korchevskii and Marochnik (1965) discussed the possibility of regulating the movement of blood in the human system by applying the magnetic field. It was observed by these authors that high strengths of the magnetic field slow down the speed of blood and these results can be very much useful during the surgical process. However, the published literature lacks the analysis of the magnetic effect on blood flow through an inclined branched artery. If a magnetic field is applied to a moving electrically conducting liquid, it induces electric and magnetic fields. The effect of radially variable magnetic field on narrow arteries is also not investigated earlier.

It is very important to consider the rheological properties of the blood flow when it flows through narrow blood vessels such as arterioles and venules. Many researchers (Federspiel, 1989; Fedosov et al., 2010; Ishii and Hibiki, 2010) have been investigated the two-phase behavior of blood flow (having cell-free plasma region and RBC containing core region) with the help of *in vivo* and *in vitro* analysis. However, with the help of the literature and to the best knowledge of the authors it is found that the effects of mass transfer on two-phase blood flow have not gained much attention from the researchers. In the present study, we consider the mass transfer phenomenon as an important part of the investigation. Effects of Joule heating and viscous dissipation with first-order chemical reaction are also observed on both core and plasma regions separately considering hematocrit dependent viscosity of the core region under the influence radially variable magnetic field. The case of temperature-dependent viscosity of the core is also discussed considering the presence elliptic shaped stenosis inside the inclined artery. The present work also investigates the influence of k^{th} order homogenous chemical reaction with radiation on

the two-layered model of blood flow. Analysis of heat transfer effects on blood flow with an extra factor of the heat source is also a part of the present work.

Hence, in the proposed work, we investigate the blood flow with radiative heat and mass transfer considering its hydromagnetic rheological nature in the presence of porous medium and variable viscosity. Since this study is carried out for a situation when the human body is subjected to an external magnetic field, therefore, it bears the promise of significant application in electromagnetic therapy. The present study also discusses the case when blood flows through a narrow artery. In which arterial length is presumed to be large enough in comparison with its radius so that negligible wall effect is observed at the inlet as well as outlet segment of the artery. The proposed study will be useful to clinicians, hematologists, and biomedical engineers because they serve as useful estimates, which are capable of throwing some light towards the understanding of the genesis of pathological states, like arteriosclerosis as well as the mechanism of gaseous exchanges that take place within tissues and blood vessels. The study will also be useful for evaluating the role of porosity and slip condition when the body is subjected to magnetic resonance imaging (MRI).

1.6 Methodology

1.6.1 Homotopy Method

Let us consider a general nonlinear differential equation

$$N[u(x)] = 0, \tag{1.6.1}$$

where N is a nonlinear operator.

Let L denote an auxiliary linear operator and we assume that $u_0(x)$ is an initial guess of $u(x)$, c_0 (which has a constant value) is a convergence-control parameter . Using the embedding parameter $q \in [0, 1]$ from homotopy theory, one may construct a family of equations as

$$(1 - q)L[u(x; q) - u_0(x; q)] = c_0 q N[u(x; q)]. \tag{1.6.2}$$

The given eq.(1.6.2) is the $zero^{th}$ order deformation equation, whose solution varies continuously with respect to the embedding parameter $q \in [0, 1]$.
The linear equation

$$L\left[U(x;q) - u_0(x;q)\right] = 0, \tag{1.6.3}$$

with known initial guess $U(x;0) = u_0(x)$ when $q = 0$, but it is equivalent to the original non linear differential equation $N[u(x)] = 0$ when $q = 1$ i.e. $U(x;1) = u(x)$. Therefore, as values of q vary from 0 to 1 solution $U(x;q)$ of the $zero^{th}$ order deformation equation varies from the chosen initial guess $u_0(x)$ to the solution $u(x)$ of the given non linear differential eq.(1.6.1).
Now, using the Taylor series expansion we expand the $U(x;q)$ about $q = 0$ and get the homotopy-Maclaurin series as

$$U(x;q) = u_0(x) + \sum_{m=1}^{\infty} u_m(x) q^m. \tag{1.6.4}$$

Now, we consider the convergence-control parameter c_0 of $zero^{th}$ order deformation equation such that the above series eq.(1.6.4) is convergent for $q = 1$ and we get the homotopy-series solution as

$$u(x) = u_0(x) + \sum_{m=1}^{\infty} u_m(x). \tag{1.6.5}$$

Using the $zero^{th}$ order deformation equation, one can directly derive the governing equation of $u_m(x)$ as

$$L[u_m(x) - X_m u_{(m-1)}(x)] = c_0 R_m[u_0, u_1, \ldots\ldots, u_{(m-1)}], \tag{1.6.6}$$

the given eq.(1.6.4) is known as m^{th} order deformation equation, in which the right-hand side R_m is dependent only upon the known results $u_0, u_1, ..., u_(m-1)$ and can be obtained easily using computer algebra software and in equation $X_1 = 0$ and $X_k = 1$ for $k > 1$. Following the given procedure and without the assumption of any small/large physical parameters the original nonlinear equation is transferred into an infinite number of linear ones.

Since the homotopy analysis method(HAM) (Liao (2013)) is based on homotopy, its provide the freedom to choose the initial guess $u_0(x)$, linear operator and the convergence-control parameter for $zero^{th}$ order deformation equation. Thus, the HAM gives freedom to choose the equation-type of the high-order deformation equation and the base functions of its solution. After calculating the general form for the chosen initial guess and linear operator, the optimal value of the convergence-control parameter c_0 is determined by the minimum of the squared residual error of governing equations and/or boundary conditions. Therefore, This is a promising way to find the convergence of the homotopy series solution.

1.6.2 Shooting Method

The shooting method is the numerical method which is used to solve the boundary value problems(BVP). In the first step of this method, we reduce the given BVP into a initial value problem. Further, in this, we apply trial and error or some scientific approach to get as close to the boundary value as possible. For a boundary value problem of a second-order ordinary differential equation, the method is stated as follows.
Let

$$\dot{x} = f(x,t) \quad x \in R^n \quad \text{with boundary conditions,} \tag{1.6.7}$$

$$B : R^n \times R^n \to R^n \quad \text{such that} \quad B(x(a), x(b)) = 0. \tag{1.6.8}$$

Let $x(t_f, s^0)$ is the solution of the BVP eq.(1.6.7) at time t_f with initial condition as $x(t_0) = s^0$. Then the shooting function (error function) is given by

$$E_r(s^0) \coloneqq B\left(s^0, x\left(t_f, s^0\right)\right).$$

The system of algebraic nonlinear eqs.(1.6.8) in s^0 can be solved using Newton's root finding algorithm as described in algorithm(1).

Algorithm 1 Single shooting method

1: **procedure** ROOT OF THE FUNCTION E_r
2: Choose appropriate initial guess s and the error tolerance bound $\delta > 0$.
3: **Stopping Criterion:**
4: **if** $\| E_r(s) \|_\infty < \delta$ **then** Stop.
5: **end if**
6: Calculate Δs by solving the linear system $d_s E_r(s)\Delta s = -E_r(s)$.
7: Update the value of $s = s + \Delta s$.
8: **go to Stopping Criterion**.
9: **end procedure**

1.7 Thesis Organization

In this thesis, we proposed and analyzed mathematical models to understand the dynamics of the hydrodynamical flow of blood through a diseased coronary artery. Effects of different physical parameters (such as magnetic field, chemical reaction and radiation parameters etc.) which directly affect the flow behavior of blood have been examined graphically. Results of their analysis on blood flow are widely applicable in many bio-engineering problems such as cancer treatment, atherosclerosis treatment and regulating blood flow. Following this introductory part, the thesis is organized as follows: **Chapter 1** describes the brief background of the problem and provides the aim and objectives of the thesis as well as gaps in existing research by giving the literature survey. In **Chapter 2**, we discussed the effects of heat transfer on blood flow through the inclined stenosed porous artery with the heat source in the presence of an external magnetic field. In the model, the viscosity of blood flow is considered as hematocrit dependent. Further, in **Chapter 3**, we extended this work and analyzed the effects of both heat and mass transfer on blood flow with the first order of the homogeneous chemical reaction. We solved the governing nonlinear partial differential equations analytically using homotopy perturbation method. The **Chapter 4** discussed a case of the two-phase model of blood flow in which we investigated heat and mass transfer effects with radiation in the presence

of an external magnetic field. We expanded this work in **Chapter 5** by explaining the mathematical model which described the effects of both heat and mass transfer on the two-phase model of blood flow through a stenosed vertical narrowed artery with chemical reaction. We got an exact solution to the given problem. In **Chapter 6**, we studied Joule heating and viscous dissipation effects on two-phase blood flow model under the influence of variable magnetic field treating viscosity of the core region as hematocrit dependent. We applied both the analytical and numerical approach to solve the given mathematical model. **Chapter 7** helped to analyze a mixed convection problem of two-phase blood flow through the inclined stenosed artery in which viscosity of the core region is assumed as temperature dependent and shape of the stenosis is considered as elliptic. Finally, the main outcomes and future scope of the thesis are summarized in **Chapter 8**.

Chapter 2

Effect of Heat Transfer on MHD Blood Flow with Variable Viscosity and Heat Source

2.1 Introduction

Nowadays in the industrialized world, blood flow in our body through arteries is a major cause of health risks. In the circulatory system of the human body highly, oxygenated blood and nutrients delivered from the heart to each cell of the body through arteries. Deposition of matter in an artery affects its function and this type of abnormal elongation of arterial thickness is the first smallest step in the formation of atherosclerosis. The accumulation of substances in the artery is known as stenosis and its presence changes the flow behavior and hemodynamic conditions of the artery that were existing before catheterization (Ellahi et al., 2014c; Rabby et al., 2013). In the presence of stenosis because of fatty deposition on an artery wall, it is increasingly difficult for oxygenated rich blood to reach the heart muscle and the larger scale of artery blockage causes heart attacks (Ollivier et al., 2009; Salomone et al., 1996). As hemodynamics is directly related to overall human health, recently it has gained a serious attention of researchers, physiologists and clinical persons to study the blood flow through arteries. Excellent works in the context of arterial blood flow in the presence of stenosis have been reported by Lipscomb and

Hooten (1978), Mekheimer and Kot (2008) and Nadeem et al. (2011).

The erythrocyte (Red blood cell) in the blood is a highly specialized cell with a small negative charge on it, so the presence of the magnetic field can influence the motion of red blood cells. Biomagnetic fluid dynamics (BFD) is the science in which we study the dynamics of biological fluids in the presence of a magnetic field. MHD differs from BFD in the sense that it deals with magnetic properties of electrically conducting fluids and under the influence of magnetic field flow is not affected by the magnetization or polarization of the fluid. MHD has numerous proposed applications in bioengineering and medical sciences (Mallikarjuna reddy C, 2011), therefore in this area Tzirtzilakis (2008) analyzed the model of the blood flow in an artery having mild stenosis under the influence of the magnetic field. Influence of radially varying MHD on the peristaltic flow in an annulus with heat and mass transfer studied by Nadeem and Akbar (2010b). A model reported by Sharma et al. (2015b) which shows the effect of the external uniform magnetic field on flow parameters of both blood and magnetic particles using magnetohydrodynamics (MHD) approach. Sharma et al. (2013) with Joule effect numerically investigated the heat and mass transfer effect in magneto-biofluid through a non-Darcian porous medium. Magnetic particle capture for biomagnetic fluid flow in stenosed aortic is discussed by Abdullah et al. (2011), Bose and Banerjee (2015). Misra et al. (2011b) proposed a model of blood flow in a porous vessel having double stenoses in the presence of an external magnetic field. The flow of an electrically conducting fluid characterizing blood through the arteries having irregularly shaped multi-stenoses in the environment of a uniform transverse magnetic field is analyzed by Mustapha et al. (2009) and by Mekheimer et al. (2011). Ikbal et al. (2009) investigated a model for non-Newtonian flow of blood through a stenosed artery in the presence of a transverse magnetic field. In which blood is characterized by a generalized Power law model. Above mentioned research has been done for showing the magnetic field effects on blood flow but their studies are restricted in consideration of variable viscosity.

However, In a real physiological system, the blood viscosity is not constant, it may vary either in hematocrit ratio or depends on temperature and pressure(Shit and Majee, 2015). Layek et al. (2009) analyzed the functional dependence of blood viscosity on

hematocrit, viscosity increases with the increasing value of the hematocrit parameter. In the same direction, Sinha and Misra (2014) presented a model of a dually stenosed artery with hematocrit-dependent viscosity. The influence of heat transfer with temperature dependent viscosity is analyzed by Massoudi and Christie (1995), Pantokratoras (2006), Nadeem and Akbar (2009). In the same direction, effects of temperature dependent viscosity with thermal conductivity on heat transfer and fluid flow are analyzed by Umavathi et al. (2016), Makinde and Onyejekwe (2011). Nadeem and Akbar (2010a); Nadeem et al. (2009) proposed the model for peristaltic flow when the viscosity is not constant.

In the case of stenosis when cholesterol deposits on the artery wall and artery-clogging blood clots in the lumen of the coronary artery this stage in the blood flow can be considered as equivalent to a fictitious porous medium El-Shahed (2003) reported a model for pulsatile flow of blood through a stenosed porous artery under the periodic body acceleration. Akbarzadeh (2016) numerically investigated the effect of periodic body acceleration and periodic body pressure gradient on MHD blood flow through a porous artery. Kumar et al. (2005) presented computational techniques for blood flow in arteries with porous effects. Bhatti and Abbas presented a model for Jeffrey fluid which shows the effects of slip and MHD on peristaltic blood flow through a porous medium. Petrofsky et al. (2009) examined the skin blood flow response to the effect of moisture content of the heat source through data. Prakash et al. (2011) formulated a model for bifurcated arteries to study the effects of heat source on MHD blood flow. In the same direction, Eldesoky (2012) studied the effects of heat source on MHD blood flow which passes through a parallel plate channel.

Motivated by the above analysis, this paper presents an analytical study of the effect of heat transfer on MHD blood flow through a stenosed inclined porous artery having variable viscosity and heat source. In the mathematical model of the given problem, momentum and energy equations of the blood flow are solved under the well-defined boundary conditions using homotopy perturbation method (Demir et al., 2013; Hemeda, 2012; Roozi et al., 2011). Effects of different physical parameters such as the inclination angle of the artery, porosity parameter, heat source parameter and magnetic field parameter on velocity and temperature profile of the blood flow have been plotted through

graphs.

2.2 The Mathematical Model

The blood flow is assumed to be flowing through a cylindrically shaped non-tapered artery, in the axial direction of the artery as shown in fig.2.1. Blood is electrically conducting in such a way that a uniform magnetic field (M) is applied perpendicular to the flow direction. Throughout the region of the blood flow in the uniform arterial tube, a non-uniform suspension viscosity is considered, which varies with the packed cell volume of the red blood cells. A case of symmetrically shaped mild stenosis is considered in order to make the model in dimensionless form.

Let us Consider an incompressible magnetohydrodynamic(MHD) Newtonian fluid of density ρ and variable viscosity $\mu(\bar{r})$ flowing through a porous medium in a tube having finite length L. Artery with stenosis is inclined at an angle γ from the vertical axis. Consider the cylindrical coordinate system (r, θ, z)in such a way that $\bar{u}$,$\bar{v}$ and $\bar{w}$ are the velocity component in $\bar{r}$, $\bar{\theta}$ and $\bar{z}$ directions respectively. The governing equations for the model are as follows

Momentum equation (r- direction)

$$\rho\left[\bar{u}\frac{\partial\bar{u}}{\partial\bar{r}}+\bar{w}\frac{\partial\bar{u}}{\partial\bar{z}}\right]=-\frac{\partial\bar{P}}{\partial\bar{r}}+\frac{\partial}{\partial\bar{r}}\left[2\mu(\bar{r})\frac{\partial\bar{u}}{\partial\bar{r}}\right]+2\frac{\mu(\bar{r})}{\bar{r}}\left[\frac{\partial\bar{u}}{\partial\bar{r}}-\frac{\bar{u}}{\bar{r}}\right]+\frac{\partial}{\partial\bar{z}}\left[\mu(\bar{r})\left(\frac{\partial\bar{u}}{\partial\bar{z}}+\frac{\partial\bar{w}}{\partial\bar{r}}\right)\right], \tag{2.2.1}$$

Momentum equation (z- direction)

$$\begin{aligned}\rho\left[\bar{u}\frac{\partial\bar{w}}{\partial\bar{r}}+\bar{w}\frac{\partial\bar{w}}{\partial\bar{z}}\right]=&-\frac{\partial\bar{P}}{\partial\bar{z}}+\frac{\partial}{\partial\bar{z}}\left[2\mu(\bar{r})\frac{\partial\bar{w}}{\partial\bar{z}}\right]+\frac{1}{\bar{r}}\frac{\partial}{\partial\bar{r}}\left[\mu(\bar{r})\bar{r}\left(\frac{\partial\bar{u}}{\partial\bar{z}}+\frac{\partial\bar{w}}{\partial\bar{r}}\right)\right]\\&-\sigma_1\bar{\mu_m}^2{H_0}^2\bar{w}+\rho g\alpha\left(\bar{T}-\bar{T_0}\right)\cos\gamma-\frac{\mu(\bar{r})\bar{w}}{k_1},\end{aligned} \tag{2.2.2}$$

Energy equation

$$\rho c_p\left[\bar{u}\frac{\partial\bar{T}}{\partial\bar{r}}+\bar{w}\frac{\partial\bar{T}}{\partial\bar{z}}\right]=\frac{k}{\bar{r}}\frac{\partial}{\partial\bar{r}}\left(\bar{r}\frac{\partial\bar{T}}{\partial\bar{r}}\right)+\mu(\bar{r})\left(\frac{\partial\bar{w}}{\partial\bar{r}}\right)^2-A(\bar{T}-\bar{T}_0), \tag{2.2.3}$$

where $\bar{u}$, $\bar{v}$ and $\bar{w}$ are the respective velocity component in the radial and axial directions. c_p is specific heat at constant pressure, k is the thermal conductivity, σ_1 is the electrical

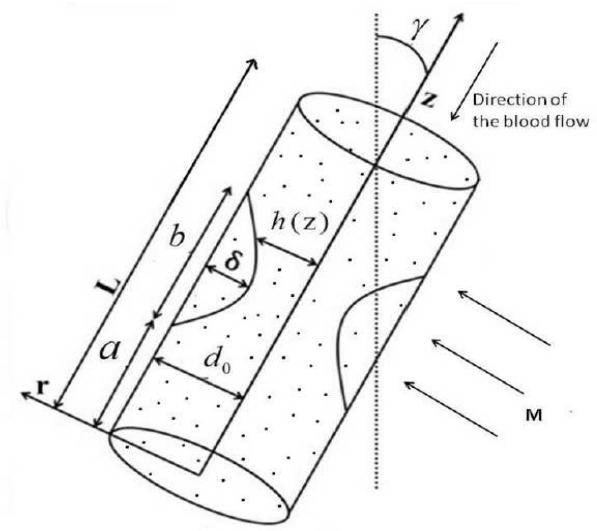

Figure 2.1: Geometry of the artery

conductivity and k_1 is the permeability, $\bar{p}$ is the pressure, $\bar{T}$ is the temperature, ρ is the density, $\mu(\bar{r})$ is the viscosity and H_0 is applied magnetic field.

Variable viscosity of the blood flow is defined by the formula

$$\mu(\bar{r}) = \mu_0(1 + \lambda\hbar(\bar{r})), \tag{2.2.4}$$

where

$$\hbar(\bar{r}) = H\left[1 - \left(\frac{\bar{r}}{d_0}\right)^m\right],$$

and $H_r = \lambda H$, in which λ is a constant having the value 2.5 and H is the maximum hematocrit at the center of an artery. Where m is the parameter that determines the exact shape of the velocity profile of blood and H_r is the hematocrit parameter (Sinha and Misra, 2014).

Geometry of the stenosis located at point z with it's maximum height of δ, is defined by the formula (Mekheimer and Kot, 2008)

$$h(\bar{z}) = \begin{cases} d(\bar{z})[1 - \eta(b^{n-1}(\bar{z} - a) - (\bar{z} - a)^n)] & \text{when} \quad a \leq \bar{z} \leq a + b, \\ d(\bar{z}) \qquad \text{otherwise}, \end{cases} \tag{2.2.5}$$

where $d(z)$ is the radius of the tapered artery in stenotic region with

$$d(\bar{z}) = d_0 + \xi\bar{z}.$$

In eq.(2.2.5), n is the shape parameter which determines the shape of the constriction profile. Value $n = 2$ results symmetrically shaped stenosis and for non symmetric stenosis case n considers the values $n \geq 2$. d_0 is the radius of the non-tapered artery and ξ is the tapering parameter which is defined by $\xi = \tan(\phi)$, where ϕ is known as tapered angle and it considers the values $\phi < 0$, $\phi > 0$ and $\phi = 0$ for the case of converging, diverging and non tapered artery respectively (Mekheimer and Kot, 2008).

In eq.(2.2.5) parameter η is defined as

$$\eta = \frac{\delta^* n^{\frac{n}{n-1}}}{d_0 b^n (n-1)}, \tag{2.2.6}$$

where δ is the maximum height of the stenosis located at

$$\bar{z} = a + \frac{b}{n^{\frac{n}{n-1}}}.$$

In order to represent the model in dimensionless form, let us introduce the non-dimensional variables as follows:

$$\begin{cases} \bar{u} = \frac{uu_0\delta}{b}, \quad \bar{r} = rd_0, \quad \bar{z} = zb, \quad \bar{w} = wu_0, \quad \bar{h} = hd_0, \\ \bar{P} = \frac{u_0 b\mu_0 P}{{d_0}^2}, \quad Re = \frac{\rho b u_0}{\mu_0}, \quad \Theta = \frac{(\bar{T}-\bar{T_0})}{\bar{T_0}}, \quad Pr = \frac{\mu c_p}{k}, \quad Ec = \frac{{u_0}^2}{c_p T_0}, \\ Z = \frac{k_1}{{d_0}^2}, \quad M^2 = \frac{\sigma_1 {H_0}^2 {d_0}^2}{\mu_0}, \quad Q = A\frac{{d_0}^2}{k}, \quad Gr = \frac{g\alpha {d_0}^3 \bar{T_0}}{v^2}, \end{cases} \tag{2.2.7}$$

where Re is the Reynolds number, Ec is the Eckert number, Pr is the Prandtl number and Gr is the thermal Grashof number, M, Q, Z and Hr are magnetic field, heat source, porosity and hematocrit parameters, respectively.

In the case of mild stenosis $\frac{\delta^*}{d_0} \ll 1$ and other two additional conditions (Mekheimer and Kot, 2008)

$$\frac{Re\delta^* n^{\frac{1}{n-1}}}{b} \ll 1, \tag{2.2.8}$$

$$\frac{d_0 n^{\frac{1}{n-1}}}{b} \sim O(1), \tag{2.2.9}$$

eqs.(2.2.1)-(2.2.3) change in the given non dimensional form

Momentum equation (r-direction)

$$\frac{\partial P}{\partial r} = 0, \tag{2.2.10}$$

Momentum equation (z-direction)

$$\frac{\partial P}{\partial z} = \left[\frac{1}{r} + H_r\left(\frac{1}{r} - (m+1)r^{m-1}\right)\right]\frac{\partial w}{\partial r} + [1 + H_r(1-r^m)]\frac{\partial}{\partial r}\left(\frac{\partial w}{\partial r}\right) - w\left(M^2 + \frac{1}{Z} + \frac{H_r}{Z}(1-r^m)\right) + Gr\Theta\cos\gamma, \tag{2.2.11}$$

Energy equation

$$\frac{1}{r}\frac{\partial}{\partial r}\left[r\frac{\partial \Theta}{\partial r}\right] + EcPr\left[\frac{\partial w}{\partial r}\right]^2 - Q\Theta = 0, \tag{2.2.12}$$

where $Br = EcPr$, Brinkman number (Br) is the ratio between heat produced by viscous dissipation and heat transported by molecular conduction.

The corresponding boundary conditions are

$$\frac{\partial w}{\partial r} = 0, \qquad \frac{\partial \Theta}{\partial r} = 0, \quad at \quad r = 0, \tag{2.2.13}$$

$$w = 0, \qquad \Theta = 0, \quad at \quad r = h(z). \tag{2.2.14}$$

In which $h(z)$ is the geometry of the stenosis in non-dimensional form when radius of the artery is of unit length ($d_0 = 1$)

$$h(\bar{z}) = \begin{cases} (1+\xi' z)[1 - \eta_1((z-l_1) - (z-l_1)^n)] & \text{when} \quad l_1 \le z \le l_1 + 1, \\ 1 \qquad \text{otherwise,} \end{cases} \tag{2.2.15}$$

in eq.(2.2.15), η_1, δ, l_1 and ξ' are defined as

$$\eta_1 = \frac{\delta n^{\frac{n}{n-1}}}{(n-1)}, \quad \delta = \frac{\delta^*}{d_0}, \quad l_1 = \frac{a}{b}, \quad \xi' = \frac{\xi b}{d_0}, \quad \xi = tan(\phi).$$

2.3 Solution

Now, we use semi-analytical technique named as homotopy perturbation method to solve the given nonlinear eqs.(2.2.10)-(2.2.12) under the given boundary conditions eqs.(2.2.13)-(2.2.14). First, formulate following homotopies for velocity and temperature profiles

$$H(q,w) = q\left[L(w) + H_r(\frac{1}{r} - (m+1)r^{m-1})\frac{\partial w}{\partial r} + H_r(1-r^m)\frac{\partial}{\partial r}(\frac{\partial w}{\partial r}) - \frac{\partial p}{\partial z}\right] \tag{2.3.1}$$
$$+ (1-q)[L(w) - L(w_0)] - q\left[w\left(M^2 + \frac{1}{Z} + H_r\frac{(1-r^m)}{Z}\right) - cos\gamma(Gr\Theta)\right],$$

where $q \in [0,1]$ is the embedding parameter and $L(w)$ is the auxiliary linear operator, defined as

$$L(w) = \frac{1}{r}\left(\frac{\partial}{\partial r}\left(r\frac{\partial w}{\partial r}\right)\right), \tag{2.3.2}$$

$$H(q,\Theta) = (1-q)[L(\Theta) - L(\Theta_0)] + q\left[L(\Theta) + EcPr\left(\frac{\partial w}{\partial r}\right)^2 - Q\Theta\right], \tag{2.3.3}$$

where

$$L(\Theta) = \frac{1}{r}\left(\frac{\partial}{\partial r}\left(r\frac{\partial \Theta}{\partial r}\right)\right). \tag{2.3.4}$$

The initial guesses used to solve these homotopies are given by

$$w_{10} = \frac{(r^2-h^2)}{4}\left(M^2 + \frac{1}{Z}\right)\left(\frac{\partial p_0}{\partial z}\right), \tag{2.3.5}$$

$$\Theta_{10} = \frac{(r^2-h^2)}{4}. \tag{2.3.6}$$

Now, the dependent variables can be decomposed as

$$w(r,q) = w_0 + qw_1 + q^2w_2 + O(q^3), \tag{2.3.7}$$

$$\Theta(r,q) = \Theta_0 + q\Theta_1 + q^2\Theta_2 + O(q^3). \tag{2.3.8}$$

Now, substitute the series expansion of above variables in eq.(2.3.1) and eq.(2.3.3), compare the coefficients of q^0, q^1 and q^2.

First by comparison the coefficient of q^0 in eq.(2.3.1),

$$L(w_0) - L(w_{10}) = 0 \quad \Rightarrow w_0 = w_{10} = \frac{(r^2-h^2)}{4}\left(M^2 + \frac{1}{Z}\right)\left(\frac{\partial p_0}{\partial z}\right), \tag{2.3.9}$$

now compare the coefficient of q^1 in eq.(2.3.1),

$$\begin{aligned} L(w_1) = -L(w_0) - H_r\left(\frac{1}{r} - (m+1)r^{(m-1)}\right)\frac{\partial w_0}{\partial r} - H_r\left(1-r^m\right)\frac{\partial}{\partial r}\left(\frac{\partial w_0}{\partial r}\right) \\ + w_0\left(M^2 + \frac{1}{Z} + H_r\frac{(1-r^m)}{Z}\right) - cos\gamma\left(Gr\Theta_0\right) + \frac{\partial p_0}{\partial z}, \end{aligned} \tag{2.3.10}$$

and by compare the coefficient of q^2 in eq.(2.3.1), get the equation as follows

$$\begin{aligned} L(w_2) = -H_r\left(\frac{1}{r} - (m+1)r^{(m-1)}\right)\frac{\partial w_1}{\partial r} - H_r(1-r^m)\frac{\partial}{\partial r}\left(\frac{\partial w_1}{\partial r}\right) \\ + w_1\left(M^2 + \frac{1}{Z} + H_r\frac{(1-r^m)}{Z}\right) - cos\gamma\left(Gr\Theta_1\right) + \frac{\partial p_1}{\partial z}. \end{aligned} \tag{2.3.11}$$

Now in eq.(2.3.3), compare coefficients of q^0, q^1 and q^2 respectively

$$q^0 : \qquad L(\Theta_0) - L(\Theta_{10}) = 0 \qquad \Rightarrow \Theta_0 = \Theta_{10} = \frac{(r^2 - h^2)}{4}, \tag{2.3.12}$$

$$q^1 : \qquad L(\Theta_1) = -L(\Theta_0) - EcPr\left(\frac{\partial w_0}{\partial r}\right)^2 + Q\Theta_0, \tag{2.3.13}$$

$$q^2 : \qquad L(\Theta_2) = -2EcPr\left(\frac{\partial w_0}{\partial r}\right)\left(\frac{\partial w_1}{\partial r}\right) + Q\Theta_1. \tag{2.3.14}$$

So with the help of initial guesses w_{10}, Θ_{10} from eq.(2.3.5) and eq.(2.3.6) and by using the definition of linear operators $L(w_0)$ and $L(\Theta_0)$ from eq.(2.3.2) and eq.(2.3.4), in eq.(2.3.10) and eq.(2.3.13), get the expressions for w_1 and Θ_1 as

$$\begin{aligned} w_1 =& \frac{(r^2 - h^2)}{4}\left(\frac{\partial p_0}{\partial z}\right)\left(1 - (M^2 + \frac{1}{Z})\right) - \frac{cos\gamma}{64}\left(r^4 + 3h^4 - 4r^2h^2\right)Gr \\ &+ \frac{H_r}{4Z}\left(\frac{\partial p_0}{\partial z}\right)\left(M^2 + \frac{1}{Z}\right)\left(\frac{r^4 + 3h^4}{16} + \frac{(h^{m+4} - r^{m+4})}{(m+4)^2} + \frac{h^2r^{m+2} - h^{m+4}}{(m+2)^2}\right) \\ &- \frac{H_r}{4Z}\left(\frac{\partial p_0}{\partial z}\right)\left(M^2 + \frac{1}{Z}\right)\left(\frac{r^2h^2}{4}\right) + \left(\frac{\partial p_0}{\partial z}\right)\left(M^2 + \frac{1}{Z}\right)^2\left(\frac{r^4}{16} + \frac{3h^4}{16} - \frac{h^2r^2}{4}\right) \\ &- \frac{H_r}{2}\left(\frac{r^2 - h^2}{2} + \frac{h^{m+2} - r^{m+2}}{m+2}\right)\left(\frac{\partial p_0}{\partial z}\right)\left(M^2 + \frac{1}{Z}\right), \end{aligned} \tag{2.3.15}$$

$$\Theta_1 = -EcPr\frac{(r^4 - h^4)}{64}\left(\frac{\partial p_0}{\partial z}\right)^2\left(M^2 + \frac{1}{Z}\right)^2 - \left(\frac{r^2 - h^2}{4}\right) + Q\left(\frac{r^4}{16} + \frac{3h^4}{16} - \frac{r^2h^2}{4}\right). \tag{2.3.16}$$

Final expressions for w_2 and Θ_2 have been calculated by putting the values of w_1, Θ_1 in eq.(2.3.11) and eq.(2.3.14) and with the help of MATLAB 2015a. We obtain full expressions for $w(r, z)$ and $\theta(r, z)$ by putting the values of w_1, w_2, θ_1 and θ_2 in eq.(2.3.7) and eq.(2.3.8) respectively.

2.4 Results and Discussion

In this section graphical results have been displayed for velocity, temperature and wall shear stress profiles of the blood flow for different quantities of interest. Default values of

the physical parameters which have been used to graphically analyze the effectiveness of the model are as follows:
d_0 =1, $h(z)$=0.9, a=0.25, b=1, $\gamma = \frac{\pi}{6}$, $Z = 0.3$, n = 2, $Gr = 2$, z= 0.5, $\delta = 0.1$, $H_r = 1$, $M = 1.5$, $Q = 1.5$, $Br = 2$.

Fig.2.2, displays the effect of the magnetic field parameter on the velocity profile of the blood flow. It can be easily seen from the figure that the velocity profile of the blood flow decreases as values of the magnetic field parameter increase. It happens because of the fact that when blood flows under the influence of the magnetic field, the action of magnetization applies a rotational motion on the charged particles of the blood flow. The continuous rotational motion of the charged particles causes red blood cells to be more suspended in the blood plasma and this effect increases the internal viscosity of the blood flow. Increased viscosity causes rise to a resistive type force called the Lorentz force. This force opposes the motion of blood particles, which reduces the velocity of the blood flow. This effect of magnetic field on the velocity profile of the blood flow follows in the same manner as proposed by the authors Sharma et al. (2015b). Fig.2.3, displays the effects of the magnetic field parameter on the temperature profile of the blood flow. From the figure, it is clear that as the values of the magnetic field parameter increase, the temperature profile of the blood flow decreases. As it has been discussed above that with the increment in the values of magnetic field parameter result in increasing values of viscosity. So by the physical law of viscosity, this follows in a right manner that with the increment in the values of the magnetic field parameter result in the direction of decreasing value of temperature profile.

In fig.2.4 , the velocity profile of the blood flow is plotted for different values of thermal Grashof number. It is clear from the figure that as values of the thermal Grashof number changes from 1 to 3, the velocity profile of the blood flow increases and this happens due to increased Boussinesq source terms. Thermal Grashof number indicates the relative effect of the thermal buoyancy force to the viscous hydrodynamic force in the boundary layer. Therefore, a rise in the velocity of the blood flow is observed due to the enhancement of thermal buoyancy force as values of the thermal Grashof number increase. Fig.2.5 is plotted to show the effects of the thermal Grashof number on the temperature

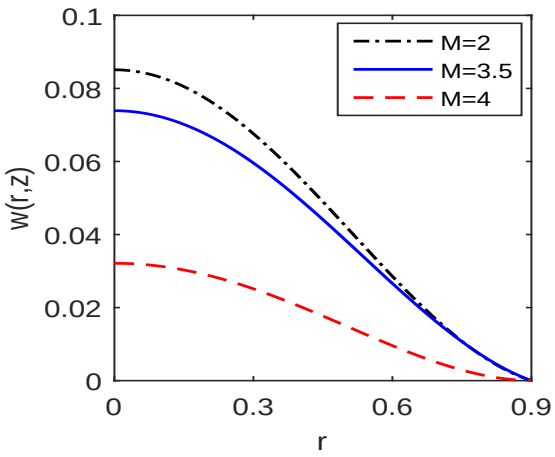

Figure 2.2: Variation of velocity profile with magnetic field parameter (M)

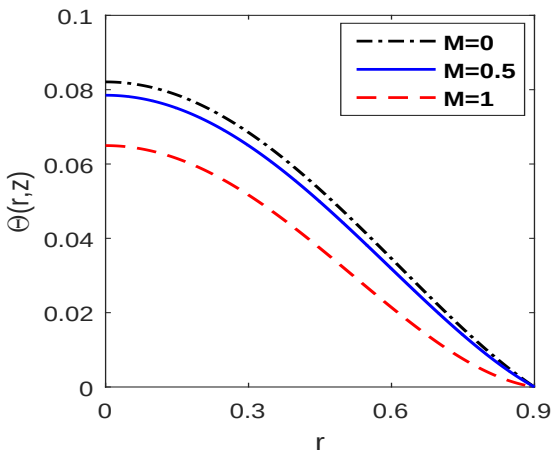

Figure 2.3: Variation of temperature profile with M

profile of the blood flow. It is clear from the figure that as values of the thermal Grashof number increase, the temperature profile of blood flow decreases.

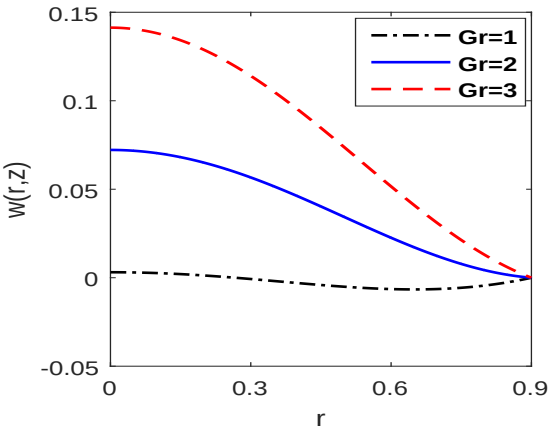

Figure 2.4: Variation of velocity profile with thermal Grashof number (Gr)

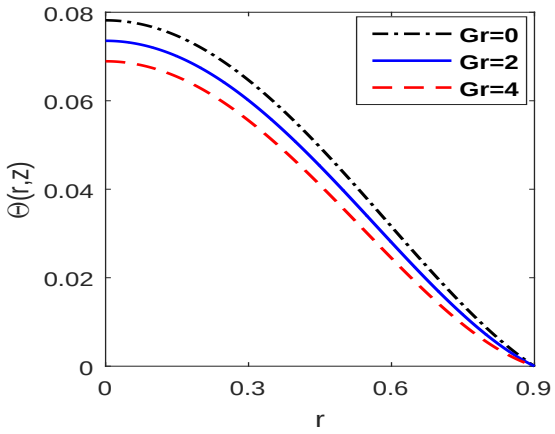

Figure 2.5: Variation of temperature profiles with Gr

Effect of the Brinkman number on the temperature profile is depicted in fig.2.6. From the figure, it is clear that as the values of the Brinkman number increase, temperature profile of blood flow decreases, respectively. It clears that for a particular value of Brinkman number, the temperature profile of blood flow decreases from the middle of the artery to the side wall of the artery. Fig.2.7 displays the effects of porosity parameter

temperature profile of the blood flow. The figure marks that the temperature profile increases with increasing values of the porosity parameter and it takes place maybe because of the viscous nature of the fluid which decreases with increasing values of velocity.

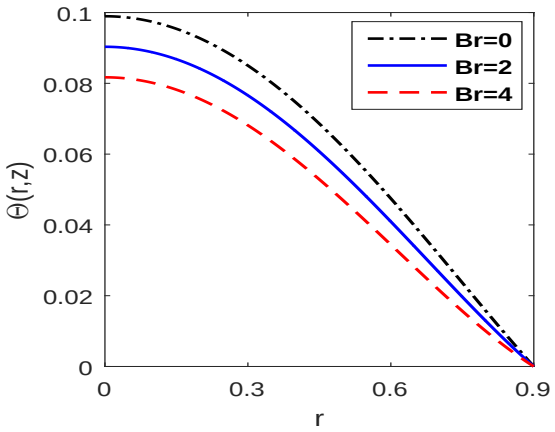

Figure 2.6: Variation of temperature profile for different values of Br

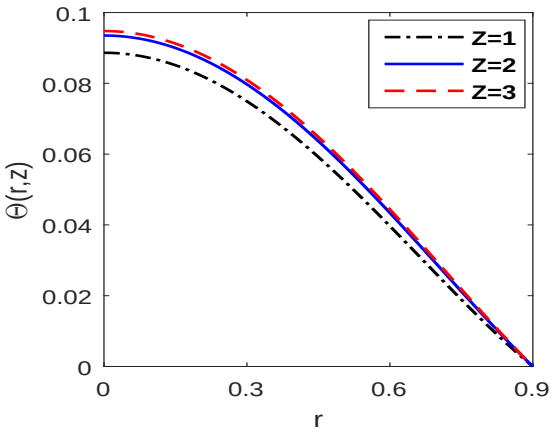

Figure 2.7: Variation of temperature profile with Z

Fig.2.8 illustrates the distribution of the velocity profile of the blood flow for different values of the hematocrit parameter. The figure shows that the velocity profile of the blood flow decreases with increasing values of the hematocrit parameter. In blood, hematocrit is the volume percentage of red blood cells and in the artery as the number of red blood cells increases in the volume, the density of blood flow increases relatively. Increased density of blood slows down the flow of blood and this causes the decreased velocity of the blood flow. The figure further reveals that velocity of the blood flow follows the parabolic profile such that for any particular value of the hematocrit parameter velocity attains maximum value at the center and it starts decreasing as we move towards the stenotic wall of the artery. Fig.2.9 illustrates the distribution of temperature profile of the blood flow for different values of the hematocrit parameter H_r. From the figure, it can be clearly observed that as the values of the hematocrit parameter increase, temperature profile of the blood flow decreases. So increase in the value of H_r directly decrease the rate of heat transfer at the stationary artery wall.

Fig.2.10 shows the variation of the velocity profile of the blood flow for different values of the heat source parameter. It can be clearly seen from the figure that as values of the

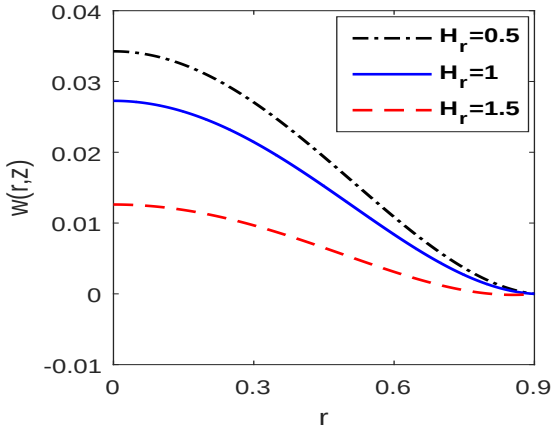

Figure 2.8: Variation of velocity profile with hematocrit parameter (H_r)

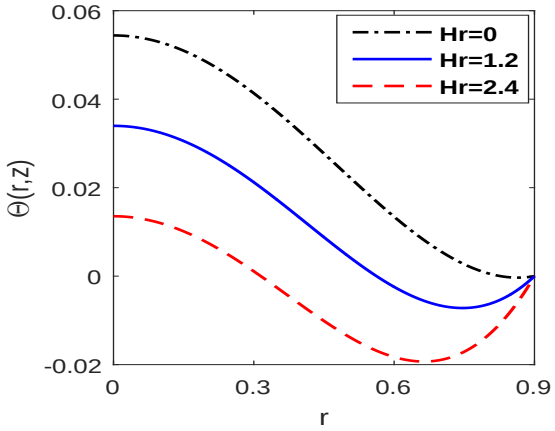

Figure 2.9: Variation of temperature profile with H_r

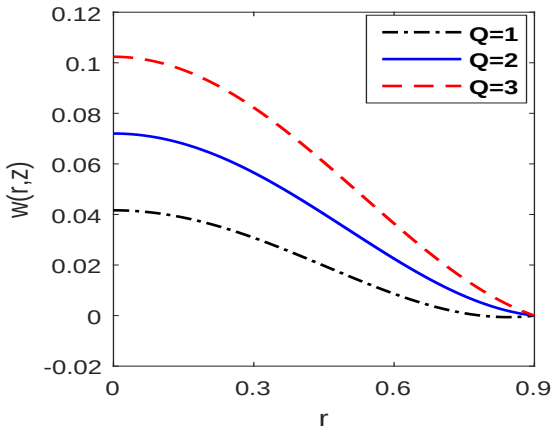

Figure 2.10: Variation of velocity profile with heat source parameter (Q)

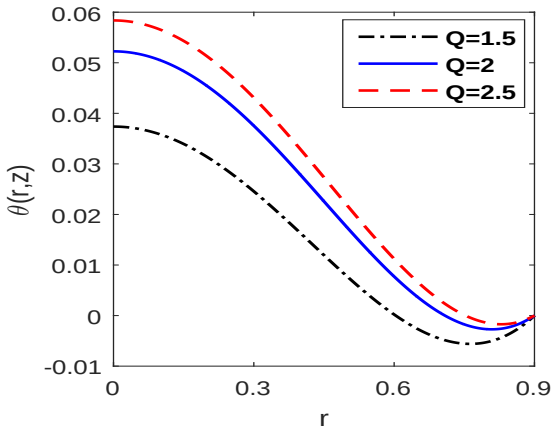

Figure 2.11: Variation of temperature profile with Q

heat source parameter increase, the velocity of the blood flow also increases. Fig.2.11 displays the variation of the temperature profile of the blood flow for different values of the heat source parameter. From the figure, it can be marked that within the blood, radiation acts as a heat source. Hence, increasing values of radiation dosage would directly increase the temperature profile of the blood flow. In the pathological state, this type of thermal therapy is very much used to expose body tissues and cancerous tumor to high temperature. The result of which kills cancer cells associated with tumors with minimal injury to normal tissues. It is observed through the figure that for a particular value of

the heat source parameter, temperature profile of the blood flow achieves its maximum value at the center of the artery and it starts decreasing as we move towards the stenotic wall.

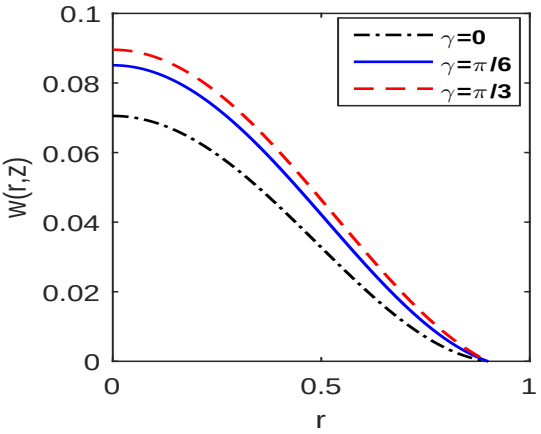

Figure 2.12: Variation of velocity profile with different values of γ

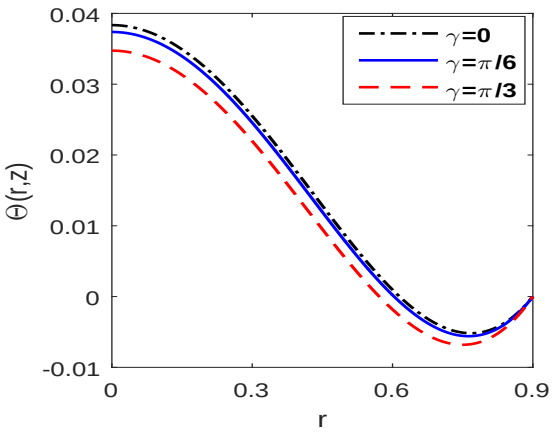

Figure 2.13: Variation of temperature profile with different values of γ

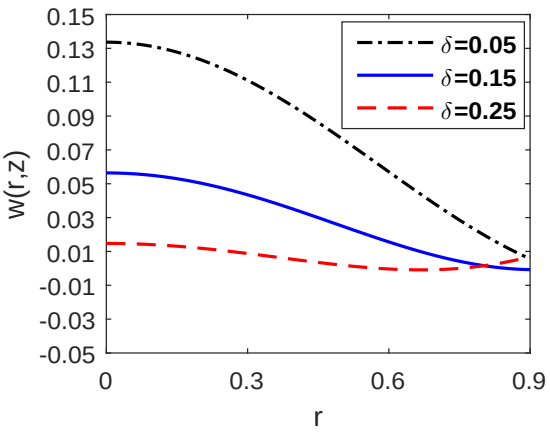

Figure 2.14: Variation of velocity profile with different height of the stenosis (δ)

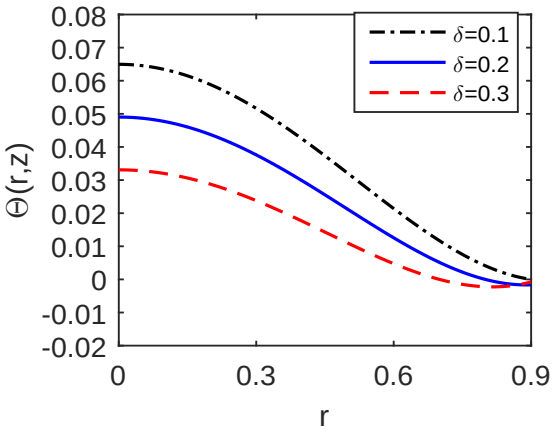

Figure 2.15: Variation of temperature profile with δ

Figs.2.12-2.13 illustrate the distribution of velocity and temperature profiles for different inclination angles of the artery, respectively. Figures show that as the angle made by the artery from vertical axes changes increasingly from 0 to $\frac{\pi}{3}$, velocity profile increases while temperature profile of the blood flow decreases, respectively, where $\gamma = 0$ is the case

of the horizontal artery.

Figs.2.14-2.15 are plotted to show the effects of the height of the stenosis (δ) on velocity and temperature profile of the blood flow, respectively. It is clear from figures that as values of the height of the stenosis increase both velocity and temperature profile of the blood flow decrease, respectively. So from these figures, it can be clearly observed that both velocity and temperature profile of the blood flow attain their minimum value at the arterial wall and maximum value at the middle of the artery. For every value of δ this satisfies the boundary conditions

Expression for the Shear Stress

The nonzero dimensionless shear stress is given by

$$\tilde{S_{rz}} = -\left(\frac{\partial w}{\partial r}\right), \tag{2.4.1}$$

expression for wall shear stress is

$$\tilde{S_{rz}} = -\left[\frac{\partial w}{\partial r}\right]_{r=h}. \tag{2.4.2}$$

To find the expression for shearing stress at the stenosis throat i.e., the wall shear at the maximum height of the stenosis located at $z = \frac{a}{b} + \frac{1}{n^{\frac{n}{n-1}}}$, put $h = (1-\delta)$. So the expression for the wall shear at the maximum height of the stenosis is given by

$$\tilde{\tau_s} = -\left[\tilde{S_{rz}}\right]_{h=(1-\delta)}. \tag{2.4.3}$$

Fig.2.16 is plotted for the wall shear stress at stenosis throat τ_s against the height of the stenosis δ for different values of the magnetic field parameter (M). From fig.2.16 it is clear that as values of the magnetic field parameter changes from 0 to 1.5, the wall shear stress at stenosis throat increases respectively. Fig.2.17 and fig.2.18 display the effects of hematocrit and porosity parameter on wall shear stress at stenosis throat, respectively. Fig.2.17 marks that as values of hematocrit parameter increase from 0 to 2, wall shear stress at stenosis throat is also increased, respectively. Fig.2.18 depicts that effects of the porosity parameter change increasingly from 0.1 to 0.4, wall shear stress at stenosis throat decreases, respectively.

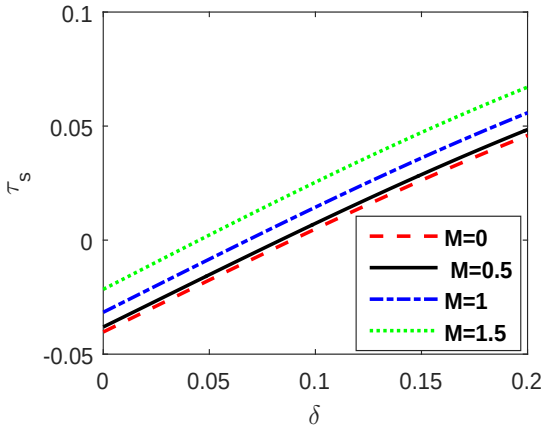

Figure 2.16: Variation of wall shear stress at stenosis throat with M

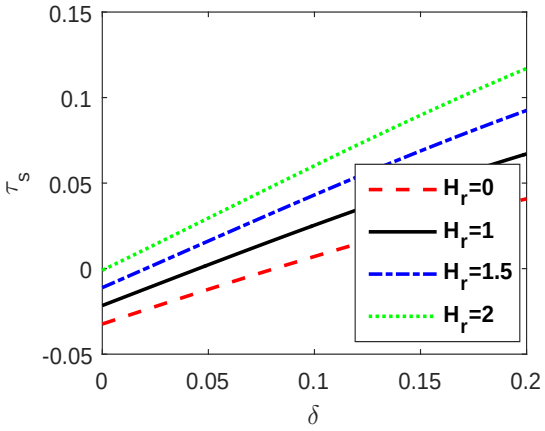

Figure 2.17: Variation of wall shear stress at stenosis throat with H_r

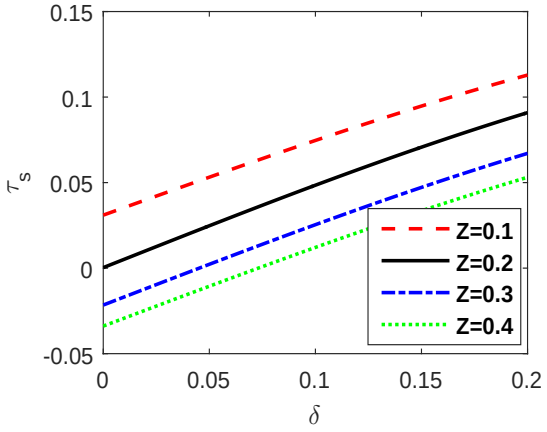

Figure 2.18: Variation of wall shear stress at stenosis throat with Z

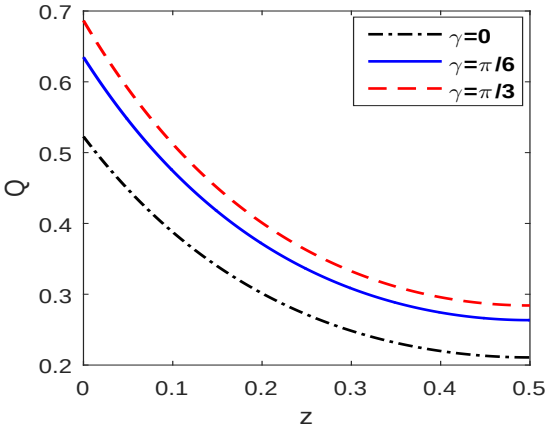

Figure 2.19: Variation of flow rate for different values of γ

The flow rate of blood flow can be calculated as

$$Q = 2\pi {d_0}^2 \int_0^{d_0} u(r)dr. \tag{2.4.4}$$

Fig.2.19 displays flow rate profile of the blood flow for different values of the inclination angle of the artery. From the figure, it is observed that as values of the inclination angle made by the artery increase from 0 to $\frac{\pi}{3}$, the flow rate of the blood flow inside a stenosed artery increases.

To draw the velocity contours following data are used:

$$M = 1, h = 0.9, \delta = 0.1, Z = 0.5, Gr = 2, \gamma = \frac{\pi}{6}, Hr = 1.$$

Figs.2.20-2.22 illustrate the flow patterns of blood in the stenosed artery for different

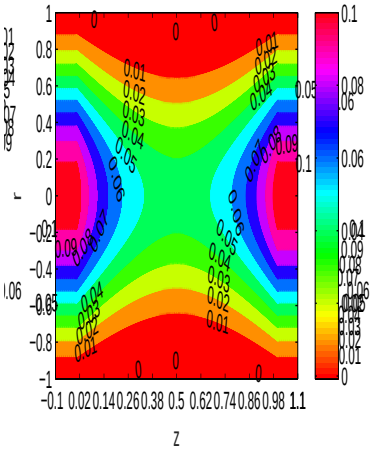

Figure 2.20: Velocity contour for 10% stenosis

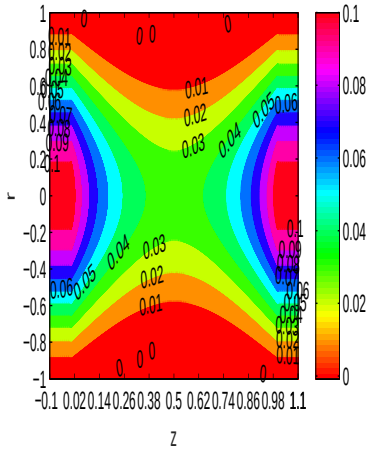

Figure 2.21: Velocity contour for 15% stenosis

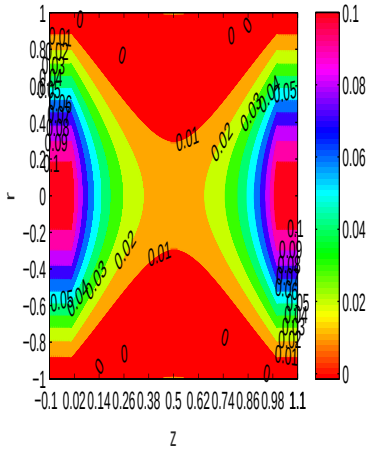

Figure 2.22: Velocity contour for 18% stenosis

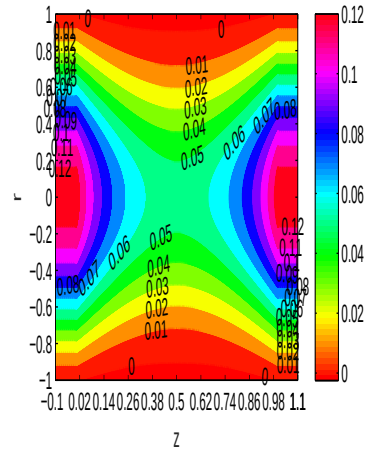

Figure 2.23: Velocity contour for $\gamma = 0$

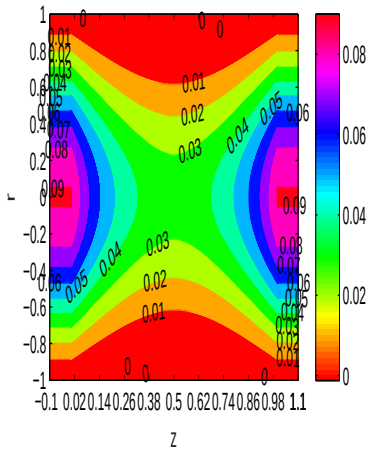

Figure 2.24: Velocity contour for $\gamma = \frac{\pi}{6}$

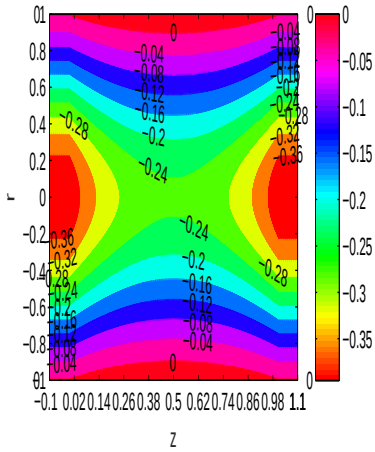

Figure 2.25: Velocity contour for $\gamma = \frac{\pi}{3}$

values of the height of the stenosis. The plots give the clear picture of flow circulation inside the artery when stenosis blocks 10% to 18% part of the artery. From figures, it is

clear that as constriction of the artery increases trapping bolus try to the shift from the downstream part of the stenosis towards the arterial wall. In figures, 0 scale streamlines show the constriction part of the artery outside of that no flow occurs. Figs2.23-2.25 exhibit the flow pattern of the blood flow through streamlines contours for different values of the inclination angles made by the artery. We observe that as the inclined angle of the artery increasingly changes from 0 to π velocity increases at stenosis throat.

2.5 Conclusions

In the article, the hemodynamics of MHD blood flow having variable viscosity through a stenosed, inclined arterial segment with heat source has been investigated. The study discusses the situation when the lumen of an arterial segment converts into a porous medium due to the deposition of fatty substances. Flow dynamics has been analyzed by the momentum and energy equation of the flow. A homotopy perturbation technique is used to get the analytical solutions for velocity and temperature equations of the blood flow. The significant findings of this paper are summarized as follows:

1. The velocity of the blood flow decreases as values of the magnetic field parameter increase and this happens due to the Lorentz force which opposes the motion of the blood flow in the artery. The given result can be very much useful to control blood flow during the surgical process.

2. The velocity profile of the blood flow increases as values of the inclination angle made by the artery increase while it shows the reverse effects on the temperature profile of the blood flow.

3. The velocity of the blood flow decreases as values of the hematocrit parameter increase. This happens due to increased density of the red blood cell inside the artery which in result slows down the flow.

4. Heat source parameter brings out an effective change in the temperature profile of the blood flow. The temperature profile of the blood flow increases as values of the

heat source parameter increase. This result is very much useful in the therapeutic procedure of hyperthermia, particularly in understanding/regulating the blood flow.

5. The shear stress at the wall of the stenosis increases as values of the hematocrit parameter increase. The flow rate of the blood flow increases as values of the inclination angle made by the artery increase.

Chapter 3

Effect of Variable Viscosity on MHD Inclined Arterial Blood Flow with Chemical Reaction

3.1 Introduction

In the circulatory system of our body, blood delivers all important substances like nutrients and oxygen from one body cell to the other body cells through arteries and veins. Arteries play an important role in the transportation of highly oxygenated blood, which drives blood from the heart to the other body parts. Systematic circulation of the blood throughout the body help to stabilize the temperature and pH scale, by providing the nourishment to the body. Extra deposition of fat inside the artery, constricts the arterial wall and directly affects the work function of the artery. The accumulation of substances in an artery is known as stenosis which changes hemodynamic conditions and flow pattern that was existing in the artery, early to catheterization (Ellahi et al., 2014c; Rabby et al., 2013; Srivastava and Saxena, 1997). Today's industrialized world blood flow in our body through arteries pose serious health risks. It is believed that one of the most widespread diseases in humans is atherosclerosis which takes place when hard plaque builds up inside the artery (Pasceri and Yeh, 1999). The presence of hard plaque limiting the flow of blood inside the artery and provides cells of blood to make blood clots near the hardened plaque.

Clots make the artery even more blocked and at that time it is increasingly difficult for oxygenated rich blood to reach the heart muscle because of the narrowing of the artery. This larger scale of coronary artery blockage causes heart attacks in the human body (Falk et al., 1995). This type of biological system related problems we deal in "Biomechanics", Which is about to study the function and structure of the living body with the help of mechanics (Fung and Cowin, 1994). Since it is directly related to the health of a human body, nowadays this has gained serious attention from researchers, physiologists, and clinical persons to study the arterial blood flow. In this field Ellahi et al. (2014b) in their paper mathematically explained a model of arterial blood flow with Composite Stenosis. Further, in this work Pralhad and Schultz (2004) presented a model for arterial stenosis and gave an idea about its application to blood diseases.

In the human body, one-milliliter blood contains about $5 * 10^{11}$ cells. Most of the cells in blood are red cells as these make up about 45% of the blood volume in the average man. Red blood cells are also known as erythrocytes. Erythrocytes are rich in hemoglobin which is an iron-containing biomolecule. Since erythrocytes have iron oxides molecules in its content, an applied magnetic field can influence the motion of the blood flow. So in the presence of a magnetic field, red blood cell shows characteristics of diamagnetic fluid when it is allocated in arteries (Baldwin and Wilson, 1994). A field in which we study the effects of applied magnetic field on biological fluids is known as biomagnetic fluid dynamics (BFD) and today it has numerous proposed applications in bioengineering and medical sciences. Magnetohydrodynamics (MHD) differs from BFD in the sense that it deals with electrically conducting fluids, and in the magnetic field, flow affects by the magnetization of the fluid (Haik et al., 1999). In order to investigate the effects of magnetic field on blood flow, Tzirtzilakis proposed a mathematical model for Newtonian blood flow under the action of applied magnetic field (Tzirtzilakis, 2005). Further, in the same direction, Misra and Sinha (2013) presented a model to study the effects of thermal radiation on MHD blood flow by using similarity transformation and boundary layer approximation. Srivastava (2014a) analytically investigated the effect of an inclined magnetic field on blood flow through an inclined porous artery with mild stenosis. In the presence of a magnetic field and with the case of double stenosis Misra et al. (2011b) proposed a model

of blood flow in a porous vessel.

The porosity of medium is a major characteristic of the artery in order to analyze the effects of different physical parameters on blood flow. In this direction Khaled and Vafai (2003) proposed a model for heat transfer, in furtherance of defining the role of porosity in biological tissues. Akbarzadeh (2016) numerically simulated a non-Newtonian model for MHD blood flows which flows through a porous blood vessel. Eldesoky (2014) concerned with a study of the unsteady MHD pulsatile flow of blood through a porous medium in a stenotic channel with slip at permeable walls. He reported that in porous medium velocity of blood flow decreases as magnetic field parameter and depth of the stenosis increases. Considering nanoparticles in the blood which is flowing through a porous vessel, Rahbari et al. (2017) explained the mathematical model of heat transfer in the presence of a magnetic field. However, none of these research considered the effects of variable viscosity as they assumed in their research viscosity as constant viscosity.

In blood, the fraction of packed cell volume differs from point to point. So In a real physiological system, the functional dependence of the blood viscosity is not constant it may vary either with hematocrit ratio or depends upon temperature and pressure (Shit and Majee, 2015). In this regard, taking functional dependence of blood viscosity on hematocrit Layek et al. (2009) analyzed the model of unsteady viscous flow in a vascular tube with an overlapping constriction and examined that as the value of hematocrit parameter increases viscosity increases respectively. Further, Sinha and Misra (2014) investigated the effects of variable viscosity and variable hematocrit on an MHD flow of blood through a dually stenosed artery. Makinde and Onyejekwe (2011) proposed a model of MHD generalized Couette flow and heat transfer with temperature dependent viscosity and reported that increasing the viscosity exponent, increases the viscous forces and slow down the fluid motion.

Recently, the study of the heat source and chemical reactions on blood has become quite interesting because of the quantitative prediction of blood rate. Heat generations are of great importance for diagnosing blood circulation illness and for the noninvasive measurement of blood glucose. In order to analyze the effects of the heat source and chemical reaction parameters on blood flowing artery Mekheimer et al. (2012) presented

a paper which investigates the influence of heat and chemical reaction parameters on blood flow through a tapered artery which is having overlapped stenosis. In the same direction, Noreen Sher Akbar (2012) studied the blood flow in a tapered artery with stenosis which shows the influence of heat and chemical reactions on a hyperbolic tangent fluid model. By treating blood as a second-grade fluid, Misra and Adhikary (2016) presented a model to study the effects of chemical reaction as well as heat and mass transfer of oscillatory MHD flow of blood.

However, the effects of both heat and mass transfer on MHD blood flow of having variable viscosity with chemical reaction have a little attention in the literature. Hence, the present article with the help of governing non-linear partial differential equations analyzes the combined effects of heat and mass transfer on Newtonian, steady, incompressible fluid flow. The analytical technique homotopy perturbation method has been used to obtain the solutions for the wall shear stress, velocity, temperature and concentration of the blood flow (Mohyud-Din and Noor, 2009). Their respective graphs have been plotted for different values of the physical parameters of the problem.

3.2 The Mathematical Model

Let us consider the two-dimensional flow of blood through a porous stenosed artery of length L, inclined at an angle γ from the vertical axis. The flow is assumed to be laminar, axially symmetric, incompressible, bio-magnetic. Blood is assumed as Newtonian fluid. Under the fully developed boundary conditions, the flow is subject to a uniform magnetic field applied perpendicular to the direction of the inclined artery as displayed in fig.3.1. The viscosity of the blood is assumed to vary in radial direction with a variable hematocrit of density ρ. The shape of the artery is assumed to cylindrical in which $\bar{u}$, $\bar{v}$ and $\bar{w}$ represent the velocity components in $\bar{r}$, $\bar{\theta}$ and $\bar{z}$ directions, respectively. Under these assumptions governing equations of the blood flow are as follows:

$$\rho\left[\bar{u}\frac{\partial\bar{u}}{\partial\bar{r}}+\bar{w}\frac{\partial\bar{u}}{\partial\bar{z}}\right]=-\frac{\partial\bar{P}}{\partial\bar{r}}+\frac{\partial}{\partial\bar{r}}\left[2\mu(\bar{r})\frac{\partial\bar{u}}{\partial\bar{r}}\right]+2\frac{\mu(\bar{r})}{\bar{r}}\left[\frac{\partial\bar{u}}{\partial\bar{r}}-\frac{\bar{u}}{\bar{r}}\right]+\frac{\partial}{\partial\bar{z}}\left[\mu(\bar{r})\left(\frac{\partial\bar{u}}{\partial\bar{z}}+\frac{\partial\bar{w}}{\partial\bar{r}}\right)\right], \tag{3.2.1}$$

$$\rho\left[\bar{u}\frac{\partial\bar{w}}{\partial\bar{r}}+\bar{w}\frac{\partial\bar{w}}{\partial\bar{z}}\right]=-\frac{\partial\bar{P}}{\partial\bar{z}}+\frac{\partial}{\partial\bar{z}}\left[2\mu(\bar{r})\frac{\partial\bar{w}}{\partial\bar{z}}\right]+\frac{1}{\bar{r}}\frac{\partial}{\partial\bar{r}}\left[\bar{r}\mu(\bar{r})\left(\frac{\partial\bar{u}}{\partial\bar{z}}+\frac{\partial\bar{w}}{\partial\bar{r}}\right)\right]-\sigma_1\bar{\mu_m}^2H_0^2\bar{w}$$
$$+\rho g\alpha\left(\bar{T}-\bar{T_0}\right)\cos\gamma+\rho g\alpha\left(\bar{C}-\bar{C_0}\right)\cos\gamma-\frac{\mu(\bar{r})}{k_1}\bar{w}, \tag{3.2.2}$$

$$\rho c_p\left[\bar{u}\frac{\partial\bar{T}}{\partial\bar{r}}+\bar{w}\frac{\partial\bar{T}}{\partial\bar{z}}\right]=\frac{k}{\bar{r}}\frac{\partial}{\partial\bar{r}}\left(\bar{r}\frac{\partial\bar{T}}{\partial\bar{r}}\right)+\mu(\bar{r})\left(\frac{\partial\bar{w}}{\partial\bar{r}}\right)^2, \tag{3.2.3}$$

$$\left(\bar{u}\frac{\partial}{\partial\bar{r}}+\bar{w}\frac{\partial}{\partial\bar{z}}\right)\bar{C}=D_f\left(\frac{\partial^2\bar{C}}{\partial^2\bar{r}}+\frac{1}{r}\frac{\partial\bar{C}}{\partial\bar{r}}+\frac{\partial^2\bar{C}}{\partial^2\bar{z}}\right)+\frac{D_fK_T}{T_m}\left(\frac{\partial^2\bar{T}}{\partial^2\bar{r}}+\frac{1}{r}\frac{\partial\bar{T}}{\partial\bar{r}}+\frac{\partial^2\bar{T}}{\partial^2\bar{z}}\right)$$
$$-L(\bar{C}-\bar{C_0}), \tag{3.2.4}$$

where $\bar{u}$, $\bar{v}$ and $\bar{w}$ are the respective velocity component in the radial and axial directions, c_p is specific heat at constant pressure, k is the thermal conductivity, σ_1 is the electrical conductivity, k_1 is the permeability, $\bar{p}$ is the pressure, $\bar{T}$ is the temperature, ρ is the density, $\mu(\bar{r})$ is the viscosity and H_0 is applied magnetic field, D_f is the coefficients of mass diffusivity, K_T is the thermal-diffusion ratio and L is the factor of chemical reaction parameter.

Variable viscosity $\mu(\bar{r})$ of the blood flow is defined as

$$\mu(\bar{r})=\mu_0(1+\lambda h(\bar{r})), \tag{3.2.5}$$

where

$$\hbar(\bar{r})=H\left[1-\left(\frac{\bar{r}}{d_0}\right)^m\right], \tag{3.2.6}$$

assume that $\lambda H=H_r$, H denotes the maximum hematocrit at the center of the artery, λ is a constant which has a numerical value 2.5, notation m determines the exact shape of the velocity profile and H_r is the hematocrit parameter (Sinha and Misra, 2014).

Geometry of the stenosis, located at point z with it's maximum height of δ is defined by the formula (Mekheimer and Kot, 2008)

$$h(\bar{z})=\begin{cases} d(\bar{z})[1-\eta(b^{n-1}(\bar{z}-a)-(\bar{z}-a)^n)] & \text{when} \quad a\le\bar{z}\le a+b,\\ d(\bar{z}), \quad \text{otherwise,}\end{cases} \tag{3.2.7}$$

where $d(\bar{z})$ is the radius of the tapered artery in stenotic region with

$$d(\bar{z})=d_0+\xi\bar{z}, \tag{3.2.8}$$

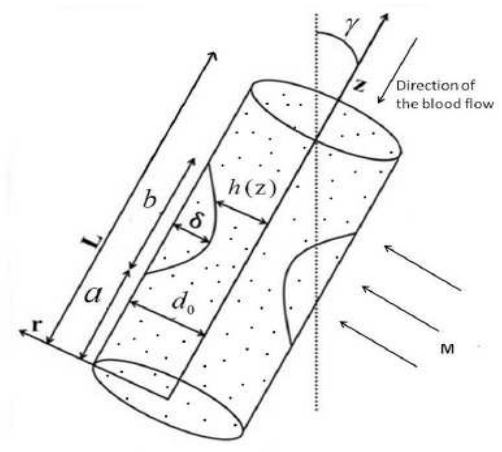

Figure 3.1: Geometry of the inclined artery with perpendicular applied magnetic field (M)

in which d_0 represents the radius of the non-tapered artery and ξ is the tapering parameter which defines by $\xi = \tan(\phi)$, where ϕ is known as the tapered angle. ϕ possess values just lower than zero ($\phi < 0$) for the case of converging tapered artery, for diverging tapered artery it takes the value greater than zero ($\phi > 0$) and the case of non- tapered artery ϕ has zero value.

In eq.(3.2.7) η is defined by

$$\eta = \frac{\delta^* n^{\frac{n}{n-1}}}{d_0 b^n (n-1)}, \tag{3.2.9}$$

where δ^* is the maximum height of the stenosis located at

$$\bar{z} = a + \frac{b}{n^{\frac{n}{n-1}}},$$

and n is the shape parameter which determines the shape of the constriction profile. Value $n = 2$ results the symmetrically shaped stenosis and non-symmetric stenosis occurs for $n \geq 2$ values.

Now the nondimensional parameters are as follows

$$\begin{cases} \bar{u} = \frac{uu_0\delta}{b}, \quad \bar{r} = rd_0, \quad \bar{z} = zb, \quad \bar{w} = wu_0, \quad \bar{h} = hd_0, \\ \bar{P} = \frac{u_0 b\mu_0 P}{{d_0}^2}, \quad Re = \frac{\rho b u_0}{\mu_0}, \quad \Theta = \frac{(\bar{T}-\bar{T}_0)}{\bar{T}_0}, \quad Pr = \frac{\mu c_p}{k}, \quad Ec = \frac{{u_0}^2}{c_p T_0}, \\ Z = \frac{k_1}{{d_0}^2}, \quad M^2 = \frac{\sigma {H_0}^2 {d_0}^2}{\mu_0} \quad Sr = \frac{\rho D k_T \bar{T}_0}{\mu_0 T_m \bar{C}_0}, \quad Sc = \frac{\mu}{D_p}, \\ \sigma = \frac{(\bar{C}-\bar{C}_0)}{\bar{C}_0}, \quad E = \frac{\rho {d_0}^2 L}{\mu}, \end{cases} \tag{3.2.10}$$

where Re is the Reynolds number, Ec is the Eckert number, Pr is the Prandtl number and Gr and Gm are the thermal and solutal Grashof number, Sc and Sr are Schmidt and Soret number, respectively and M, Q, Z, Hr, E are magnetic field, heat source, porosity, hematocrit and chemical reaction parameters, respectively.

Viscosity of the blood flow as given in eq.(3.2.5) can be written in non-dimensional form as

$$\mu(r) = \mu_0(1 + \lambda H(1 - r^m)). \tag{3.2.11}$$

In the case of mild stenosis $\left(\frac{\delta^*}{d_0} \ll 1\right)$ and by considering two other additional conditions (Mekheimer and Kot, 2008)

$$\frac{Re\delta^* n^{\frac{1}{n-1}}}{b} \ll 1, \tag{3.2.12}$$

and

$$\frac{d_0 n^{\frac{1}{n-1}}}{b} \sim O(1). \tag{3.2.13}$$

Now, the eq.(3.2.1) to eq.(3.2.4) change in given non dimensional form respectively as

$$\frac{\partial P}{\partial r} = 0, \tag{3.2.14}$$

$$\frac{\partial P}{\partial z} = \left[\frac{1}{r} + H_r\left(\frac{1}{r} - (m+1)r^{m-1}\right)\right]\frac{\partial w}{\partial r} + \left[1 + H_r(1 - r^m)\frac{\partial}{\partial r}\left(\frac{\partial w}{\partial r}\right)\right] + G_r\Theta\cos\gamma + G_m\sigma\cos\gamma - w\left[M^2 + \frac{1}{Z} + \frac{H_r}{Z}(1 - r^m)\right], \tag{3.2.15}$$

$$\frac{1}{r}\frac{\partial}{\partial r}\left[r\frac{\partial\Theta}{\partial r}\right] + EcPr\left[\frac{\partial w}{\partial r}\right]^2 = 0, \tag{3.2.16}$$

$$\frac{1}{Sc}\left[\frac{1}{r}\frac{\partial}{\partial r}\left(r\frac{\partial\sigma}{\partial r}\right)\right] + Sr\left[\frac{1}{r}\frac{\partial}{\partial r}\left(r\frac{\partial\Theta}{\partial r}\right)\right] - E\sigma = 0, \tag{3.2.17}$$

where $Br = EcPr$ known as the Brinkman number which is the ratio of viscous heat generation to external heating and E is the chemical reaction parameter.

The corresponding boundary conditions are as follows,

$$\frac{\partial w}{\partial r} = 0, \frac{\partial\Theta}{\partial r} = 0, \frac{\partial\sigma}{\partial r} = 0 \quad at \quad r = 0, \tag{3.2.18}$$

$$w = 0, \quad \Theta = 0, \quad \sigma = 0, \quad at \quad r = h(z), \tag{3.2.19}$$

where $h(z)$ is the geometry of the stenosis in non-dimensional form when radius of the artery is of unit length ($d_0 = 1$),

$$h(z) = \begin{cases} (1+\xi' z)[1-\eta_1((z-l_1)-(z-l_1)^n)] & when \qquad l_1 \le z \le l_1+1, \\ 1, \qquad otherwise, \end{cases} \tag{3.2.20}$$

where

$$\eta_1 = \frac{\delta n^{\frac{n}{n-1}}}{(n-1)}, \quad \delta = \frac{\delta^*}{d_0}, \quad l_1 = \frac{a}{b}, \quad \xi' = \frac{\xi b}{d_0}$$

.

3.3 Solution

Now, applying homotopy perturbation method(HPM) to solve non linear differential eqs.(3.2.14)-(3.2.17) under the given boundary conditions eqs.(3.2.18)-(3.2.19). In HPM , homotopies for velocity, temperature and concentration profiles are as follows

$$\begin{aligned} H(q,w) = {} & q\left[L(w) + H_r\left(\frac{1}{r} - (m+1)r^{m-1}\right)\frac{\partial w}{\partial r} + H_r(1-r^m)\frac{\partial}{\partial r}\left(\frac{\partial w}{\partial r}\right) - \frac{\partial p}{\partial z}\right] \\ & + (1-q)\left[L(w) - L(w_0)\right] - q\left[w\left(M^2 + \frac{1}{Z} + H_r\frac{(1-r^m)}{Z}\right)\right] \\ & + q\left[cos\gamma\left(G_r\Theta + G_m\sigma\right)\right], \end{aligned} \tag{3.3.1}$$

$$H(q,\Theta) = (1-q)\left[L(\Theta) - L(\Theta_0)\right] + q\left[L(\Theta) + EcPr\left(\frac{\partial w}{\partial r}\right)^2\right], \tag{3.3.2}$$

$$H(q,\sigma) = (1-q)\left[L(\sigma) - L(\sigma_0)\right] + q\left[L(\sigma) + ScSrL(\Theta) - ScE\sigma\right], \tag{3.3.3}$$

where L is the linear operator defined as

$$L(X) = \frac{1}{r}\left(\frac{\partial}{\partial r}\left(r\frac{\partial X}{\partial r}\right)\right). \tag{3.3.4}$$

The initial guesses which satisfy the corresponding boundary conditions eqs.(3.2.18)-(3.2.19) are given as,

$$w_{10} = \frac{(r^2-h^2)}{4}\left(M^2 + \frac{1}{Z}\right)\left(\frac{\partial p_0}{\partial z}\right), \tag{3.3.5}$$

$$\Theta_{10} = \frac{(r^2-h^2)}{4}, \tag{3.3.6}$$

$$\sigma_{10} = -\frac{(r^2 - h^2)}{4}. \tag{3.3.7}$$

Dependent variables can be decomposed in series form as follows:

$$w(r,q) = w_0 + qw_1 + q^2 w_2 + O(q^3), \tag{3.3.8}$$

$$\Theta(r,q) = \Theta_0 + q\Theta_1 + q^2\Theta_2 + O(q^3), \tag{3.3.9}$$

$$\sigma(r,q) = \sigma_0 + q\sigma_1 + q^2\sigma_2 + O(q^3). \tag{3.3.10}$$

Substituting the series expansion form of $w(r,q)$, $\Theta(r,q)$, $\sigma(r,q)$ from eqs.(3.3.8)-(3.3.10) in to eqs.(3.3.1)-(3.3.3) respectively, compare the coefficients of q^0, q^1 and q^2.

For eq.(3.3.1) coefficients of q^0, q^1 and q^2 are as follows,

$$q^0: \qquad L(w_0) - L(w_{10}) = 0 \quad \Rightarrow w_0 = w_{10} = \frac{\partial p_0}{\partial z}\frac{(r^2 - h^2)}{4}\left(M^2 + \frac{1}{Z}\right), \tag{3.3.11}$$

$$\begin{aligned} q^1: \qquad L\left(w_1\right) = &- L\left(w_0\right) + \frac{\partial p_0}{\partial z} - H_r\left(\frac{1}{r} - (m+1)\, r^{(m-1)}\right)\frac{\partial w_0}{\partial r} \\ &+ w_0\left(M^2 + \frac{1}{Z} + H_r\frac{(1-r^m)}{Z}\right) - cos\gamma(G_r\Theta_0 + G_m\sigma_0) \\ &- H_r\left(1 - r^m\right)\frac{\partial}{\partial r}\left(\frac{\partial w_0}{\partial r}\right), \end{aligned} \tag{3.3.12}$$

$$\begin{aligned} q^2: \qquad L(w_2) = &\frac{\partial p_1}{\partial z} - H_r(\frac{1}{r} - (m+1)r^{(m-1)})\frac{\partial w_1}{\partial r} - H_r(1-r^m)\frac{\partial}{\partial r}(\frac{\partial w_1}{\partial r}) \\ &+ w_1(M^2 + \frac{1}{Z} + H_r\frac{(1-r^m)}{Z}) - cos\gamma(G_r\Theta_1 + G_m\sigma_1). \end{aligned} \tag{3.3.13}$$

Similarly, for temperature eq.(3.3.2) coefficients of q^0, q^1 and q^2 are as follows,

$$q^0: \qquad L\left(\Theta_0\right) - L\left(\Theta_{10}\right) = 0 \quad \Rightarrow \Theta_0 = \Theta_{10} = \frac{(r^2 - h^2)}{4}, \tag{3.3.14}$$

$$q^1: \qquad L\left(\Theta_1\right) = -L\left(\Theta_0\right) - EcPr\left(\frac{\partial w_0}{\partial r}\right)^2, \tag{3.3.15}$$

$$q^2: \qquad L\left(\Theta_2\right) = -2EcPr\left(\frac{\partial w_0}{\partial r}\right)\left(\frac{\partial w_1}{\partial r}\right). \tag{3.3.16}$$

For eq.(3.3.3) coefficients of q^0, q^1 and q^2 are as follows,

$$q^0: \qquad L(\sigma_0) - L(\sigma_{10}) = 0 \quad \Rightarrow \sigma_0 = \sigma_{10} = -\frac{(r^2 - h^2)}{4}, \tag{3.3.17}$$

$$q^1 : \qquad L(\sigma_1) = -L(\sigma_0) - ScSrL(\Theta_0) + ScE\sigma_0, \tag{3.3.18}$$

$$q^2 : \qquad L(\sigma_2) = -ScSrL(\Theta_1) + ScE\sigma_1. \tag{3.3.19}$$

Now, with the help of the values w_0, Θ_0, σ_0 from eqs.(3.3.5)-(3.3.7) and by using definition of linear operator for $L(w_0)$,$L(\Theta_0)$, $L(\sigma_0)$ in to eqs.(3.3.12), (3.3.15) and (3.3.18), attain the expressions for w_1,Θ_1 and σ_1 as follows

$$\begin{aligned} w_1 =& \frac{(r^2-h^2)}{4}\left(\frac{\partial p_0}{\partial z}\right)\left(1-(M^2+\frac{1}{Z})\right) - \frac{cos\gamma}{64}\left(r^4+3h^4-4r^2h^2\right)(G_r-G_m) \\ &+ \frac{H_r}{4Z}\left(\frac{\partial p_0}{\partial z}\right)\left(M^2+\frac{1}{Z}\right)\left(\frac{r^4+3h^4}{16}+\frac{(h^{m+4}-r^{m+4})}{(m+4)^2}+\frac{h^2r^{m+2}-h^{m+4}}{(m+2)^2}\right) \\ &- \frac{H_r}{4Z}\left(\frac{\partial p_0}{\partial z}\right)\left(M^2+\frac{1}{Z}\right)\left(\frac{r^2h^2}{4}\right)+\left(\frac{\partial p_0}{\partial z}\right)\left(M^2+\frac{1}{Z}\right)^2\left(\frac{r^4}{16}+\frac{3h^4}{16}-\frac{h^2r^2}{4}\right) \\ &- \frac{H_r}{2}\left(\frac{r^2-h^2}{2}+\frac{h^{m+2}-r^{m+2}}{m+2}\right)\left(\frac{\partial p_0}{\partial z}\right)\left(M^2+\frac{1}{Z}\right), \end{aligned} \tag{3.3.20}$$

$$\Theta_1 = -\frac{(r^2-h^2)}{4} - EcPr\frac{(r^4-h^4)}{64}P^2U^2, \tag{3.3.21}$$

$$\sigma_1 = (1-ScSr)\frac{(r^2-h^2)}{4} + ScE\left(\frac{r^4}{64}+\frac{3h^4}{64}-\frac{r^2h^2}{16}\right). \tag{3.3.22}$$

After getting the expressions for w_1, θ_1 and σ_1 and by following the same steps we further calculate the values of w_2, Θ_2 and σ_2 with the help of MATLAB-2015b. We get Final expressions for velocity, temperature and concentration profiles of the blood flow by putting the values of all the calculated variables in eqs.(3.3.8)-(3.3.10) respectively.

3.4 Results and Discussion

The motivation behind the research is to analyze the effects of heat and mass transfer on blood flow through the inclined stenosed artery under the influence of an applied magnetic field with a chemical reaction.

List of all the parameters used to graphically analyze the validity of the mathematical model are given in Table.3.1, where the value of the height of the stenosis (δ) is considered 0.1 for the case of mild stenosis.

Considering the case of mild stenosis fig.3.2 provides a comparison between the present study and those reported in Misra and Shit (2007) and in Misra and Kar (1988)

for the Newtonian fluid model of the blood flow. From the figure, it is clear that the present result shows a good agreement with those published results.

Parameters	Values (Unitfree)	Source
Height of the stenosis (δ)	0.1	Srivastava (2014a), Shukla et al. (1980)
Inclination angle of the artery (γ)	$\frac{\pi}{6}$	Sanyal et al. (2007), Ramesh (2016)
Porosity parameter (Z)	0.3	Bhatti and Abbas (2016)
Chemical reaction Parameter (E)	1	Misra and Adhikary (2016)
Shape parameter for symmetric case(n)	2	Mekheimer and Kot (2008)
Grashof Number (G_r)	2	Rao et al. (2012)
Modified Grashof Number (G_m)	3	Rao et al. (2012)
Brinkaman number (Br)	2	Zaman et al. (2016a)
Hematocrit parameter (H_r)	1	Thompson et al. (2016)
Magnetic field parameter (M)	1.5	Swartz et al. (2009)
Schmidt number (Sc)	1	Zaman et al. (2016a)
Soret number (Sr)	0.5	Zaman et al. (2016a)
Ratio of $\frac{a}{b}$ (l_1)	0	Nadeem et al. (2011)
Location of the maximum height of the stenosis	0.5	Nadeem et al. (2011)

Table 3.1: Values of the parametrs

All the graphs are plotted for the range of 0 to 0.9 by assuming non-stretching stenotic wall of the artery (as the value of the height of the stenosis for mild stenosis case is assumed as 0.1). All the figures have been plotted by using the parameters values

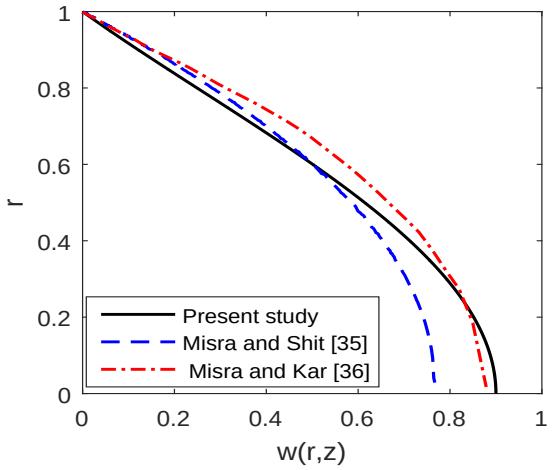

Figure 3.2: Comparision result of variation of velocity profile for Newtonian model of blood flow

as given in Table.3.1. Fig.3.3 and fig.3.4 display the radial variation of velocity and temperature profiles for different values of the inclination angle (γ) made by the non-tapered artery from the vertical axis. The magnitude of the applied magnetic field is assumed to be the same for each and every inclined position of the artery. It can be clearly observed from the fig.3.3 that as the values of the inclination angle of the artery increase, the velocity profile of the blood flow decreases, respectively. It can be clearly seen from the figure that the pattern of all velocity profiles for different inclination angles are similar in the sense that they show the decrease in their maxima as one moves away from the center of the artery and finally fall to zero at the stenotic wall. From fig.3.4 it is clear that as the value of the inclination angle of the artery increases from 0 to $\frac{\pi}{3}$, the temperature profile of the blood flow also increases.

To analyze the magnetic effects on blood flow with variable viscosity through an inclined porous artery, a magnetic field is applied perpendicular to the direction of the inclined artery, which is assumed to be inclined at an angle $\frac{\pi}{6}$ from the vertical axis. Fig.3.5 illustrates the radial distribution of the velocity profile of the blood flow for different values of magnetic field parameter (M). One can notice the half-flattened parabolic velocity profile from the figure, which decreases as the values of the applied magnetic field increases. It happens because, blood contains magnetic iron oxide particles in its content

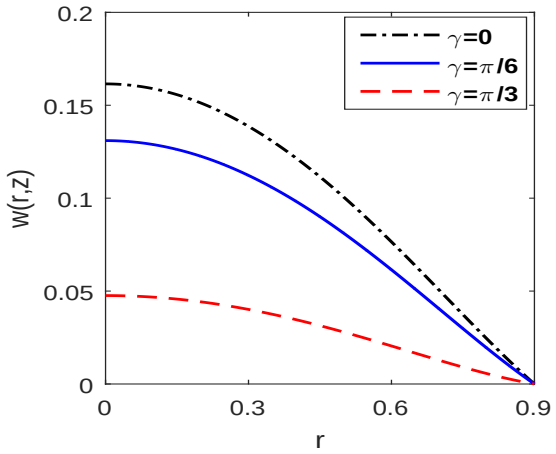

Figure 3.3: Velocity profile for different values of γ

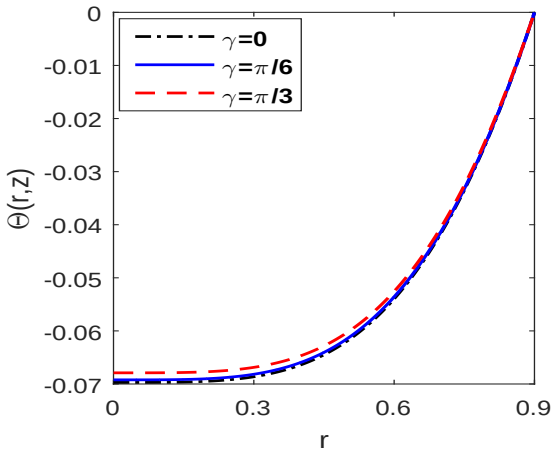

Figure 3.4: Temperature profile for different values of γ

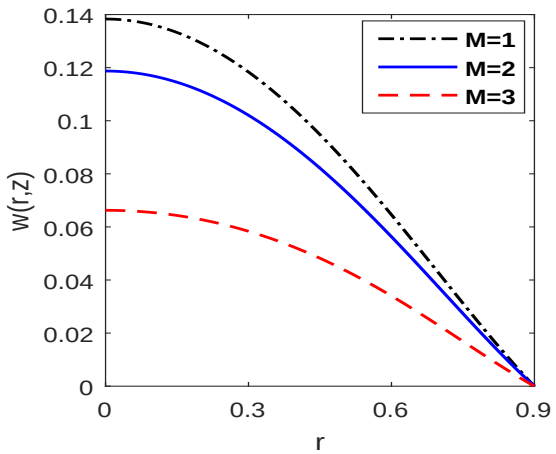

Figure 3.5: Velocity profile for different values of M

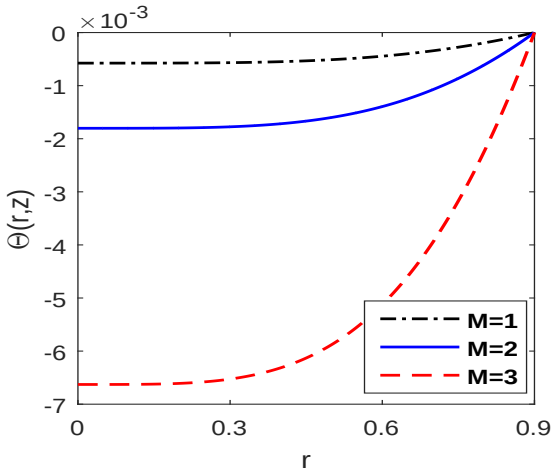

Figure 3.6: Temperature profile for different values of M

and when blood flows under the action of the applied magnetic field, it feels a strong electromotive force. This effect of magnetization causes a rotational motion of charged particles and magnetic particles of the blood. This type of orientation in blood, form red blood cells and magnetic particles more suspended in the blood plasma and increase the value of blood viscosity and that directly affects the velocity of the blood flow. So as the value of applied magnetic field parameter increases, Lorentz force which stabilizes between moving magnetic particles and applied magnetic field opposes the motion of

the blood flow and causes reduced velocity profile of the blood flow. The result for the velocity profile agrees well with the result reported by Sharma et al. (2015b). The effect of magnetic field parameter (M) on temperature profile is displayed in fig.3.6. It is noticed from the figure that temperature profile of blood flow in an inclined artery decreases as the values of the applied magnetic field which works just perpendicular to the stenosed artery, increase. Fig.3.7 displays the effects on the concentration profile of the blood flow as the intensity of the applied magnetic field varies. From figure it is clear that the concentration profile of the blood flow under variable viscosity effect, decreases as value of the applied magnetic field increases from 1 to 3 and for a particular value of magnetic field parameter concentration of the blood in the inclined porous artery decreases from the center towards the arterial wall and falls to zero at stenosis wall.

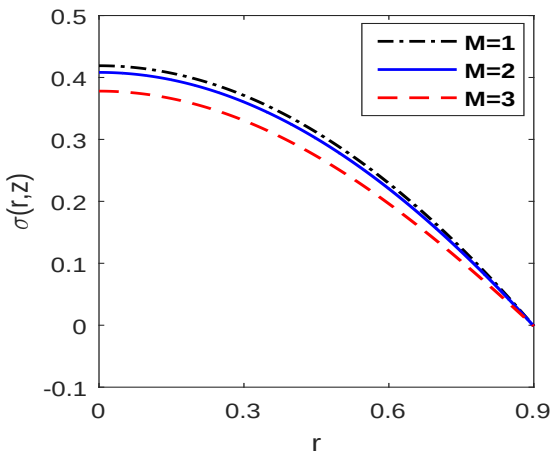

Figure 3.7: Concentration profile for different values of M

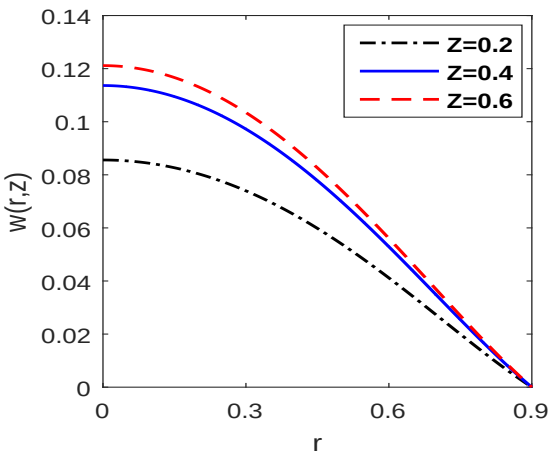

Figure 3.8: Velocity profile for different values of Z

Variations of velocity, temperature and concentration profiles of the blood flow for different values of porosity parameter (Z) have been analyzed with the help of the figs.3.8, 3.9 and 3.10, respectively. Fig.3.8 illustrates that as values of the porosity parameter increase, velocity profile of the blood flow is also increases. It describes that for a particular value of porosity parameter velocity attains its maximum value at the middle of the artery and gradually it starts decreasing towards the arterial wall. Velocity profile with porosity parameter shows this behavior may be because, when a fraction of the voids volume over

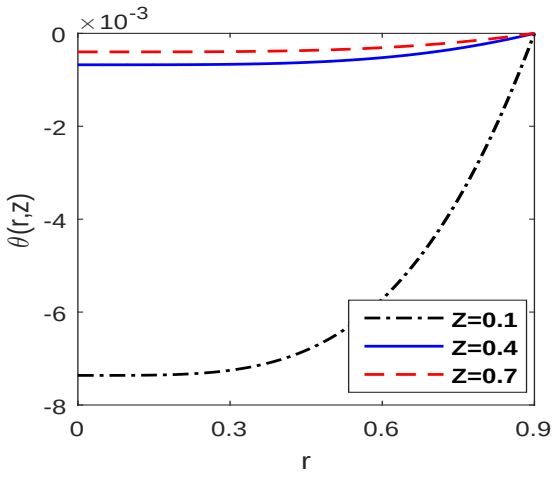

Figure 3.9: Temperature profile for different values of Z

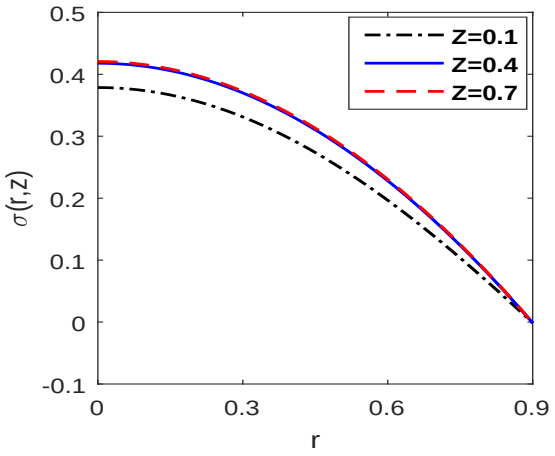

Figure 3.10: Concentration profile for different values of Z

the total volume increases, it can be more possible for fluid particles to move from one place to another place in the artery. Similarly, fig.3.9 and fig.3.10 mark that the temperature and concentration profiles of the blood flow in the stenosed artery also increase as the values of porosity parameter increase.

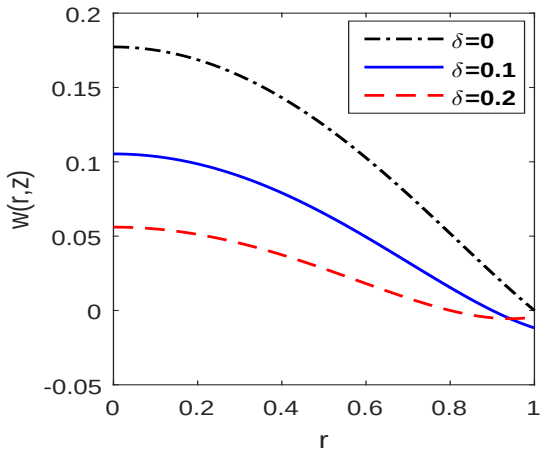

Figure 3.11: Velocity profile for different values of δ

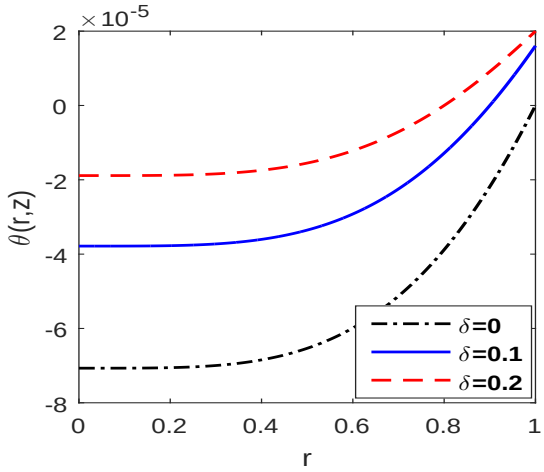

Figure 3.12: Temperature profile for different values of δ

Fig.3.11 depicts the distribution of the velocity profile of the blood flow with different sizes of the stenosis (δ). It is clear from the figure that the velocity profile of the blood flow decreases as stenosis presence in the artery increases in size. It may also be noted

that the velocity profile decreases the onset of the stenosis towards the stenosis throat. This result is in good agreement with those reported by Misra and Shit (2007). Fig.3.12 displays the effects of the height of the stenosis (δ) on the variations of the temperature profile of the blood flow. It shows that the temperature profile of the blood flow increases as the values of the height of the stenosis increase from 0 to 0.2. The first case where $\delta = 0$ is considered to analyze the distribution of velocity and temperature profiles of the blood flow in the stenosed free artery.

Fig.3.13 and fig.3.14 give the variation of concentration profiles of the blood flow with r for different values of the Schmidt number (Sc) and Soret number (Sr), respectively. Under the influence of chemical reaction, the value of concentration profiles of the blood flow reduces as the effects of both Schmidt and Soret number increase in the stenosed artery. Similar behavior of concentration profile with changing values of Schmidt number (Sc) has been observed by Kandasamy et al. (2005).

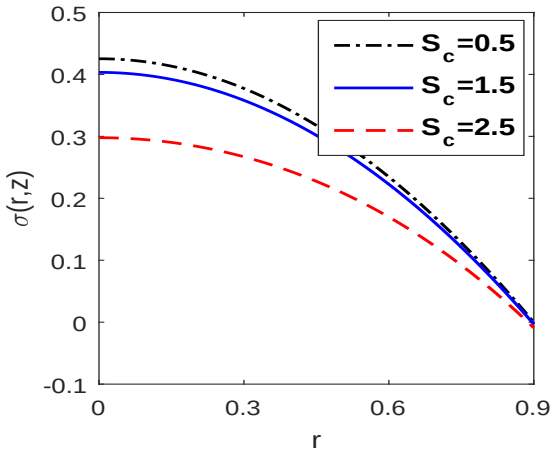

Figure 3.13: Variation of concentration profile for different values of Sc

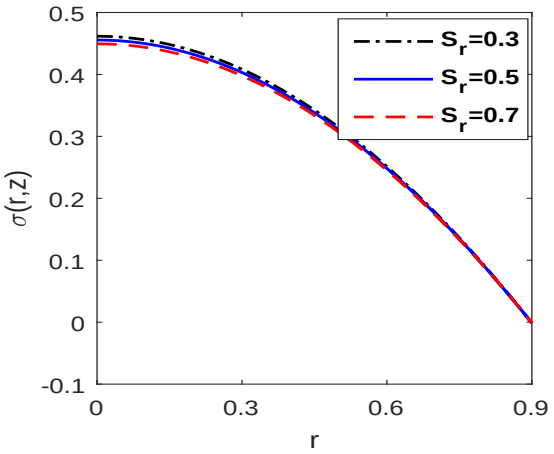

Figure 3.14: Variation of concentration profile for different values of Sr

Expression for the Shear Stress

Shear stress in arteries defines by the force per unit area on the arterial wall and it can be calculated as follows (Nadeem et al. (2011))

$$\tilde{S_{rz}} = -\left(\frac{\partial w}{\partial r}\right), \tag{3.4.1}$$

expression for wall shear stress is

$$\tilde{S_{rz}} = -\left[\frac{\partial w}{\partial r}\right]_{r=h}. \tag{3.4.2}$$

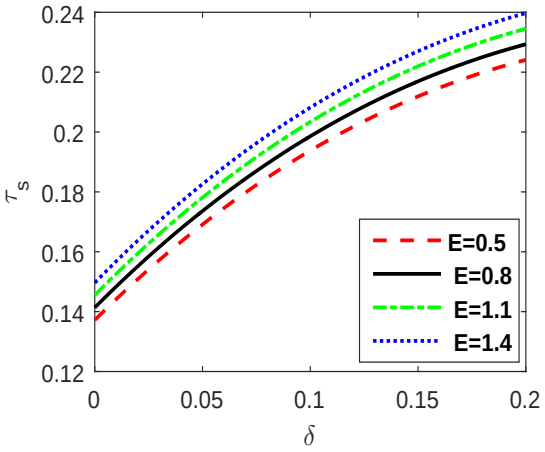

Figure 3.15: Variation of shear stress at stenosis throat for different values of E

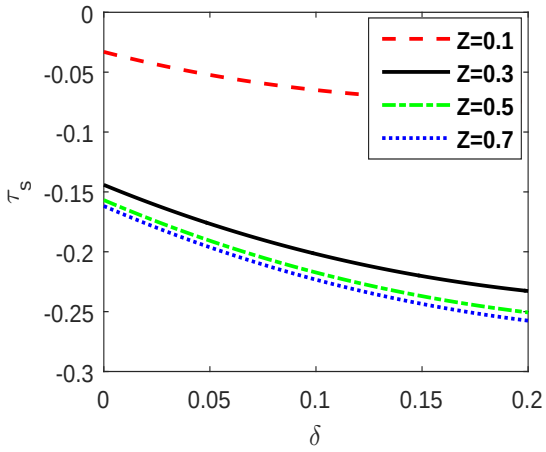

Figure 3.16: Variation of shear stress at stenosis throat for different values of Z

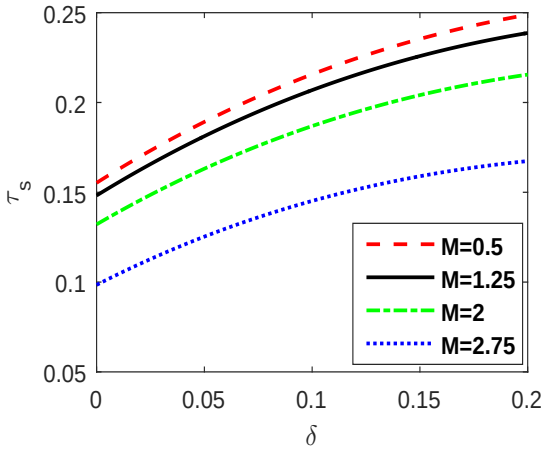

Figure 3.17: Variation of shear stress at stenosis throat for different values of M

Expression for shearing stress at the maximum height of the stenosis i.e. shear stress at stenosis throat located at $z = \frac{a}{b} + \frac{1}{n^{\frac{n}{n-1}}}$, can be defined as

$$\tilde{\tau_s} = -\left[\tilde{S_{rz}}\right]_{h=(1-\delta)}. \tag{3.4.3}$$

Fig.3.15 displays the variation of shear stress profile at stenosis throat for different values of chemical reaction (E) parameter. From the figure, it is clear that as the values of the chemical reaction parameter increase, shear stress at stenosis throat of the artery also increases. Further for different values of the porosity and magnetic field parameters fig.3.16 and fig.3.17 show the variations of shear stress profile at the stenosis throat of an inclined porous artery. It can be clearly observed from these figures that as values of the porosity parameter increase, shear stress profile at stenosis throat decreases and it also decreases with the increased value of the magnetic field parameter.

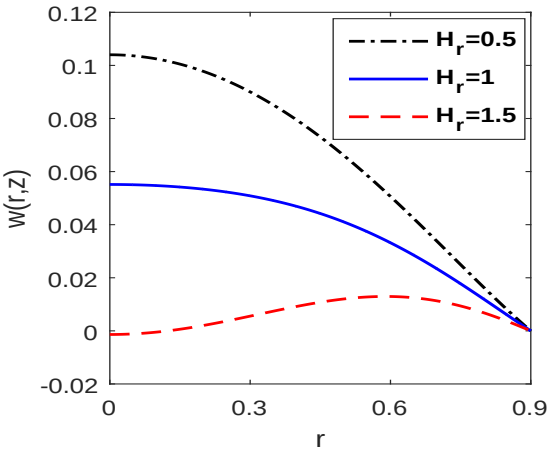

Figure 3.18: Radial distribution of velocity profile for different values of H_r

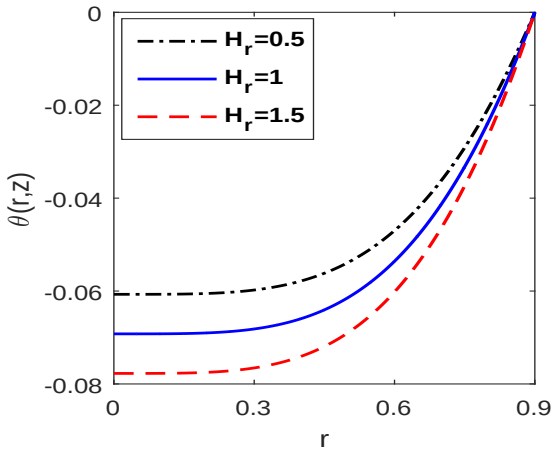

Figure 3.19: Radial distribution of temperature profile for different values of (H_r)

Fig.3.18 and fig.3.19 are prepared to analyze the effect of hematocrit parameter (H_r) on velocity and temperature profiles of the blood flow in an inclined porous artery. Fig.3.18 shows that as the values of hematocrit parameter increase, the velocity profile decreases receptively. From eq.(3.2.11) it is clear that the hematocrit ratio of the blood directly affects the viscosity of the blood flow. So, as the number of red blood cell present in the blood volume increases, it will be relatively difficult for blood particles to move from one place to another place because of the higher viscosity and this results in the decreased value of the velocity profile of the blood flow. Fig.3.19 illustrates that as the values of hematocrit parameter increase from 0.5 to 1.5, the temperature profile of the blood flow decreases, respectively.

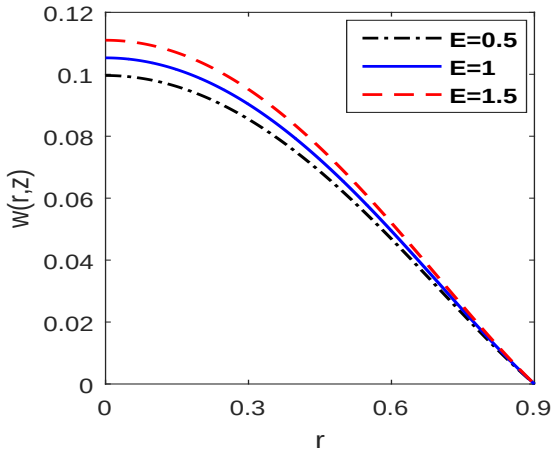

Figure 3.20: Radial variation of velocity profile for different values of E

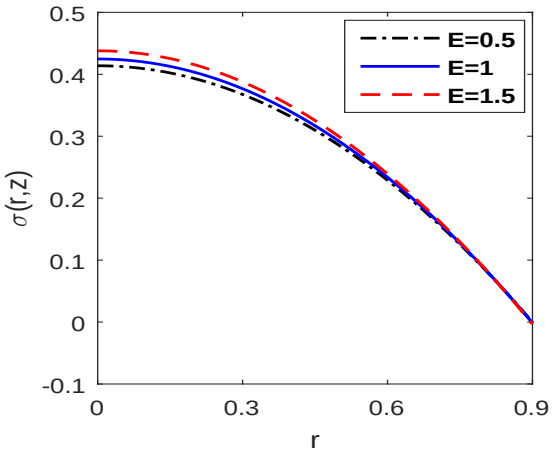

Figure 3.21: Radial distribution of concentration profile for different values of E

Fig.3.20 and fig.3.21 focus on variation of velocity and concentration profiles distribution for different values of chemical reaction parameter (E). From fig.3.20, it can be clearly observed that as values of the chemical reaction parameter increases, velocity profile also increases. Fig.3.21 indicates that as the values of chemical reaction parameter increase, the concentration profile of the MHD blood flow in an inclined porous artery increases. Further, those figures reveal that for a fixed value of chemical reaction parameter, both the velocity and concentration profiles decrease as we move gradually from the middle of the artery towards the stenosed arterial wall.

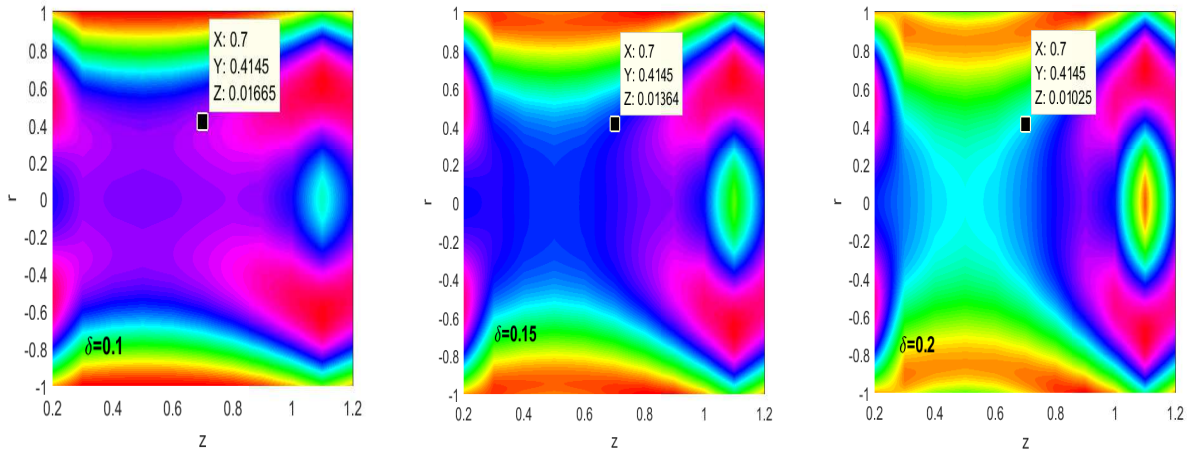

Figure 3.22: Velocity contour plots for different values of height of the stenosis (δ)

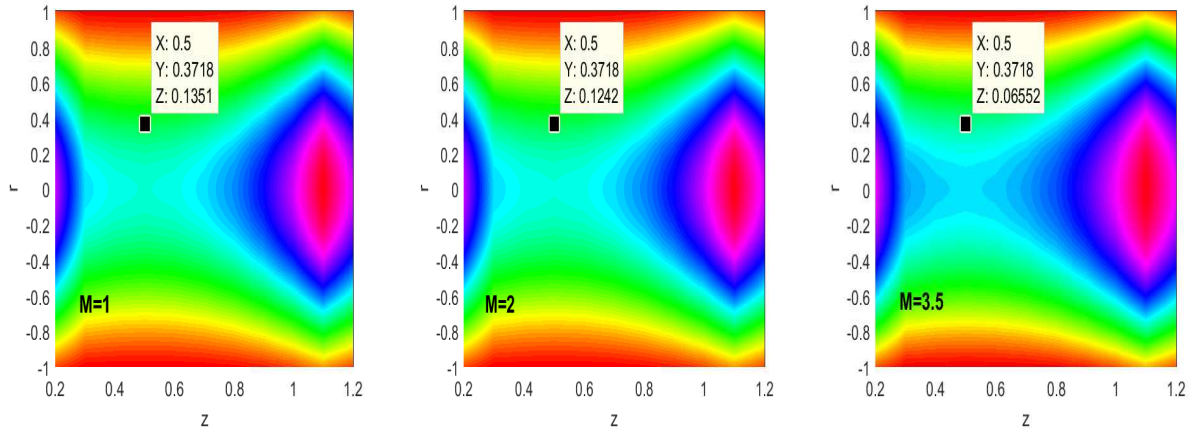

Figure 3.23: Velocity contour plots for different values of magnetic field parameter (M)

Fig.3.22 and fig.3.23 are prepared by using the values of physical parameters as given in Table.(3.1), to display the contour plots for the variation of the velocity profile of the blood flow for different values of the height of the stenosis (δ) and magnetic field parameter. In these figures X, Y, Z display the scale of the axial distance, radial distance and velocity at that point respectively. Contours are plotted for stenosis region $z = 0.2$ to $z = 1.2$, in which maximum height of stenosis is located at $z = 0.7$. So as the height of the stenosis (δ) increases, size of the trapped bolus also increases and slowly it slows down the flow of blood at the maximum height of the stenosis. In fig.3.23 as the effect of magnetic field parameter increases, trapped bolus also increases in size which gradually reduces the velocity of the blood flow. As it cleared that at point $(0.5, 0.3718)$ value of the velocity reduces from 0.1351 to 0.06552 as the influence of the magnetic field increases from 1 to 3.5.

3.5 Conclusions

In this investigation, the effects of chemical reaction with heat and mass transfer have been analyzed on blood flow of having variable viscosity through an inclined artery under the influence of the applied magnetic field. Governing nonlinear differential equations have been solved by using homotopy perturbation method under the given boundary conditions. Effects of the physical parameters used in the problem as chemical reaction

parameter (E), porosity parameter(Z), Schmidt number (Sc), Soret number(Sr), thermal Grashof number(G_r), solutal Grashof number (G_m), hematocrit parameter (H_r) on velocity, temperature and concentration profiles have been sketched graphically. Some effective findings of the article are elaborated below

1. Blood Velocity in the inclined artery increases as we increase the effects of porosity and chemical reaction parameters while it decreases when values of the magnetic field and hematocrit parameters increase. This type of controlled behavior of the velocity profile under the effects of the applied magnetic field can help medical persons during their surgical procedure.

2. As the value of the inclination angle of the artery from the vertical axis increases, the velocity of blood flow decreases while the temperature of the artery increases.

3. Height of the stenosis affects the velocity and temperature profiles of the blood flow in the inclined artery in the sense that as the size of the stenotic region increases both velocity and temperature profiles of the MHD blood flow decrease.

4. Concentration profile enhances as the magnitude of magnetic field parameter increases while it reduces with the increased value of the porosity parameter.

Chapter 4

MHD Pulsatile Two-Phase Blood Flow through a Stenosed Artery with Heat and Mass Transfer

4.1 Introduction

To estimate the hemodynamic resistance and analyze the heat and mass transfer process in arterioles and venules a quantitative comprehension of the blood flow is necessary. A major characteristic of the blood depends upon the hematocrit level as it is the percentage of whole blood occupies by the red blood cells(RBC) (Medvedev and Fomin, 2011). In the artery, the hematocrit level of the blood flow depends upon the diameter of the artery, and this relationship has important implications for physiological phenomena related to blood flow. Fåhræus effect explains this relationship which states that as the value of arterial diameter decreases, hematocrit level present in the artery also decreases. Due to the Fåhræus effect in arteries having the diameter less than 500 μm, erythrocytes move towards the center of the artery and thus forming the cell depleted plasma layer near the wall (Barbee and Cokelet, 1971; Fahraeus and Lindqvist, 1931). In smaller arteries, due to the higher concentration of red blood cell near the center and existence of cell-free plasma layer near the arterial wall, blood flow is considered as two-phase fluid flow (Verma, 2014).

Cokelet and Goldsmith (1991) through *In vitro* analysis have documented the phenomenon in more fully tube of 172-μm diameter and found that the two-phase flow of a suspension may lead to a decrease in hydrodynamic resistance. They suggested that in vertical tubes at very low shear stress, decreased hydrodynamic resistance depends upon the aggregation of red blood cells and the magnitude of this effect increases as the degree of the aggregation cells increases. They also identified that in the core region with the effect of gravity hydrodynamic resistance is greater in upward than the downward flowing suspension. The importance of the two-phase flow come to light with decreasing size of the vessel, however, for single phase flow, the flow characteristic is independent of the vessel size. Sharan and Popel (2001) presented a two-phase model of blood flow in narrow arteries assuming different viscosity of the core region than the cell depleted plasma region. Through their work, they found that due to the dissipation of energy the effective viscosity of the plasma region in a tube of fixed diameter increases as the level of the hematocrit increases.

Cardiovascular system transports nutrients and waste product from one body part to other. To supply proper oxygen-rich blood to all the tissues through arteries an adequate blood circulation is necessary (Ku, 1997). Any type of intrusion of fat into the arterial wall, block the way of blood flow. Hard plaque formation in the artery is known as stenosis which causes a well-known disease in the human body named as atherosclerosis (Alexopoulos et al., 2014), a major cause of heart attacks. To analyze the two-phase blood flow behavior under these hemodynamical disturbances, Ponalagusamy (2016) stabilized the two-fluid model for blood flow through a tapered stenotic artery considering core region as couple stress fluid and a peripheral region of plasma as a Newtonian fluid. The author reported that wall shear stress is high in the case of converging tapered stenosis and it is low in the case of non-tapered diverging stenosis. Further, for the case of symmetric and axisymmetric stenosis, Sankar (2011) proposed a mathematical model for two-phase blood flow and investigated that presence of cell-depleted peripheral layer near the wall helps in the functioning of the diseased arterial system. Many authors explored the two-phase blood flow modeling of the stenosed artery considering the extra effect of the magnetic field. In the artery to recognize the existence of the atherosclerosis disease,

the presence of which alters the velocity field a non-invasive technique based on MRI devices is used (Cavalcanti, 1995). The MRI device uses the strong magnetic field to work and when performs over the particular area of our body it affects the velocity field of that area. Now, it has gained serious attention by researches to study the blood flow through the stenosed artery under the influence of the applied magnetic field.

Magnetohydrodynamics (MHD) is about to study the motion of highly conducting fluid under the influence of the magnetic field. Blood is an electrically conducting fluid because the erythrocytes contain iron oxide molecules in its content. When magnetic field applies on blood flow, it induces electric as well as magnetic fields, interactions of which generates a mechanical force on the body known as Lorentz force (Mekheimer, 2008; Mekheimer and El Kot, 2008; Shit et al., 2014). Many researchers have been shown the effects of magnetization on the arterial vessel by considering the two-phase fluid model of the blood flow. Ponalagusamy and Selvi (2015) examined the effect of magnetic field on the two-phase model of oscillatory blood flow assuming both core and plasma regions as a Newtonian fluid in the presence of an arterial stenosis. They solved the model for both core and plasma regions separately using boundary conditions at the arterial wall as well as for interface region. The authors reported that as the value of the magnetic field increases, the flow resistance of the blood flow in the stenosed artery also increases. Further, Ponalagusamy and Priyadharshini (2018) examined the effect of magnetic field on two-phase blood flow through a tapered stenosed artery, assuming micropolar fluid in the core region and Newtonian fluid in the plasma region. A mathematical model presented by Mirza et al. (2016) analyzes the effect of magnetic field on a transient laminar electromagnetic-hydrodynamic two-phase blood flow using the continuum approach. Solving the model analytically they displayed the effect of the magnetic field for both blood velocity and particles velocity separately and concluded that as the effects of the magnetic field increases, both blood and particles velocities decrease for electromagnetic-hydrodynamic two-phase blood flow.

Above mentioned studies were focused on analyzing momentum and heat transfer phenomenon for two-phase models of blood flow with the horizontal artery. To show the effect of total movement of the mass from one place to the other place in the two-

phase model of blood flow, our study includes mass transfer as an important part of the investigation, which has not been done earlier. The present article analyzes the effects of radiation, chemical reaction and the external applied the magnetic field on the two-phase model of blood flow considering mild stenosis in the artery. The exact solutions for the velocity, temperature and concentration profiles have been calculated for both core and plasma regions and graphs have been plotted against the radial distance for different values of parameters used in the problem. With the aim of having adequate insight into the two-phase flow behavior of blood flow through a stenosed arterial segment flow resistance, total flow rate and wall shear stress have been estimated and graphs have been plotted with varying values of the applied magnetic field parameter, the ratio of the viscosity parameter and radiation parameter. A comparative study has been done with experimental data to show the effectiveness of the two-phase model of blood flow and observed that the two-phase model fits more appropriately with the experimental data as compared to single phase model.

4.2 The Mathematical Model

Consider the continuum model of unsteady, incompressible, pulsatile two-phase blood flow through a vertically stenosed coronary artery of length L in the presence of applied magnetic field M as shown in fig.4.1. In the cylindrical artery of radius r, the two-phase model of blood flow consists of a core region of radius r_c which contains erythrocytes (a suspension of the uniform hematocrit of viscosity $\bar{\mu_c}$) and a plasma region of radius r_p having the cell-depleted plasma layer with viscosity $\bar{\mu_p}$. Therefore, viscosities of the fluid for core and plasma regions are given by

$$\bar{\mu}(\bar{r}) = \begin{cases} \bar{\mu_c} & \text{for} \quad 0 \leq r \leq r_c(\bar{z}), \\ \bar{\mu_p} & \text{for} \quad r_c(\bar{z}) \leq r_p(\bar{z}). \end{cases}$$

Note that the artery is assumed to be of cylindrical shape with $(\bar{u_c}, \bar{v_c}, \bar{w_c})$ as the velocity vector for core region and $(\bar{u_p}, \bar{v_p}, \bar{w_p})$ as the velocity vector for plasma region along $(\bar{r}, \bar{\theta}, \bar{z})$ direction in the cylindrical coordinates. Shear stresses are considered high enough so that the fluid can be treated as Newtonian in both the regions (Sharan and Popel, 2001).

Let $\bar{T}_w$ and $\bar{C}_w$ be the temperature and concentration of the outer wall of the artery respectively. The temperature $\bar{T}_w$ is assumed high enough at the wall to induce radiative heat transfer.

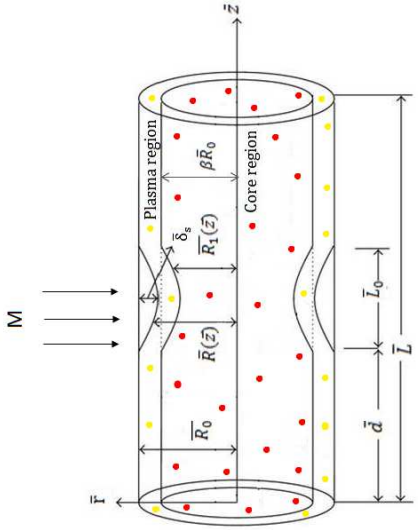

Figure 4.1: Geometry of the vertical stenosed artery of length $\bar{L}$

Geometry of the stenosis in plasma region, which is assumed symmetric about the radial direction, is defined as (Mekheimer and Kot, 2008),

$$\frac{\bar{R}(\bar{z})}{\bar{R}_0} = \begin{cases} 1 - \frac{\bar{\delta}_s n^{\frac{n}{n-1}}}{\bar{R}_0 \bar{L}_0^n (n-1)} \left(\bar{L}_0^{n-1}(\bar{z} - \bar{d}) - (\bar{z} - \bar{d})^n \right) & \text{for} \quad \bar{d} \leq \bar{z} \leq \bar{d} + \bar{L}_0, \\ 1, & \text{otherwise}, \end{cases} \tag{4.2.1}$$

and in core region geometry of the stenosis is defined as (Sankar and Lee, 2007),

$$\frac{\bar{R}_1(\bar{z})}{\bar{R}_0} = \begin{cases} \beta - \frac{\bar{\delta}_s n^{\frac{n}{n-1}}}{\bar{R}_0 \bar{L}_0^n (n-1)} \left(\bar{L}_0^{n-1}(\bar{z} - \bar{d}) - (\bar{z} - \bar{d})^n \right) & \text{for} \quad \bar{d} \leq \bar{z} \leq \bar{d} + \bar{L}_0, \\ \beta, & \text{otherwise}, \end{cases} \tag{4.2.2}$$

where $\bar{L}_0$ is the length of the stenosis, β is the ratio of the central core radius to the normal artery radius, $\bar{R}_0$ is the radius of the artery and n determines the shape of the constriction profile (Nadeem et al., 2011) and $\bar{\delta}_s$ indicates the maximum height of the stenosis located at

$$\bar{z} = \bar{d} + \frac{\bar{L}_0}{n^{\frac{1}{(n-1)}}}. \tag{4.2.3}$$

For the symmetric case, i.e., $n = 2$, maximum height of the stenosis occurs at mid point of the stenotic region

$$\bar{z} = \bar{d} + \frac{\bar{L}_0}{2}.$$

Note that the fluid flow in both the regions is in the axial direction and applied magnetic field is acting perpendicular to the flow direction. Under these assumptions the equations for momentum, energy and concentration for the core region are given by

$$\bar{\rho_c}\frac{\partial \bar{u}_c}{\partial \bar{t}} = -\frac{\partial \bar{p}}{\partial \bar{z}} + \bar{\mu}_c\left(\frac{\partial^2 \bar{u}_c}{\partial \bar{r}^2} + \frac{1}{\bar{r}}\frac{\partial \bar{u}_c}{\partial \bar{r}}\right) - \bar{\sigma}{\bar{B}_0}^2\bar{u_c} + \bar{g}\bar{\rho_c}\bar{\beta}\left(\bar{T}_c - \bar{T}_0\right) + \bar{g}\bar{\rho_c}\bar{\gamma}\left(\bar{C}_c - \bar{C}_0\right), \tag{4.2.4}$$

$$\bar{\rho_c}\bar{c_c}\frac{\partial \bar{T}_c}{\partial \bar{t}} = \bar{K}_c\left(\frac{\partial^2 \bar{T}_c}{\partial \bar{r}^2} + \frac{1}{\bar{r}}\frac{\partial \bar{T}_c}{\partial \bar{r}}\right) - \frac{\partial \bar{q}_c}{\partial \bar{r}}, \tag{4.2.5}$$

$$\frac{\partial \bar{C}_c}{\partial \bar{t}} = \bar{D}_c\left(\frac{\partial^2 \bar{C}_c}{\partial \bar{r}^2} + \frac{1}{\bar{r}}\frac{\partial \bar{C}_c}{\partial \bar{r}}\right) - \bar{E}'_c\left(\bar{C}_c - \bar{C}_0\right), \tag{4.2.6}$$

where $\bar{B}_0$ is the magnetic field intensity, $\bar{\sigma}$ is the electrical conductivity, $\frac{\partial \bar{\bar{p}}}{\partial \bar{\bar{z}}}$ represents the pressure gradient, $\bar{D}_c$ is the coefficient of mass diffusivity, $\bar{\rho_c}$ is the density, $\bar{c_c}$ is the specific heat, $\bar{E}'_c$ is the chemical reaction parameter, $\bar{K}_c$ is the thermal conductivity, $\bar{u_c}$ is the velocity of the fluid in radial direction, $\bar{T}_c$ is the temperature and $\bar{C}_c$ is the concentration of fluid(blood) in the core region.

Similarly, the governing equations of momentum, energy and concentration for plasma region are given by

$$\bar{\rho_p}\frac{\partial \bar{u}_p}{\partial \bar{t}} = -\frac{\partial \bar{p}}{\partial \bar{z}} + \bar{\mu}_p\left(\frac{\partial^2 \bar{u}_p}{\partial \bar{r}^2} + \frac{1}{\bar{r}}\frac{\partial \bar{u}_p}{\partial \bar{r}}\right) - \bar{\sigma}{\bar{B}_0}^2\bar{u_p} + \bar{g}\bar{\rho_p}\bar{\beta}\left(\bar{T}_p - \bar{T}_0\right) + \bar{g}\bar{\rho_p}\bar{\gamma}\left(\bar{C}_p - \bar{C}_0\right), \tag{4.2.7}$$

$$\bar{\rho_p}\bar{c_p}\frac{\partial \bar{T}_p}{\partial \bar{t}} = \bar{K}_p\left(\frac{\partial^2 \bar{T}_p}{\partial \bar{r}^2} + \frac{1}{\bar{r}}\frac{\partial \bar{T}_p}{\partial \bar{r}}\right) - \frac{\partial \bar{q}_p}{\partial \bar{r}}, \tag{4.2.8}$$

$$\frac{\partial \bar{C}_p}{\partial \bar{t}} = \bar{D}_p\left(\frac{\partial^2 \bar{C}_p}{\partial \bar{r}^2} + \frac{1}{\bar{r}}\frac{\partial \bar{C}_p}{\partial \bar{r}}\right) - \bar{E}'_p\left(\bar{C}_p - \bar{C}_0\right), \tag{4.2.9}$$

where $\bar{D}_p$ is the coefficient of mass diffusivity, $\bar{\rho_p}$ is the density, $\bar{c_p}$ is the specific heat, $\bar{E}'_p$ is the chemical reaction parameter and $\bar{K}_p$ is the thermal conductivity of plasma in the peripheral region.

Remark 4.1. Terms $\frac{\partial \bar{q}_c}{\partial \bar{r}}$ in eq.(4.2.5) and $\frac{\partial \bar{q}_p}{\partial \bar{r}}$ in eq.(4.2.8) are due to the radiation effect of heat transfer, where $\bar{q}_c$ and $\bar{q}_p$ represent the radiative heat flux in core and plasma regions respectively.

Therefore, the radiative heat fluxes for core and plasma regions respectively can be expressed as explained in eq.(1.4.4):

$$\frac{\partial \bar{q}_c}{\partial \bar{r}} = 4\bar{\alpha_c}^2 \left(\bar{T_c} - \bar{T_0}\right), \quad \frac{\partial \bar{q}_p}{\partial \bar{r}} = 4\bar{\alpha_p}^2 \left(\bar{T_p} - \bar{T_0}\right), \tag{4.2.10}$$

where $\bar{q_c}$ and $\bar{q_p}$ represent the radiative heat transfer coefficients, and $\bar{\alpha_c}$ and $\bar{\alpha_p}$ are the mean radiation absorption coefficients for core and plasma regions respectively.

Remark 4.2. Note that the mean radiation absorption coefficients $\bar{\alpha_c}$ and $\bar{\alpha_p}$, in general, are considered less than unity ($\bar{\alpha} \lll 1$) in view of the fact that fluids like plasma and blood in the physiological conditions are optically thin with low density (Ogulu and Abbey, 2005).

To solve the momentum, energy and concentration equations of the two-phase model of the blood flow no-slip boundary conditions are considered on the arterial wall. It is assumed that the functions of velocity, temperature and concentration are continuous at the interface of core and plasma regions so their values of both core and plasma regions are equal at that point and due to symmetry their gradient vanishes along with the axis. It is believed that at the interface of core and plasma regions heat and mass transfer effects are same for both the regions (Sharan and Popel, 2001). The appropriate boundary conditions for the model under consideration are as follows:

$$\begin{cases} \bar{u_p} = 0, \quad \bar{T_p} = \bar{T_w}, \quad \bar{C_p} = \bar{C_w} \quad at \quad \bar{r} = \bar{R}(\bar{z}), \\ \bar{u_c} = \bar{u_p}, \quad \bar{T_p} = \bar{T_c}, \quad \bar{C_p} = \bar{C_c} \quad at \quad \bar{r} = \bar{R_1}(\bar{z}), \\ \frac{\partial \bar{u_c}}{\partial \bar{r}} = 0, \quad \frac{\partial \bar{T_c}}{\partial \bar{r}} = 0, \quad \frac{\partial \bar{C_c}}{\partial \bar{r}} = 0 \quad at \quad \bar{r} = 0, \\ \bar{\tau_c} = \bar{\tau_p}, \quad \frac{\partial \bar{T_c}}{\partial \bar{r}} = \frac{\partial \bar{T_p}}{\partial \bar{r}}, \quad \frac{\partial \bar{C_c}}{\partial \bar{r}} = \frac{\partial \bar{C_p}}{\partial \bar{r}} \quad at \quad \bar{r} = \bar{R_1}(\bar{z}). \end{cases} \tag{4.2.11}$$

Now, we introduce the following dimensionless parameters:

$$u_c = \frac{\bar{u_c}}{\bar{u_0}}, \quad r = \frac{\bar{r}}{\bar{R_0}}, \quad z = \frac{\bar{z}}{\bar{R_0}}, \quad t = \bar{\omega}\bar{t}, \quad R(z) = \frac{\bar{R}(\bar{z})}{\bar{R_0}}, \quad R_1(z) = \frac{\bar{R_1}(\bar{z})}{\bar{R_0}},$$

$$p = \frac{\bar{R_0}\bar{p}}{\bar{u_0}\bar{\mu_p}}, \quad Re = \frac{\bar{\rho_p}\bar{R_0}^2\omega}{\bar{\mu_p}}, \quad \theta_c = \frac{(\bar{T_c} - \bar{T_0})}{\bar{T_w} - \bar{T_0}}, \quad \sigma_c = \frac{(\bar{C_c} - \bar{C_0})}{\bar{C_w} - \bar{C_0}}, \quad u_p = \frac{\bar{u_p}}{\bar{u_0}},$$

$$\delta = \frac{\bar{\delta}_s}{\bar{R}_0} \quad \theta_p = \frac{(\bar{T}_p - \bar{T}_0)}{\bar{T}_w - \bar{T}_0}, \quad N^2 = \frac{4\bar{R}_0{}^2\bar{\alpha}_p{}^2}{\bar{K}_p}, \quad M^2 = \frac{\bar{\sigma}\bar{B}_0{}^2\bar{R}_0{}^2}{\bar{\mu}_p}, \quad \sigma_p = \frac{(\bar{C}_p - \bar{C}_0)}{\bar{C}_w - \bar{C}_0},$$

$$Pe = \frac{\bar{\rho}_p\bar{c}_p\bar{R}_0{}^2\bar{\omega}}{\bar{K}_p}, \quad Sc = \frac{\bar{\mu}_p}{\bar{D}_p\bar{\rho}_p}, \quad Gr = \frac{\bar{g}\bar{\rho}_p\bar{\beta}\bar{R}_0{}^2\left(\bar{T}_w - \bar{T}_0\right)}{\bar{u}_0\bar{\mu}_p}, \quad D_0 = \frac{\bar{D}_p}{\bar{D}_c},$$

$$\tau_c = \frac{\bar{\tau}_c\bar{R}_0{}^2}{\bar{u}_0\bar{\mu}_p}, \quad \tau_p = \frac{\bar{\tau}_p\bar{R}_0{}^2}{\bar{u}_0\bar{\mu}_p}, \quad \rho_0 = \frac{\bar{\rho}_p}{\bar{\rho}_c}, \quad \mu_0 = \frac{\bar{\mu}_p}{\bar{\mu}_c}, \quad \bar{E}'_p = \frac{E\bar{\mu}_p}{\bar{\rho}_p\bar{R}_0{}^2}, \quad E_0 = \frac{\bar{E}_p}{\bar{E}_c}.$$

Therefore, equations of momentum, energy and concentration eqs.(4.2.4)-(4.2.6) of the core region is represented in terms of these non-dimensional parameters as

$$\left(\frac{Re}{\rho_0}\right)\frac{\partial u_c}{\partial t} = -\frac{\partial p}{\partial z} + \frac{1}{\mu_0}\left(\frac{\partial^2 u_c}{\partial r^2} + \frac{1}{r}\frac{\partial u_c}{\partial r}\right) - M^2 u_c + \left(\frac{Gr}{\rho_0}\right)\theta_c + \left(\frac{Gm}{\rho_0}\right)\sigma_c, \quad (4.2.12)$$

$$\frac{PeK_0}{\rho_0 s_0}\left(\frac{\partial \theta_c}{\partial t}\right) = \left(\frac{\partial^2 \theta_c}{\partial r^2} + \frac{1}{r}\frac{\partial \theta_c}{\partial r}\right) - \frac{K_0}{\alpha_0}N^2\theta_c, \quad (4.2.13)$$

$$Re\left(\frac{\partial \sigma_c}{\partial t}\right) = \frac{1}{D_0}\left(\frac{1}{Sc}\right)\left(\frac{\partial^2 \sigma_c}{\partial r^2} + \frac{1}{r}\frac{\partial \sigma_c}{\partial r}\right) - \frac{E}{E_0}\sigma_c, \quad (4.2.14)$$

and, equations of momentum, energy and concentration eqs.(4.2.7)-(4.2.9) of the plasma region is represented in terms of these non-dimensional parameters as

$$Re\frac{\partial u_p}{\partial t} = -\frac{\partial p}{\partial z} + \left(\frac{\partial^2 u_p}{\partial r^2} + \frac{1}{r}\frac{\partial u_p}{\partial r}\right) - M^2 u_p + Gr\theta_p + Gm\sigma_p, \quad (4.2.15)$$

$$Pe\frac{\partial \theta_p}{\partial t} = \left(\frac{\partial^2 \theta_p}{\partial r^2} + \frac{1}{r}\frac{\partial \theta_p}{\partial r}\right) - N^2\theta_p, \quad (4.2.16)$$

$$Re\left(\frac{\partial \sigma_p}{\partial t}\right) = \left(\frac{1}{Sc}\right)\left(\frac{\partial^2 \sigma_p}{\partial r^2} + \frac{1}{r}\frac{\partial \sigma_p}{\partial r}\right) - E\sigma_p, \quad (4.2.17)$$

where α_0 is the ratio of mean radiation absorption coefficient in the plasma region to mean radiation absorption coefficient in the core region, K_0 is the ratio of thermal conductivity of plasma to core region, s_0 is the specific heat ratio of plasma to core region, E_0 is the ratio of chemical moles present in the plasma region to chemical moles in the core region and N, M and E are factors of thermal radiation, applied magnetic field and chemical reaction for both core and plasma regions.

The dimensionless form of geometry of the stenosis in core and plasma regions are given by

$$R(z) = \begin{cases} 1 - \eta\left((z-l) - (z-l)^n\right) & \text{for} \quad l \leq z \leq 1+l, \\ 1 & \text{otherwise}, \end{cases} \tag{4.2.18}$$

$$R_1(z) = \begin{cases} \beta - \eta\left((z-l) - (z-l)^n\right) & \text{for} \quad l \leq z \leq 1+l, \\ \beta & \text{otherwise}, \end{cases} \tag{4.2.19}$$

where

$$\eta = \frac{\delta n^{\frac{n}{n-1}}}{(n-1)}, \quad l = \frac{\bar{d}}{\bar{L_0}}, \quad \delta = \frac{\bar{\delta_s}}{\bar{R_0}}.$$

Similarly, the corresponding boundary conditions eq.(4.2.11) in non-dimensional form for both core and plasma regions are given as

$$\begin{cases} u_p = 0, & \theta_p = 1, & \sigma_p = 1 & at & r = R(z), \\ u_p = u_c, & \theta_p = \theta_c, & \sigma_p = \sigma_c & at & r = R_1(z), \\ \tau_c = \tau_p, & \frac{\partial \theta_c}{\partial r} = \frac{\partial \theta_p}{\partial r}, & \frac{\partial \sigma_c}{\partial r} = \frac{\partial \sigma_p}{\partial r} & at & r = R_1(z), \\ \frac{\partial u_c}{\partial r} = 0, & \frac{\partial \theta_c}{\partial r} = 0, & \frac{\partial \sigma_c}{\partial r} = 0 & at & r = 0. \end{cases} \tag{4.2.20}$$

4.3 Solution

In this section, we solve the momentum, energy and concentration eqs.(4.2.12)-(4.2.17) in both core and plasma regions under the given boundary conditions eq.(4.2.20). In view of the fact that the pumping action of the heart results in a pulsatile blood flow, pressure gradient can be represented as

$$-\frac{\partial p}{\partial z} = P_0 e^{i\bar{\omega}\bar{t}},$$

where P_0 represents the constant pressure. This assumption is limited to cases of harmonic oscillatory motion (San and Staples, 2012).

As eqs.(4.2.12)-(4.2.17) are linear, we are allowed to express velocity, temperature and concentration in the form of:

$$\begin{cases} u_c(r,t) = u_{c_0}(r)e^{i\omega t}, & u_p(r,t) = u_{p_0}(r)e^{i\omega t}, \\ \theta_c(r,t) = \theta_{c_0}(r)e^{i\omega t}, & \theta_p(r,t) = \theta_{p_0}(r)e^{i\omega t}, \\ \sigma_c(r,t) = \sigma_{c_0}(r)e^{i\omega t}, & \sigma_p(r,t) = \sigma_{p_0}(r)e^{i\omega t}. \end{cases} \tag{4.3.1}$$

Therefore, using eq.(4.3.1), eqs.(4.2.12)-(4.2.14) can be reduced as

$$\left(\frac{\partial^2 u_{c_0}}{\partial r^2}+\frac{1}{r}\frac{\partial u_{c_0}}{\partial r}\right)-\left(M^2+\frac{\mu_0 Re}{\rho_0}i\right)u_{c_0}=-\left(P_0+\frac{Gr\theta_{c_0}}{\rho_0}+\frac{Gm\sigma_{c_0}}{\rho_0}\right)\mu_0, \tag{4.3.2}$$

$$\frac{\partial^2\theta_{c_0}}{\partial r^2}+\frac{1}{r}\frac{\partial\theta_{c_0}}{\partial r}-\left(\frac{K_0N^2}{\alpha_0}+i\frac{Pe}{\rho_0}\left(\frac{K_0}{s_0}\right)\right)\theta_{c_0}=0, \tag{4.3.3}$$

$$\frac{\partial^2\sigma_{c_0}}{\partial r^2}+\frac{1}{r}\frac{\partial\sigma_{c_0}}{\partial r}-\left(iReD_0Sc+\frac{E}{E_0}D_0Sc\right)\sigma_{c_0}=0. \tag{4.3.4}$$

Similarly, substituting eq.(4.3.1) into eqs.(4.2.15)-(4.2.17), we get

$$\left(\frac{\partial^2 u_{p_0}}{\partial r^2}+\frac{1}{r}\frac{\partial u_{p_0}}{\partial r}\right)-\left(M^2+Rei\right)u_{p_0}=-\left(P_0+\frac{Gr\theta_{p_0}}{\rho_0}+\frac{Gm\sigma_{p_0}}{\rho_0}\right), \tag{4.3.5}$$

$$\frac{\partial^2\theta_{p_0}}{\partial r^2}+\frac{1}{r}\frac{\partial\theta_{p_0}}{\partial r}-\left(N^2+iPe\right)\theta_{p_0}=0, \tag{4.3.6}$$

$$\frac{\partial^2\sigma_{p_0}}{\partial r^2}+\frac{1}{r}\frac{\partial\sigma_{p_0}}{\partial r}-\left(iReSc+ESc\right)\sigma_{p_0}=0. \tag{4.3.7}$$

Remark 4.3. Note that the system of ODEs eqs.(4.3.2)-(4.3.7) along with the boundary conditions eq.(4.2.20) admits an exact solution using Bessel functions.

To find the solution of eq.(4.3.3) and eq.(4.3.6) under the given boundary conditions eq.(4.2.20), we rewrite the energy equations of core and plasma regions in standard Bessel differential equations form as

$$\frac{\partial^2\theta_{c_0}}{\partial r^2}+\frac{1}{r}\frac{\partial\theta_{c_0}}{\partial r}+\beta_1\theta_{c_0}=0, \tag{4.3.8}$$

$$\frac{\partial^2\theta_{p_0}}{\partial r^2}+\frac{1}{r}\frac{\partial\theta_{p_0}}{\partial r}+\beta_2\theta_{p_0}=0, \tag{4.3.9}$$

where

$$\beta_1=-\left(\frac{K_0N^2}{\alpha_0}+i\frac{Pe}{\rho_0}\left(\frac{K_0}{s_0}\right)\right),\quad \beta_2=-\left(N^2+iPe\right).$$

Hence, solution for the energy equations of core and plasma regions are

$$\theta_{c_0}(r) = \left[U_1\left(\frac{\sqrt{\beta_2}Y_1(\sqrt{\beta_2}R_1)}{U_3Y_0(\sqrt{\beta_2}R)} - \frac{\sqrt{\beta_1}U_2J_1(\sqrt{\beta_1}R_1)}{U_3}\right) + U_2\right]J_0(\sqrt{\beta_1}(r)), \tag{4.3.10}$$

$$\theta_{p_0}(r) = \left[\left(\frac{\sqrt{\beta_2}Y_1(\sqrt{\beta_2}R_1)}{U_3Y_0(\sqrt{\beta_2}R)} - \frac{\sqrt{\beta_1}U_2J_1(\sqrt{\beta_1}R_1)}{U_3}\right)\left(J_0(\sqrt{\beta_2}r) - \frac{J_0(\sqrt{\beta_2}R}{Y_0(\sqrt{\beta_2}R}Y_0(\sqrt{\beta_2}r)\right)\right] + \frac{Y_0(\sqrt{\beta_2}r)}{Y_0(\sqrt{\beta_2}R)}, \tag{4.3.11}$$

where $J_n(x)$ and $Y_n(x)$ are respectively the Bessel function of first and second kind. Expressions for the constants U_1, U_2 and U_3 are given in Appendix A.

Final expressions for temperature considering unsteady flow of core and plasma regions respectively, are as follows

$$\theta_c(r,t) = \left[\left(U_1\left(\frac{\sqrt{\beta_2}Y_1(\sqrt{\beta_2}R_1)}{U_3Y_0(\sqrt{\beta_2}R)} - \frac{\sqrt{\beta_1}U_2J_1(\sqrt{\beta_1}R_1)}{U_3}\right) + U_2\right)J_0(\sqrt{\beta_1}(r))\right]e^{i\omega t}, \tag{4.3.12}$$

$$\begin{aligned}\theta_p(r,t) = &\left(\frac{\sqrt{\beta_2}Y_1(\sqrt{\beta_2}R_1)}{U_3Y_0(\sqrt{\beta_2}R)} - \frac{\sqrt{\beta_1}U_2J_1(\sqrt{\beta_1}R_1)}{U_3}\right)J_0(\sqrt{\beta_2}r)e^{i\omega t}\\ &- \left(\frac{\sqrt{\beta_2}Y_1(\sqrt{\beta_2}R_1)}{U_3Y_0(\sqrt{\beta_2}R)} - \frac{\sqrt{\beta_1}U_2J_1(\sqrt{\beta_1}R_1)}{U_3}\right)\frac{J_0(\sqrt{\beta_2}R)}{Y_0(\sqrt{\beta_2}R)}Y_0(\sqrt{\beta_2}r)e^{i\omega t}\\ &+ \frac{Y_0(\sqrt{\beta_2}r)}{Y_0(\sqrt{\beta_2}R)}e^{i\omega t}.\end{aligned} \tag{4.3.13}$$

In a similar manner, the concentration eq.(4.3.4) and eq.(4.3.7) of core and plasma region can be rewritten in the standard Bessel differential equation form as

$$\frac{\partial^2\sigma_{c_0}}{\partial r^2} + \frac{1}{r}\frac{\partial\sigma_{c_0}}{\partial r} + \gamma_1\sigma_{c_0} = 0, \tag{4.3.14}$$

$$\frac{\partial^2\sigma_{p_0}}{\partial r^2} + \frac{1}{r}\frac{\partial\sigma_{p_0}}{\partial r} + \gamma_2\sigma_{p_0} = 0, \tag{4.3.15}$$

where

$$\gamma_1 = -\left(iReD_0Sc + \frac{E}{E_0}D_0Sc\right), \quad \gamma_2 = -\left(iReSc + ESc\right).$$

Therefore, solutions for concentration equations satisfying the given boundary conditions eq.(4.2.20) for both core and plasma regions are calculated as

$$\sigma_{c_0}(r) = \left[U_4\left(\frac{\sqrt{\gamma_2}Y_1(\sqrt{\gamma_2}R_1)}{U_6Y_0(\sqrt{\gamma_2}R)} - \frac{\sqrt{\gamma_1}U_5J_1(\sqrt{\gamma_1}R_1)}{U_6}\right) + U_5\right]J_0(\sqrt{\gamma_1}(r)), \tag{4.3.16}$$

and

$$\sigma_{p_0}(r) = \left[\left(\frac{\sqrt{\gamma_2}Y_1(\sqrt{\gamma_2}R_1)}{U_6Y_0(\sqrt{\gamma_2}R)} - \frac{\sqrt{\gamma_1}U_5J_1(\sqrt{\gamma_1}R_1)}{U_6}\right)\left(J_0(\sqrt{\gamma_2}r) - \frac{J_0(\sqrt{\gamma_2}R}{Y_0(\sqrt{\gamma_2}R}Y_0(\sqrt{\gamma_2}r)\right)\right] + \frac{Y_0(\sqrt{\gamma_2}r)}{Y_0(\sqrt{\gamma_2}R)}, \tag{4.3.17}$$

Consequently, concentration for unsteady flow in core and plasma regions are as follows

$$\sigma_c(r,t) = \left[U_4\left(\frac{\sqrt{\gamma_2}Y_1(\sqrt{\gamma_2}R_1)}{U_6Y_0(\sqrt{\gamma_2}R)} - \frac{\sqrt{\gamma_1}U_5J_1(\sqrt{\gamma_1}R_1)}{U_6}\right) + U_5\right]J_0(\sqrt{\gamma_1}(r))e^{i\omega t}, \tag{4.3.18}$$

$$\begin{aligned}\sigma_p(r,t) = &\left(\frac{\sqrt{\gamma_2}Y_1(\sqrt{\gamma_2}R_1)}{U_6Y_0(\sqrt{\gamma_2}R)} - \frac{\sqrt{\gamma_1}U_5J_1(\sqrt{\gamma_1}R_1)}{U_6}\right)J_0(\sqrt{\gamma_2}r)e^{i\omega t}\\ &- \left(\frac{\sqrt{\gamma_2}Y_1(\sqrt{\gamma_2}R_1)}{U_6Y_0(\sqrt{\gamma_2}R)} - \frac{\sqrt{\gamma_1}U_5J_1(\sqrt{\gamma_1}R_1)}{U_6}\right)\frac{J_0(\sqrt{\gamma_2}R)}{Y_0(\sqrt{\gamma_2}R)}Y_0(\sqrt{\gamma_2}r)e^{i\omega t}\\ &+ \frac{Y_0(\sqrt{\gamma_2}r)}{Y_0(\sqrt{\gamma_2}R)}e^{i\omega t},\end{aligned} \tag{4.3.19}$$

where expressions for the constants U_4, U_5 and U_6 are given in Appendix A.

To find the solution for velocity profile in core region, we substitute the values of θ_{c_0} and σ_{c_0} from eq.(4.3.10) and eq.(4.3.16) into eq.(4.3.2) and obtains the following non-homogeneous differential equations by assuming

$$\left(\frac{\partial^2 u_{c_0}}{\partial r^2} + \frac{1}{r}\frac{\partial u_{c_0}}{\partial r}\right) + \lambda_1 u_{c_0} = -\left(P_0 + \frac{Gr\theta_{c_0}}{\rho_0} + \frac{Gm\sigma_{c_0}}{\rho_0}\right)\mu_0. \tag{4.3.20}$$

where

$$\lambda_1 = -\left(M^2 + \frac{\mu_0 Re}{\rho_0}i\right). \tag{4.3.21}$$

The general solution of the eq.(4.3.20) is calculated using variation of parameters method as

$$u_{c_0} = C_1J_0\sqrt{\lambda_1}r + C_2Y_0\sqrt{\lambda_1}r + A_1J_0\sqrt{\lambda_1}r + B_1Y_0\sqrt{\lambda_1}r, \tag{4.3.22}$$

where C_1, C_2 are the arbitrary constants and A_1, A_2 are defined as

$$A_1 = -\frac{\pi r}{2}\int Y_0\sqrt{\lambda_1}r\left(P_0 + \frac{Gr\theta_{c_0}}{\rho_0} + \frac{Gm\sigma_{c_0}}{\rho_0}\right)\mu_0 \quad dr,$$

$$B_1 = \frac{\pi r}{2}\int J_0\sqrt{\lambda_1}r\left(P_0 + \frac{Gr\theta_{c_0}}{\rho_0} + \frac{Gm\sigma_{c_0}}{\rho_0}\right)\mu_0 \quad dr.$$

Now for eq.(4.3.5) of plasma region, we assume that

$$\lambda_2 = -\left(M^2 + Rei\right). \tag{4.3.23}$$

So,the eq.(4.3.5) convert in terms of λ_2 as

$$\left(\frac{\partial^2 u_{p_0}}{\partial r^2} + \frac{1}{r}\frac{\partial u_{p_0}}{\partial r}\right) + \lambda_2 u_{p_0} = -\left(P_0 + \frac{Gr\theta_{p_0}}{\rho_0} + \frac{Gm\sigma_{p_0}}{\rho_0}\right). \tag{4.3.24}$$

So, the general solution of the given eq.(4.3.24) can be calculated as

$$u_{p_0} = C_3 J_0\sqrt{\lambda_1}r + C_4 Y_0\sqrt{\lambda_1}r + A_2 J_0\sqrt{\lambda_1}r + B_2 Y_0\sqrt{\lambda_1}r, \tag{4.3.25}$$

where C_3, C_4 are arbitrary constants and A_2, B_2 are expressed as

$$A_2 = -\frac{\pi r}{2}\int Y_0\sqrt{\lambda_2}r\left(P_0 + \frac{Gr\theta_{c_0}}{\rho_0} + \frac{Gm\sigma_{c_0}}{\rho_0}\right) \quad dr,$$

$$B_2 = \frac{\pi r}{2}\int J_0\sqrt{\lambda_2}r\left(P_0 + \frac{Gr\theta_{c_0}}{\rho_0} + \frac{Gm\sigma_{c_0}}{\rho_0}\right) \quad dr.$$

After applying the boundary conditions eq.(4.2.20) into the eq.(4.3.22) and eq.(4.3.25), we get $C_2 = 0$ and the linear system in terms of C_1, C_3, C_4 as

$$\begin{pmatrix} J_0(\sqrt{\lambda_1}R_1) & -J_0(\sqrt{\lambda_2}R_1) & -Y_0(\sqrt{\lambda_2}R_1) \\ 0 & J_0(\sqrt{\lambda_2}R) & Y_0(\sqrt{\lambda_2}R) \\ -\sqrt{\lambda_1}J_1(\sqrt{\lambda_1}R_1) & \sqrt{\lambda_2}J_1(\sqrt{\lambda_2}R_1) & \sqrt{\lambda_2}Y_1(\sqrt{\lambda_2}R_1) \end{pmatrix}\begin{pmatrix} C_1 \\ C_3 \\ C_4 \end{pmatrix} = \begin{pmatrix} D_1 \\ D_2 \\ D_3 \end{pmatrix} \tag{4.3.26}$$

where D_1, D_2 and D_3 are expressed in Appendix A. Under the given set of boundary conditions the linear system eq.(4.3.26) admits a unique solution.

4.4 Results and Discussion

For having adequate insight into the two-phase flow behavior of blood through a stenosed arterial segment, flow resistance, total flow rate, and wall shear stress have been estimated assuming pulsatile, Newtonian nature of the blood flow for both core and plasma regions. A computational study has been carried out to show the effects of cell-depleted plasma layer on blood flow with the variation of different quantities of interest. Default values

Parameters	Values (Unit free)	Source
Magnetic field Parameter (M)	1.5-3	Swartz et al. (2009); Trivedi et al. (2004)
Schmidt Parameter (Sc)	0.5-1.5	Zaman et al. (2016a)
Radiation Parameter (N)	2-5	Ogulu and Abbey (2005)
Chemical reaction Parameter (E)	0.5-2	Misra and Adhikary (2016)
Peclet Number (Pe)	0.87	Sharan et al. (1997)
Grashof Number (Gr)	2-3	Misra and Adhikary (2016)
Modified Grashof Number (Gm)	2-3	Misra and Adhikary (2016)
Ratio of Thermal Conductivity in core and plasma regions (K_0)	0.4-0.8	Ponalagusamy and Selvi (2015)
Ratio of Specific heat in core and plasma regions (s_0)	1.0	Ponalagusamy and Selvi (2015)
Ratio of density in core and plasma regions (ρ_0)	1.05	Medvedev and Fomin (2011)
Ratio of mean radiation absobtion coefficients in core and plasma region (α_0)	1.0	Ponalagusamy and Selvi (2015)
Reynold Number(Re)	0.005	Fujiwara et al. (2009); Sharan et al. (1997)
Ratio of viscosities in core and plasma region (μ_0)	1.2	Medvedev and Fomin (2011); Sharan and Popel (2001)
Pressure gradient (P_0)	10	Ponalagusamy and Selvi (2015)

Table 4.1: Values of the parameters

of the parameters used to graphically analyze the effectiveness of the model are given in Table.4.1. In all the figures, continuous lines show the respective profile for the core

region while dotted lines display the same for the plasma region.

Fig.4.2 displays the comparative studies between single phase (where we assume that plasma and red blood cells are uniformly distributed over the region and their flow dynamics are also same) and two-phase model of the blood flow with the experimental results of Bugliarello and Sevilla (1970), who through their *In Vitro* experimental studies in a fine glass tube under the steady flow conditions measured the cell velocity distribution of blood containing 40% hematocrit. The results of the present model seems to be closer to those of Bugliarello and Sevilla for values $\delta = 0$, $Re = 5$, $Pe = 1$, $M = 0$ and $R_1 = 0.7$. Comparison result shows that the data of the present model for two-phase blood flow ($R_1 = 0.7$) shows a good agreement with the experimental result as compared to single phase data ($R_1 = 1$). Mean squared errors (MSE) for the measured data of two-phase and single-phase blood flow as compared with the experimental data are calculated as

$$\frac{1}{n}\sum_{i=1}^{n}(\widehat{\mathbf{Y}}_{\mathbf{EX}_i} - \mathbf{Y}_{\mathbf{T}_i})^2 = 0.003094882, \tag{4.4.1}$$

$$\frac{1}{n}\sum_{i=1}^{n}(\widehat{\mathbf{Y}}_{\mathbf{EX}_i} - \mathbf{Y}_{\mathbf{S}_i})^2 = 0.010313676, \tag{4.4.2}$$

where $\widehat{\mathbf{Y}}_{\mathbf{EX}}$ represents the experimental data (Bugliarello and Sevilla, 1970), $\mathbf{Y_T}$ is the two-phase model data and $\mathbf{Y_S}$ shows single phase model data. The result shows that two-phase model data fit with the experimental data more appropriately than the single phase model data as it has 0.3% mean squared error than the single phase model data of 1% mean squared error.

Fig.4.3 shows the effect of variable applied a magnetic field on the velocity profile of the blood flow. Hence, it is clear from the figure that as the value of uniform applied magnetic field increases from 0.5 to 3 velocity profiles for both core and plasma regions decrease, respectively. This happens because of the mature red blood cells contain high concentration hemoglobin molecules in their content which basically are the oxides of iron. Therefore, when blood flows under the influence of a magnetic field, erythrocytes orient with their own disk plane parallel to the direction of the applied magnetic field. This action increases the concentration of red blood cells and causes an increase in the

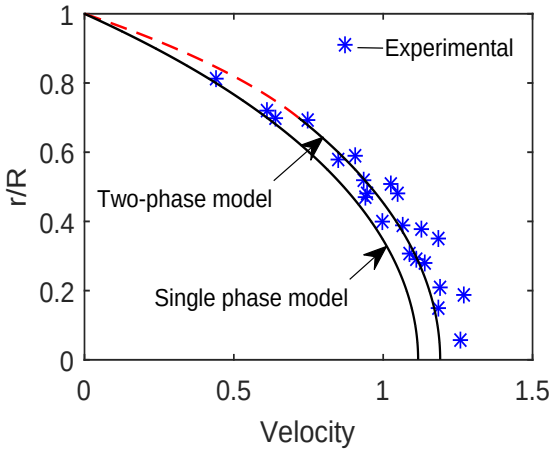

Figure 4.2: Comparative results of velocity profiles for two-phase and single phase blood flow model with the experimental results of Bugliarello and Sevilla (1970)

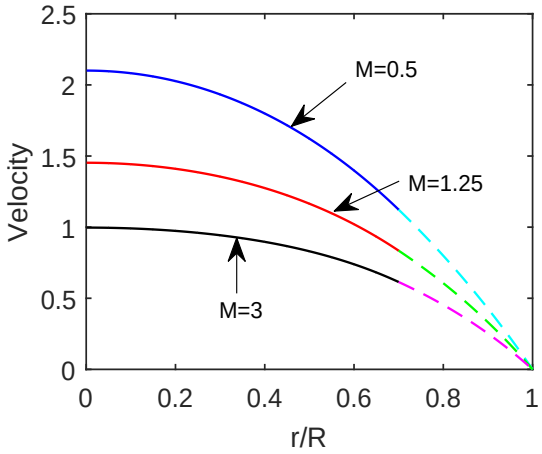

Figure 4.3: Variation of velocity profile of two-phase blood flow with different values of magnetic field parameter (M), where $\delta = 0.1$, $t = 1$, $R_1 = 0.7$

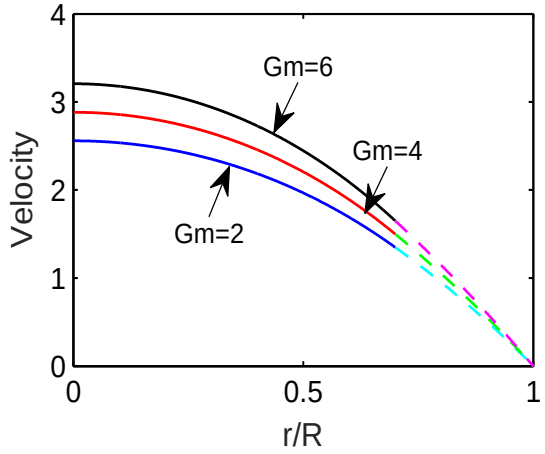

Figure 4.4: Variation of velocity profile of two-phase blood flow with Gm

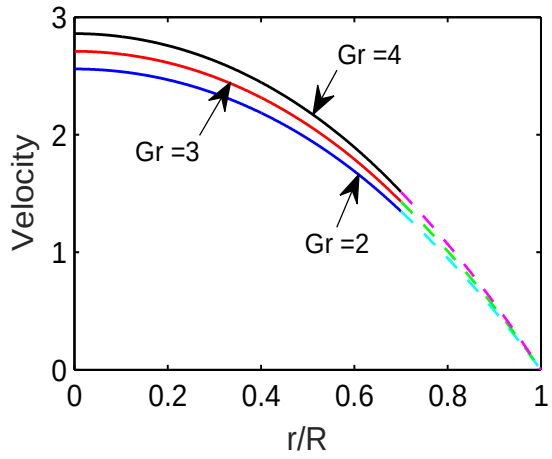

Figure 4.5: Variation of velocity profile of two-phase blood flow with Gr

internal blood viscosity (Haik et al., 2001). In the model as boundary condition shows the continuous behavior of the flow at the interface, the reduced velocity of the red blood cells direct affects the velocity of the plasma by resulting angular velocity for the plasma fluid. The difference between the angular velocities of plasma and red blood cell create the viscous torque which results in the decreased velocity of the plasma region as well.

This leads to a decrease in the blood velocity as Lorentz force opposes the flow of blood (Tzirtzilakis, 2005). Fig.4.4 and fig.4.5 show the variation of axial velocity profiles with solutal Grashof number and thermal Grashof number, respectively. It can be clearly observed from the figures that as we increase the value of solutal Grashof number and thermal Grashof number, velocity profiles increase respectively for both core and plasma regions.

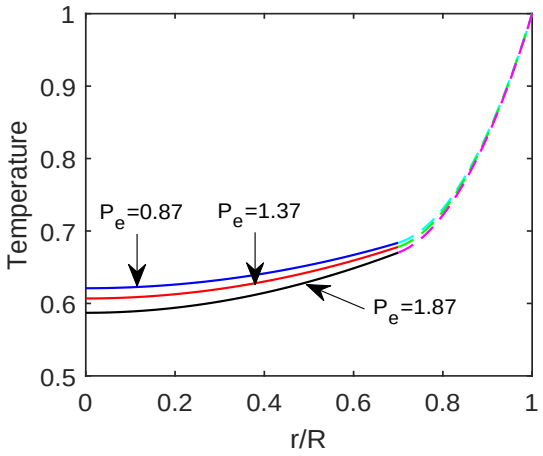

Figure 4.6: Variation of temperature profile of two-phase blood flow with Pe

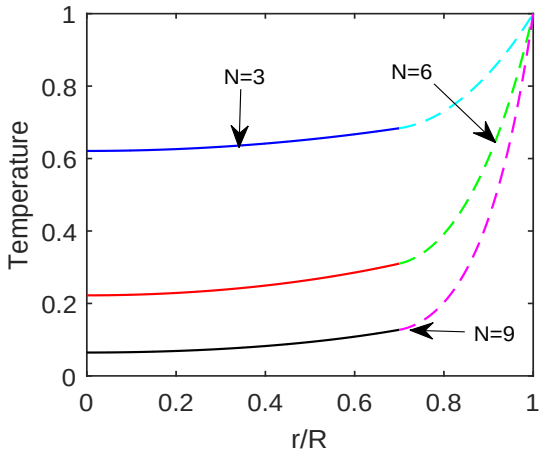

Figure 4.7: Variation of temperature profile of two-phase blood flow with N

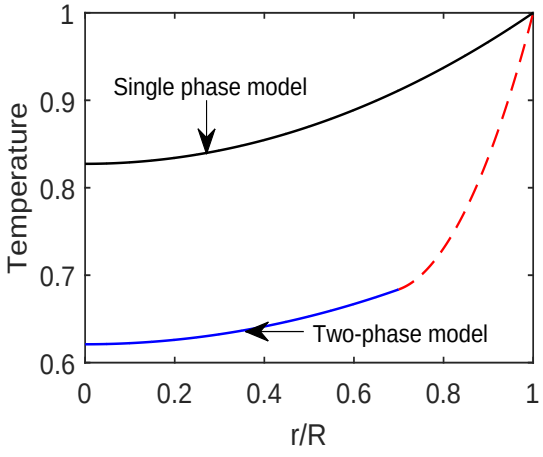

Figure 4.8: Comparative results of temperature profiles of single and two-phase model

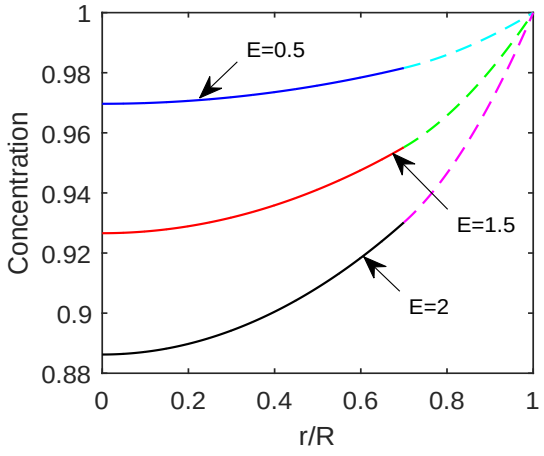

Figure 4.9: Effects of the chemical reaction parameter (E) on concentration profile of two-phase blood flow

Fig.4.6 illustrates the variations of the temperature profile of the blood flow for different values of the Peclet number (Pe). It can be observed from the figure that as values of the Peclet number increase, temperature profile of the blood flow decreases in both core and plasma regions. Fig.4.7 illustrates the behavior of the temperature profile of the blood flow for different values of the radiation parameter. It can be clearly observed from the figure that for a particular value of radiation parameter (N), temperature profile start increases from mid of the artery towards the interface region of the core and plasma regions and it continuously increases up to the arterial wall. Further, as we increase the values of the radiation parameter, temperature profile decreases in both core and plasma regions of the artery (Ogulu and Abbey, 2005). Comparative results for temperature profiles for single phase and two-phase model of blood flow have been displayed in fig.4.8, by considering parameters value from Table.4.1. It is clear from the fig.4.8 that temperature profile of the two-phase blood flow along the radial direction of the artery attains lower values than the temperature profile of the single phase model of the blood flow in which we assume that plasma and red blood cells are uniformly distributed over the artery.

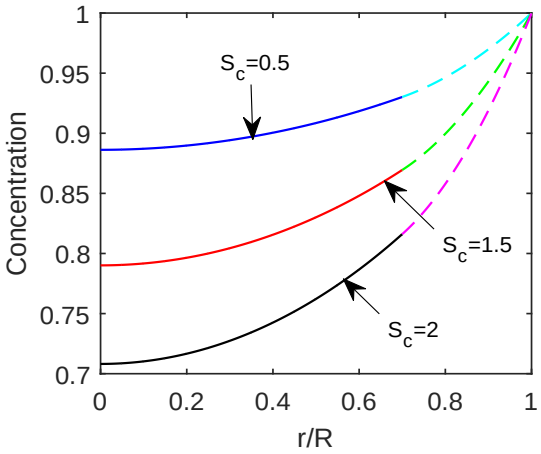

Figure 4.10: Effects of the Schmidt number (Sc) on concentration profile of two-phase blood flow

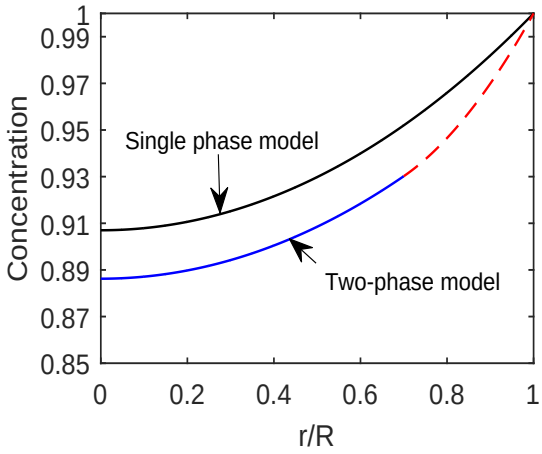

Figure 4.11: Comparative results of concentration profiles of two-phase and single phase flow

Fig.4.9 and fig.4.10 reveal that under the purview of the present computational study, concentration profiles for both core and plasma regions decrease as the values of the chem-

ical reaction parameter and Schmidt number increase, respectively. For a particular value of the chemical reaction parameter and Schmidt number, concentration profile increases, as we move from mid of the artery towards the interface region and it increases up to the arterial wall. With chemical reaction parameter, concentration profile shows this behavior because higher values of chemical reaction parameter resulted to a fall into the molecular diffusivity which directly suppresses the species concentration. Therefore, the concentration decreases at all point of the flow field with increasing values of the chemical reaction parameter. Fig.4.11 shows the comparison result for the concentration profile of the single-phase blood flow as $R_1 = 1$ and for the two-phase blood flow when $R_1 = 0.7$. It is clear from the figure that, concentration profile along the radial direction of the artery attains higher values for single phase blood flow (in which blood components are uniformly distributed over the artery) than the two-phase model of the blood flow.

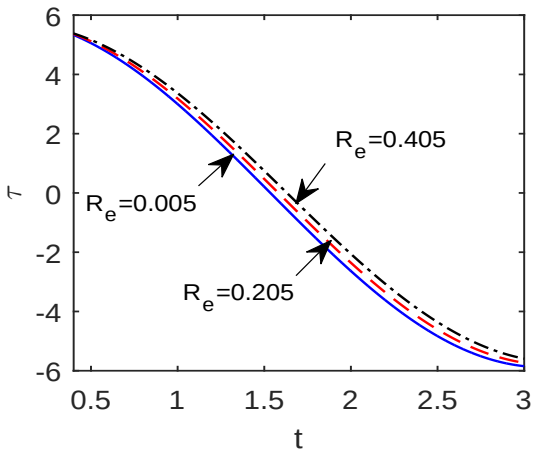

Figure 4.12: Variation of wall shear stress with time for different values of Re

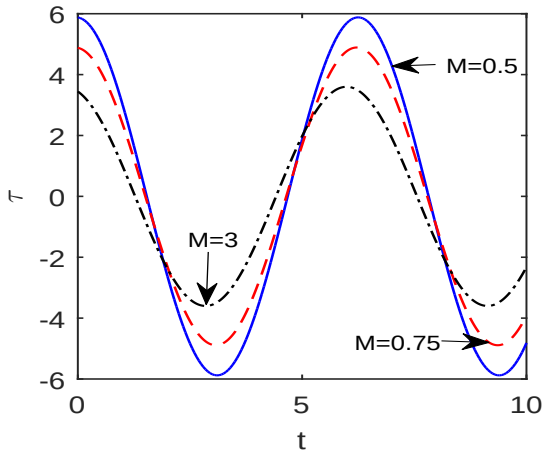

Figure 4.13: Variation of wall shear stress with time for different values of M

In the artery, vascular tissue shows histological and morphological alterations, when it is physically stressed then the role of wall shear stress comes into the picture. So in the study of stenosed arterial blood flow, wall shear stress is a major flow component to measure (Cavalcanti, 1992). The shear stress at the interface wall of core and the plasma region is obtained as

$$\tau = -\left(\frac{\partial u_c}{\partial r}\right). \tag{4.4.3}$$

At the outer wall of the artery shear stress is determined as

$$\tau' = -\frac{1}{\mu_0}\left(\frac{\partial u_p}{\partial r}\right), \tag{4.4.4}$$

where μ_0 is the ratio of the viscosity in plasma and core regions, respectively.

For unsteady blood flow, fig.4.12 displays the variation of wall shear stress along with the time (which includes only one cycle for t), for different values of the Reynolds number. It can be clearly observed from the figure that as values of the Reynolds number increase from 0.005 to 0.405 along with the time cycle, shear stress at the wall of the artery also increases. Here, we consider only the plasma velocity (due to the existence of the plasma layer near the arterial wall) to evaluate the wall shear stress in the stenosed artery. Fig.4.13 depicts the variation of wall shear stress along with time as the values of the uniform applied magnetic field increase. From the figure, it is clear that for different values of the magnetic field parameter wall shear stress shows the oscillatory behavior due to the pulsatile nature of the blood flow.

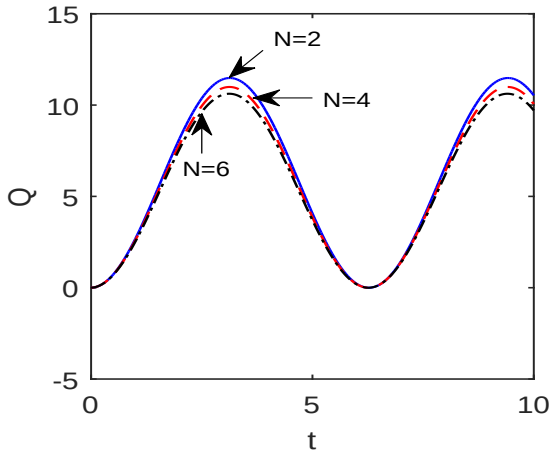

Figure 4.14: Variation of total flow rate with time for different values of N

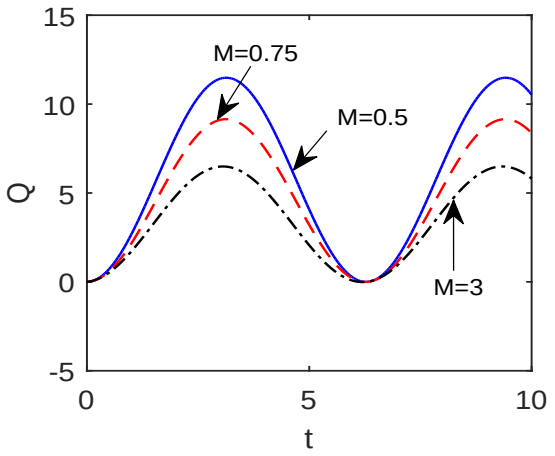

Figure 4.15: Variation of total flow rate with time for different values of M

The total volumetric flow rate of the blood flow in the artery is calculated as

$$Q = 2\pi R^2 \int_0^{R_1} u_c(r,t)dr + 2\pi R^2 \int_{R_1}^{R} u_p(r,t)dr. \tag{4.4.5}$$

Fig.4.14 and fig.4.15 respectively show the flow rate profile of the blood flow along with time t for different values of the radiation and magnetic field parameter. Further, these

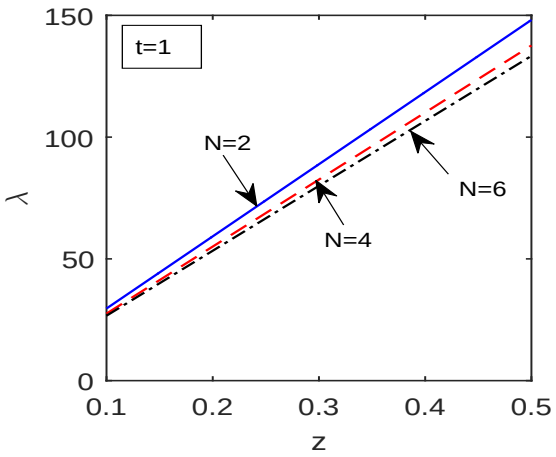

Figure 4.16: Variation of flow impedence for different values of N

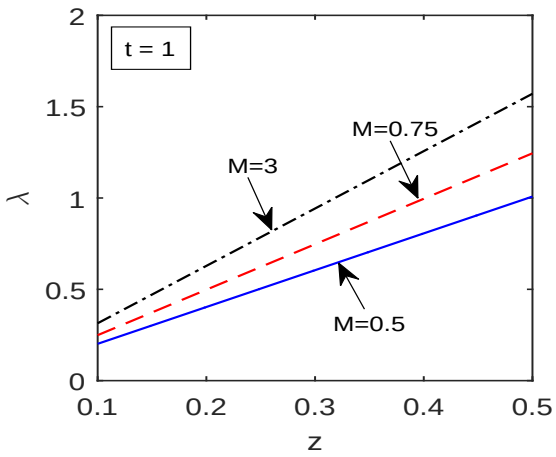

Figure 4.17: Variation of flow impedence for different values of M

figures reveal that as values of the radiation and magnetic field parameter increase, flow rate decreases. Flow rate displays this behavior with magnetic field parameter because blood behaves as electrically conducting fluid and induces electric as well as magnetic field around when it flows under the influence of magnetic field. Therefore, the combined effect of both the forces produces a body force known as "Lorentz force", which has the tendency to oppose the fluid motion (Shit and Roy, 2016).

The flow impedance gives the strong correlation between the localization of stenosis and arterial wall as it important to understand the development of arterial disease. Flow resistance in two-phase blood flow is calculated as

$$\lambda = \int_0^z \frac{P_0 e^{i\omega t}}{Q} dz, \tag{4.4.6}$$

using the value of Q from eq.(4.4.5), we get the final expression for λ. Fig.4.16 and fig.4.17 are plotted to show the impedance profile against the axial distance for different values of the radiation and magnetic field parameter, respectively. From these figures, it can be clearly observed that as values of the radiation parameter increase from 2 to 6, total impedance of the blood flow decreases while impedance shows the reverse effect as values of the magnetic field parameter increase.

Now, to observe the phase difference between pressure gradient and flow rate for pulsatile flow, expression of the longitudinal impedance (which relates the forces acting

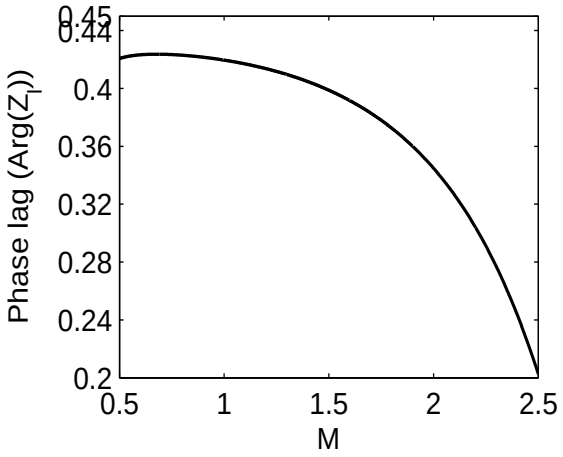

Figure 4.18: Phase lag between pressure gradient and flow resistance with M

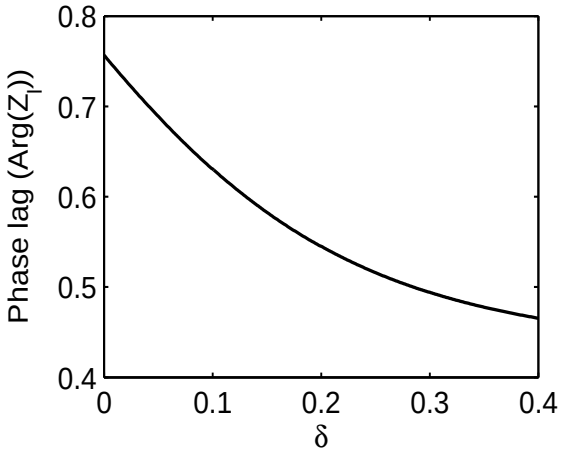

Figure 4.19: Phase lag between pressure gradient and flow resistance with δ

on blood due to the local pressure gradient with the movement of the blood) is used as

$$Z_l = -\frac{1}{Q}\left(\frac{\partial p}{\partial z}\right), \tag{4.4.7}$$

where Q is the flow rate. For pulsatile flow, impedance function is very much important in the analysis of wave propagation, reflection of pressure and flow pulses traveling through an arterial system. Therefore, for pulsatile blood flow figs.4.18-4.19 displays the phase difference between pressure gradient and flow rate with magnetic field parameter and with the variable height of the stenosis, respectively. Fig.4.18 shows that $Arg(Z_l)$ decreases with increase in the magnetic field parameter (M). For smaller values of magnetic field parameter phase difference between pressure gradient and the flow rate is $\frac{\pi}{12}$. From the same figure, we conclude that for high values of magnetic field parameter ($M > 0.5$) phase difference is decreasing between pressure gradient and flow rate. Fig.4.19 illustrates that $Arg(Z_l)$ significantly decreases as the value of the height of the stenosis increases. Further, the same figure reveals that the pressure gradient and flow rate are in the phase difference of $\frac{\pi}{4}$ when there is no stenosis present in the arterial segment and it slowly decreases as values of the height of the stenosis increases.

Figs.4.20-4.25 focuses on displaying the contour plots for the two-phase model of the blood flow through the constricted part of the artery under the action of an applied magnetic field. Under a range of hemodynamic flow, all the contour plots have been

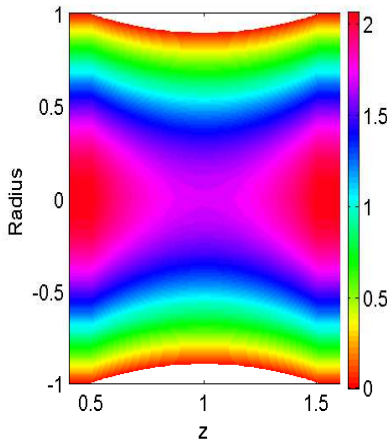

Figure 4.20: Flow analysis for 10% stenosis

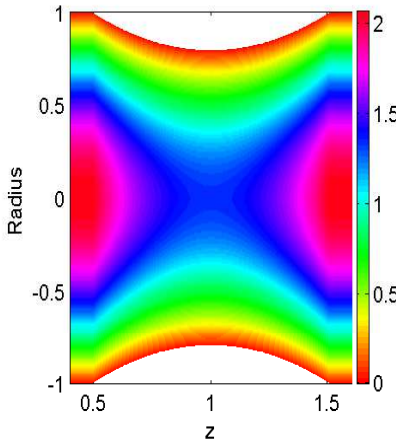

Figure 4.21: Flow analysis for 20% stenosis

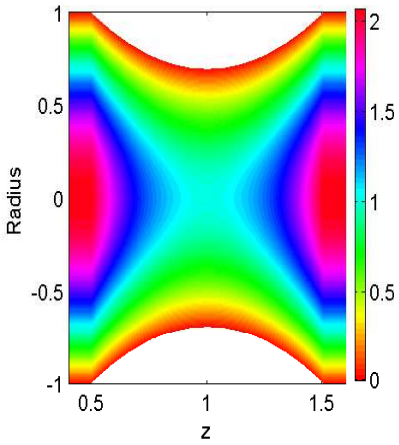

Figure 4.22: Flow analysis for 30% stenosis

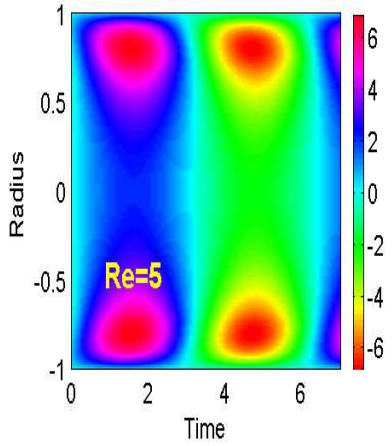

Figure 4.23: Flow analysis at $Re = 10$

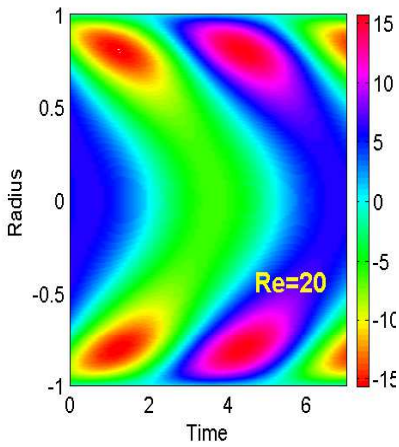

Figure 4.24: Flow analysis at $Re = 30$

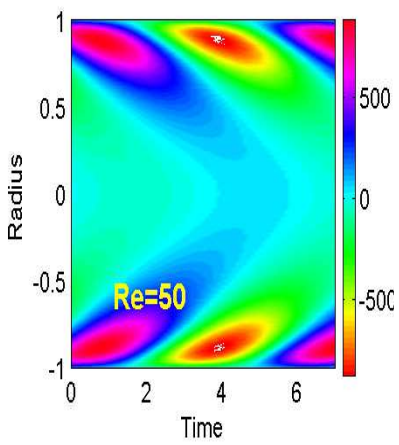

Figure 4.25: Flow analysis at $Re = 50$

plotted by using the data given in Table.4.1. Figs.4.20-4.22 show the velocity contour along the axial direction of the artery as blockage of the artery increases while considering the fixed value of the applied magnetic field as $M = 1$. These figures illustrate the flow patterns of blood in different positions of the artery, viz., entry section, onset, throat and downstream of the stenosis, outlet, where diseased part of the artery varies from $z = 0.5$ to $z = 1.5$ along the artery. It can be clearly noticed from the figures that as blockage of the artery increases the velocity contours strongly gets distorted at the downstream and

slowly appearing trapping bolus shift toward the arterial wall, thereby velocity decreases. For unsteady flow, figs.4.23-4.25 exhibit the flow patterns of blood through the contours of the two-phase blood flow against time for different values of the Reynolds number. These figures capture flow circulation at 10% constriction of the artery when Reynold number varies from $Re = 5$ to $Re = 50$. We observe that the region of flow circulation is small when $Re = 5$ and flow become turbulent for high values of Reynold number and it makes flow locally unstable with respect to large-scale disturbances (Ahmed and Giddens, 1983).

4.5 Conclusions

The main focus of the present study is to investigate the combined effects of the plasma layer thickness, heat and mass transfer on the blood flow through narrow stenosed arteries. Effects of different parameters such as magnetic field, radiation and chemical reaction on flow have been presented for core and plasma regions separately. Important findings obtained from the graphical results are listed herewith:

1. The velocity of the blood flow in narrow arteries decreases as values of the magnetic field parameter increase and velocity of the plasma region attains lower value than the core region. The given result is very much applicable in the medical field since during the surgical process in narrow arteries blood flow can be regulated at the desired level.

2. Increase in the peripheral plasma layer thickness leads to decrease velocity, temperature and concentration profile of the blood flow.

3. The temperature of the blood flow reduces to an appreciable extent in both core and plasma regions, as the values of the radiation parameter increase. Hence, the present study reveals that the temperature of blood flow can be regulated in the narrow arteries by reducing or increasing the effects of the radiation parameter. The result is very much useful in radiation therapy which is used to treat cancer.

4. The concentration profile decreases with increasing the chemical reaction parameter. This happens due to increased molecular diffusivity which directly suppresses the

concentration profile of the flow.

5. The investigation shows that Peclet and Schmidt's number have reducing effects on temperature and concentration of the blood flow, respectively.

6. The high intensity of the magnetic field causes the reduction of the flow rate while it has an enhancing effect on flow impedance.

7. Both flow rate and flow impedance decrease as values of the radiation parameter increase.

8. A comparative study between the present result and the experimental result in a fine glass tube of the cell velocity distribution of blood containing 40% hematocrit, validate the present model. The comparative result shows that the present result gives a good agreement with the experimental results.

9. For pulsatile flow, the phase difference between the pressure gradient and flow rate decreases with applied magnetic field and height of the stenosis.

Chapter 5

Influence of Heat and Mass Transfer on MHD Two-Phase Blood Flow with Radiation

5.1 Introduction

In today's industrialized world, blood flow in our body through arteries pose serious health risks. It is believed that one of the most widespread diseases in humans is atherosclerosis which takes place when hard plaque builds up inside the artery (Pasceri and Yeh, 1999). The hard plaque formation inside the artery limits the flow of blood inside the artery and provides cells of blood to make blood clots near the hardened plaque. Blood clots make the artery even more blocked, and at that time it is increasingly difficult for oxygenated rich blood to reach the heart muscle because of the narrowing of the artery. Nowadays it has gained serious attention from physiologist and researchers to study the blood flow dynamics.

Fåhræus-Lindqvist effect explains when blood flows through a narrow artery then there exists a cell-free plasma layer near the arterial wall (Barbee and Cokelet, 1971). Therefore, in the narrow artery due to the higher concentration of red blood cell near the center and existence of cell-free plasma layer near the arterial wall, blood flow is considered as two-phase fluid flow (Medvedev and Fomin, 2011). Cokelet and Goldsmith (1991)

through In vitro analysis observed the phenomenon in a tube of 172-μm diameter and suggested that the two-phase flow of a suspension may lead to a decrease in the hydrodynamic resistance. Ponalagusamy and Selvi (2011) presented a mathematical model of two-phase blood flow, considering axially variable peripheral layer thickness and obtained the analytic expressions for peripheral layer thickness, core viscosity, slip velocity and wall shear stress.

Many cardiovascular diseases such as stenosis which is responsible for the deaths of people are mainly related to the flow behavior and hemodynamic conditions of an artery. Srivastava (1996) presented a two-phase model of blood flow in the presence of a peripheral plasma layer, considering the presence of the stenosis inside an artery. Further, Riahi (2016) proposed the modeling of two-phase blood flow through a stenosed artery by choosing its form based on the available experimental data. He found that in narrow artery blood pressure gradient gets affected and increased significantly in the presence of stenosis.

Blood is an electrically conducting fluid which is greatly affected by the presence of an external magnetic field. Magnetohydrodynamics (MHD) is the study which deals with the magnetic properties of an electrically conducting fluid, including Lorentz force due to induced electric as well as the magnetic fields (Sharma et al., 2015b). Ali et al. (2017) studied the MHD effects on blood flow assuming blood as a Casson fluid, along with the magnetic particles. With the help of their study, they found that the magnetic field reduces the velocities of both magnetic particles and as well as the blood. To study the effects of magnetic field on two-phase blood flow, Ponalagusamy and Selvi (2015) presented a mathematical model of heat transfer on two-phase blood flow considering the effects of an applied magnetic field. Further, Ponalagusamy and Priyadharshini (2018) analyzed a two-fluid model of blood flow in the presence of an external magnetic field by assuming the characteristics of a micropolar fluid in the core region and Newtonian nature of the fluid in the plasma region. Authors reported that increased intensity of an applied magnetic field increases the resistive impedance which reduces the required amount of blood supply to vital organs.

In the past, there have been a number of studies to examine the heat transfer effect in

narrow arteries. A numerical investigation of unsteady flow has been done by Majee and Shit (2017) to investigate the heat transfer effects on MHD blood flow through a stenosed arterial segment. They reported that the temperature profile of the blood flow increases as values of the magnetic field parameter increase. They found that the given result is very much applicable in the hyperthermic treatment of the tumor. Garcia and Riahi (2014) examined the heat transfer effect on the two-phase blood flow through a stenosed artery with viscous heating effect. They analyzed that the generation of heat in the blood due to the viscous heating effect is significant enough to make the blood temperature higher than the temperature on the surface of the artery. Abbas et al. (2014) studied the MHD two-phase fluid flow with heat transfer in an inclined channel by considering velocity slip and thermal slip conditions. They investigated that the temperature profile of blood flow increases as the values of thermal slip parameter increase.

All the above-mentioned studies were focused on analyzing the momentum and heat transfer phenomenon on the two-phase model of the blood flow. With the help of the literature and to the best knowledge of the authors, it is found that the influence of mass transfer on two-phase blood flow is still not done by the researchers. The present article analyzes the heat and mass transfer effects on two-phase blood flow through a stenosed artery in the presence of an external magnetic field with radiation. Exact solutions have been calculated for the nonlinear differential equations of momentum, energy and concentration, considering the pulsatile nature of the flow. With the aim of having an adequate insight into the problem graphs for flow resistance, total flow rate and wall shear stress have been plotted with different quantities of interest.

5.2 Mathematical Model

Let us consider the two-phase model of the blood flow consists of a core region (a suspension of the uniform hematocrit) of radius $\bar{R}_1(\bar{z})$ and a cell-free plasma layer of radius $\bar{R}(\bar{z})$ through a cylindrical stenosed artery of radius $\bar{R}_0$. It is assumed that blood flows through the stenosed artery under the influence of an external magnetic field with radiation. In which magnetic field works perpendicular to the flow direction as shown in fig.5.1. In the

artery, shear rates are considered to be high enough so that the fluid can be treated as Newtonian in the core and the plasma layer (Sharan and Popel, 2001). Viscosities of the core and the plasma regions are taken as

$$\bar{\mu}(\bar{r}) = \begin{cases} \bar{\mu_c} & for \quad 0 \leq r \leq \bar{R_1}(\bar{z}), \\ \bar{\mu_p} & for \quad \bar{R_1}(\bar{z}) \leq r \leq \bar{R}(\bar{z}). \end{cases}$$

Geometry of the stenosis in plasma and core regions are defined as (Sankar and Lee, 2007).

$$\frac{\bar{R}(\bar{z})}{\bar{R_0}} = \begin{cases} 1 - \frac{\bar{\delta_s} n^{\frac{n}{n-1}}}{\bar{R_0} \bar{L_0}^n (n-1)} \left(\bar{L_0}^{n-1} (\bar{z} - \bar{d}) - (\bar{z} - \bar{d})^n \right) & \text{for} \quad \bar{d} \leq \bar{z} \leq \bar{d} + \bar{L}_0, \\ 1, & \text{otherwise}, \end{cases} \tag{5.2.1}$$

$$\frac{\bar{R}(\bar{z})}{\bar{R_0}} = \begin{cases} \beta - \frac{\bar{\delta_s} n^{\frac{n}{n-1}}}{\bar{R_0} \bar{L_0}^n (n-1)} \left(\bar{L_0}^{n-1} (\bar{z} - \bar{d}) - (\bar{z} - \bar{d})^n \right) & \text{for} \quad \bar{d} \leq \bar{z} \leq \bar{d} + \bar{L}_0, \\ \beta, & \text{otherwise}, \end{cases} \tag{5.2.2}$$

where β is the ratio of the central core radius to the normal artery radius, n determines the shape of the constriction profile (Nadeem et al., 2011) and $\bar{\delta_s}$ indicates the maximum height of the stenosis located at $\bar{z} = \bar{d} + \frac{\bar{L_0}}{n^{\frac{1}{(n-1)}}}$.

Now, under all these assumptions, equations for momentum, energy and concentration for the core region are given by

$$\bar{\rho_c} \frac{\partial \bar{u}_c}{\partial \bar{t}} = -\frac{\partial \bar{p}}{\partial \bar{z}} + \bar{\mu_c} \left(\frac{\partial^2 \bar{u}_c}{\partial \bar{r}^2} + \frac{1}{\bar{r}} \frac{\partial \bar{u}_c}{\partial \bar{r}} \right) - \bar{\sigma} {\bar{B_0}}^2 \bar{u_c}, \tag{5.2.3}$$

$$\bar{\rho_c} \bar{c_c} \frac{\partial \bar{T}_c}{\partial \bar{t}} = \bar{K_c} \left(\frac{\partial^2 \bar{T}_c}{\partial \bar{r}^2} + \frac{1}{\bar{r}} \frac{\partial \bar{T}_c}{\partial \bar{r}} \right) - \frac{\partial \bar{q_c}}{\partial \bar{r}}, \tag{5.2.4}$$

$$\frac{\partial \bar{C}_c}{\partial \bar{t}} = \bar{D_c} \left(\frac{\partial^2 \bar{C}_c}{\partial \bar{r}^2} + \frac{1}{\bar{r}} \frac{\partial \bar{C}_c}{\partial \bar{r}} \right). \tag{5.2.5}$$

Similarly, the governing equations of momentum, energy and concentration for plasma region are given by

$$\bar{\rho_p} \frac{\partial \bar{u}_p}{\partial \bar{t}} = -\frac{\partial \bar{p}}{\partial \bar{z}} + \bar{\mu_p} \left(\frac{\partial^2 \bar{u}_p}{\partial \bar{r}^2} + \frac{1}{\bar{r}} \frac{\partial \bar{u}_p}{\partial \bar{r}} \right) - \bar{\sigma} {\bar{B_0}}^2 \bar{u_p}, \tag{5.2.6}$$

$$\bar{\rho_p} \bar{c_p} \frac{\partial \bar{T}_p}{\partial \bar{t}} = \bar{K_p} \left(\frac{\partial^2 \bar{T}_p}{\partial \bar{r}^2} + \frac{1}{\bar{r}} \frac{\partial \bar{T}_p}{\partial \bar{r}} \right) - \frac{\partial \bar{q_p}}{\partial \bar{r}}, \tag{5.2.7}$$

$$\frac{\partial \bar{C}_p}{\partial \bar{t}} = \bar{D_p} \left(\frac{\partial^2 \bar{C}_p}{\partial \bar{r}^2} + \frac{1}{\bar{r}} \frac{\partial \bar{C}_p}{\partial \bar{r}} \right), \tag{5.2.8}$$

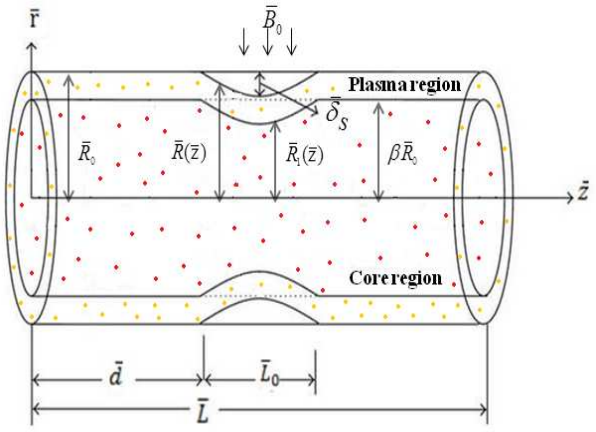

Figure 5.1: Geometry of the stenosed artery of length $\bar{L}$

from eqs.(5.2.3)-(5.2.8) subscripts c and p stand for the coefficients defined in core and plasma regions respectively. Where $\bar{B}_0$ is the magnetic field intensity, $\bar{\sigma}$ represents the electrical conductivity of the blood, $\frac{\partial \bar{p}}{\partial \bar{z}}$ stands for the pressure gradient. $\bar{D}$ is the coefficient of mass diffusivity, $\bar{\rho}$ is the density, $\bar{c}$ is the specific heat and $\bar{K}$ represents the thermal conductivity and $\bar{u}$, $\bar{T}$ and $\bar{C}$ are the velocity, temperature and concentration of the blood flow. Terms $\frac{\partial \bar{q}_c}{\partial \bar{r}}$ in eq.(5.2.4) and $\frac{\partial \bar{q}_p}{\partial \bar{r}}$ in eq.(5.2.7) are due to the radiation effect and these are defined as

$$\frac{\partial \bar{q}_c}{\partial \bar{r}} = 4\bar{\alpha_c}^2 \left(\bar{T}_c - \bar{T}_0\right), \quad \frac{\partial \bar{q}_p}{\partial \bar{r}} = 4\bar{\alpha_p}^2 \left(\bar{T}_p - \bar{T}_0\right). \tag{5.2.9}$$

Note that as plasma and blood in the physiological conditions are optically thin fluids of very low density the values of mean radiation absorption coefficient $\bar{\alpha_c}$ and $\bar{\alpha_p}$ of core and plasma are considered here $\bar{\alpha} \lll 1$, (Ogulu and Abbey, 2005).

The appropriate boundary conditions for the model under consideration are as follows:

$$\begin{cases} \bar{u_p} = 0, \quad \bar{T}_p = \bar{T_w}, \quad \bar{C_p} = \bar{C_w} \quad at \quad \bar{r} = \bar{R}(\bar{z}), \\ \bar{u_c} = \bar{u_p}, \quad \bar{T}_p = \bar{T_c}, \quad \bar{C_p} = \bar{C_c} \quad at \quad \bar{r} = \bar{R}_1(\bar{z}), \\ \frac{\partial \bar{u_c}}{\partial \bar{r}} = 0, \quad \frac{\partial \bar{T_c}}{\partial \bar{r}} = 0, \quad \frac{\partial \bar{C_c}}{\partial \bar{r}} = 0 \quad at \quad \bar{r} = 0, \\ \bar{\tau_c} = \bar{\tau_p}, \quad \frac{\partial \bar{T_c}}{\partial \bar{r}} = \frac{\partial \bar{T_p}}{\partial \bar{r}}, \quad \frac{\partial \bar{C_c}}{\partial \bar{r}} = \frac{\partial \bar{C_p}}{\partial \bar{r}} \quad at \quad \bar{r} = \bar{R}_1(\bar{z}). \end{cases} \tag{5.2.10}$$

Now, we introduce the following dimensionless parameters:

$$u_c = \frac{\bar{u_c}}{\bar{u_0}}, \quad r = \frac{\bar{r}}{\bar{R}_0}, \quad z = \frac{\bar{z}}{\bar{R}_0}, \quad t = \bar{\omega}\bar{t}, \quad R(z) = \frac{\bar{R}(\bar{z})}{\bar{R}_0}, \quad D_0 = \frac{\bar{D}_p}{\bar{D}_c},$$

$$p=\frac{\bar{R}_0\bar{p}}{\bar{u}_0\bar{\mu}_p},\quad \delta=\frac{\bar{\delta}_s}{\bar{R}_0}, Re=\frac{\bar{\rho}_p{\bar{R}_0}^2\omega}{\bar{\mu}_p},\quad \theta_c=\frac{(\bar{T}_c-\bar{T}_0)}{\bar{T}_w-\bar{T}_0},\quad \sigma_c=\frac{(\bar{C}_c-\bar{C}_0)}{\bar{C}_w-\bar{C}_0},\quad u_p=\frac{\bar{u}_p}{\bar{u}_0},$$

$$\theta_p=\frac{(\bar{T}_p-\bar{T}_0)}{\bar{T}_w-\bar{T}_0},\quad \sigma_p=\frac{(\bar{C}_p-\bar{C}_0)}{\bar{C}_w-\bar{C}_0},\quad \mu_0=\frac{\bar{\mu}_p}{\bar{\mu}_c},\quad N^2=\frac{4{\bar{R}_0}^2{\bar{\alpha}_p}^2}{\bar{K}_p},\quad M^2=\frac{\bar{\sigma}{\bar{B}_0}^2{\bar{R}_0}^2}{\bar{\mu}_p},$$

$$Pe=\frac{\bar{\rho}_p\bar{c}_p{\bar{R}_0}^2\bar{\omega}}{\bar{K}_p},\quad Sc=\frac{\bar{\mu}_p}{\bar{D}_p\bar{\rho}_p},\quad \rho_0=\frac{\bar{\rho}_p}{\bar{\rho}_c}.$$

Meaning of the above mentioned notations are already given in earlier chapters 2, 3 and 4.

Therefore, eqs.(5.2.3)-(5.2.5) of the core region in non dimensional form can be represented as

$$\left(\frac{Re}{\rho_0}\right)\frac{\partial u_c}{\partial t}=-\frac{\partial p}{\partial z}+\frac{1}{\mu_0}\left(\frac{\partial^2 u_c}{\partial r^2}+\frac{1}{r}\frac{\partial u_c}{\partial r}\right)-M^2u_c, \tag{5.2.11}$$

$$\frac{PeK_0}{\rho_0 s_0}\left(\frac{\partial\theta_c}{\partial t}\right)=\left(\frac{\partial^2\theta_c}{\partial r^2}+\frac{1}{r}\frac{\partial\theta_c}{\partial r}\right)-\frac{K_0}{\alpha_0}N^2\theta_c, \tag{5.2.12}$$

$$Re\left(\frac{\partial\sigma_c}{\partial t}\right)=\frac{1}{D_0}\left(\frac{1}{Sc}\right)\left(\frac{\partial^2\sigma_c}{\partial r^2}+\frac{1}{r}\frac{\partial\sigma_c}{\partial r}\right), \tag{5.2.13}$$

and, eqs.(5.2.6)-(5.2.8) of the plasma region can be expressed as

$$Re\frac{\partial u_p}{\partial t}=-\frac{\partial p}{\partial z}+\left(\frac{\partial^2 u_p}{\partial r^2}+\frac{1}{r}\frac{\partial u_p}{\partial r}\right)-M^2u_p, \tag{5.2.14}$$

$$Pe\frac{\partial\theta_p}{\partial t}=\left(\frac{\partial^2\theta_p}{\partial r^2}+\frac{1}{r}\frac{\partial\theta_p}{\partial r}\right)-N^2\theta_p, \tag{5.2.15}$$

$$Re\left(\frac{\partial\sigma_p}{\partial t}\right)=\left(\frac{1}{Sc}\right)\left(\frac{\partial^2\sigma_p}{\partial r^2}+\frac{1}{r}\frac{\partial\sigma_p}{\partial r}\right). \tag{5.2.16}$$

Similarly, the corresponding boundary conditions eq.(5.2.10) in non-dimensional form are given as

$$\begin{cases} u_p=0, & \theta_p=1, & \sigma_p=1 & at & r=R(z),\\ u_p=u_c, & \theta_p=\theta_c, & \sigma_p=\sigma_c & at & r=R_1(z),\\ \tau_c=\tau_p, & \frac{\partial\theta_c}{\partial r}=\frac{\partial\theta_p}{\partial r}, & \frac{\partial\sigma_c}{\partial r}=\frac{\partial\sigma_p}{\partial r} & at & r=R_1(z),\\ \frac{\partial u_c}{\partial r}=0, & \frac{\partial\theta_c}{\partial r}=0, & \frac{\partial\sigma_c}{\partial r}=0 & at & r=0. \end{cases} \tag{5.2.17}$$

5.3 Solution

In this section, we solve the momentum, temperature and concentration eqs.(5.2.11)-(5.2.16) for both core and plasma regions under the given boundary conditions eq.(5.2.17). Since pumping action of the heart results in the pulsatile nature of the blood flow, we assume pressure gradient, velocity, temperature and concentration are in the form of

$$\begin{cases} -\frac{\partial p}{\partial z} = P_0 e^{i\omega t}, \quad u_c(r,t) = u_{c_0}(r)e^{i\omega t}, \quad u_p(r,t) = u_{p_0}(r)e^{i\omega t}, \\ \theta_c(r,t) = \theta_{c_0}(r)e^{i\omega t}, \quad \theta_p(r,t) = \theta_{p_0}(r)e^{i\omega t}, \\ \sigma_c(r,t) = \sigma_{c_0}(r)e^{i\omega t}, \quad \sigma_p(r,t) = \sigma_{p_0}(r)e^{i\omega t}. \end{cases} \tag{5.3.1}$$

Now using eq.(5.3.1), eqs.(5.2.11)-(5.2.13) can be converted in the form of

$$\left(\frac{\partial^2 u_{c_0}}{\partial r^2} + \frac{1}{r}\frac{\partial u_{c_0}}{\partial r}\right) - \left(M^2 + \frac{\mu_0 Re}{\rho_0} i\right) u_{c_0} = -P_0\mu_0, \tag{5.3.2}$$

$$\frac{\partial^2 \theta_{c_0}}{\partial r^2} + \frac{1}{r}\frac{\partial \theta_{c_0}}{\partial r} - \left(\frac{K_0 N^2}{\alpha_0} + i\frac{Pe}{\rho_0}\left(\frac{K_0}{s_0}\right)\right)\theta_{c_0} = 0, \tag{5.3.3}$$

$$\frac{\partial^2 \sigma_{c_0}}{\partial r^2} + \frac{1}{r}\frac{\partial \sigma_{c_0}}{\partial r} - (iReD_0Sc)\,\sigma_{c_0} = 0. \tag{5.3.4}$$

Similarly, substituting eq.(5.3.1) into eqs.(5.2.14)-(5.2.16), we get

$$\left(\frac{\partial^2 u_{p_0}}{\partial r^2} + \frac{1}{r}\frac{\partial u_{p_0}}{\partial r}\right) - \left(M^2 + Rei\right) u_{p_0} = -P_0, \tag{5.3.5}$$

$$\frac{\partial^2 \theta_{p_0}}{\partial r^2} + \frac{1}{r}\frac{\partial \theta_{p_0}}{\partial r} - \left(N^2 + iPe\right)\theta_{p_0} = 0, \tag{5.3.6}$$

$$\frac{\partial^2 \sigma_{p_0}}{\partial r^2} + \frac{1}{r}\frac{\partial \sigma_{p_0}}{\partial r} - iReSc\sigma_{p_0} = 0. \tag{5.3.7}$$

Remark 5.1. Note that the system of ODEs, eqs.(5.3.2)-(5.3.7) along with the boundary conditions (eq.(5.2.17)) admits an exact solution using the definition of Bessel functions.

Therefore, final solutions for temperature and concentration considering unsteady flow of core and plasma regions respectively, are as follows

$$\theta_c(r,t) = \left[(U_1S_1 + U_2)\,J_0(\sqrt{\beta_1}(r))\right] e^{i\omega t}, \tag{5.3.8}$$

$$\theta_p(r,t) = \left[S_1\left(J_0(\sqrt{\beta_2}r) - \frac{J_0(\sqrt{\beta_2}R}{Y_0(\sqrt{\beta_2}R}Y_0(\sqrt{\beta_2}r)\right) + \frac{Y_0(\sqrt{\beta_2}r)}{Y_0(\sqrt{\beta_2}R)}\right] e^{i\omega t}. \tag{5.3.9}$$

$$\sigma_c(r,t) = [U_4 S_2 + U_5]\, J_0(\sqrt{\gamma_1'}(r)) e^{i\omega t}, \tag{5.3.10}$$

$$\sigma_p(r,t) = \left[S_2 \left(J_0(\sqrt{\gamma_2'} r) - \frac{J_0(\sqrt{\gamma_2'} R}{Y_0(\sqrt{\gamma_2'} R}) Y_0(\sqrt{\gamma_2'} r) \right) + \frac{Y_0(\sqrt{\gamma_2'} r)}{Y_0(\sqrt{\gamma_2'} R)} \right] e^{i\omega t}, \tag{5.3.11}$$

where $S_1 = \frac{\sqrt{\beta_2} Y_1(\sqrt{\beta_2} R_1)}{U_3 Y_0(\sqrt{\beta_2} R)} - \frac{\sqrt{\beta_1} U_2 J_1(\sqrt{\beta_1} R_1)}{U_3}$, $S_2 = \left(\frac{\sqrt{\gamma_2'} Y_1(\sqrt{\gamma_2'} R_1)}{U_6 Y_0(\sqrt{\gamma_2'} R)} - \frac{\sqrt{\gamma_1'} U_5 J_1(\sqrt{\gamma_1'} R_1)}{U_6} \right)$ and constants β_1, β_2, γ_1', γ_2', U_1, U_2, U_3, U_4, U_5 and U_6 are given in Appendix A.

Now, we calculate the solution for the eq.(5.3.2)

$$\left(\frac{\partial^2 u_{c_0}}{\partial r^2} + \frac{1}{r} \frac{\partial u_{c_0}}{\partial r} \right) - \left(M^2 + \frac{\mu_0 Re}{\rho_0} i \right) u_{c_0} = -P_0 \mu_0. \tag{5.3.12}$$

The general solution of the eq.(5.3.12) is calculated using variation of parameters method as

$$u_{c_0} = C_1 J_0(\sqrt{\lambda_1} r) + C_2 Y_0(\sqrt{\lambda_1} r) + A_1 J_0(\sqrt{\lambda_1}) r + B_1 Y_0(\sqrt{\lambda_1} r). \tag{5.3.13}$$

where C_1, C_2 are the arbitrary constants and A_1, B_1 are defined as

$$A_1 = -\frac{\pi r}{2} \int Y_0(\sqrt{\lambda_1} r) P_0 \mu_0 \quad dr,$$
$$B_1 = \frac{\pi r}{2} \int J_0(\sqrt{\lambda_1} r) P_0 \mu_0 \quad dr.$$

Similarly, for the plasma region the general solution for the eq.(5.3.5) is

$$u_{p_0} = C_3 J_0(\sqrt{\lambda_2} r) + C_4 Y_0(\sqrt{\lambda_2} r) + A_2 J_0(\sqrt{\lambda_2} r) + B_2 Y_0(\sqrt{\lambda_2} r). \tag{5.3.14}$$

Now, using boundary conditions eq.(5.2.17) into eq.(5.3.13) and eq.(5.3.14), we get $C_2 = 0$ and the linear system in terms of C_1, C_3, C_4 as

$$\begin{pmatrix} J_0(\sqrt{\lambda_1} R_1) & -J_0(\sqrt{\lambda_2} R_1) & -Y_0(\sqrt{\lambda_2} R_1) \\ 0 & J_0(\sqrt{\lambda_2} R) & Y_0(\sqrt{\lambda_2} R) \\ -\sqrt{\lambda_1} J_1(\sqrt{\lambda_1} R_1) & \sqrt{\lambda_2} J_1(\sqrt{\lambda_2} R_1) & \sqrt{\lambda_2} Y_1(\sqrt{\lambda_2} R_1) \end{pmatrix} \begin{pmatrix} C_1 \\ C_3 \\ C_4 \end{pmatrix} = \begin{pmatrix} D_1 \\ D_2 \\ D_3 \end{pmatrix} \tag{5.3.15}$$

where values of λ_1, λ_2,D_1, D_2 and D_3 are given in Appendix A. Under the given set of boundary conditions the linear system eq.(5.3.15) admits a unique solution.

5.4 Results and Discussion

In this section, graphical results are presented to analyze the effects of various dimensionless parameters on velocity, temperature and concentration profiles of the blood flow. In which value of the radius of the core region is taken as 0.7, by considering the radius of the stenosed artery as 0.9. In all the graphical results, the effect of a particular parameter on plasma region has been displayed using the dim black dotted lines. Default values which have been used to graphically analyze the effectiveness of the model are as follows: $N = 2$, $K_0 = 0.4$, $\rho_0 = 1.05$, $Pe = 0.87$ $Sc = 0.5$, $Re = 0.9$, $L_0 = 1$, $M = 3$, $\delta = 0.1$.

Fig.5.2 shows the variation of the velocity profile of blood flow for different values of the magnetic field parameter (M). It is clear from the figure that as the values of the magnetic field parameter increase, the value of the velocity profile decreases in both core as well as in plasma regions. This happens due to the Lorentz force which acts as a resistive drag force. An action of which makes red blood cell more suspended in the fluid by increasing the internal viscosity of the fluid. This results in a decrease velocity profile of the core region which directly affects the velocity of the plasma region due to the continuous behavior of the flow lines at the interface region of core and plasma. Therefore, the velocity of the plasma region also decreases as values of the magnetic field parameter increase. Fig.5.3 displays the variation of the temperature profile of the core

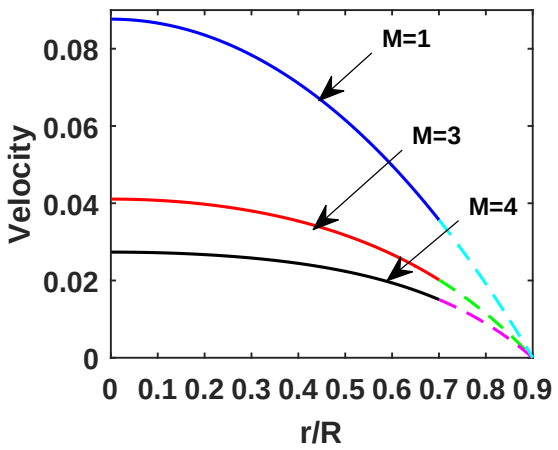

Figure 5.2: Variation of velocity profile with M.

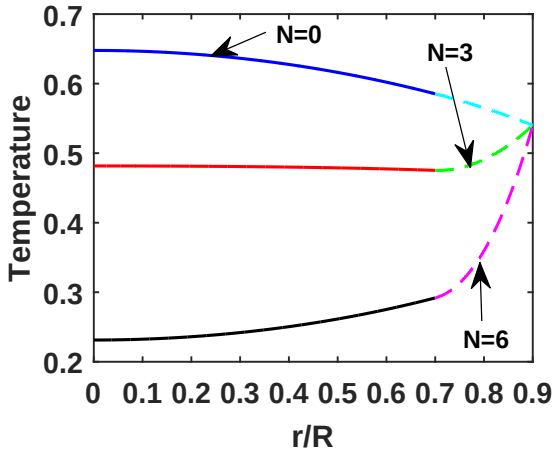

Figure 5.3: Variation of temperature profile with N.

and plasma regions with radiation parameter (N). It can be clearly observed from the figure that as the values of the radiation parameter increase, temperature profile of the blood flow decreases. Therefore, when plasma separates from the red blood cell as in two-phase analysis, temperature profile attains lower values in core region than in the plasma region because of the buoyancy force which exists due to the radiation effect. Further, the same figure reveals that with no radiation effect, temperature profile shows exactly opposite behavior for core and plasma regions by attaining higher values in the core region than the plasma region. Variation of concentration profile for different values

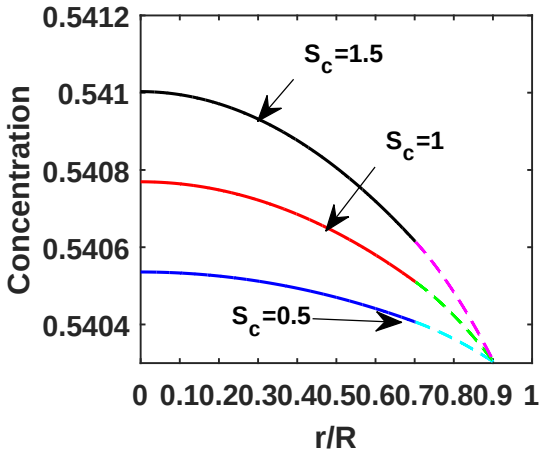

Figure 5.4: Variation of concentration profile with Sc.

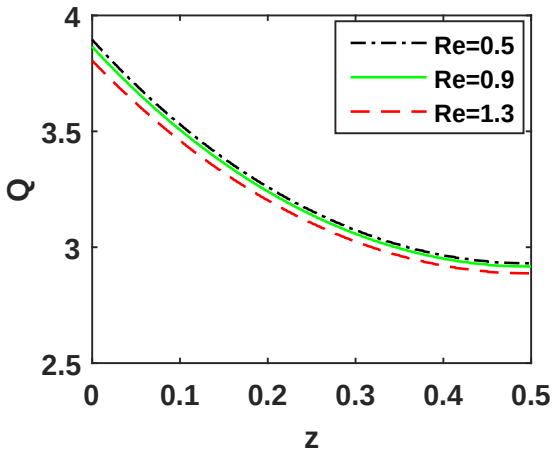

Figure 5.5: Variation of flow rate for different values of Re.

of the Schmidt number (Sc) has been displayed in fig.5.4. From the figure, it is clear that as values of the Schmidt number increase, the concentration profile of the core and the plasma regions increases. Further, the same figure exhibits that for any particular value of the Schmidt number concentration profile of the core region attains higher values than the concentration profile of the plasma region.

The total volumetric flow rate (Q) and flow resistance (λ) are calculated as

$$Q = 2\pi R^2 \int_0^{R_1} u_c(r,t)dr + 2\pi R^2 \int_{R_1}^{R} u_p(r,t)dr, \tag{5.4.1}$$

$$\lambda = \int_0^z \frac{P_0 e^{i\omega t}}{Q} dz. \tag{5.4.2}$$

Fig.5.5 has been plotted for the flow rate profile of the blood flow against the axial distance z of the artery (values of which covers only the diseased part of the artery) for different values of the Reynolds number. It can be clearly observed from the figure that as values of the Reynolds number increase, flow rate of the blood flow within the stenosed artery decreases. Fig.5.6 displays the flow impedance profile of the blood flow against the axial

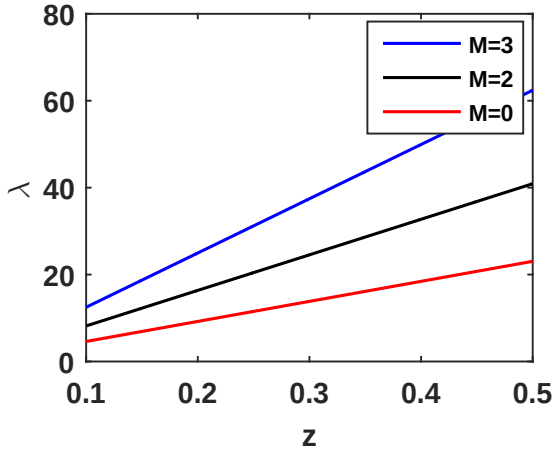

Figure 5.6: Flow impedance for different values of M.

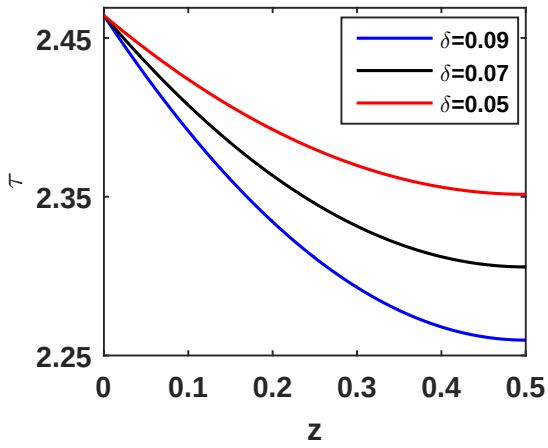

Figure 5.7: Variation of wall shear stress with δ.

distance for different values of the magnetic field parameter. From the figure, it can be noticed that as values of the magnetic field parameter increase, the impedance profile also increases. This happens because the high intensity of the applied magnetic field increases the internal viscosity of the fluid which directly affects the fluid resistance to flow.

At the outer wall of the artery shear stress is determined as

$$\tau = -\frac{1}{\mu_0}\left(\frac{\partial u_p}{\partial r}\right). \tag{5.4.3}$$

Fig.5.7 shows the variation of wall shear stress against the axial distance with variable height of the stenosis. From the figure, it is clear that as values of the height of the stenosis increase from 0.05 to 0.09, shear stress at stenosis throat decreases, respectively.

Comparison of results

Table. 5.1 gives a comparison between the results computed on the basis of the present study with those of Sharma et al. (2015b). Values of the parameters for both of these studies are considered as $N = 0$, $Pe = 0.1$, $Sc = 0.1$ $Re = 0.9$, $\delta = 0$ $M = 1$, $P0 = 2.16$. Present study converts to the case of a single phase blood flow (in which plasma and red blood cell are uniformly distributed throughout the artery by following the same flow dynamics) with no radiation effect when we consider values as $R1 = 1$, $N = 0$ and $R = 1$. For the given value of the parameters, result in the Table 5.1 displays that the present model maintains a good agreement with the result given by Sharma et al. (2015b).

Table 5.1: Comparative results of Velocity distribution.

r	0.00276243	0.198895	0.400552	0.599448	0.798343	1
Sharma **et al.**	0.264906	0.256981	0.232075	0.187925	0.11434	0
Our result	0.2717	0.2647	0.2407	0.1939	0.1154	0

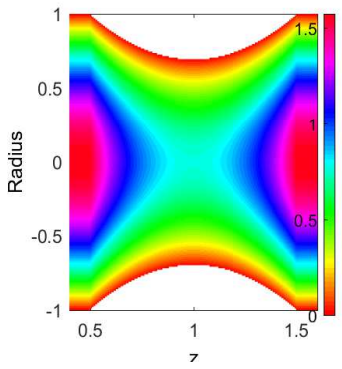

Figure 5.8: Velocity Contour for 20% stenosis.

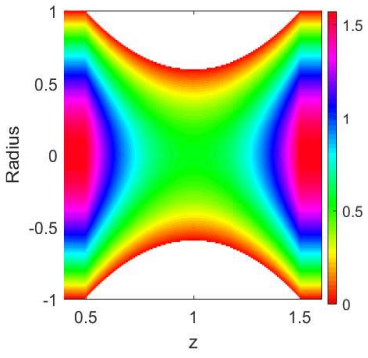

Figure 5.9: Velocity Contour for 40% stenosis.

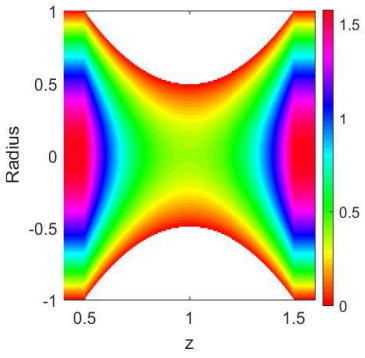

Figure 5.10: Velocity Contour 50% stenosis.

Figs.5.8-5.10 show the magnetic field induced streamlines for 20%, 40% and 50% of the arterial blockage. From the figures, it is clear that the showing symmetry about the center line these streamlines reveal that as the height of the blocked area increases more and more re-circulation zones appear around the center of the artery. To compare these results one may also record from these patterns that the number of flow lines increases

near the center of the artery as the height of the stenosis increases. Thus the deviation of the patterns of flow lines can be used to estimate the influence of increasing height of the stenosis on blood flow.

5.5 Conclusions

In the present study, we have theoretically analyzed the effects of heat and mass transfer on the two-phase model of the blood flow through a stenosed artery, under the influence of an applied magnetic field with thermal radiation. Considering Newtonian fluid in the core and the plasma regions, the mathematical model of coupled nonlinear differential equations have been developed for momentum, concentration, and energy equations of the blood flow. The study enables us to conclude the following:

1. It is evident from the graphical result that the increasing intensity of an applied magnetic field leads to the decreased velocity of both core and the plasma regions. It implies that the blood velocity in the narrow artery can be regulated under the influence of an applied magnetic field. This result can be helpful for the medical personnel at the time of the surgical process in a human body.

2. The high values of the radiation parameter in the narrow artery decreases the temperature of the blood flow. This result has important relevance in the therapeutic procedure of hyperthermia which treats cancer.

3. The study reveals that increasing values of the Schmidt number give rise to an increased concentration of the blood flow.

4. Results show that the flow rate of the blood flow in narrow artery decreases as values of the Reynolds number increase and the shear stress at stenosis throat decreases with increasing values of the height of the stenosis.

Chapter 6

Influence of Heat and Mass Transfer on Two-Phase Blood Flow with Joule Heating and Variable Viscosity In the Presence of Variable Magnetic Field

6.1 Introduction

To quantitate the analysis of the blood flow through the smaller size of blood vessels as arterioles and venules, it is necessary to consider the rheological properties of the blood flow. One of the major characteristics of blood flow is the volume percentage of the erythrocytes in the blood. In the literature, it has been already shown through *in vitro* and *in vivo* analysis that when the blood flows through a narrow artery, there exists a cell-free plasma layer near the wall due to Fåhræus effect (Chebbi, 2015; Cokelet and Goldsmith, 1991; Sharan and Popel, 2001). Therefore, when blood flows through narrow arteries, the two-phase nature of blood as a suspension becomes significant as the diameter of the red blood cell becomes comparable to the arterial diameter. Therefore, in the smaller arteries at very low shear stress, aggregation of red blood cells leads to the

two-phase flow which consists of an inner core region of red blood cells surrounded by cell depleted plasma layer. According to the fluid mosaic model, both red blood cells in the core region (as they are mostly composed of water) and the plasma layer near the arterial wall itself shows the fluid properties (Rubenstein et al., 2015).

Considering different viscosity of the core region than the plasma region and assuming erythrocyte distribution by the step function, Medvedev and Fomin (2011) compared the experimental values with the calculated values of relative observed viscosity. With the help of *in vitro* and *in vivo* data Pries et al. (1992, 1994, 1990) established an empirical relationship between relative apparent viscosity and mean tube hematocrit as a function of tube diameter and discharge hematocrit. Authors found a significantly higher blood flow resistance in tubes of diameters less than 40 μm "*in vivo* viscosity law" compared with the results of "*in vitro* viscosity law" in a smooth glass tube. Ponalagusamy and Selvi (2013) presented a mathematical model for narrow arteries with a core region containing red blood cells and cell-free region of plasma. Considering radially varying viscosity of the core region with the hematocrit level, they observed that increased viscosity of the core fluid enhances the resistance force which slows down the velocity of the flow of blood.

In the cardiovascular system of our human body, narrowing of an artery due to the deposition of fatty substances and cholesterol causes to a medical condition known as stenosis (Bakheet et al., 2016). Presence of stenosis inside an inner wall of the artery changes its flow pattern and hemodynamic conditions. Recently, many theoretical, as well as experimental studies, have been done to investigate the flow characteristics of the arterial lumen of a blood vessel due to the presence of stenosis (Ikbal et al., 2009; Majee and Shit, 2017; Misra and Shit, 2006). For two-phase blood flow, considering Newtonian fluid in both core and plasma regions, Srivastava (1996) examined the effects of red cell concentration and peripheral layer on flow characteristics in the presence of mild stenosis. Sankar and Lee (2007) analyzed the effects of stenosis on two-phase blood flow assuming core region as a Herschel-Bulkley fluid and the plasma in the peripheral layer as a Newtonian fluid and reported that the plug core radius and resistance to flow increase as the size of the stenosis increases.

There are so many important technological problems that concern the flow of chem-

ically reacting fluid mixtures. Therefore, it has gained serious importance from the researchers to study the presence of chemical reaction effects during various physiological functions. Many researchers have studied various aspects of blood flow including the chemical reaction effects for single-phase arterial blood flow. As Mekheimer **et al.** (Mekheimer et al., 2012) presented a theoretical model to study the impact of heat and chemical reaction on blood flow with overlapping stenosis. Further, Misra and Adhikary (2016) studied the problem of MHD flow of blood in presence of chemical reaction and an external magnetic field. They investigated with the help of their study that in blood flow, the mass transfer rate is strongly dependent on the chemical reaction and it decreases as effects of the chemical reaction increase. By assuming non-Newtonian characteristics of the blood flow El-Sayed et al. (2011) develop a mathematical model to analyze the MHD heat and mass transfer of chemical reaction fluid flow over a moving vertical plate in the presence of heat source with convective surface boundary condition. However, in none of the aforesaid studies mentioned above, the effect of chemical reaction on two-phase blood flow has been incorporated.

Blood is a physiological fluid which shows the characteristics of biomagnetic fluids as it gets affected by the applied magnetic field. A mathematical study presented by Misra et al. (2011b) for the single-phase model of the stenosed arterial blood flow in which they examined the complex flow behavior of blood under the influence of applied magnetic field. The study reveals that the variation in the values of applied magnetic field influences the wall shear stress of the stenosed artery in such a way, that high intensity of applied magnetic field can rupture the stenosed arterial wall and in result concerned portion of the body may become paralyzed. By neglecting the induced magnetic and electric fields effects Khan et al. (2017b), described the bioconvective flow of Maxwell nanofluid containing microorganisms, in the presence of a magnetic field. Ponalagusamy and Selvi (2015) introduced a mathematical model for narrow arteries to analyze the external magnetic field effects on two-phase blood flow, consisting central core region of suspended erythrocytes and a cell-free layer surrounding the core. They observed that velocity profiles for both core and plasma regions decrease, under the increased intensity of the applied magnetic field. For radially varying values of applied magnetic

field Bhatti and Zeeshan (2016) developed a mathematical model for single-phase blood flow which resulted that the pressure rise increases with increased values of the applied magnetic field. Bhatti and Rashidi (2017) studied the effects of heat and mass transfer on magnetohydrodynamic blood flow with joule heating effect. Further, Khan et al. (2017a) established a mathematical model to study the effects of both viscous dissipation and Joule heating on MHD stagnation point flow. They found that high intensity of magnetic field has a reducing effect on both velocity and temperature profile of the fluid. However, in the above-mentioned studies, no authors discussed the heat and mass transfer effects on two-phase blood flow with viscous dissipation and Joule heating effect in the presence of an applied magnetic field.

The analysis of various physiological systems has been reported by many scientists during the past few years. They show unpredictable and chaotic behavior. In such type of systems, the analysis of heat and mass transfer involves great interest which arises due to its complex combination of stochastic and deterministic physiological processes. Blood flow enhances when a person performs different physical activities and in this situations, blood circulation remains unstable. When the environmental temperature fluctuates then heat transfer takes place from the skin through the process of evaporation or the human body loses heat through conduction and radiation processes. In such types of cases, entropy plays an important role to scrutinize such systems. Bejan (1982) developed the entropy generation optimization method and introduced its applications in science and engineering field. Rashidi et al. (2016) presented the entropy generation on the MHD blood flow of a nanofluid influenced by the thermal radiation. Considering heat generation and absorption effects, Hayat et al. (2016) characterize the phenomenon of heat transfer to addresses the effect of melting heat in the flow. Further, Hayat et al. (2017) studied the flow of micropolar nano-fluid with thermal radiation and Newtonian heating and analyzed that both heat and mass transfer rate increases as values of the radiation parameter increase. Considering the nonlinear radiative effects, Farooq et al. (2016) presented a mathematical model for stretched flow of viscoelastic fluid by assuming nonlinear radiative effects. With the help of their study, they resulted from that surface heat flux increases for large values of the radiation parameter. Recently, Tripathi and

Sharma (2018a) discussed the effect of heat and mass transfer on the two-phase model of the blood flow through a horizontal stenosed artery. The blood flow is considered as Newtonian fluid in both the core and the plasma region.

Above mentioned studies were focused on analyzing the momentum and the heat transfer phenomenon for the two-phase model of the blood flow. With the help of the literature and to the best knowledge of the authors, it is found that the influence of mass transfer on two-phase blood flow having variable viscosity with chemical reaction has not gained much attention by the researchers. To show the effect of total movement of the mass from one place to the other place in the two-phase model of blood flow we consider the mass transfer phenomenon as an important part of the investigation. The present article investigates the simultaneous effects of viscous dissipation and Joule heating with the chemical reaction to the problem of unsteady two-phase blood flow through a stenosed artery under the presence of variable applied magnetic field. The present mathematical model with nonlinear partial differential equations of energy and concentration have been solved using a shooting method for both core and plasma regions separately. To get physical insight into the problem, flow resistance, total flow rate, wall shear stress, heat and mass transfer have been estimated and their respective graphs have been plotted with different values of stenosis size and magnetic field. A comparative study has been done with experimental data to show the effectiveness of the two-phase model of blood flow and it is observed that the two-phase model fits more appropriately with the experimental data as compared to single-phase model.

6.2 The Mathematical Model

Let us consider a two-layered model of blood flow through a cylindrically shaped stenosed artery having core region which contains erythrocytes (suspension of the uniform hematocrit), and a cell-free layer outside the core containing plasma as shown in fig.6.1. To investigate the flow dynamics of blood flow under the influence of radially varying applied magnetic field, a fully developed, unsteady, laminar, incompressible fluid is considered both in the core as well as plasma regions. Arterial length is presumed to be large enough

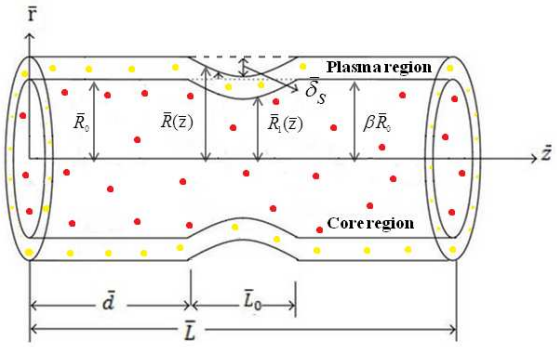

Figure 6.1: Geometry of the stenosed artery of length $\bar{L}$

in comparison with its radius so that wall effects can be neglected at the inlet as well as outlet segment of the artery. Due to the large length of the blood vessel and high rates of shear stress, nature of the blood flow is considered as Newtonian in both the core as well as in plasma regions (Noutchie, 2009). We consider the flow of two immiscible Newtonian fluids, consisting of a core region of having hematocrit dependent viscosity and plasma region of constant viscosity.

The viscosity of the fluid for the core region is given by

$$\mu_c(\bar{r}) = \bar{\mu_p}\left(1 + \beta_1 h(\bar{r})\right),$$

now we use following the empirical formula for (Sinha and Misra, 2014)

$$h(\bar{r}) = h_m\left[\left(\frac{R_1}{R_0}\right)^m - \left(\frac{\bar{r}}{R_0}\right)^m\right], \tag{6.2.1}$$

where $m \geqslant 2$, which is valid only for very dilute suspension of spherically shaped erythrocytes and $H_r = \beta_1 h_m$, in which β_1 is a constant value (for blood it has value nearly 2.5).

Geometry of the stenosis in plasma region (assumed to be symmetric) is defined as (Mekheimer and Kot, 2008),

$$\bar{R}(\bar{z}) = \begin{cases} 1 - \eta^*\left(\bar{L}_0^{n-1}(\bar{z} - \bar{d}) - (\bar{z} - \bar{d})^n\right) & \text{for} \quad \bar{d} \leq \bar{z} \leq \bar{d} + \bar{L}_0, \\ 1 & \text{otherwise}, \end{cases} \tag{6.2.2}$$

in the core region, geometry of the stenosis is defined as (Sankar and Lee, 2007),

$$\frac{\bar{R}_1(\bar{z})}{\bar{R}_0} = \begin{cases} \beta - \eta^* \left(\bar{L}_0^{n-1}(\bar{z} - \bar{d}) - (\bar{z} - \bar{d})^n \right) & \text{for} \quad \bar{d} \leq \bar{z} \leq \bar{d} + \bar{L}_0, \\ 1 & \text{otherwise}, \end{cases} \tag{6.2.3}$$

in which η^* is expressed as

$$\eta^* = \frac{\bar{\delta}_s n^{\frac{n}{n-1}}}{\bar{R}_0 \bar{L}_0^n \, (n-1)}, \tag{6.2.4}$$

where $n = 2$ for the case of symmetric stenosis (Nadeem et al., 2011) and the maximum height of the stenosis is located at

$$\bar{z} = \bar{d} + \frac{\bar{L}_0}{n^{\frac{1}{(n-1)}}}. \tag{6.2.5}$$

Note that the artery is assumed to be of cylindrically shaped in which velocity components $(\bar{u}_c, \bar{v}_c, \bar{w}_c)$ and $(\bar{u}_p, \bar{v}_p, \bar{w}_p)$ are considered in the $(\bar{r}, \bar{\theta}, \bar{z})$ directions, respectively. Having all these assumptions, the governing equations of the flow of blood in the core arterial segment are as follows (Hayat et al., 2008; Pal and Talukdar, 2011; Tripathi and Sharma, 2018a):

$$\bar{\rho}_c \frac{\partial \bar{u}_c}{\partial \bar{t}} = -\frac{\partial \bar{p}}{\partial \bar{z}} + \frac{1}{\bar{r}} \frac{\partial}{\partial \bar{r}} \left(\bar{r} \bar{\mu}_c(\bar{r}) \left(\frac{\partial \bar{u}_c}{\partial \bar{r}} \right) \right) - \bar{\sigma}_1 \bar{B}_0(\bar{r})^2 \bar{u}_c, \tag{6.2.6}$$

$$\bar{\rho}_c \bar{c}_c \frac{\partial \bar{T}_c}{\partial \bar{t}} = \bar{K}_c \left(\frac{\partial^2 \bar{T}_c}{\partial \bar{r}^2} + \frac{1}{\bar{r}} \frac{\partial \bar{T}_c}{\partial \bar{r}} \right) + \bar{\mu}_c(\bar{r}) \left(\frac{\partial \bar{u}_c}{\partial \bar{r}} \right)^2 + \bar{\sigma}_1 \bar{B}_0(\bar{r})^2 {\bar{u}_c}^2, \tag{6.2.7}$$

$$\frac{\partial \bar{C}_c}{\partial \bar{t}} = \bar{D}_c \left(\frac{\partial^2 \bar{C}_c}{\partial \bar{r}^2} + \frac{1}{\bar{r}} \frac{\partial \bar{C}_c}{\partial \bar{r}} \right) - \bar{E}'_c \left(\bar{C}_c - \bar{C}_0 \right). \tag{6.2.8}$$

The equations for momentum, energy and concentration for plasma region are as follows

$$\bar{\rho}_p \frac{\partial \bar{u}_p}{\partial \bar{t}} = -\frac{\partial \bar{p}}{\partial \bar{z}} + \bar{\mu}_p \left(\frac{\partial^2 \bar{u}_p}{\partial \bar{r}^2} + \frac{1}{\bar{r}} \frac{\partial \bar{u}_p}{\partial \bar{r}} \right) - \bar{\sigma}_1 \bar{B}_0(\bar{r})^2 \bar{u}_p, \tag{6.2.9}$$

$$\bar{\rho}_p \bar{c}_p \frac{\partial \bar{T}_p}{\partial \bar{t}} = \bar{K}_p \left(\frac{\partial^2 \bar{T}_p}{\partial \bar{r}^2} + \frac{1}{\bar{r}} \frac{\partial \bar{T}_p}{\partial \bar{r}} \right) + \bar{\mu}_p \left(\frac{\partial \bar{u}_p}{\partial \bar{r}} \right)^2 + \bar{\sigma}_1 \bar{B}_0(\bar{r})^2 {\bar{u}_p}^2, \tag{6.2.10}$$

$$\frac{\partial \bar{C}_p}{\partial \bar{t}} = \bar{D}_p \left(\frac{\partial^2 \bar{C}_p}{\partial \bar{r}^2} + \frac{1}{\bar{r}} \frac{\partial \bar{C}_p}{\partial \bar{r}} \right) - \bar{E}'_p \left(\bar{C}_p - \bar{C}_0 \right). \tag{6.2.11}$$

In eqs.(6.2.6) and (6.2.9), terms $\bar{\sigma_1} \bar{B_0}(\bar{r})^2 \bar{u_c}$ and $\bar{\sigma_1} \bar{B_0}(\bar{r})^2 \bar{u_p}$ are appeared because of the Lorentz force that is considered due to the electrical conductivity of the blood flow (Tashtoush and Magableh, 2008). Term $\bar{\mu}_c(\bar{r}) \left(\frac{\partial \bar{u}_c}{\partial \bar{r}} \right)^2$ in eq.(6.2.7) and term $\bar{\mu}_p \left(\frac{\partial \bar{u}_p}{\partial \bar{r}} \right)^2$ in eq.(6.2.10) are for the viscous dissipation which directly affects the mechanism of heat transfer of the blood flow. This phenomenon has a great importance in a pathological state of an arterial segment during deep heat muscle treatment (Dessie and Kishan, 2014). Further, last terms in eqs.(6.2.7) and (6.2.10) represent the Joule heating effect while chemical reaction terms are incorporated in concentration eqs.(6.2.8) and (6.2.11) for both core as well as plasma region.

In the model, It is also assumed that the outer arterial wall as a solid surface by considering no-slip boundary conditions (Prabhakara and Deshpande, 2004). A continuous behavior of velocity, temperature, and concentration have been taken at the interface of core and plasma regions. It is presumed that in the core region due to symmetry, velocity, temperature and concentration gradient vanish along with the center of artery (Sharan and Popel, 2001). Under all these assumption boundary conditions to solve the mathematical model eqs.(6.2.6)-(6.2.11) for both core and plasma regions are as follows:

$$\begin{cases} \bar{u_p} = 0, \quad \bar{T_p} = \bar{T_w}, \quad \bar{C_p} = \bar{C_w} \quad at \quad \bar{r} = \bar{R}(\bar{z}), \\ \bar{u_c} = \bar{u_p}, \quad \bar{T_p} = \bar{T_c}, \quad \bar{C_p} = \bar{C_c} \quad at \quad \bar{r} = \bar{R_1}(\bar{z}), \\ \frac{\partial \bar{u}_c}{\partial \bar{r}} = 0, \quad \frac{\partial \bar{T_c}}{\partial \bar{r}} = 0, \quad \frac{\partial \bar{C_c}}{\partial \bar{r}} = 0 \quad at \quad \bar{r} = 0, \\ \bar{\tau_c} = \bar{\tau_p}, \quad \frac{\partial \bar{T_c}}{\partial \bar{r}} = \frac{\partial \bar{T_p}}{\partial \bar{r}}, \quad \frac{\partial \bar{C_c}}{\partial \bar{r}} = \frac{\partial \bar{C_p}}{\partial \bar{r}} \quad at \quad \bar{r} = \bar{R_1}(\bar{z}). \end{cases} \tag{6.2.12}$$

Now, let us introduce following non-dimensional parameters as follows

$$u_c = \frac{\bar{u_c}}{\bar{u_0}}, \quad r = \frac{\bar{r}}{\bar{R_0}}, \quad z = \frac{\bar{z}}{\bar{R_0}}, \quad t = \bar{\omega} \bar{t}, \quad \frac{\bar{R}(\bar{z})}{\bar{R_0}} = R(Z), \quad \frac{\bar{R}(\bar{z})}{\bar{R_0}} = R_1(z),$$

$$u_p = \frac{\bar{u_p}}{\bar{u_0}}, \quad p = \frac{\bar{R_0} \bar{p}}{\bar{u_0} \bar{\mu_p}}, \quad Re = \frac{\bar{\rho_p} \bar{R_0} u_0}{\bar{\mu_p}}, \quad \theta_c = \frac{(\bar{T_c} - \bar{T_0})}{\bar{T_w} - \bar{T_0}}, \quad \sigma_c = \frac{(\bar{C_c} - \bar{C_0})}{\bar{C_w} - \bar{C_0}},$$

$$\delta = \frac{\bar{\delta_s}}{\bar{R_0}}, \quad \theta_p = \frac{(\bar{T_p} - \bar{T_0})}{\bar{T_w} - \bar{T_0}}, \quad {M_1}^2(r) = \frac{\bar{\sigma} \bar{B_0}(\bar{r})^2 {\bar{R_0}}^2}{\bar{\mu_p}}, \quad \sigma_p = \frac{(\bar{C_p} - \bar{C_0})}{\bar{C_w} - \bar{C_0}},$$

$$Pe = \frac{\bar{\rho_p}\bar{c_p}{\bar{R_0}}^2\bar{\omega}}{\bar{K_p}}, \quad Sc = \frac{\bar{\mu_p}}{\bar{D_p}\bar{\rho_p}}, \quad D_0 = \frac{\bar{D_p}}{\bar{D_c}},$$

$$\tau_c = \frac{\bar{\tau_c}{\bar{R_0}}^2}{\bar{u_0}\bar{\mu_p}}, \quad \tau_p = \frac{\bar{\tau_p}{\bar{R_0}}^2}{\bar{u_0}\bar{\mu_p}}, \quad \rho_0 = \frac{\bar{\rho_p}}{\bar{\rho_c}}, \quad \mu_0 = \frac{\bar{\mu_p}}{\bar{\mu_c}}, \quad \bar{E_p'} = \frac{E\bar{\mu_p}}{\bar{\rho_p}{\bar{R_0}}^2} \quad E_0 = \frac{\bar{E_p}}{\bar{E}c}.$$

where expression for variable magnetic field (Bhatti and Zeeshan, 2016) is considered as

$$M_1(r) = \frac{M}{r}. \tag{6.2.13}$$

where M is the magnetic field parameter and meaning of the other mentioned notations are already given in earlier chapters 2, 3 and 4.

The dimensionless form of the geometry of the stenosis in core and plasma regions are given by

$$R(z) = \begin{cases} 1 - \eta\left((z-l) - (z-l)^n\right) & \text{for} \quad l \le z \le 1+l, \\ 1 & \text{otherwise}, \end{cases} \tag{6.2.14}$$

$$R_1(z) = \begin{cases} \beta - \eta\left((z-l) - (z-l)^n\right) & \text{for} \quad l \le z \le 1+l, \\ \beta & \text{otherwise}, \end{cases} \tag{6.2.15}$$

where

$$\eta = \frac{\delta n^{\frac{n}{n-1}}}{(n-1)}, \quad l = \frac{\bar{d}}{\bar{L_0}}, \quad \delta = \frac{\bar{\delta_s}}{\bar{R_0}}.$$

The governing equations for core region in dimensionless form as described in eqs.(6.2.6)-(6.2.8) can be written as

$$\begin{aligned}\left(\frac{Re}{\rho_0}\right)\left(\frac{\partial u_c}{\partial t}\right) = &-\left(\frac{\partial p}{\partial z}\right) + \left(\frac{\partial^2 u_c}{\partial r^2}\right)\left[1 + \beta h_m\left(\left(\frac{R_1}{R_0}\right)^{m_2} - r^{m_2}\right)\right] \\ &+ \frac{1}{r}\left(\frac{\partial u_c}{\partial r}\right)\left[1 + \beta h_m\left(\left(\frac{R_1}{R_0}\right)^{m_2} - (m_2+1)r^{m_2}\right)\right] - \frac{M^2}{r^2}u_c,\end{aligned} \tag{6.2.16}$$

$$\begin{aligned}\left(\frac{1}{\rho_0 s_0}\right)\left(\frac{\partial \theta_c}{\partial t}\right) = &\frac{1}{K_0 Pe}\left(\frac{\partial^2 \theta_c}{\partial r^2} + \frac{1}{r}\frac{\partial \theta_c}{\partial r}\right) + \frac{M^2}{r^2}\left(\frac{Ec}{Re}\right){u_c}^2 \\ &+ \left(\frac{Ec}{Re}\right)\left[1 + \beta h_m\left(\left(\frac{R_1}{R_0}\right)^{m_2} - r^{m_2}\right)\right]\left(\frac{\partial u_c}{\partial r}\right)^2,\end{aligned} \tag{6.2.17}$$

$$Re\left(\frac{\partial \sigma_c}{\partial t}\right) = \frac{1}{D_0}\left(\frac{1}{Sc}\right)\left(\frac{\partial^2 \sigma_c}{\partial r^2} + \frac{1}{r}\frac{\partial \sigma_c}{\partial r}\right) - \frac{E}{E_0}\sigma_c. \tag{6.2.18}$$

Equations of the plasma region eqs.(6.2.9)-(6.2.11) can be transformed in non dimensional form as

$$Re\left(\frac{\partial u_p}{\partial t}\right) = -\left(\frac{\partial P}{\partial z}\right) + \left(\frac{\partial^2 u_p}{\partial r^2} + \frac{1}{r}\frac{\partial u_p}{\partial r}\right) - \frac{M^2}{r^2}u_p, \tag{6.2.19}$$

$$\left(\frac{\partial \theta_p}{\partial t}\right) = \frac{1}{Pe}\left(\frac{\partial^2 \theta_p}{\partial r^2} + \frac{1}{r}\frac{\partial \theta_p}{\partial r}\right) + \frac{Ec}{Re}\left(\frac{\partial u_p}{\partial r}\right)^2 + \frac{M^2}{r^2}\frac{Ec}{Re}{u_p}^2, \tag{6.2.20}$$

$$Re\left(\frac{\partial \sigma_p}{\partial t}\right) = \left(\frac{1}{Sc}\right)\left(\frac{\partial^2 \sigma_p}{\partial r^2} + \frac{1}{r}\frac{\partial \sigma_p}{\partial r}\right) - E\sigma_p. \tag{6.2.21}$$

Henceforth, the corresponding boundary conditions eq.(6.2.12) in nondimensional form are given by

$$\begin{cases} u_p = 0, & \theta_p = 1, & \sigma_p = 1 & at & r = R(z), \\ u_p = u_c, & \theta_p = \theta_c, & \sigma_p = \sigma_c & at & r = R_1(z), \\ \tau_c = \tau_p, & \frac{\partial \theta_c}{\partial r} = \frac{\partial \theta_p}{\partial r}, & \frac{\partial \sigma_c}{\partial r} = \frac{\partial \sigma_p}{\partial r} & at & r = R_1(z), \\ \frac{\partial u_c}{\partial r} = 0, & \frac{\partial \theta_c}{\partial r} = 0, & \frac{\partial \sigma_c}{\partial r} = 0 & at & r = R_c. \end{cases} \tag{6.2.22}$$

It is a well-studied fact that pumping action of the heart results into a pulsatile nature of the blood flow, and therefore the pressure gradient is assumed in the following form (Ponalagusamy and Selvi, 2015)

$$-\frac{\partial p}{\partial z} = P_0 e^{i\omega t}, \tag{6.2.23}$$

where P_0 is the constant pressure. This assumption holds for harmonic oscillatory flows, and in these cases, the real part of the eq.(6.2) gives the corresponding flow, as discussed in details by Womersley (1955). For the selected form of the pressure gradient, solution of velocity, temperature and concentration for both core and plasma regions can be written in the form of

$$\begin{cases} u_c(r,t) = u_{c_0}(r)e^{i\omega t}, & u_p(r,t) = u_{p_0}(r)e^{i\omega t}, \\ \theta_c(r,t) = \theta_{c_0}(r)e^{i\omega t}, & \theta_p(r,t) = \theta_{p_0}(r)e^{i\omega t}, \\ \sigma_c(r,t) = \sigma_{c_0}(r)e^{i\omega t}, & \sigma_p(r,t) = \sigma_{p_0}(r)e^{i\omega t}. \end{cases} \tag{6.2.24}$$

Substituting the expressions from eq.(6.2.24) in to eqs.(6.2.16)-(6.2.18), we get

$$\begin{aligned} \left(i\frac{Re}{\rho_0} + \frac{M^2}{r^2}\right)u_{c_0} =& P_0 + \left(\frac{\partial^2 u_{c_0}}{\partial r^2}\right)\left[1 + \beta h_m\left(\left(\frac{R_1}{R_0}\right)^{m_2} - r^{m_2}\right)\right] \\ &+ \frac{1}{r}\left(\frac{\partial u_{c_0}}{\partial r}\right)\left[1 + \beta h_m\left(\left(\frac{R_1}{R_0}\right)^{m_2} - (m_2+1)r^{m_2}\right)\right], \end{aligned} \tag{6.2.25}$$

$$\left(i\frac{1}{\rho_0 s_0}\right)\theta_{c_0} = \frac{1}{K_0 Pe}\left(\frac{\partial^2\theta_{c_0}}{\partial r^2}+\frac{1}{r}\frac{\partial\theta_{c_0}}{\partial r}\right)+\left(\frac{M}{r}\right)^2\frac{Ec}{Re}{u_{c_0}}^2 e^{i\omega t} + \left(\frac{Ec}{Re}\right)\left[1+\beta h_m\left(\left(\frac{R_1}{R_0}\right)^{m_2}-r^{m_2}\right)\right]\left(\frac{\partial u_{c_0}}{\partial r}\right)^2 e^{i\omega t}, \tag{6.2.26}$$

$$\frac{\partial^2\sigma_{c_0}}{\partial r^2}+\frac{1}{r}\frac{\partial\sigma_{c_0}}{\partial r}-\left(iReD_0Sc+\frac{E}{E_0}D_0Sc\right)\sigma_{c_0}=0, \tag{6.2.27}$$

and eqs.(6.2.19)-(6.2.21) of plasma region change in the form of

$$\left(iRe+\left(\frac{M}{r}\right)^2\right)u_{p_0} = P_0+\left(\frac{\partial^2 u_{p_0}}{\partial r^2}+\frac{1}{r}\frac{\partial u_{p_0}}{\partial r}\right), \tag{6.2.28}$$

$$i\theta_{p_0} = \frac{1}{Pe}\left(\frac{\partial^2\theta_{p_0}}{\partial r^2}+\frac{1}{r}\frac{\partial\theta_{p_0}}{\partial r}\right)+\left(\frac{M}{r}\right)^2\frac{Ec}{Re}{u_{p_0}}^2 e^{i\omega t}+\left(\frac{Ec}{Re}\right)\left(\frac{\partial u_{p_0}}{\partial r}\right)^2 e^{i\omega t}, \tag{6.2.29}$$

$$\frac{\partial^2\sigma_{p_0}}{\partial r^2}+\frac{1}{r}\frac{\partial\sigma_{p_0}}{\partial r}-\left(iReSc+ESc\right)\sigma_{p_0}=0. \tag{6.2.30}$$

6.3 Solution

Since eqs.(6.2.25) and (6.2.26) are the coupled non-linear ordinary differential equations (containing an independent variable r), we employ a numerical technique named single shooting method to solve the equations with the given boundary conditions eq.(6.2.22).

Shooting method

Shooting methods are used to solve boundary value problems (BVP). In this technique, an initial guess is chosen for the unknown initial value problem(IVP) and the IVP is further solved. Subsequently, the initial guess is improved by comparing the error between the known values and computed values at the terminal node (Ha, 2001; Ja, 1983). In the model let us assume $x(1)=u, x(2)=\theta, x(3)=\frac{\partial u}{\partial r}$ and $x(4)=\frac{\partial\theta}{\partial r}$.
Therefore, first order nonlinear system for eqs.(6.2.25) and (6.2.26) can be represented as

$$\dot{x}(1)=x(3), \tag{6.3.1}$$

$$\dot{x}(2)=x(4), \tag{6.3.2}$$

$$\dot{x}(3) = \frac{1}{\phi}\left(-P_0 - \frac{1}{r}\left(\phi - \beta h_m(m_2+1)r^{m_2}\right)x(3)\right) + \left(\left(\frac{M}{r}\right)^2 + \frac{iRe}{\rho_0}\right)\frac{x(1)}{\phi}, \tag{6.3.3}$$

$$\dot{x}(4) = -\frac{1}{r}x(4) - \frac{K_0 PeEc}{Re\,\phi}x(3)^2 e^{i\omega t} + \frac{K_0 Pe}{\rho_0 c_0}x(2) - \left(\frac{M}{r}\right)^2 \frac{K_0 PeEc}{Re}x(1)^2 e^{i\omega t}, \tag{6.3.4}$$

where $\phi = 1 + \beta h_m\left(\left(\frac{R_1}{R_0}\right)^{m_2} - r^{m_2}\right)$. Now, first order system for eqs.(6.2.28) and (6.2.29) are as follows

$$\dot{x}(1) = x(3), \tag{6.3.5}$$

$$\dot{x}(2) = x(4), \tag{6.3.6}$$

$$\dot{x}(3) = -P_0 + \left(\left(\frac{M}{r}\right)^2 + i\alpha^2\right)x(1) - \frac{1}{r}x(3), \tag{6.3.7}$$

$$\dot{x}(4) = iPe\,x(2) - \frac{1}{r}Pe\,x(4) - \frac{PeEc}{Re}x(3)^2 e^{i\omega t} - \frac{PeEc}{Re}\left(\frac{M}{r}\right)^2 e^{i\omega t}x(1). \tag{6.3.8}$$

Now, we apply all the steps as given in algorithm((1)) to solve the given problem using single shooting method.

Eqs.(6.2.27) and (6.2.30) are the ordinary differential equations which we solve using the definition of Bessel differential equation and calculate their exact solutions. To solve these equations under the given boundary conditions eq.(6.2.22), first we assume

$$\gamma_1 = -\left(iReD_0Sc + \frac{E}{E_0}D_0Sc\right), \tag{6.3.9}$$

$$\gamma_2 = -\left(iReSc + ESc\right). \tag{6.3.10}$$

So the eqs.(6.2.27) and (6.2.30) become

$$\frac{d^2\sigma_{c_0}}{dr^2} + \frac{1}{r}\frac{d\sigma_{c_0}}{dr} + \gamma_1\sigma_{c_0} = 0, \tag{6.3.11}$$

$$\frac{d^2\sigma_{p_0}}{dr^2} + \frac{1}{r}\frac{d\sigma_{p_0}}{dr} + \gamma_2\sigma_{p_0} = 0. \tag{6.3.12}$$

Therefore, Solution of concentration for core and plasma regions is calculated as

$$\sigma_{c_0}(r) = \left[U_4\left(\frac{\sqrt{\gamma_2}Y_1(\sqrt{\gamma_2}R_1)}{U_3Y_0(\sqrt{\gamma_2}R)} - \frac{\sqrt{\gamma_1}U_5J_1(\sqrt{\gamma_1}R_1)}{U_6}\right) + U_5\right]J_0(\sqrt{\gamma_1}(r)), \tag{6.3.13}$$

and

$$\sigma_{p_0}(r) = \left[\left(\frac{\sqrt{\gamma_2}Y_1(\sqrt{\gamma_2}R_1)}{U_3Y_0(\sqrt{\gamma_2}R)} - \frac{\sqrt{\gamma_1}U_5J_1(\sqrt{\gamma_1}R_1)}{U_6}\right)\left(J_0(\sqrt{\gamma_2}r) - \frac{J_0(\sqrt{\gamma_2}R}{Y_0(\sqrt{\gamma_2}R}Y_0(\sqrt{\gamma_2}r)\right)\right] + \frac{Y_0(\sqrt{\gamma_2}r)}{Y_0(\sqrt{\gamma_2}R)}, \tag{6.3.14}$$

Consequently, concentration for unsteady flow in core and plasma regions are as follows

$$\sigma_c(r,t) = \left[U_4\left(\frac{\sqrt{\gamma_2}Y_1(\sqrt{\gamma_2}R_1)}{U_3Y_0(\sqrt{\gamma_2}R)} - \frac{\sqrt{\gamma_1}U_5J_1(\sqrt{\gamma_1}R_1)}{U_6}\right) + U_5\right]J_0(\sqrt{\gamma_1}(r))e^{i\omega t}, \tag{6.3.15}$$

$$\begin{aligned}\sigma_p(r,t) = &\left(\frac{\sqrt{\gamma_2}Y_1(\sqrt{\gamma_2}R_1)}{U_3Y_0(\sqrt{\gamma_2}R)} - \frac{\sqrt{\gamma_1}U_5J_1(\sqrt{\gamma_1}R_1)}{U_6}\right)J_0(\sqrt{\gamma_2}r)e^{i\omega t} \\ &- \left(\frac{\sqrt{\gamma_2}Y_1(\sqrt{\gamma_2}R_1)}{U_3Y_0(\sqrt{\gamma_2}R)} - \frac{\sqrt{\gamma_1}U_5J_1(\sqrt{\gamma_1}R_1)}{U_6}\right)\frac{J_0(\sqrt{\gamma_2}R)}{Y_0(\sqrt{\gamma_2}R)}Y_0(\sqrt{\gamma_2}r)e^{i\omega t} \\ &+ \frac{Y_0(\sqrt{\gamma_2}r)}{Y_0(\sqrt{\gamma_2}R)}e^{i\omega t},\end{aligned} \tag{6.3.16}$$

where expressions for the constants U_4, U_5 and U_6 are given in Appendix A.

6.4 Results and Discussion

Parameters	Values (Unitfree)	Source
Eckert number (Ec)	0.1-10	Fakour et al. (2015); Ramzan et al. (2013)
Reynold Number(Re)	0.005-0.4	Fujiwara et al. (2009); Ku (1997)
Height of the stenosis (δ)	0.1-0.2	Misra et al. (1993)

Table 6.1: Values of the parametrs

The aim of the present model is to analyze the flow, heat and mass transfer effects on two-phase blood flow through a stenosed artery under the influence of varying applied magnetic

field along with the Joule heating and viscous dissipation. The viscosity of the core region is assumed to be varying with the hematocrit ratio while the viscosity of the plasma region is assumed constant. In order to illustrate the applicability of the given model, solutions for velocity, the temperature of both core as well as plasma regions have been computed numerically using single shooting method. Now, for having the adequate insight of two-layered model of blood flow, computational results have been plotted graphically to show the effects of cell-free plasma layer on blood flow with the variation of different quantities of interest. Default values of the parameters used in graphs are specified in Table.(5.1) and Table.(6.1) to analyze the effectiveness of the model.

The value of the plasma layer thickness is assumed as 0.2 on the scale of the radius of the artery and height of the stenosis (δ) is taken as 0.1, to draw all the graphical results. Taking these default values of parameters, flow, heat and mass transfer characteristics of blood flow in narrow artery have been analyzed by considering range of the core region from 0.1 to 0.7 (in which viscosity varies with hematocrit ratio) and the plasma region (constant viscosity) from 0.7 to 0.9 on the scale of 0 to 1. In figures dotted lines display the variation of velocity, temperature and concentration profiles of the blood flow in the core region and continuous lines show the same inside the plasma region.

Fig.6.2 presents a comparative study between the present model and the experimental data provided by Bugliarello and Sevilla (1970) with the help of their *In Vitro* experimental studies in which they examined the cell velocity distribution in a fine glass tube of blood containing 40% hematocrit. The figure shows that the present model for a given set of values as $\delta = 0$, $Re = 5$, $M = 0$ and $R_1 = 0.6$ (core region is in the 60% part of the artery), has a good agreement with the experimental data.

Fig.6.3 illustrates the behavior of the velocity profile of the blood flow characterized by the Newtonian fluids in both the core as well as plasma regions in the presence of the radially varying applied magnetic field. From the figure, it is clear that as the value of the magnetic field parameter increases, the velocity profile of both core and plasma regions decrease, respectively. This happens due to an increase in the viscosity for the blood flow under the influence of applied magnetic field as red blood cells contain hemoglobin molecules which are oxides of iron and highly influenced by the presence of the magnetic

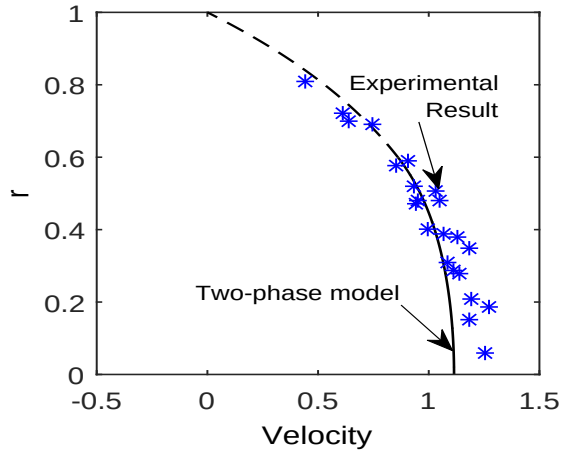

Figure 6.2: Comparative results of velocity distribution of single and two-phase blood flow with the experimetal data (Bugliarello and Sevilla, 1970)

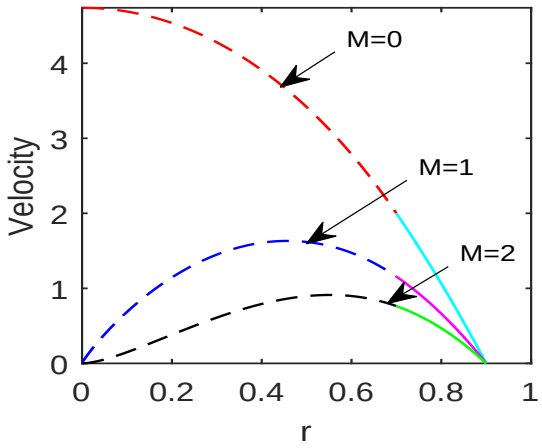

Figure 6.3: Variation of velocity profile of two-phase blood flow for different values of $M = 0$, $M = 1$ and $M = 2$ when δ=0.1 and R_1=0.7

effect. This behavior is related to the existence of the magnetic torque which results in the erythrocytes to orient with their disk plane parallel to the direction of the applied magnetic field. This orientation makes red blood cell more concentrated along the fluid flow and the results of which decreases the velocity profile of the core region. In the model as boundary condition provides the continuous behavior of the flow at the interface between core and plasma, the velocity of the plasma region gets affected due to the decreased velocity of the red blood cells. The difference between the angular velocities of red blood cells and plasma create the viscous torque which results in the decreased velocity of the blood plasma. It is also observed that under the variable magnetic strengths, the velocity of the red blood cells decreases more rapidly than the velocity of plasma. The velocity of the core region attains higher values than the plasma region if there is no magnetic field, while the reverse effect is observed for the strong magnetic field. Therefore, in the narrow artery magnetic field is very influential in order to perform the surgical operation.

Fig.6.4 displays the variation of the velocity profile of the blood flow for different values of the height of the stenosis. It can be clearly observed from the figure that as the height of the stenosis increases inside the artery then the velocity profile decrease in both the

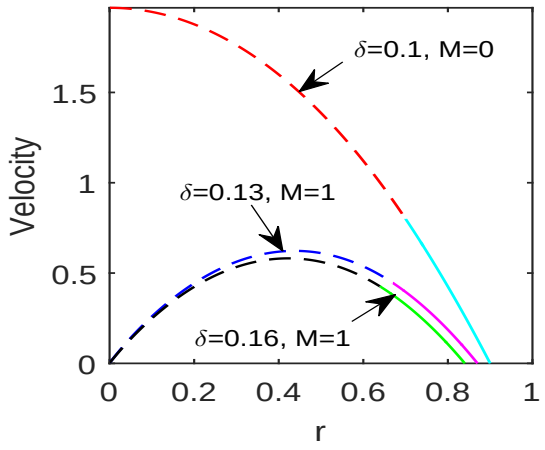

Figure 6.4: Variation of velocity profile with r for different values of δ

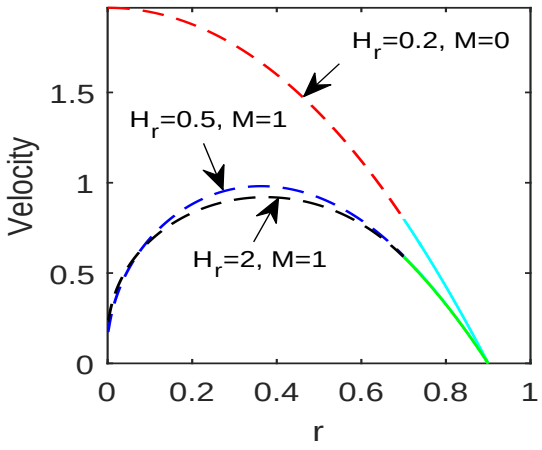

Figure 6.5: Variation of velocity profile for different values of H_r

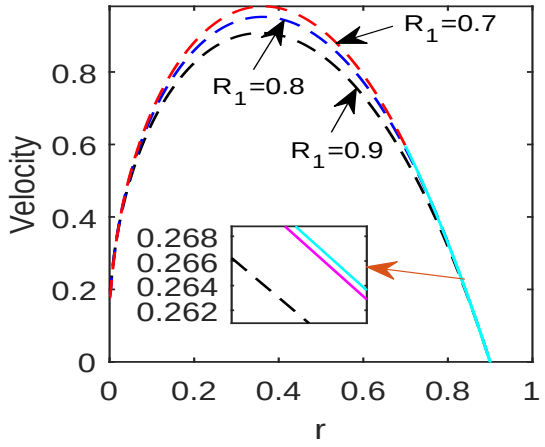

Figure 6.6: Variation of velocity profile for different values of plasma layer thickness

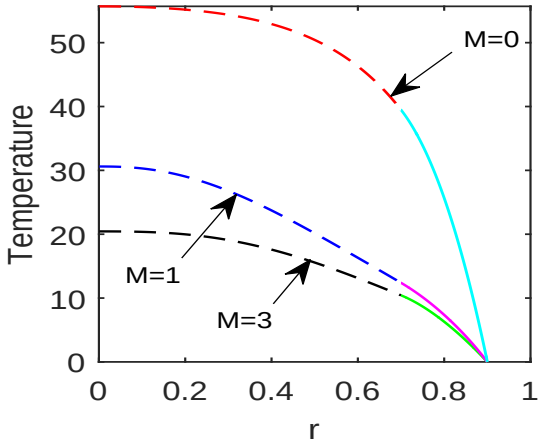

Figure 6.7: Variation of temperature profile for different values of M

core as well as plasma regions due to constriction of the artery. Further, the figure reveals that with no magnetic effect and for the case of 10% arterial occlusion, core velocity profile attains higher values than the velocity profile in the plasma region. It can be seen clearly that in the presence of magnetic field velocity profile of the blood flow from the center displays the symmetric parabolic profile, in both the cases of 13% and 16% arterial occlusion. Fig.6.5 shows the variation of the velocity profile of blood flow for different values of hematocrit parameter. In the proposed model viscosity of the core

region varies with the hematocrit ratio while the viscosity of the plasma is assumed to be constant. From the figure, it is clear that as values of hematocrit parameter increase, the velocity of the core region decreases due to rising in the concentration of erythrocyte. It is noticed that the velocity of cell-free plasma layer is not affected by the variable hematocrit parameter. Further, the figure depicts that the velocity profile of the core region attains higher values than the plasma region by following the parabolic velocity profile around the center in the absence of a magnetic field. It is also observed that in the presence of a magnetic field, velocity profile possesses the same values near the center of the artery for different values of hematocrit parameter. For a fixed value of stenosis height ($\delta = 0.1$), fig.6.6 depicts the effects of variable plasma layer thickness on the velocity profile of blood flow in the narrow artery. It is observed that as the radius of the core region increases (so plasma layer thickness decreases), the velocity profile of both core and plasma layer decrease.

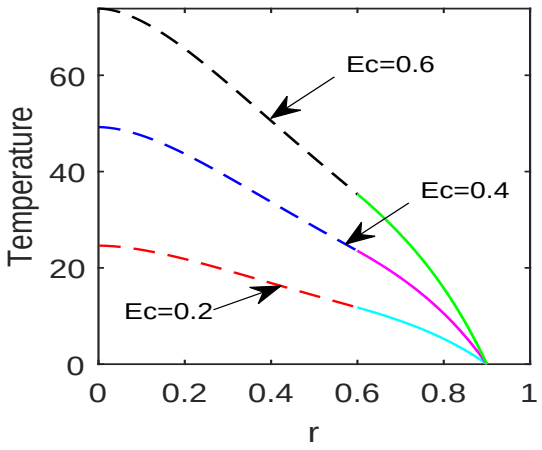

Figure 6.8: Variation of temperature profile for different values of Ec

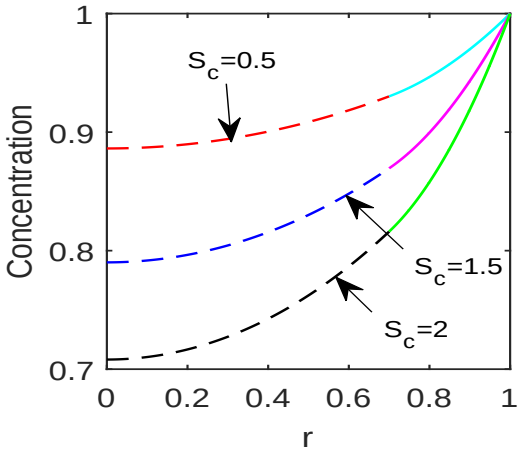

Figure 6.9: Variation of concentration profile for different values of Sc

Fig.6.7 presents the variation of the temperature profile in the radial direction for different values of the magnetic field parameter. The figure reveals that the temperature profile of blood flow decreases with increasing values of the magnetic field parameter. This happens due to the magnetic field which acts as a retarding force and slows down the motion of fluid particles. As a result of this, the kinetic energy decreases and thus

temperature decreases by increasing the magnetic field parameter. This result shows the good agreement with the result obtained by (Hayat et al., 2015). Fig.6.8 shows the

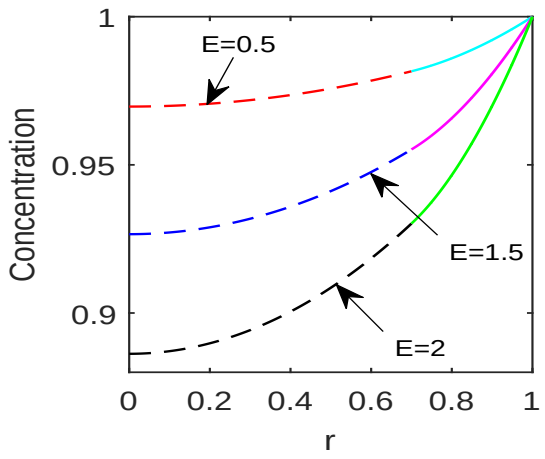

Figure 6.10: Variation of concentration profile for different values of E

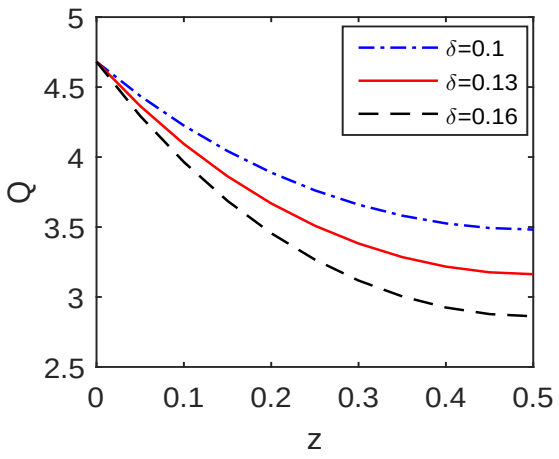

Figure 6.11: Variation of flow rate for different values of δ

behavior of the temperature profile of blood flow for different values of the Eckert number. The figure shows that as the values of the Eckert number increase, the temperature profile of the blood flow also increases. The reason behind this is the fact that the effect of viscous dissipation becomes more significant. It can be seen from the figure that for a fixed value of the Eckert number (Ec), temperature profile starts decreasing from the center of the artery towards the interface region of core and plasma and continuously decreases up to the arterial wall.

Fig.6.9 displays the variation of the concentration profile of the blood flow for different values of the Schmidt number. As the values of the Schmidt number increase, the concentration profile of the blood flow decreases. This happens due to the buoyancy effects in which high value of Schmidt number implies weaker mass diffusion coefficient, the influence of which reduces the concentration profile of the blood flow. Fig.6.10 shows the effects of chemical reaction in both the core as well as plasma regions. The figure reveals that the concentration profile of the blood flow decreases as the values of the chemical reaction parameter increase. Physically, an increase in chemical reaction parameter suppresses the concentration of the fluid due to a fall in the chemical molecular diffusivity

of the species concentration. Thus the species concentration experiences retarding effect and reduce the total mass transfer of both the fluids.

The total volumetric flow rate of the blood flow in the artery is calculated as

$$Q = 2\pi R^2 \int_0^{R_1} u_c(r,t)dr + 2\pi R^2 \int_{R_1}^{R} u_p(r,t)dr. \tag{6.4.1}$$

The shear stress at the interface wall of core and the plasma region is given by

$$\tau = -\left(\frac{\partial u_c}{\partial r}\right)_{R_1}. \tag{6.4.2}$$

Flow resistance in the two-phase blood flow is defined as

$$\lambda = \int_0^z \frac{P_0 e^{i\omega t}}{Q} dz. \tag{6.4.3}$$

The variation in the total volumetric flow rate of blood along with the axis of the artery

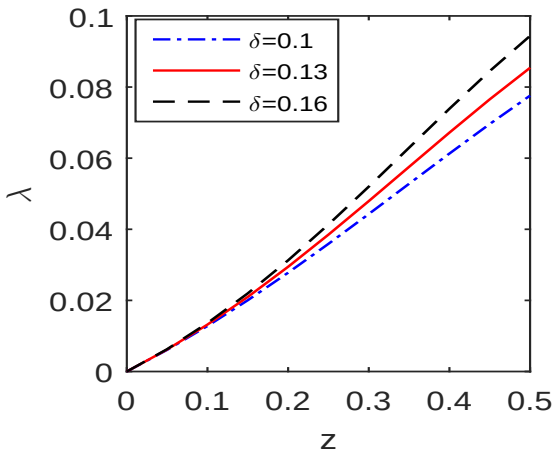

Figure 6.12: Variation of flow resistance with z for different values of δ

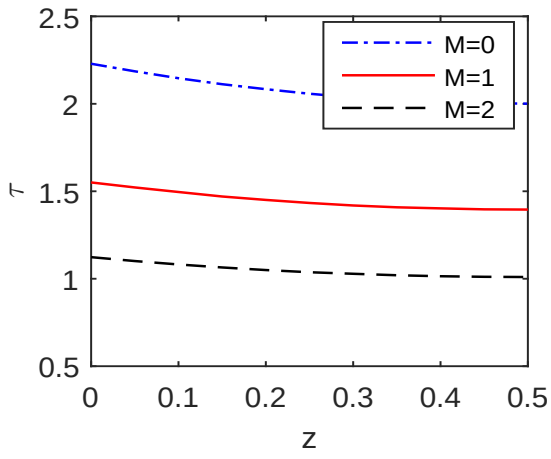

Figure 6.13: Variation of wall shear stress with z for different values of M

for different values of the height of the stenosis is illustrated in fig.6.11. The range of z includes only the diseased region of the artery by assuming the maximum height of the stenosis at the point $z = 0.5$ for the case of symmetric stenosis. It is observed that the flow rate is minimum at the throat of stenosis irrespective of the stenosis size. This can be further notable that the volumetric flow rate decreases as values of the height of the stenosis increase. The flow impedance establishes the strong correlation

between the localization of stenosis and arterial wall which is important to understand the development of arterial disease. Fig.6.12 displays the flow resistance profile of the blood flow along with the axial direction (includes only the stenotic region) for different values of the height of the stenosis. It is observed from the figure that the resistance to flow or the impedance experienced by the streaming fluid distribution over the stenosed arterial segment increases with the increased height of the stenosis. Wall shear stress is one of the important flow characteristics of blood flow. Distribution of wall shear stress along the axial direction(includes only the diseased part of the artery) has been displayed in fig.6.13, for different values of the magnetic field parameter. The wall shear stress is found to be reduced due to the increasing strength of the applied magnetic field. Since the applied magnetic field tends to impede the flow motion and thus reduce the surface friction force.

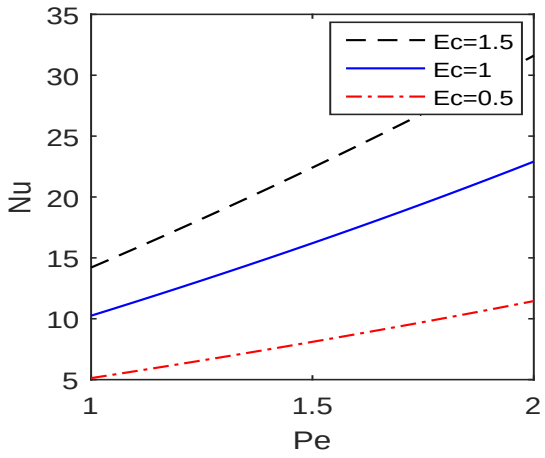

Figure 6.14: Nusselt number for two-phase blood flow with Ec

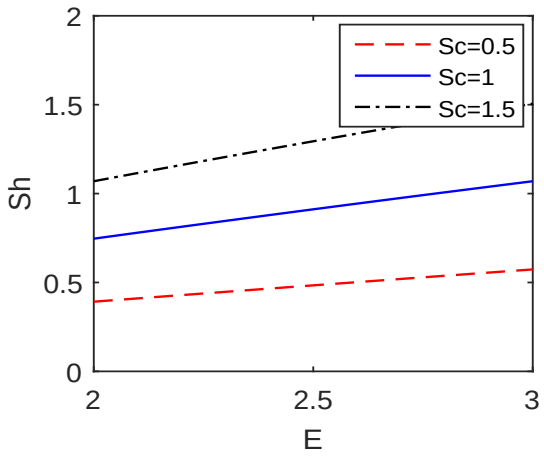

Figure 6.15: Sherwood number for two-phase blood flow with Sc

The heat and mass transfer coefficients across the upper wall (upper wall) of the stenosed artery respectively are calculated as

$$Nu = -\left(\frac{\partial \theta_p}{\partial r}\right)_R, \tag{6.4.4}$$

and

$$Sh = -\left(\frac{\partial \sigma_p}{\partial r}\right)_R. \tag{6.4.5}$$

Fig.6.14 shows the variations of heat transfer coefficient (Nusselt number) with the Peclet number for different values of the Eckert number. It can be clearly observed from the figure that as values of the Eckert number increase, the Nusselt number also increases and for a fixed value of the Eckert number it monotonically increases with Peclet number. This is due to the fact that heat energy is stored in the fluid due to frictional heating which directly affects the heat transfer coefficients.

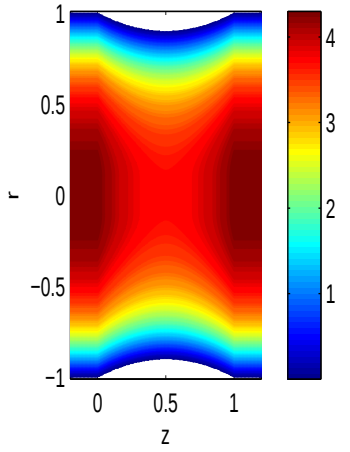

Figure 6.16: Velocity contour for 10% of the arterial blockage when $M = 0$

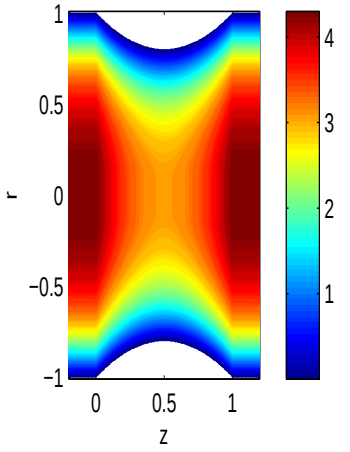

Figure 6.17: Velocity contour for 20% of the arterial blockage when $M = 0$

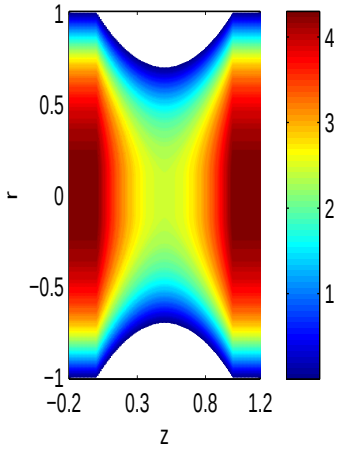

Figure 6.18: Velocity contour for 30% of the arterial blockage when $M = 0$

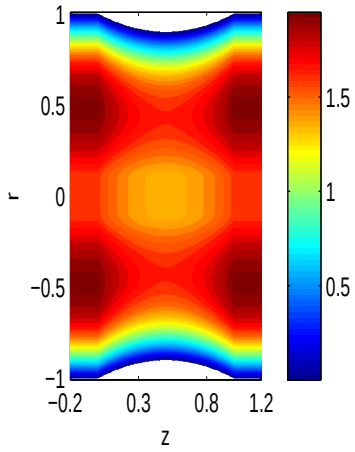

Figure 6.19: Velocity contour for $M = 0$ when $\delta = 0.1$

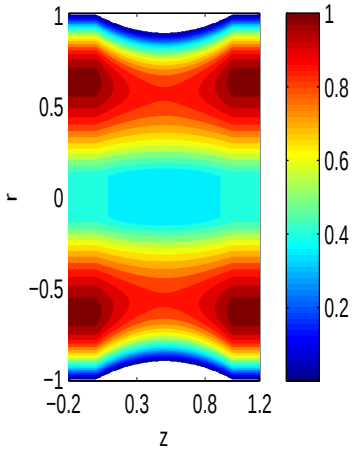

Figure 6.20: Velocity contour for $M = 2$ when $\delta = 0.1$

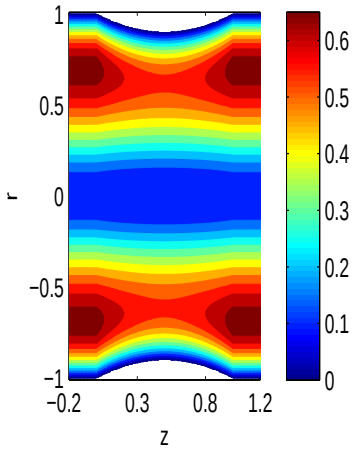

Figure 6.21: Velocity contour for $M = 3$ when $\delta = 0.1$

Fig.6.15, displays the variations of mass transfer coefficient (Sherwood number) with chemical reaction parameter for different values of the Schmidt number. The figure shows that as values of the Schmidt number increase, the Sherwood number increases.

Figs.6.16 to 6.18 display velocity contours (measure of the flow disturbances) in the downstream of the stenosis for 10%, 20% and 30% arterial occlusion. In figures, the range of the diseased part of the artery has been taken from 0 to 1 in the axial direction of the artery. From figures, it can be observed that under no magnetic effects and for the case of 10% stenosis, the contour lines get generated near the center of the artery at the downstream of the stenosis. As the blockage of the artery increases, the velocity contours strongly get distorted at the downstream and thereby slowly velocity reduces at that point. These plots provide a clear indication of the circulation zone of the flow.

Velocity contours of the stenosed artery having 10% stenosis and for different values of the applied magnetic field have been displayed in figs.6.19 to 6.21. From these figures, it can clearly be observed that as the strength of an applied magnetic field increases, the flow lines tend to increase near the stenotic wall by producing low flow lines near the center of the artery. These figures give a clear idea to find flow separation and reattachment points under the influence of the applied magnetic field.

6.5 Conclusions

Combined effects of Joule heating and viscous dissipation with chemical reaction have been investigated on the two-layered model of blood flow through a stenosed artery in the presence of variable applied the magnetic field. The two-layered model of blood flow contains a cell-free plasma layer of having constant viscosity and erythrocytes suspended core region of hematocrit dependent viscosity. Shooting method is applied to solve nonlinear partial differential equations in order to get the expressions for important flow characteristics such as flow rate, flow impedance and wall shear stress. Based on the simulation results following are the important conclusions:

1. To validate our model, a comparative study has been done between the present result and the experimental result which shows that the present result has a good

agreement with the experimental data of cell velocity distribution of blood containing 40% hematocrit.

2. The study reveals that the magnetic field parameter and hematocrit parameter have reducing effects on the velocity distribution of both the core as well as plasma regions. Since it is the situation when the human body directly subjected to an external magnetic field, it carries the promise of significant application in magnetic and electromagnetic therapy. Application of this result can be useful particularly for people having a heart problem.

3. The temperature profile of the blood flow in narrow artery decreases under the effect of high magnetic strengths while it shows the reverse effect for Eckert number. Hence the present study reveals that the temperature of the body can be regulated by applying the external magnetic field. This result can be very much useful to treat cancer.

4. The present study concludes that the concentration profile of blood flow decreases with increased values of the Schmidt number due to the buoyancy effect.

5. The concentration profile of the blood flow decreases as values of chemical reaction parameter increase. This happens due to a fall in the chemical molecular diffusivity of the species concentration which directly affects the concentration profile of core and plasma regions.

6. The study reveals that the Eckert number and Schmidt number have enhancing effects on both heat and mass transfer coefficients of the blood flow, respectively.

7. Increasing values of the height of the stenosis increase the flow impedance profile while it has reverse effects on flow rate profile of the blood flow.

Chapter 7

Modeling and Analysis of MHD Two-Phase Blood Flow through a Stenosed Artery having Temperature-Dependent Viscosity

7.1 Introduction

Blood is a bodily fluid which contains erythrocytes or RBCs, leukocytes or WBCs, platelets, and plasma (contain different types of molecules and ions) in its content. It is necessary to consider the physical properties of blood flow to measure the analysis of blood flow through the small size of blood vessels as in arterial and venules. One of the major characteristics of blood flow is the percentage of erythrocytes in the blood. Fåhræus effect explains that when blood passes from larger size of the blood vessel to a smaller size of the blood vessel (almost at least 0.3 mm), hematocrit level decreases and there exists a cell-free plasma layer at the corner of the smaller vessel (Barbee and Cokelet, 1971; Fedosov et al., 2010). The apparent viscosity of the blood flow also decreases as vessel diameter decreases as described in Fåhræus and Lindqvist effect (Fahraeus and Lindqvist, 1931). It is well known by Haynes' marginal theory that the blood flow through a small blood vessel follows the two-layered model of blood flow which consists the core region con-

taining red blood cells and a cell-free plasma layer (Chebbi, 2015). Many researchers have been studied Fåhræus and Lindqvist effect with the help of *in vitro* as well as through *in vivo* analysis (Cokelet and Goldsmith, 1991; Sharan and Popel, 2001). Sharan and Popel (2001) presented a two-phase model of the blood flow through a narrow artery consisting a central core of suspended erythrocytes and a cell-free layer surrounding the core. Medvedev and Fomin (2011) developed the two-phase model of the blood flow through both large and small blood vessels. With the help of their study, they described the analytical dependence for the blood velocity and viscosity as functions of the blood vessel diameter and hematocrit level.

In a closed system like our human circulatory system, state of hemodynamic equilibrium can be affected by the velocity, pressure, flow rate and viscosity of blood. As viscosity is the property of the fluid (when it is in motion), which measures by the resistance of fluid acts against the flow. In our human body friction between the blood elements and the vessel lumen provides the resistance to blood for circulation. The application of energy is essential to make a fluid flow. In our human circulatory system, blood pressure as well as the velocity of the blood flow, are some forms of energy. It is observed that the viscosity of biofluids shows noticeable variations with different values of temperature. As for the case of water, increased values of temperature from 10^0C to 50^0C reduce the viscosity of the water 240%. This behavior is not only seen for low viscosity fluid like water but also happens with the high viscous fluid such as blood and glycerin etc. It is observed with the help of quantitative data that the viscosity of blood increases 26% as values of temperature reduce from 36.5^0C to 22^0C, which directly affects the flow rate of blood flow by reducing its value by 20.72% (Çinar et al., 2001; Hooman and Gurgenci, 2008; Torrance and Turcotte, 1971). Hence, it is very much interesting to study the behavior of blood flow by establishing the relationship between the energy of the circulatory system and the viscosity level of blood. Many authors presented different models of blood flow by taking the temperature-dependent viscosity of blood flow rather than assuming it constant. In this regard, Siddiqa et al. (2018) discussed the influence of temperature dependent viscosity on heat transfer of blood flow through a rectangular vessel. Also, Siddiqa et al. (2017b) explained the mathematical model of the blood

flow through a rectangular channel considering the exponential model for the variation of viscosity with the temperature. In their study, it was observed that the strong viscosity of the fluid causes more disturbances in the fluid and also increases the temperature of the fluid. All the above-mentioned studies are focused on analyzing the influence of temperature dependent viscosity for single phase model of blood flow.

In the cardiovascular system of the human body, any obstruction to blood flow due to the accumulation of fatty substances such as cholesterol and saturated fats within the arteries creates a medical condition called stenosis. Presence of stenosis inside an arterial blood vessel changes its flow pattern and hemodynamics conditions and its continuous growth inside the blood vessel increase the chance of heart failure, significantly (Cooper et al., 2014; Jean et al., 1994). Since stenosis is directly related to human health, many researchers have studied its effects on the blood flow due to various shapes and sizes of stenosis. Mekheimer and Kot (2008) presented the mathematical model for the geometry of the stenosis by defining the shape and tapering parameters. With the help of their study, they resulted that impedance experienced by the streaming fluid distribution over the whole arterial segment decreases with increasing values of the stenosis length and stenosis shape parameter, while it increases as the size of the stenosis increases. Kamangar et al. (2014) numerically computed the simulations of steady and transient blood flow for different geometrical shapes of stenosis(triangular, elliptical, and trapezium) having 70% (moderate), 80% (intermediate), and 90% (severe) area stenosis. Considering the case of a diseased artery, Tripathi and Sharma (2018a) described a mathematical model for narrow arteries by defining the geometry of stenosed artery for both core and plasma regions separately. They showed that the velocity profile of blood flow decreases in both core and plasma regions as the maximum height of the stenosis increases inside an artery.

The role of magnetohydrodynamics (in which we study about the magnetic property of electrically conducting fluid) is very important in the medical science as it helps to treat hyperthermia, a cancerous tumor or magnetic wounds, bleeding reduction during surgeries (Bhatti and Zeeshan, 2016). As blood shows the characteristics of biomagnetic fluids, magnetohydrodynamics laws are very much used to study the flow of blood through an artery under the influence of the magnetic field. Misra et al. (2011c) developed a

mathematical model to understand the behavior of blood flow under the influence of externally applied magnetic field considering artery as $2D$ channel. They Investigated that velocity of the blood can be controlled (increase or decrease) by varying the strengths of an applied magnetic field. Bhatti et al. (2017b) analyzed the effects of transverse magnetic field, heat and mass transfer on peristaltic motion of two-phase flow as particle fluid suspension through a planar channel. They resulted that the temperature profile of the flow increases as the influence of magnetic field increases. Further, Ponalagusamy and Selvi (2013) explained the effects of the magnetic field for two-phase blood flow consisting RBC containing core region and cell-free plasma region. With the help of their model, they resulted that both wall shear stress and impedance increase as strengths of the external applied magnetic field increase.

Recently, heat generated by viscous dissipation and Joule heating has attracted attentions by many researchers. Joule heating is the process in which heat is generated due to collision among the moving particles and in this procedure kinetic energy is transformed into heat which enhances the temperature of the human body (Hayat et al., 2018; Sharma et al., 2013). On the other hand, viscous dissipation is calculated through the work done by the velocity against viscous stresses, known as viscous dissipation of energy (Kumar et al., 2018). Sharma et al. (2015a) developed a mathematical model considering pulsatile hydro-magnetic rheological nature of the blood flow with joule heating and viscous dissipation effects. By paying attention to the viscous dissipation and Joule heating effects, Chakraborty et al. (2013) discussed the thermal characteristics of electro-magneto-hydrodynamics flow in microchannels. They resulted that increasing Joule heating effect enhances the liquid temperature in a homogeneous manner while the increased value of viscous heating increase temperature of the wall.

On the other hand, to study the chemical reaction effect in fluids is important in view of several physiological functions. As in drug dynamics(which describes the effects of the drug on the body) a role of the chemical reaction is important to study. In most of the chemical reaction, reaction rate based on the concentration of the species itself whether they are heterogeneous or homogeneous depends upon the where it occurs at an interface or as a single phase volume reaction. If the reaction rate of any chemical reaction is

directly proportional to the concentration it is called as a first-order homogeneous chemical reaction. The reaction in which the reaction rate is proportional to the n^{th} power of the concentration is considered n order chemical reaction. Makinde (2010) analyzed the mixed convection problem for vertical porous plate considering n^{th} order homogeneous chemical reaction between the fluid and the diffusing species. Further, Tripathi and Sharma (2018b) explained the effects of first-order chemical reaction on the two-phase model of blood flow and resulted that the concentration profile decreases in both core and plasma regions as values of the chemical reaction parameter increase.

However, in none of the aforesaid studies mentioned above, a problem of two-phase blood flow with k^{th} order chemical reaction has been incorporated. The present study deals the MHD problem of two-phase blood flow through a stenosed inclined artery having Joule heating and viscous dissipation effects with radiation and k^{th} order of chemical reaction. In two-phase blood flow viscosity of the core region is assumed as temperature dependent while the viscosity of the plasma region is treated constant. The governing non-linear partial differential equations of the present mathematical model have been solved by applying a single shooting method. Solutions which have been calculated for flow resistance, total flow rate, wall shear stress, heat and mass transfer and simultaneously their respective graphs, give the physical insight of blood flow.

7.2 The Mathematical Model

Considered the cylindrical stenosed narrow artery of length L in which blood flow is assumed to be a two-layered flow viz. core layer and plasma layer as shown in fig.7.1. The core layer contains erythrocytes (suspension of uniform hematocrit) and another one plasma layer is the RBC cell-free. Length of the arterial vessel and applied shear stress are assumed to be large enough so that the Newtonian nature of the blood flow can be observed in both core and plasma regions, separately (Noutchie, 2009). In order to investigate the flow dynamics of blood flow under the effect of applied magnetic field, a fully developed, unsteady, laminar, incompressible fluid is considered both in the core as well as in plasma regions. It is assumed that in the core region viscosity of the fluid varies

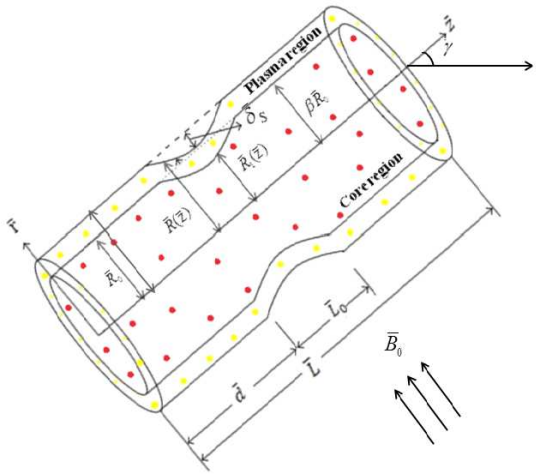

Figure 7.1: Geometry of the inclined stenosed artery of length $\bar{L}$

with temperature, while, the viscosity of the plasma region is constant.

The temperature dependent viscosity of the fluid for the core region is given by (Siddiqa et al., 2018)

$$\mu_c(\bar{T}) = \bar{\mu_p}\exp\left[\lambda\left(\frac{1}{2} - \frac{\bar{T}_c - \bar{T}_0}{\bar{T}_w - \bar{T}_0}\right)\right].$$

Geometry of the elliptical shape stenosis in plasma region (assumed to be symmetric) is defined as (Kamangar et al., 2014),

$$\bar{R}(\bar{z}) = \begin{cases} 1 - \frac{\bar{\delta}_s^*}{\bar{R}_0}\sin\pi\left(\frac{\bar{z}-\bar{d}}{\bar{L}_0}\right) & \text{for} \quad \bar{d} \le \bar{z} \le \bar{d} + \bar{L}_0, \\ 1 & \text{otherwise.} \end{cases} \tag{7.2.1}$$

In the core region, geometry of the elliptical shape stenosis is defined as

$$\frac{\bar{R}_1(\bar{z})}{\bar{R}_0} = \begin{cases} \beta - \frac{\bar{\delta}_s^*}{\bar{R}_0}\sin\pi\left(\frac{\bar{z}-\bar{d}}{\bar{L}_0}\right) & \text{for} \quad \bar{d} \le \bar{z} \le \bar{d} + \bar{L}_0, \\ 1 & \text{otherwise,} \end{cases} \tag{7.2.2}$$

where $\bar{\delta}_s^*$ is the maximum height of the stenosis, located at

$$\bar{z} = \bar{d} + \frac{\bar{L}_0}{n^{\frac{1}{(n-1)}}}. \tag{7.2.3}$$

Note that in cylindrically shaped artery, velocity components in $(\bar{r}, \bar{\theta}, \bar{z})$ directions are considered as $(\bar{u_c}, \bar{v_c}, \bar{w_c})$ and $(\bar{u_p}, \bar{v_p}, \bar{w_p})$, respectively. Under these assumptions, the governing equations for core region are as follows:

$$\bar{\rho_c}\frac{\partial \bar{u}_c}{\partial \bar{t}} = -\frac{\partial \bar{p}}{\partial \bar{z}} + \frac{1}{\bar{r}}\frac{\partial}{\partial \bar{r}}\left(\bar{r}\mu_c(\bar{r})\left(\frac{\partial \bar{u}_c}{\partial \bar{r}}\right)\right) - \bar{\sigma_1}{\bar{B_0}}^2\bar{u_c} + \bar{g}\bar{\rho_c}\bar{\beta}\left(\bar{\theta_c} - \bar{\theta_0}\cos\gamma\right) + \bar{g}\bar{\rho_c}\bar{\gamma}\left(\bar{\sigma_c} - \bar{\sigma_0}\right)\cos\gamma, \tag{7.2.4}$$

$$\bar{\rho_c}\bar{c_c}\frac{\partial \bar{T}_c}{\partial \bar{t}} = \bar{K_c}\left(\frac{\partial^2 \bar{T}_c}{\partial \bar{r}^2} + \frac{1}{\bar{r}}\frac{\partial \bar{T}_c}{\partial \bar{r}}\right) + \bar{\mu}_c(\bar{r})\left(\frac{\partial \bar{u}_c}{\partial \bar{r}}\right)^2 + \bar{\sigma_1}\bar{B_0}(\bar{r})^2{\bar{u_c}}^2 - \frac{\partial \bar{q_c}}{\partial \bar{r}}, \tag{7.2.5}$$

$$\frac{\partial \bar{C}_c}{\partial \bar{t}} = \bar{D_c}\left(\frac{\partial^2 \bar{C}_c}{\partial \bar{r}^2} + \frac{1}{\bar{r}}\frac{\partial \bar{C}_c}{\partial \bar{r}}\right) - \bar{E_c'}\left(\bar{C_c} - \bar{C_0}\right)^k. \tag{7.2.6}$$

Also, momentum, energy and concentration equations for plasma region are as follows

$$\bar{\rho_p}\frac{\partial \bar{u}_p}{\partial \bar{t}} = -\frac{\partial \bar{p}}{\partial \bar{z}} + \bar{\mu}_p\left(\frac{\partial^2 \bar{u}_p}{\partial \bar{r}^2} + \frac{1}{\bar{r}}\frac{\partial \bar{u}_p}{\partial \bar{r}}\right) - \bar{\sigma_1}\bar{B_0}(\bar{r})^2\bar{u_p} + \bar{g}\bar{\rho_p}\bar{\beta}\left(\bar{\theta_p} - \bar{\theta_0}\cos\gamma\right) + \bar{g}\bar{\rho_p}\bar{\gamma}\left(\bar{\sigma_p} - \bar{\sigma_0}\right)\cos\gamma, \tag{7.2.7}$$

$$\bar{\rho_p}\bar{c_p}\frac{\partial \bar{T}_p}{\partial \bar{t}} = \bar{K_p}\left(\frac{\partial^2 \bar{T}_p}{\partial \bar{r}^2} + \frac{1}{\bar{r}}\frac{\partial \bar{T}_p}{\partial \bar{r}}\right) + \bar{\mu}_p\left(\frac{\partial \bar{u}_p}{\partial \bar{r}}\right)^2 + \bar{\sigma_1}\bar{B_0}(\bar{r})^2{\bar{u_p}}^2 - \frac{\partial \bar{q_p}}{\partial \bar{r}}, \tag{7.2.8}$$

$$\frac{\partial \bar{C}_p}{\partial \bar{t}} = \bar{D_p}\left(\frac{\partial^2 \bar{C}_p}{\partial \bar{r}^2} + \frac{1}{\bar{r}}\frac{\partial \bar{C}_p}{\partial \bar{r}}\right) - \bar{E_p'}\left(\bar{C_p} - \bar{C_0}\right)^k. \tag{7.2.9}$$

In eqs.(7.2.4) and (7.2.7), $\bar{\sigma_1}{\bar{B_0}}^2\bar{u_c}$ and $\bar{\sigma_1}\bar{B_0}(\bar{r})^2\bar{u_p}$ are due to Lorentz force which acts in the particular direction of the inclined artery as displayed in fig.7.1. Term $\bar{\mu}_c(\bar{r})\left(\frac{\partial \bar{u}_c}{\partial \bar{r}}\right)^2$ in eq.(7.2.5) and $\bar{\mu}_p\left(\frac{\partial \bar{u}_p}{\partial \bar{r}}\right)^2$ in eq.(7.2.8) represent the viscous dissipation effect which greatly influence the heat transfer mechanics of blood flow. Similarly, last terms in eqs.(7.2.5) and (7.2.8) are because of the Joule heating effect, while last term in eqs.(7.2.6), (7.2.9), (7.2.6) (7.2.9) are incorporated for chemical reaction effect. Here we consider the case of non homogeneous chemical reaction of order k^{th}, where k is any constant.

In the model, outer wall is taken solid by following the no-slip boundary conditions at the wall. It is assumed that the velocity, temperature, and concentration follow a continuous behavior at the interface of core and plasma regions. Velocity, temperature and

concentration gradient are assumed to be vanishing along with the center of artery due to symmetry (Sharan and Popel, 2001). Therefore, having all these assumption boundary conditions for the given mathematical model are as follows:

$$\begin{cases} \bar{u_p} = 0, \quad \bar{T_p} = \bar{T_w}, \quad \bar{C_p} = \bar{C_w} \quad at \quad \bar{r} = \bar{R}(\bar{z}), \\ \bar{u_c} = \bar{u_p}, \quad \bar{T_p} = \bar{T_c}, \quad \bar{C_p} = \bar{C_c} \quad at \quad \bar{r} = \bar{R_1}(\bar{z}), \\ \frac{\partial \bar{u}_c}{\partial \bar{r}} = 0, \quad \frac{\partial \bar{T_c}}{\partial \bar{r}} = 0, \quad \frac{\partial \bar{C_c}}{\partial \bar{r}} = 0 \quad at \quad \bar{r} = 0, \\ \bar{\tau_c} = \bar{\tau_p}, \quad \frac{\partial \bar{T_c}}{\partial \bar{r}} = \frac{\partial \bar{T_p}}{\partial \bar{r}}, \quad \frac{\partial \bar{C_c}}{\partial \bar{r}} = \frac{\partial \bar{C_p}}{\partial \bar{r}} \quad at \quad \bar{r} = \bar{R_1}(\bar{z}). \end{cases} \tag{7.2.10}$$

Now, we introduce the following non-dimensional parameters,

$$u_c = \frac{\bar{u_c}}{\bar{u_0}}, \quad r = \frac{\bar{r}}{\bar{R_0}}, \quad z = \frac{\bar{z}}{\bar{R_0}}, \quad t = \bar{\omega}\bar{t}, \quad \frac{\bar{R}(\bar{z})}{\bar{R_0}} = R(Z), \quad \frac{\bar{R_1}(\bar{z})}{\bar{R_0}} = R_1(z),$$

$$u_p = \frac{\bar{u_p}}{\bar{u_0}}, \quad p = \frac{\bar{R_0}\bar{p}}{\bar{u_0}\bar{\mu_p}}, \quad Re = \frac{\bar{\rho_p}\bar{R_0}u_0}{\bar{\mu_p}}, \quad \theta_c = \frac{(\bar{T_c} - \bar{T_0})}{\bar{T_w} - \bar{T_0}}, \quad \sigma_c = \frac{(\bar{C_c} - \bar{C_0})}{\bar{C_w} - \bar{C_0}},$$

$$Gm = \frac{\bar{g}\bar{\rho_p}\bar{\beta}{\bar{R_0}}^2\left(\bar{C_w} - \bar{C_0}\right)}{\bar{u_0}\bar{\mu_p}}, \quad \theta_p = \frac{(\bar{T_p} - \bar{T_0})}{\bar{T_w} - \bar{T_0}}, \quad M = \frac{\bar{\sigma}\bar{B_0}(\bar{r})^2{\bar{R_0}}^2}{\bar{\mu_p}}, \quad \sigma_p = \frac{(\bar{C_p} - \bar{C_0})}{\bar{C_w} - \bar{C_0}},$$

$$Pe = \frac{\bar{\rho_p}\bar{c_p}{\bar{R_0}}^2\bar{\omega}}{\bar{K_p}}, \quad Sc = \frac{\bar{\mu_p}}{\bar{D_p}\bar{\rho_p}}, \quad D_0 = \frac{\bar{D_p}}{\bar{D_c}}, Gr = \frac{\bar{g}\bar{\rho_p}\bar{\beta}{\bar{R_0}}^2\left(\bar{T_w} - \bar{T_0}\right)}{\bar{u_0}\bar{\mu_p}}, \quad \delta = \frac{\bar{\delta_s}}{\bar{R_0}}$$

$$\tau_c = \frac{\bar{\tau_c}{\bar{R_0}}^2}{\bar{u_0}\bar{\mu_p}}, \quad \tau_p = \frac{\bar{\tau_p}{\bar{R_0}}^2}{\bar{u_0}\bar{\mu_p}}, \quad \rho_0 = \frac{\bar{\rho_p}}{\bar{\rho_c}}, \quad \mu_0 = \frac{\bar{\mu_p}}{\bar{\mu_c}}, \quad \bar{E_p'} = \frac{E\bar{\mu_p}}{\bar{C_w} - {\bar{C_0}}^k\bar{\rho_p}{\bar{R_0}}^2}, \quad E_0 = \frac{\bar{E_p}}{\bar{E_c}},$$

where k is any constant and meaning of the other mentioned notations are already given in earlier chapters 2, 3 and 4.

Using the non-dimensional parameters, the dimensionless form of the geometry of the stenosis for core and plasma regions respectively are as follows

$$R(z) = \begin{cases} \frac{1}{R_0}\left(1 - \delta \sin \pi\left(z - l\right)\right) & \text{for} \quad l \leq z \leq 1 + l, \\ 1 & \text{otherwise}, \end{cases} \tag{7.2.11}$$

$$R_1(z) = \begin{cases} \beta - \delta \sin \pi\left(z - l\right) & \text{for} \quad l \leq z \leq 1 + l, \\ \beta & \text{otherwise}, \end{cases} \tag{7.2.12}$$

where

$$l = \frac{\bar{d}}{\bar{L}_0}, \quad \delta = \frac{\bar{\delta}_s^{\,*}}{\bar{R}_0}.$$

The governing eqs.(7.2.4)-(7.2.6) for core region in dimensionless form are as follows

$$\left(\frac{Re}{\rho_0}\right)\left(\frac{\partial u_c}{\partial t}\right) = -\left(\frac{\partial p}{\partial z}\right) + \exp\left(\lambda\left(\frac{1}{2}-\theta_c\right)\right) + \frac{1}{r}\frac{\partial}{\partial r}\left(r\left(\frac{\partial u_c}{\partial r}\right)\right) - Mu_c + \frac{\theta_c}{\rho_0}\cos\gamma + \frac{\sigma_c}{\rho_0}\cos\gamma, \tag{7.2.13}$$

$$\left(\frac{1}{\rho_0 s_0}\right)\left(\frac{\partial \theta_c}{\partial t}\right) = \frac{1}{K_0 Pe}\left(\frac{\partial^2\theta_c}{\partial r^2} + \frac{1}{r}\frac{\partial\theta_c}{\partial r}\right) + M\left(\frac{E_c}{Re}\right){u_c}^2 - \left(\frac{N^2}{Pe{\alpha_0}^2}\right)\theta_c + \left(\frac{E_c}{Re}\right)\exp\left(\lambda\left(\frac{1}{2}-\theta_c\right)\right)\left(\frac{\partial u_c}{\partial r}\right)^2, \tag{7.2.14}$$

$$Re\left(\frac{\partial \sigma_c}{\partial t}\right) = \frac{1}{D_0}\left(\frac{1}{Sc}\right)\left(\frac{\partial^2\sigma_c}{\partial r^2} + \frac{1}{r}\frac{\partial\sigma_c}{\partial r}\right) - \frac{E}{E_0}{\sigma_c}^k. \tag{7.2.15}$$

The governing eqs.(7.2.7)-(7.2.9) for the plasma region can be written in non dimensional form as

$$Re\left(\frac{\partial u_p}{\partial t}\right) = -\left(\frac{\partial P}{\partial z}\right) + \left(\frac{\partial^2 u_p}{\partial r^2} + \frac{1}{r}\frac{\partial u_p}{\partial r}\right) - Mu_p, \tag{7.2.16}$$

$$\left(\frac{\partial \theta_p}{\partial t}\right) = \frac{1}{Pe}\left(\frac{\partial^2\theta_p}{\partial r^2} + \frac{1}{r}\frac{\partial\theta_p}{\partial r}\right) + \frac{E_c}{Re}\left(\frac{\partial u_p}{\partial r}\right)^2 + M\frac{E_c}{Re}{u_p}^2 - \left(\frac{N^2}{Pe}\right)\theta_p, \tag{7.2.17}$$

$$Re\left(\frac{\partial \sigma_p}{\partial t}\right) = \left(\frac{1}{Sc}\right)\left(\frac{\partial^2\sigma_p}{\partial r^2} + \frac{1}{r}\frac{\partial\sigma_p}{\partial r}\right) - E{\sigma_p}^k. \tag{7.2.18}$$

The corresponding boundary conditions eq.(7.2.10) in non dimensional form are as follows

$$\begin{cases} u_p = 0, & \theta_p = 1, & \sigma_p = 1 & at & r = R(z), \\ u_p = u_c, & \theta_p = \theta_c, & \sigma_p = \sigma_c & at & r = R_1(z), \\ \tau_c = \tau_p, & \frac{\partial\theta_c}{\partial r} = \frac{\partial\theta_p}{\partial r}, & \frac{\partial\sigma_c}{\partial r} = \frac{\partial\sigma_p}{\partial r} & at & r = R_1(z), \\ \frac{\partial u_c}{\partial r} = 0, & \frac{\partial\theta_c}{\partial r} = 0, & \frac{\partial\sigma_c}{\partial r} = 0 & at & r = R_c. \end{cases} \tag{7.2.19}$$

As pumping action of the heart results into a pulsatile nature of the blood flow. Therefore, we consider the following form for pressure gradient (Ponalagusamy and Selvi, 2015)

$$-\frac{\partial p}{\partial z} = P_0 e^{i\omega t}, \tag{7.2.20}$$

where P_0 denotes the constant pressure. As described by Womersley (1955), the given assumption eq.(7.2.20) can be applied to the harmonic oscillatory flows in which real part of the equation provides the corresponding flow.

For preferred form of the pressure gradient, solution of velocity, temperature and concentration for both core and plasma regions can be written in the form of

$$\begin{cases} u_c(r,t) = u_{c_0}(r)e^{i\omega t}, & u_p(r,t) = u_{p_0}(r)e^{i\omega t}, \\ \theta_c(r,t) = \theta_{c_0}(r)e^{i\omega t}, & \theta_p(r,t) = \theta_{p_0}(r)e^{i\omega t}, \\ \sigma_c(r,t) = \sigma_{c_0}(r)e^{i\omega t}, & \sigma_p(r,t) = \sigma_{p_0}(r)e^{i\omega t}. \end{cases} \tag{7.2.21}$$

Substituting the given expressions from eq.(7.2.21) in to eqs.(7.2.13)-(7.2.15), we get the equation of core region

$$\begin{aligned} \left(i\frac{Re}{\rho_0} + M\right) u_{c_0} =& P_0 + \exp\left(\lambda\left(\frac{1}{2} - \theta_c\right)\right)\left[\left(\frac{\partial^2 u_{c_0}}{\partial r^2}\right) + \frac{1}{r}\left(\frac{\partial u_{c_0}}{\partial r}\right)\right] \\ &+ \frac{\cos\gamma}{\rho_0}\left(Gr\theta_{c_0} + Gm\sigma_{c_0}\right), \end{aligned} \tag{7.2.22}$$

$$\begin{aligned} \left(i\omega\frac{1}{\rho_0 s_0} + \left(\frac{N^2}{Pe}\right)\left(\frac{1}{\alpha_0}\right)^2\right)\theta_{c_0} =& \frac{1}{K_0 Pe}\left(\frac{\partial^2\theta_{c_0}}{\partial r^2} + \frac{1}{r}\frac{\partial\theta_{c_0}}{\partial r}\right) + M\frac{E_c}{Re}e^{i\omega t}{u_{c_0}}^2 \\ &+ \left(\frac{E_c}{Re}\right)\exp\left(\lambda\left(\frac{1}{2} - \theta_{c_0}\right)\right)e^{i\omega t}\left(\frac{\partial u_{c_0}}{\partial r}\right)^2, \end{aligned} \tag{7.2.23}$$

$$iReD_0 Sc\sigma_{c_0} + \frac{E}{E_0}D_0 Sc{\sigma_{c_0}}^k e^{i(k-1)t} = \frac{\partial^2\sigma_{c_0}}{\partial r^2} + \frac{1}{r}\frac{\partial\sigma_{c_0}}{\partial r}, \tag{7.2.24}$$

and eqs.(7.2.16)-(7.2.18) of plasma region convert in the form of

$$\left(iRe + M\right)u_{p_0} = P_0 + \left(\frac{\partial^2 u_{p_0}}{\partial r^2} + \frac{1}{r}\frac{\partial u_{p_0}}{\partial r}\right) + \cos\gamma\left(Gr\theta_{p_0} + Gm\sigma_{p_0}\right), \tag{7.2.25}$$

$$i\omega\theta_{p_0} = \frac{1}{Pe}\left(\frac{\partial^2\theta_{p_0}}{\partial r^2} + \frac{1}{r}\frac{\partial\theta_{p_0}}{\partial r}\right) + M\frac{E_c}{Re}e^{i\omega t}{u_{p_0}}^2 + e^{i\omega t}\left(\frac{E_c}{Re}\right)\left(\frac{\partial u_{p_0}}{\partial r}\right)^2 - \frac{N^2}{Pe}\theta_p, \tag{7.2.26}$$

$$\frac{\partial^2\sigma_{p_0}}{\partial r^2} + \frac{1}{r}\frac{\partial\sigma_{p_0}}{\partial r} - iReSc\sigma_{p_0} + ESc\sigma_{p_0}^k e^{i(k-1)t} = 0. \tag{7.2.27}$$

7.3 Solution

Since given equations of core region from eqs.(7.2.22)-(7.2.24) and equations for plasma region from eqs.(7.2.25)-(7.2.27) are coupled nonlinear differential equations. We apply a

numerical technique named as single shooting method to solve following model under the given boundary conditions eq.(7.2.19), simultaneously.

To execute the single shooting method on the given eqs.(7.2.22) and (7.2.24) we assume $x(1) = u$, $x(2) = \theta$ and $x(3) = \sigma$, $x(4) = \frac{\partial u}{\partial r}$, $x(5) = \frac{\partial \theta}{\partial r}$ and $x(6) = \frac{\partial \sigma}{\partial r}$. We convert them in first order nonlinear system as

$$\dot{x}(1) = x(4), \tag{7.3.1}$$

$$\dot{x}(2) = x(5), \tag{7.3.2}$$

$$\dot{x}(3) = x(6), \tag{7.3.3}$$

$$\dot{x}(4) = \left(\frac{i\omega Re}{\rho_0} + M\right)\frac{x(1)}{\chi} - \frac{P_0}{\chi} - \frac{\cos\gamma}{\rho_0}\left(Grx(2) + Gmx(3)\right)\frac{1}{\chi} - \frac{x(4)}{r}, \tag{7.3.4}$$

$$\dot{x}(5) = -\left(\frac{EcK0Pe\chi}{Re}\right)x(4)^2 e^{i\omega t} - \left(\frac{MEcK0Pe}{Re}\right)x(1)^2 e^{i\omega t} - \frac{x(5)}{r} + \tag{7.3.5}$$

$$(PeK0)\left(\frac{i\omega}{\rho_0 s_0} + \frac{N^2}{Pe{\alpha_0}^2}\right)x(2),$$

$$\dot{x}(6) = iReD_0 Scx(3) + \frac{E}{E_0}D_0 Scx(3)^k e^{(k-1)t}, \tag{7.3.6}$$

where $\chi = \exp\left(\lambda\left(\frac{1}{2} - \theta_{c_0}\right)\right)$. Now, first order system for eqs.(7.2.25) and (7.2.27) can be written as follows

$$\dot{x}(1) = x(4), \tag{7.3.7}$$

$$\dot{x}(2) = x(5), \tag{7.3.8}$$

$$\dot{x}(3) = x(6), \tag{7.3.9}$$

$$\dot{x}(4) = (iRe + M)\,x(1) - P_0 - \cos\gamma\left(Grx(2) + Gmx(3)\right) - \frac{x(4)}{r}, \tag{7.3.10}$$

$$\dot{x}(5) = -\left(\frac{EcPe}{Re}\right)x(4)^2 e^{i\omega t} - \left(\frac{MEcPe}{Re}\right)x(1)^2 e^{i\omega t} + iPe\omega x(2) + \left(\frac{N^2}{Pe}\right)x(2) - \frac{x(5)}{r}, \tag{7.3.11}$$

$$\dot{x}(6) = iReScx(3) + EScx(3)^k e^{(k-1)t} - \frac{x(6)}{r}. \tag{7.3.12}$$

We solve these system of ODEs applying single shooting method as described in algorithm((1)) with the help of MATLAB 2015.

7.4 Results and Discussion

The present model describes heat and mass transfer effects on two-phase blood flow through a inclined stenosed artery considering Joule heating and viscous dissipation effects with k^{th} order chemical reaction and radiation effect. As viscosity of bio fluids gives noticeable variations with different values of temperature therefore in the present model viscosity of the core region region is assumed as temperature dependent treating viscosity of plasma region as constant. The effects of various physical parameters are analyzed on the inclined artery which made γ angle from the horizontal axis. With the help of computed results for velocity, temperature and concentration, different graphs have been plotted to analyze the influence of various physical parameters on blood flow in this section. The values of physical parameters which have been used in this model are given in Table.(5.1) and Table.(6.1).

In order to get the physical insight of the problem core region is considered from 0 to 0.6 on the scale of 0 to 1, having a plasma layer thickness of 0.1, in which maximum height of the stenosis is assumed as $\delta = 0.2$. In all the figures, continuous lines display the effects of the physical parameter on core region, while, dotted lines show the effects for cell-free plasma layer.

Fig.7.2 displays the variations of the velocity profile of blood flow for different values of magnetic field parameter (M). In the figure, individual effects of magnetic field on velocity profiles of both core and plasma regions can be seen observed. From the figure, it is clear that as the influence of an external magnetic field increases from 0 to 4, the

velocity profile of blood flow decreases in both core and plasma region. In the core region, it decreases more as compared to the plasma region. This is due to the fact that the core region contains red blood cells which consist mainly of hemoglobin, an iron-containing protein. Therefore, change in the strength of an external magnetic field create magnetic torque, influence of which results in erythrocytes to orient with their disk plane parallel to the direction of the applied magnetic field. This type of orientation makes red blood cell to be more suspended in the blood which directly increases the viscosity of the blood flow and the velocity of blood flow in the core region decreases with high strength of magnetic field. Continuous behavior of flow at the interface of core and plasma directly affects the velocity of the plasma layer by decreasing its value with high strength of the magnetic field. This result follows in the same manner as proposed by Ponalagusamy and Priyadharshini (2018). Fig.7.3 shows the variations of the velocity profile of blood flow as the maximum height of the stenosis changes from 0 to 0.2. The figure shows the behavior of velocity profile for the cases (i) when there is no blockage and core region varies from 0 to 0.9 and (ii) with blockage up to 20% and core layer covers 0 to 0.7 region of the artery. It can be seen from the figure that velocity shows mixed behavior with different height of the stenosis as it increases near the center of the artery as values of δ increase. It decreases for rest of the region covered by core and plasma with increasing values of δ. Fig.7.4 illustrates the effects of different inclination angle (made by the artery from the

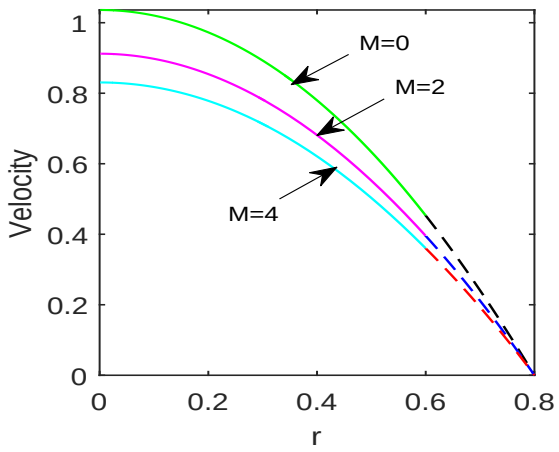

Figure 7.2: Velocity distribution with different values of M

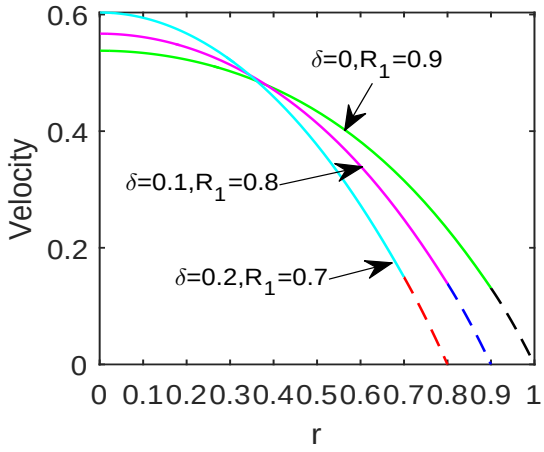

Figure 7.3: Velocity distribution with different values of δ

horizontal axis) on the velocity profile of blood flow. From the figure, it can be clearly seen that as values of the inclination angle changes from $\frac{\pi}{6}$ to $\frac{\pi}{3}$, velocity profile of both core and plasma regions decrease, respectively. For all the given inclination angle of the artery, velocity in the core region attains higher value than the plasma region. It attains its maximum value at the middle of the artery and started decreasing towards the interface region of both core and plasma region and fall to zero at the outer wall by following the parabolic profile. Effects of Grashof number and modified Grashof number have been displayed in figs.7.5 and 7.6, respectively. It is observed that as the values of Grashof number and modified Grashof number increase velocity profile in both core and plasma regions decrease, respectively. In both, the figures velocity profile of the core region shows significant variations as compared to the plasma region with increasing values of Grashof and solutal Grashof number.

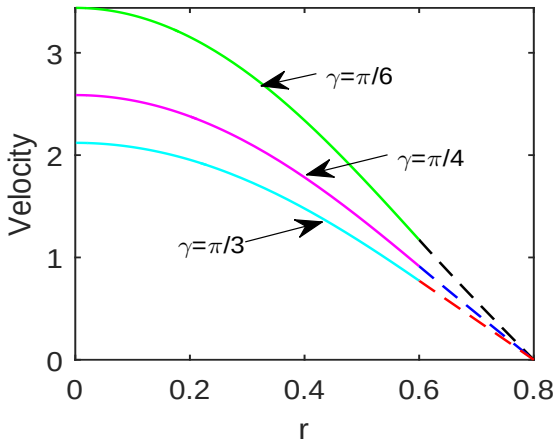

Figure 7.4: Variation of velocity profile with different values of γ

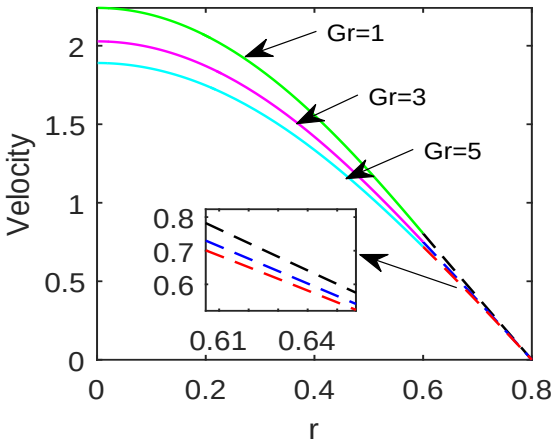

Figure 7.5: Variation of the velocity profile for different values of Gr

The temperature profile of blood flow shows variations with different values of magnetic field parameter due to Joule heating effect as shown in fig.7.7. As it can be seen from the figure that as values of magnetic field parameter increase from 0 to 4, the temperature profile of blood flow in both core and plasma regions increase, respectively. This is due to the Lorentz force which acts as retarding force and slows down the velocity of both the core region and plasma region, respectively. This resisting force creates more heat inside

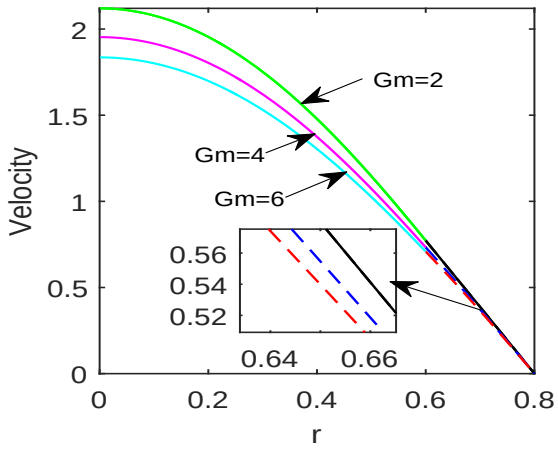

Figure 7.6: Velocity profile for different values of Gm

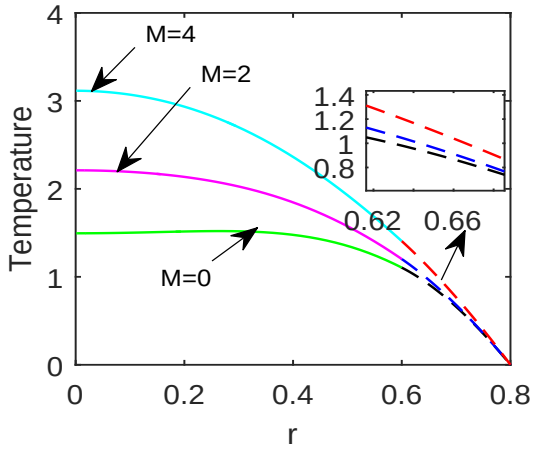

Figure 7.7: Temperature distribution for different values of M

the regions and increases the temperature profile of blood flow in both the regions. The temperature profile of the blood flow for different values of the radiation parameter has been depicted in fig.7.8. The figure illustrates that as values of the radiation parameter increase from $N = 0$ to $N = 4$, the temperature profile of the blood flow in both core and plasma regions also increase, respectively. For each value of the radiation parameter temperature profile of the core region attains higher value than the temperature profile of the plasma region. Although, in both of the regions effective variations with different values of the radiation parameter can be observed. This happens because radiation works as a heat source within the blood and as radiation dosage increases temperature profile also increases. This result is very much applicable to treat some pathological situations like thermal therapy in which body tissues and cancerous cells are exposed to high temperature. High values of temperature due to thermal radiation absorption make the cancerous cell more sensitive to radiation and action of which damages and kill cancer cells associated with tumors (Dewhirst et al., 2003).

Fig.7.9 reveals the variation of the concentration profile of the blood flow for different values of chemical reaction parameter where the order of chemical reaction is taken as $n = 1$. The figure exhibits that as values of the chemical reaction parameter increase concentration profile of the blood flow in both core and plasma regions increase, respectively.

Following the parabolic profile, concentration profile attains higher value at the middle of the artery and it starts decreasing towards the interface region of the core and plasma region and fall to zero at the outer wall.

Variation of the concentration profile of blood flow for different values of modified Grashof number has been displayed in fig.7.10. The figure elucidates that the concentration profile in both core and plasma regions decreases rapidly as effects of modified Grashof number increase. Fig.7.11 shows the concentration profile of the blood flow when order of the chemical reaction changes from $n = 1$ to $n = 5$. The figure illustrates that the first and fifth order of the chemical reaction has the higher value of the concentration profile as compared to the second, third and fourth order of chemical reaction.

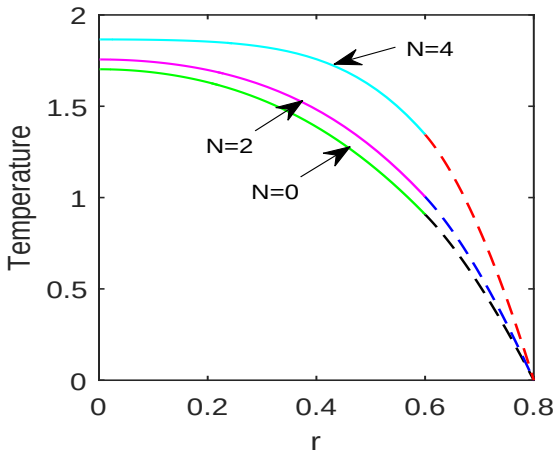

Figure 7.8: Variation of temperature profile for different values of N

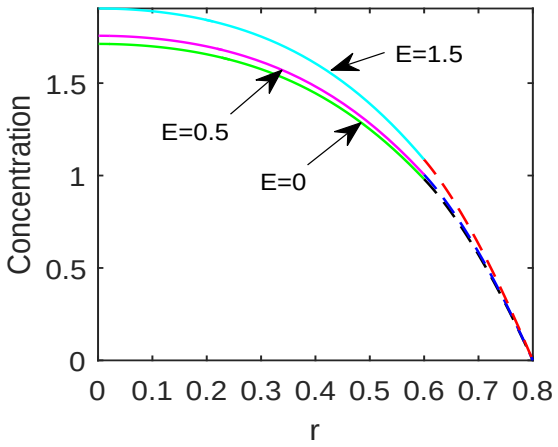

Figure 7.9: Concentration distribution for different values of E

The total volumetric flow rate for different values of a magnetic field parameter, the height of the stenosis and viscosity parameter have been shown in figs.7.12, 7.13 and 7.14, respectively. In all the figures value of z covers only the stenosed region of the artery. It can be noticed from the fig.7.12 that as the intensity of the magnetic field increases from $M = 0$ to $M = 4$, flow rate decreases and this happens due to Lorentz force which opposes the flow of fluid. Considering elliptically shaped stenosis, fig.7.13 reveals that the increasing height of the stenosis slows down the flow rate of the blood flow. In the stenosed region $z = 0$ to $z = 0.5$, from its higher value flow rate starts decreasing

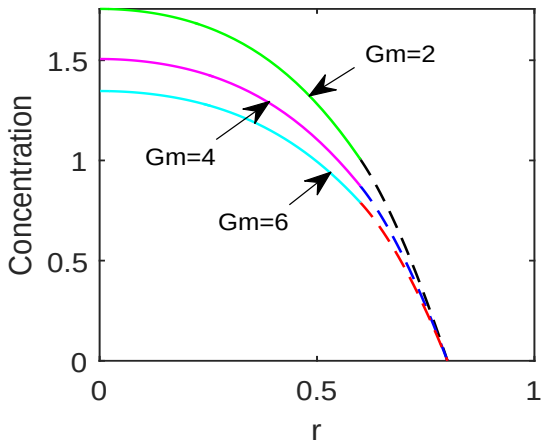

Figure 7.10: Variation of concentration profile for different values of Gm

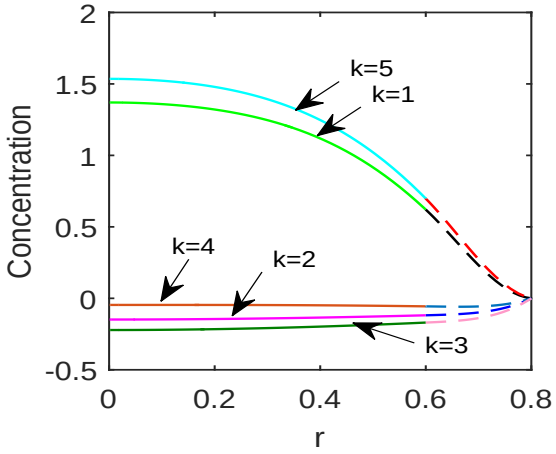

Figure 7.11: Variation of concentration profile for different values of k

as the height of the stenosis increases. Fig.7.14 displays that as values of the viscosity parameter increase, flow rate inside the stenosed artery decreases due to the assumption of temperature-dependent viscosity of the core region.

The total volumetric flow rate of blood flow in the artery is calculated as

$$Q = 2\pi R^2 \int_0^{R_1} u_c(r,t)dr + 2\pi R^2 \int_{R_1}^{R} u_p(r,t)dr. \tag{7.4.1}$$

The shear stress at the interface of core and the plasma region is given by

$$\tau = -\left(\frac{\partial u_c}{\partial r}\right)_{R_1}. \tag{7.4.2}$$

Flow resistance in the two-phase blood flow is defined as

$$\lambda_i = \int_0^z \frac{P_0 e^{i\omega t}}{Q} dz. \tag{7.4.3}$$

Variations of Wall shear stress (which is one of the most important flow characteristics of blood flow) for different values of Eckert number and radiation parameter have been displayed in figs.7.15 and 7.16, respectively. The fig.7.15 illustrates that as values of Eckert number (which characterize the heat dissipation) increase, wall shear stress decreases while, reverse effect is observed for radiation parameter as shown in fig.7.16.

Effects of different values of plasma layer thickness and Reynolds number on flow impedance (which develops the correlation between the localization of stenosis and arterial

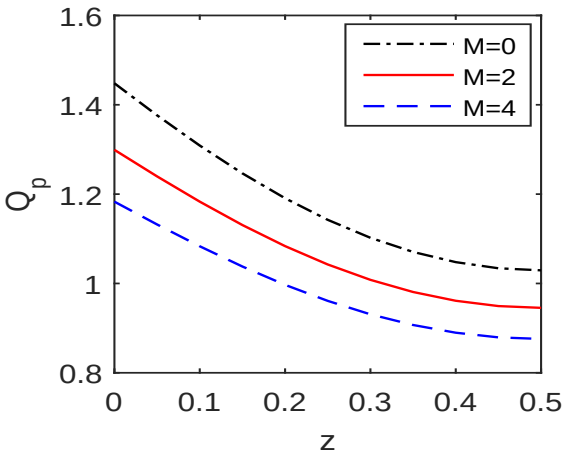

Figure 7.12: Variation of flow rate for different values of M

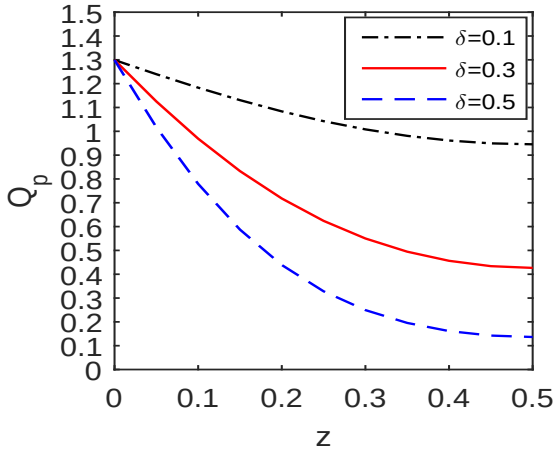

Figure 7.13: Variation of flow rate with z for different values of δ

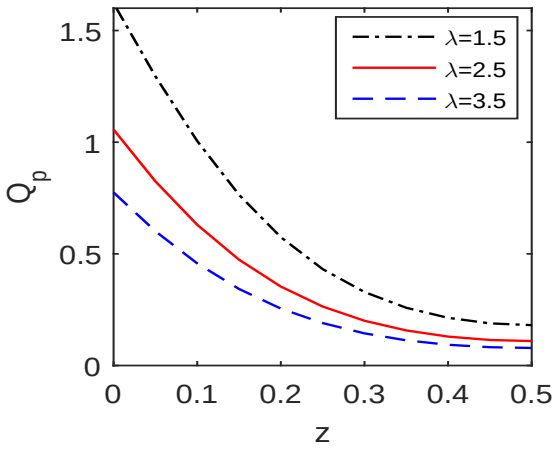

Figure 7.14: Variation of flow rate with z for different values of λ

wall) have been discussed with the help of figs.7.17 and 7.18, respectively. Fig.7.17 reveals that for fixed height of the stenosis ($\delta = 0.2$), as radius of the core region increases (which results decreasing radius of plasma region) from 0.7 to 0.9 (simultaneously radius of plasma region decreases from 0.1 to 0.3) total impedance of the blood flow over the stenosed arterial segment decreases, respectively. Further, fig.7.18 clearly displays that the resistance to flow decreases as values of the Reynolds number increase. This happens because high values of Reynolds number create more turbulence in the fluid which results in the decreased impedance profile of blood flow.

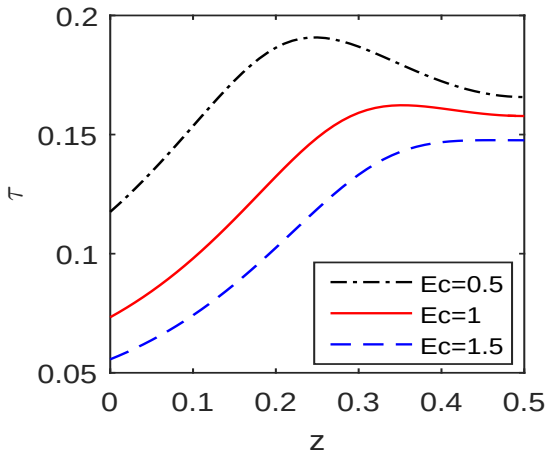

Figure 7.15: Variation of shear stress with z for different values of Ec

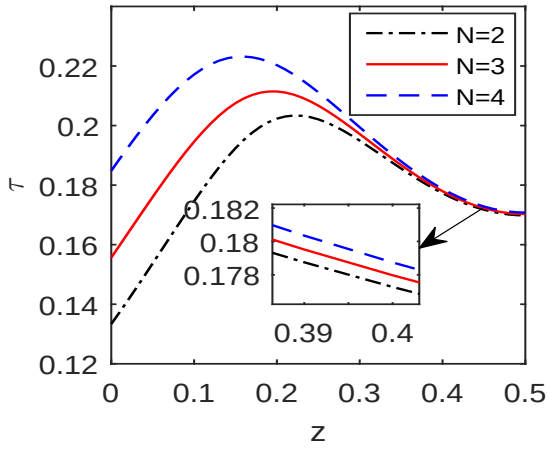

Figure 7.16: Variation of shear stress with z for different values of N

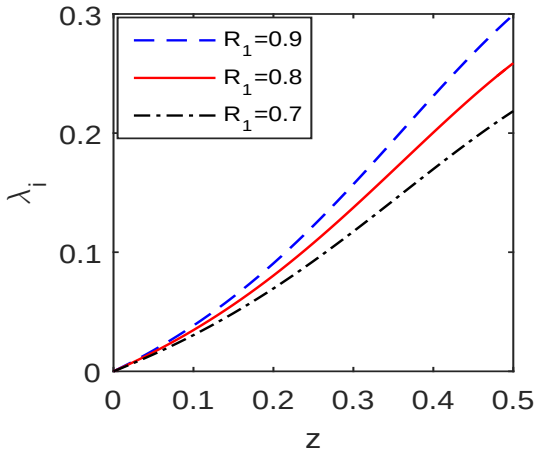

Figure 7.17: Variation of flow resistance with z for different values of R_1

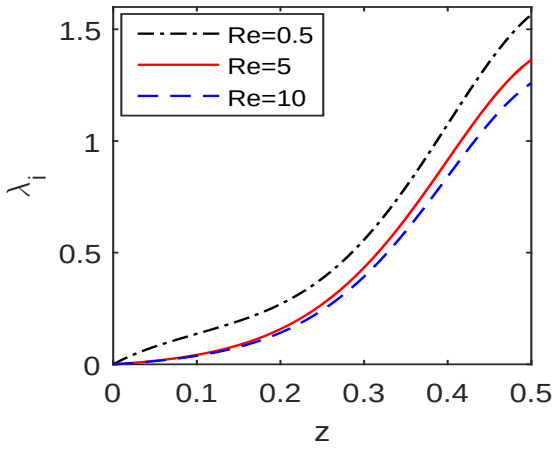

Figure 7.18: Variation of flow resistance with z for different values of Re

7.5 Conclusions

Combined heat and mass transfer effects with k^{th} order homogeneous chemical reaction have been investigated on MHD two-layered model of blood flow through an inclined stenosed artery. In the two-layer model of blood flow viscosity of erythrocytes suspended core region is considered as temperature dependent while the viscosity of cell-free plasma layer is treated as constant. Single shooting method is applied to solve governing nonlinear partial differential equations in order to get the flow characteristics such as flow rate, flow

impedance and wall shear stress. Based on the simulation some important observation of the present analysis are as follows:

1. Study reveals that the Grashof number and modified Grashof number have reducing effects on the velocity profile of blood flow. Magnetic field parameter also has a reducing effect on the velocity profile of blood flow. Since the result shows that blood velocity can be very much controlled with regulating the strength of an external magnetic field. Therefore, it can be practically applied in magnetic and electromagnetic therapy.

2. The temperature profile of the blood flow in narrow artery increases as effects of radiation increase. The result describes the possibility to provide the heat to the blood capillaries of the affected area of the human body directly by using infrared radiation and the technique is widely used in heat therapy for rehabilitation purposes. Further, the temperature profile also increases as effects of magnetic field increase. Hence, the result reveals that the temperature of the body can be controlled by changing the strength of an external magnetic field. This result is very much useful to treat cancer disease.

3. Result of the present study concludes that the concentration profile of blood flow increases with increased values of the chemical reaction parameter. For different order of the homogeneous chemical reaction, concentration profile follows the different path as fifth order of the chemical reaction shows the higher value of concentration profile as compared to the second, third and fourth order of chemical reaction.

4. Total flow rate of the blood flow decreases as values of the height of the stenosis and viscosity parameter increases.

5. The study reveals that the Eckert number which establishes the relationship between flow's kinetic energy and the boundary layer enthalpy has to reduce the effect on wall shear stress, while, reverse effect on wall shear stress has been observed for radiation parameter.

6. Increasing values of core layer thickness increase the flow impedance profile, while, Reynolds number has reverse effects on flow impedance profile of the blood flow.

Chapter 8

Conclusions and Future Scope

In this chapter, the main outcomes of my research work have been discussed in the conclusion section and the new directions which can be the possibilities for the further research work have been presented in the future scope section.

8.1 Conclusions

In the thesis, we have analyzed the effects of heat and mass transfer on blood flow through a stenosed artery. First two chapters explain the phenomenon of blood flow through a stenosed porous artery considering hematocrit dependent viscosity of the blood flow in the presence of an external magnetic field. In which chapter 2 explains the heat transfer effects on blood flow through an inclined artery with a heat source while extended work in chapter 3 describes both heat and mass transfer effects on blood flow with chemical reaction effect. The governing mathematical models have been solved using homotopy perturbation method. To analyze the effects of different physical parameters on blood flow, different graphs have been plotted for flow rate and shear stress. Results show that the magnetic field has reducing effects on the velocity profile of the blood flow. This happens due to the Lorentz force which opposes the motion of the blood flow in the artery. The given result is very useful to control blood flow during the surgical process. The results indicate that changes in the values of the heat source parameter show an effective change in the temperature of the blood flow and it increases as values of the heat

source parameter increase. This result is very effective in understanding/regulating blood flow, especially for the therapeutic process of hyperthermia.

Chapter 4, chapter 5, chapter 6 and chapter 7 analyze the phenomenon of Fåhræus – Lindqvist effect for narrow stenosed arteries. It is experimentally observed that when blood flows through a narrow artery then there exists a cell-free plasma layer near the arterial wall. In chapter 4 we focus on analyzing the effects of the plasma layer thickness on the blood flow through a vertical stenosed artery having radiation and chemical reaction effects in the presence of a magnetic field. In the founding of the given chapter, effects of different physical parameters such as magnetic field, radiation parameter, chemical reaction parameter on velocity, temperature and concentration profile of both core and plasma regions have been displayed graphically. It is found that the velocity of both core and plasma regions decreases as the strength of an applied external magnetic field increases. Further, the result reveals that under the influence of the magnetic field the velocity of plasma layer attains lower values than the velocity of the core layer. With the help of this result during the surgical process in narrow arteries, blood flow can be regulated at the desired level. The result of the given chapter explains that in the narrow arteries concentration profile of blood flow decreases as values of the chemical reaction parameter increase and this happens due to increased molecular diffusivity which directly suppresses the concentration profile of the blood flow. The work further has been extended in chapter 5 in which the effects of heat and mass transfer on two-phase blood flow through a horizontal stenosed artery with radiation have been analyzed. The exact solution has been found for the given problem after taking assumption on pressure gradient due to pulsatile behavior of the blood flow. Results show that the flow rate of the blood flow in narrow artery decreases as values of the Reynolds number increase and the shear stress at stenosis throat decreases with increasing values of the height of the stenosis. Chapter 6 analyzes the Joule heating and viscous dissipation effects on two-phase blood flow in the presence of radially varying magnetic field. In the model, the viscosity of the core region is assumed as hematocrit dependent and plasma viscosity is considered as constant. The study shows that the Eckert number and Schmidt number have enhancing effects on both heat and mass transfer coefficients of the blood flow. Increasing values of the height of

the stenosis increase the flow impedance profile while it shows reverse effects on flow rate profile of the blood flow. Considering the case of elliptically shaped stenosis, chapter 7 presents the study on two-phase blood flow having temperature-dependent viscosity of blood flow in the core region and constant viscosity of blood flow in the plasma region. The problem also discusses the case of n^{th} order homogeneous chemical reaction. The coupled non-linear partial differential equations of the given problem have been solved using a single shooting method. With the help of the results, we can conclude that Increasing values of core layer thickness increase the flow impedance profile of the blood flow. The result of the present study concludes that as values of the chemical reaction parameter increase the concentration profile of blood flow also increases. It follows the different path for a different order of the homogeneous chemical reaction, as fifth order of the chemical reaction shows the higher value of concentration profile as compared to the second, third and fourth order of chemical reaction. Results for the variations of the temperature profile of the blood flow with radiation parameter describes the possibility to provide the heat to the blood capillaries of the affected area of the human body directly by using infrared radiation, which is widely used in heat therapy for rehabilitation purposes.

8.2 Future Scope

Mathematical models examined in this thesis basically describe the single-phase or two-phase phenomenon of blood flow. We have analyzed the effects of different quantities of interest on blood flow and have solved the governing mathematical models analytically as well as numerically. Following aspects of research work can be explored in future:

1. The modeling of two-phase blood flow has been analyzed in the thesis, further this work can be extended by considering the effects of nanoparticles on blood flow.

2. In two-phase modeling, a continuous behavior of flow is taken at the interface of both core and plasma regions, the work further can be extended in which miscible behavior of flow may be considered.

3. Modeling of optimal targeted drug delivery (magnetic nanoparticles) in blood flow

under the influence of a controlled magnetic field can be explored for both single and two-phase models.

A Appendix

$$\beta_1 = -\left(\frac{K_0 N^2}{\alpha_0} + i\frac{P_e}{\rho_0}\left(\frac{K_0}{s_0}\right)\right), \quad \beta_2 = -\left(N^2 + iP_e\right).$$

$$\gamma_1 = -\left(iReD_0S_c + \frac{E}{E_0}D_0S_c\right), \quad \gamma_2 = -\left(iReS_c + ES_c\right).$$

$$\lambda_1 = -\left(M^2 + \frac{\mu_0 Re}{\rho_0}i\right), \quad \lambda_2 = -\left(M^2 + Rei\right).$$

$$U_1 = \left(\frac{J_0(\sqrt{\beta_2}R_1)}{J_0(\sqrt{\beta_1}R_1)} - \frac{J_0(\sqrt{\beta_2}R)}{Y_0(\sqrt{\beta_2}R)}\frac{Y_0(\sqrt{\beta_2}R_1)}{J_0(\sqrt{\beta_1}R_1)}\right), U_2 = \frac{Y_0(\sqrt{\beta_2}R_1))}{J_0(\sqrt{\beta_1}R_1)Y_0(\sqrt{\beta_2}R)}.$$

$$U_3 = \sqrt{\beta_1}U_1J_1(\sqrt{\beta_1}R_1) - \sqrt{\beta_2}\left(J_1(\sqrt{\beta_2}R_1) - \frac{J_0(\sqrt{\beta_2}R)}{Y_0(\sqrt{\beta_2}R)}Y_1(\sqrt{\beta_2}R_1)\right).$$

$$U_4 = \left(\frac{J_0(\sqrt{\gamma_2}R_1)}{J_0(\sqrt{\gamma_1}R_1)} - \frac{J_0(\sqrt{\gamma_2}R)}{J_0(\sqrt{\gamma_1}R_1)}\frac{Y_0(\sqrt{\gamma_2}R_1)}{Y_0(\sqrt{\gamma_2}R)}\right), U_5 = \frac{Y_0(\sqrt{\gamma_2}R_1))}{J_0(\sqrt{\gamma_1}R_1)Y_0(\sqrt{\gamma_2}R)}.$$

$$U_6 = \sqrt{\gamma_1}U_5J_1(\sqrt{\gamma_1}R_1) - \sqrt{\gamma_2}\left(J_1(\sqrt{\gamma_2}R_1) - \frac{J_0(\sqrt{\gamma_2}R)}{Y_0(\sqrt{\gamma_2}R)}.Y_1(\sqrt{\gamma_2}R_1)\right).$$

$$D_1 = -A_1(R_1)J_0(\sqrt{\lambda_1}R_1) - B_1(R_1)Y_0(\sqrt{\lambda_1}R_1) + A_2(R_1)J_0(\sqrt{\lambda_2}R_1) + B_2(R_1)Y_0(\sqrt{\lambda_2}R_1).$$

$$D_2 = -A_2(R)J_0(\sqrt{\lambda_2}R) - B_2(R)Y_0(\sqrt{\lambda_2}R).$$

$$D_3 = -\frac{\partial A_1(R_1)}{\partial r}J_0(\sqrt{\lambda_1}R_1) + A_1(R_1)\sqrt{\lambda_1}J_1(\sqrt{\lambda_1}R_1) - \frac{\partial B_1(R_1)}{\partial r}Y_0(\sqrt{\lambda_1}R_1)$$

$$+B_1(R_1)\sqrt{\lambda_1}Y_1(\sqrt{\lambda_1}R_1) + \frac{\partial A_2(R_1)}{\partial r}J_0(\sqrt{\lambda_2}R_1) + \frac{\partial B_2(R_1)}{\partial r}Y_0(\sqrt{\lambda_2}R_1)$$

$$- A_2(R_1)\sqrt{\lambda_2}J_1(\sqrt{\lambda_2}R_1) - B_2(R_1)\sqrt{\lambda_2}Y_1(\sqrt{\lambda_2}R_1).$$

$$\gamma_1' = -iReD_0S_c, \qquad \gamma_2' = -iReS_c.$$

Bibliography

Abbas, Z., Hasnain, J., and Sajid, M. (2014). Mhd two-phase fluid flow and heat transfer with partial slip in an inclined channel. *Thermal Science*, 20(5):1435–1446.

Abbasi, F., Hayat, T., and Ahmad, B. (2016). Numerical analysis for peristalsis of carreau–yasuda nanofluid in an asymmetric channel with slip and joule heating effects. *Journal of Engineering Thermophysics*, 25(4):548–562.

Abbasi, F., Hayat, T., and Alsaedi, A. (2015). Effects of inclined magnetic field and joule heating in mixed convective peristaltic transport of non-newtonian fluids. *Bulletin of the polish academy of sciences technical sciences*, 63(2):501–514.

Abdullah, I., Amin, N., and Hayat, T. (2011). Magnetohydrodynamic effects on blood flow through an irregular stenosis. *International Journal for Numerical Methods in Fluids*, 67(11):1624–1636.

Ahmed, S. A. and Giddens, D. P. (1983). Velocity measurements in steady flow through axisymmetric stenoses at moderate reynolds numbers. *Journal of biomechanics*, 16(7):505509–507516.

Akbarzadeh, P. (2016). Pulsatile magneto-hydrodynamic blood flows through porous blood vessels using a third grade non-Newtonian fluids model. *Computer methods and programs in biomedicine*, 126:3–19.

Alexopoulos, N., Katritsis, D., and Raggi, P. (2014). Visceral adipose tissue as a source of inflammation and promoter of atherosclerosis. *Atherosclerosis*, 233(1):104–112.

Ali, F., Sheikh, N. A., Khan, I., and Saqib, M. (2017). Magnetic field effect on blood flow of casson fluid in axisymmetric cylindrical tube: A fractional model. *Journal of Magnetism and Magnetic Materials*, 423:327–336.

Alongi, F., Arcangeli, S., Filippi, A. R., Ricardi, U., and Scorsetti, M. (2012). Review and uses of stereotactic body radiation therapy for oligometastases. *The oncologist*, pages 2012–0092.

Asghar, S., Hussain, Q., Hayat, T., and Alsaadi, F. (2014). Hall and ion slip effects on peristaltic flow and heat transfer analysis with ohmic heating. *Applied Mathematics and Mechanics*, 35(12):1509–1524.

Bakheet, A., Alnussaiyri, E. A., Ismail, Z., and Amin, N. (2016). Blood flow through an inclined stenosed artery. *Applied Mathematical Sciences*, 10(5):235–254.

Baldwin, A. and Wilson, L. M. (1994). Stationary red blood cells induce a negative charge on mucosal capillary endothelium. *American Journal of Physiology-Gastrointestinal and Liver Physiology*, 266(4):685–694.

Bali, R. and Awasthi, U. (2007). Effect of a magnetic field on the resistance to blood flow through stenotic artery. *Applied Mathematics and Computation*, 188(2):1635–1641.

Barbee, J. H. and Cokelet, G. R. (1971). The fahraeus effect. *Microvascular research*, 3(1):6–16.

Bejan, A. (1982). *Entropy generation through heat and fluid flow*. Wiley.

Bhatti, M. and Abbas, M. A. (2016). Simultaneous effects of slip and mhd on peristaltic blood flow of jeffrey fluid model through a porous medium. *Alexandria Engineering Journal*, 55(2):1017–1023.

Bhatti, M. and Rashidi, M. (2017). Study of heat and mass transfer with joule heating on magnetohydrodynamic (mhd) peristaltic blood flow under the influence of hall effect. *Propulsion and Power Research*, 6(3):177–185.

Bhatti, M. and Zeeshan, A. (2017). Heat and mass transfer analysis on peristaltic flow of particle–fluid suspension with slip effects. *Journal of Mechanics in Medicine and Biology*, 17(02):1750028–1750044.

Bhatti, M., Zeeshan, A., and Ellahi, R. (2017a). Simultaneous effects of coagulation and variable magnetic field on peristaltically induced motion of jeffrey nanofluid containing gyrotactic microorganism. *Microvascular research*, 110:32–42.

Bhatti, M., Zeeshan, A., Ellahi, R., and Ijaz, N. (2017b). Heat and mass transfer of two-phase flow with electric double layer effects induced due to peristaltic propulsion in the presence of transverse magnetic field. *Journal of Molecular Liquids*, 230:237–246.

Bhatti, M. M. and Zeeshan, A. (2016). Study of variable magnetic field and endoscope on peristaltic blood flow of particle-fluid suspension through an annulus. *Biomedical Engineering Letters*, 6(4):242–249.

Biswas, G. (2003). *Introduction to Fluid Mechanics and Fluid Machines, 2e*. Tata McGraw-Hill Education.

Bose, S. and Banerjee, M. (2015). Magnetic particle capture for biomagnetic fluid flow in stenosed aortic bifurcation considering particle-fluid coupling. *Journal of Magnetism and Magnetic Materials*, 385:32 – 46.

Brinkman, H. (1951). Heat effects in capillary flow i. *Applied Scientific Research*, 2(1):120.

Bugliarello, G. and Sevilla, J. (1970). Velocity distribution and other characteristics of steady and pulsatile blood flow in fine glass tubes. *Biorheology*, 7(2):85–107.

Cavalcanti, S. (1992). Wall shear stress in stenotic artery. In *Engineering in Medicine and Biology Society, 1992 14th Annual International Conference of the IEEE*, volume 2, pages 421–422. IEEE.

Cavalcanti, S. (1995). Hemodynamics of an artery with mild stenosis. *Journal of Biomechanics*, 28(4):387–399.

Cengel, Y. A., Pérez, H., et al. (2004). Heat transfer: a practical approach. transferencia de calor.

Chakraborty, R., Dey, R., and Chakraborty, S. (2013). Thermal characteristics of electromagnetohydrodynamic flows in narrow channels with viscous dissipation and joule heating under constant wall heat flux. *International Journal of Heat and Mass Transfer*, 67:1151–1162.

Chakraborty, U. S., Biswas, D., and Paul, M. (2011). Suspension model blood flow through an inclined tube with an axially non-symmetrical stenosis. *Korea-Australia Rheology Journal*, 23(1):25–32.

Chakravarty, S. and Mandal, P. (1994). Mathematical modelling of blood flow through an overlapping arterial stenosis. *Mathematical and computer modelling*, 19(1):59–70.

Chandran, K. B., Rittgers, S. E., and Yoganathan, A. P. (2006). *Biofluid mechanics: the human circulation*. CRC press.

Chebbi, R. (2015). Dynamics of blood flow: modeling of the fåhræus–lindqvist effect. *Journal of biological physics*, 41(3):313–326.

Chen, I. I. and Sana, S. (1985). Analysis of an intensive magnetic field on blood flow: part 2. *Journal of Bioelectricity*, 4(1):55–62.

Çinar, Y., Şenyol, A. M., and Duman, K. (2001). Blood viscosity and blood pressure: role of temperature and hyperglycemia. *American journal of hypertension*, 14(5):433–438.

Cokelet, G. R. and Goldsmith, H. L. (1991). Decreased hydrodynamic resistance in the two-phase flow of blood through small vertical tubes at low flow rates. *Circulation research*, 68(1):1–17.

Cooper, C. J., Murphy, T. P., Cutlip, D. E., Jamerson, K., Henrich, W., Reid, D. M., Cohen, D. J., Matsumoto, A. H., Steffes, M., Jaff, M. R., et al. (2014). Stenting and medical therapy for atherosclerotic renal-artery stenosis. *New England Journal of Medicine*, 370(1):13–22.

Craciunescu, O. I. and Clegg, S. T. (2001). Pulsatile blood flow effects on temperature distribution and heat transfer in rigid vessels. *Journal of biomechanical engineering*, 123(5):500–505.

Demir, A., Erman, S., Özgür, B., and Korkmaz, E. (2013). Analysis of the new homotopy perturbation method for linear and nonlinear problems. *Boundary Value Problems*, 2013(1):61–72.

Desjardins, C. and Duling, B. R. (1987). Microvessel hematocrit: measurement and implications for capillary oxygen transport. *American Journal of Physiology-Heart and Circulatory Physiology*, 252(3):494–503.

Dessie, H. and Kishan, N. (2014). Mhd effects on heat transfer over stretching sheet embedded in porous medium with variable viscosity, viscous dissipation and heat source/sink. *Ain shams engineering journal*, 5(3):967–977.

Devi, S. A. and Ganga, B. (2009). Viscous dissipation effects on nonlinear mhd flow in a porous medium over a stretching porous surface. *International Journal of Applied Mathematics and Mechanics*, 5:45–59.

Dewhirst, M., Viglianti, B. L., Lora-Michiels, M., Hoopes, P. J., and Hanson, M. A. (2003). Thermal dose requirement for tissue effect: experimental and clinical findings. In *Thermal Treatment of Tissue: Energy Delivery and Assessment II*, volume 4954, pages 37–58. International Society for Optics and Photonics.

El-Sayed, M., Eldabe, N., Ghaly, A., and Sayed, H. (2011). Effects of chemical reaction, heat, and mass transfer on non-newtonian fluid flow through porous medium in a vertical peristaltic tube. *Transport in porous media*, 89(2):185.

El-Shahed, M. (2003). Pulsatile flow of blood through a stenosed porous medium under periodic body acceleration. *Applied Mathematics and Computation*, 138(2):479–488.

Eldesoky, I. M. (2012). Mathematical analysis of unsteady mhd blood flow through parallel plate channel with heat source. *World Journal of Mechanics*, 2(3):131–137.

Eldesoky, I. M. (2014). Unsteady MHD pulsatile blood flow through porous medium in stenotic channel with slip at permeable walls subjected to time dependent velocity (injection/suction). *Walailak Journal of Science and Technology*, 11(11):901–922.

Ellahi, R., Bhatti, M. M., and Vafai, K. (2014a). Effects of heat and mass transfer on peristaltic flow in a non-uniform rectangular duct. *International Journal of Heat and Mass Transfer*, 71:706–719.

Ellahi, R., Rahman, S., Gulzar, M. M., Nadeem, S., and Vafai, K. (2014b). A mathematical study of non-Newtonian micropolar fluid in arterial blood flow through composite stenosis. *Applied Mathematics & Information Sciences*, 8(4):1567.

Ellahi, R., Rahman, S., and Nadeem, S. (2014c). Blood flow of jeffrey fluid in a catherized tapered artery with the suspension of nanoparticles. *Physics Letters A*, 378(40):2973 – 2980.

Faber, T. E. (1995). *Fluid dynamics for physicists*. Cambridge university press.

Fahraeus, R. and Lindqvist, T. (1931). The viscosity of the blood in narrow capillary tubes. *American Journal of Physiology-Legacy Content*, 96(3):562–568.

Fakour, M., Vahabzadeh, A., and Ganji, D. (2015). Study of heat transfer and flow of nanofluid in permeable channel in the presence of magnetic field. *Propulsion and Power Research*, 4(1):50–62.

Falk, E., Shah, P. K., and Fuster, V. (1995). Coronary plaque disruption. *Circulation*, 92(3):657–671.

Farooq, M., Khan, M. I., Waqas, M., Hayat, T., Alsaedi, A., and Khan, M. I. (2016). Mhd stagnation point flow of viscoelastic nanofluid with non-linear radiation effects. *Journal of molecular liquids*, 221:1097–1103.

Federspiel, W. J. (1989). Pulmonary diffusing capacity: implications of two-phase blood flow in capillaries. *Respiration physiology*, 77(1):119–134.

Fedosov, D. A., Caswell, B., Popel, A. S., and Karniadakis, G. E. (2010). Blood flow and cell-free layer in microvessels. *Microcirculation*, 17(8):615–628.

Fetecau, C., Akhtar, S., Pop, I., and Fetecau, C. (2017). Unsteady general solution for mhd natural convection flow with radiative effects, heat source and shear stress on the boundary. *International Journal of Numerical Methods for Heat & Fluid Flow*, 27(6):1266–1281.

Frank, S., Johnson, A., and Ross Jr, J. (1973). Natural history of valvular aortic stenosis. *British heart journal*, 35(1):41–46.

Fujiwara, H., Ishikawa, T., Lima, R., Matsuki, N., Imai, Y., Kaji, H., Nishizawa, M., and Yamaguchi, T. (2009). Red blood cell motions in high-hematocrit blood flowing through a stenosed microchannel. *Journal of Biomechanics*, 42(7):838–843.

Fung, Y. and Cowin, S. (1994). Biomechanics: mechanical properties of living tissues. *Journal of Applied Mechanics*, 61:1007.

Fung, Y.-C. (1993). *Mechanical properties and active remodeling of blood vessels*. Springer.

Gabryś, E., Rybaczuk, M., and Kkedzia, A. (2006). Blood flow simulation through fractal models of circulatory system. *Chaos, Solitons & Fractals*, 27(1):1–7.

Garcia, A. E. and Riahi, D. N. (2014). Two-phase blood flow and heat transfer in an inclined stenosed artery with or without a catheter. *International Journal of Fluid Mechanics Research*, 41(1):16–30.

Ha, S. N. (2001). A nonlinear shooting method for two-point boundary value problems. *Computers & Mathematics with Applications*, 42(10):1411–1420.

Habibi, M. R., Ghassemi, M., and Shahidian, A. (2012). Investigation of biomagnetic fluid flow under nonuniform magnetic fields. *Nanoscale and Microscale Thermophysical Engineering*, 16(1):64–77.

Haik, Y., Pai, V., and Chen, C.-J. (1999). Development of magnetic device for cell separation. *Journal of Magnetism and Magnetic Materials*, 194(1):254 – 261.

Haik, Y., Pai, V., and Chen, C.-J. (2001). Apparent viscosity of human blood in a high static magnetic field. *Journal of Magnetism and Magnetic Materials*, 225(1):180–186.

Hayat, T., Abbas, Z., and Sajid, M. (2008). Heat and mass transfer analysis on the flow of a second grade fluid in the presence of chemical reaction. *Physics letters A*, 372(14):2400–2408.

Hayat, T., Ayub, S., Tanveer, A., and Alsaedi, A. (2018). Slip and joule heating effects on peristaltic transport in an inclined channel. *Journal of Thermal Science and Engineering Applications*, 10(3):031004–031012.

Hayat, T., Khan, M. I., Alsaedi, A., and Khan, M. I. (2016). Homogeneous-heterogeneous reactions and melting heat transfer effects in the mhd flow by a stretching surface with variable thickness. *Journal of Molecular Liquids*, 223:960–968.

Hayat, T., Khan, M. I., Waqas, M., Alsaedi, A., and Khan, M. I. (2017). Radiative flow of micropolar nanofluid accounting thermophoresis and brownian moment. *International Journal of Hydrogen Energy*, 42(26):16821–16833.

Hayat, T., Nisar, Z., Ahmad, B., and Yasmin, H. (2015). Simultaneous effects of slip and wall properties on mhd peristaltic motion of nanofluid with joule heating. *Journal of Magnetism and Magnetic Materials*, 395:48–58.

Haynes, R. H. (1960). Physical basis of the dependence of blood viscosity on tube radius. *American Journal of Physiology-Legacy Content*, 198(6):1193–1200.

Hemeda, A. A. (2012). Homotopy perturbation method for solving systems of nonlinear coupled equations. *Applied Mathematical Sciences*, 6(96):4787 – 4800.

Hooman, K. and Gurgenci, H. (2008). Effects of temperature-dependent viscosity on benard convection in a porous medium using a non-darcy model. *International Journal of Heat and Mass Transfer*, 51(5-6):1139–1149.

Horiuchi, K. and Dutta, P. (2004). Joule heating effects in electroosmotically driven microchannel flows. *International journal of heat and mass transfer*, 47(14-16):3085–3095.

Hussain, A., Malik, M., Bilal, S., Awais, M., and Salahuddin, T. (2017). Computational analysis of magnetohydrodynamic sisko fluid flow over a stretching cylinder in the presence of viscous dissipation and temperature dependent thermal conductivity. *Results in Physics*, 7:139–146.

Ikbal, M., Chakravarty, S., Wong, K. K., Mazumdar, J., and Mandal, P. (2009). Unsteady response of non-newtonian blood flow through a stenosed artery in magnetic field. *Journal of Computational and Applied Mathematics*, 230(1):243 – 259.

Ishii, M. and Hibiki, T. (2010). *Thermo-fluid dynamics of two-phase flow*. Springer Science & Business Media.

Ja, Y. (1983). Using the shooting method to solve boundary-value problems involving nonlinear coupled-wave equations. *Optical and quantum electronics*, 15(6):529–538.

Jean, W. J., Al-Bitar, I., Zwicke, D. L., Port, S. C., Schmidt, D. H., and Bajwa, T. K. (1994). High incidence of renal artery stenosis in patients with coronary artery disease. *Catheterization and cardiovascular diagnosis*, 32(1):8–10.

JW, P. (1962). The physics of blood flood in capillaries. ii. the capillary resistance to flow. *Biophysical Journal*, 2(2 Pt 1):199–212.

Kamangar, S., Kalimuthu, G., Anjum Badruddin, I., Badarudin, A., Salman Ahmed, N., and Khan, T. (2014). Numerical investigation of the effect of stenosis geometry on the coronary diagnostic parameters. *The Scientific World Journal*, 2014:1–7.

Kandasamy, R., Periasamy, K., and Prabhu, K. S. (2005). Effects of chemical reaction, heat and mass transfer along a wedge with heat source and concentration in the presence of suction or injection. *International journal of heat and mass transfer*, 48(7):1388–1394.

Khaled, A.-R. and Vafai, K. (2003). The role of porous media in modeling flow and heat transfer in biological tissues. *International Journal of Heat and Mass Transfer*, 46(26):4989–5003.

Khan, M. I., Hayat, T., Khan, M. I., and Alsaedi, A. (2017a). A modified homogeneous-heterogeneous reactions for mhd stagnation flow with viscous dissipation and joule heating. *International Journal of Heat and Mass Transfer*, 113:310–317.

Khan, M. I., Waqas, M., Hayat, T., Khan, M. I., and Alsaedi, A. (2017b). Behavior of stratification phenomenon in flow of maxwell nanomaterial with motile gyrotactic

microorganisms in the presence of magnetic field. *International Journal of Mechanical Sciences*, 131:426–434.

Khonsari, M. M. and Booser, E. R. (2017). *Applied tribology: bearing design and lubrication*. John Wiley & Sons.

Knudson, D. (2007). *Fundamentals of biomechanics*. Springer Science & Business Media.

Kobu, Y. (1999). Effects of infrared radiation on intraosseous blood flow and oxygen tension in the rat tibia. *The Kobe journal of medical sciences*, 45(1):27–39.

Kolin, A. (1936). An electromagnetic flowmeter. principle of the method and its application to bloodflow measurements. *Proceedings of the Society for Experimental Biology and Medicine*, 35(1):53–56.

Koppensteiner, R. (1996). Blood rheology in emergency medicine. In *Seminars in thrombosis and hemostasis*, volume 22, pages 89–91. Copyright© 1996 by Thieme Medical Publishers, Inc.

Korchevskii, E. and Marochnik, L. (1965). Magnetohydrodynamic version of movement of blood. *Biophysics*, 10(2):411–414.

Koriko, O. K., Oreyeni, T., Oreyeni, T., and Oyem, O. A. (2018). On the analysis of variable thermophysical properties of thermophoretic viscoelastic fluid flow past a vertical surface with nth order of chemical reaction. *Open Access Library Journal*, 5(06):1–17.

Krishna, M. V., Swarnalathamma, B., and Prakash, J. (2018). Heat and mass transfer on unsteady mhd oscillatory flow of blood through porous arteriole. In *Applications of Fluid Dynamics*, pages 207–224. Springer.

Ku, D. N. (1997). Blood flow in arteries. *Annual review of fluid mechanics*, 29(1):399–434.

Kumar, A., Varshney, C. L., and Sharma, G. C. (2005). Computational technique for flow in blood vessels with porous effects. *Applied Mathematics and Mechanics*, 26(1):63–72.

Kumar, R., Kumar, R., Shehzad, S. A., and Sheikholeslami, M. (2018). Rotating frame analysis of radiating and reacting ferro-nanofluid considering joule heating and viscous dissipation. *International Journal of Heat and Mass Transfer*, 120:540–551.

Layek, G., Mukhopadhyay, S., and Gorla, R. S. R. (2009). Unsteady viscous flow with variable viscosity in a vascular tube with an overlapping constriction. *International journal of engineering science*, 47(5):649–659.

Liao, S. (2013). *Advances in the homotopy analysis method*. World Scientific.

Lin, T., Hawks, K., and Leidenfrost, W. (1983). Analysis of viscous dissipation effect on thermal entrance heat transfer in laminar pipe flows with convective boundary conditions. *Wärme-und stoffübertragung*, 17(2):97–105.

Lipscomb, K. and Hooten, S. (1978). Effect of stenotic dimensions and blood flow on the hemodynamic significance of model coronary arterial stenoses. *The American Journal of Cardiology*, 42(5):781 – 792.

Majee, S. and Shit, G. (2017). Numerical investigation of mhd flow of blood and heat transfer in a stenosed arterial segment. *Journal of Magnetism and Magnetic Materials*, 424:137–147.

Makinde, O. (2010). Mhd mixed-convection interaction with thermal radiation and nth order chemical reaction past a vertical porous plate embedded in a porous medium. *Chemical Engineering Communications*, 198(4):590–608.

Makinde, O. and Onyejekwe, O. (2011). A numerical study of mhd generalized couette flow and heat transfer with variable viscosity and electrical conductivity. *Journal of Magnetism and Magnetic Materials*, 323(22):2757 – 2763.

Mallikarjuna reddy C, Rambhupal reddy B., K. r. (2011). Mathematical model governing magnetic field effect on bio magnetic fluid flow and orientation of red blood cells. *Pacific-Asian Journal of Mathematics*, 5(1):344–356.

Marcus, M. L., Doty, D. B., Hiratzka, L. F., Wright, C. B., and Eastham, C. L. (1982). Decreased coronary reserve: a mechanism for angina pectoris in patients with aortic

stenosis and normal coronary arteries. *New England Journal of Medicine*, 307(22):1362–1366.

Massoudi, M. and Christie, I. (1995). Effects of variable viscosity and viscous dissipation on the flow of a third grade fluid in a pipe. *International Journal of Non-Linear Mechanics*, 30(5):687 – 699.

Mazumdar, J. (2015). *Biofluid mechanics*. World Scientific.

Medvedev, A. and Fomin, V. (2011). Two-phase blood-flow model in large and small vessels. *Doklady Physics*, 56(12):610–613.

Mekheimer, K. S. (2008). Effect of the induced magnetic field on peristaltic flow of a couple stress fluid. *Physics Letters A*, 372(23):4271–4278.

Mekheimer, K. S. and El Kot, M. (2008). Influence of magnetic field and hall currents on blood flow through a stenotic artery. *Applied Mathematics and Mechanics*, 29(8):1093–1104.

Mekheimer, K. S., Haroun, M. H., and El Kot, M. (2012). Influence of heat and chemical reactions on blood flow through an anisotropically tapered elastic arteries with overlapping stenosis. *Appl. Math*, 6(2):281–292.

Mekheimer, K. S., Haroun, M. H., and Elkot, M. A. (2011). Effects of magnetic field, porosity, and wall properties for anisotropically elastic multi-stenosis arteries on blood flow characteristics. *Applied Mathematics and Mechanics*, 32(8):1047–1064.

Mekheimer, K. S. and Kot, M. A. E. (2008). The micropolar fluid model for blood flow through a tapered artery with a stenosis. *Acta Mechanica Sinica*, 24(6):637–644.

Minasyan, H. (2016). Bactericidal capacity of erythrocytes in human cardiovascular system. *Int Clin Pathol J*, 2(5):104–106.

Mirza, I., Abdulhameed, M., Vieru, D., and Shafie, S. (2016). Transient electro-magneto-hydrodynamic two-phase blood flow and thermal transport through a capillary vessel. *Computer Methods and Programs in Biomedicine*, 137(2016):149–166.

Misra, J. and Adhikary, S. (2016). Mhd oscillatory channel flow, heat and mass transfer in a physiological fluid in presence of chemical reaction. *Alexandria Engineering Journal*, 55(1):287 – 297.

Misra, J. and Kar, B. (1988). Momentum integral method for studying flow characteristics of blood through a stenosed vessel. *Biorheology*, 26(1):23–35.

Misra, J., Patra, M., and Misra, S. (1993). A non-newtonian fluid model for blood flow through arteries under stenotic conditions. *Journal of biomechanics*, 26(9):1129–1141.

Misra, J. and Shit, G. (2006). Blood flow through arteries in a pathological state: A theoretical study. *International Journal of Engineering Science*, 44(10):662–671.

Misra, J. and Shit, G. (2007). Role of slip velocity in blood flow through stenosed arteries: a non-newtonian model. *Journal of Mechanics in Medicine and Biology*, 7(03):337–353.

Misra, J., Shit, G., Chandra, S., and Kundu, P. (2011a). Hydromagnetic flow and heat transfer of a second-grade viscoelastic fluid in a channel with oscillatory stretching walls: application to the dynamics of blood flow. *Journal of Engineering Mathematics*, 69(1):91–100.

Misra, J., Sinha, A., and Shit, G. (2011b). Mathematical modeling of blood flow in a porous vessel having double stenoses in the presence of an external magnetic field. *International Journal of Biomathematics*, 4(02):207–225.

Misra, J., Sinha, A., and Shit, G. (2011c). A numerical model for the magnetohydrodynamic flow of blood in a porous channel. *Journal of Mechanics in Medicine and Biology*, 11(03):547–562.

Misra, J. C. and Sinha, A. (2013). Effect of thermal radiation on MHD flow of blood and heat transfer in a permeable capillary in stretching motion. *Heat and Mass Transfer*, 49(5):617–628.

Mohyud-Din, S. T. and Noor, M. A. (2009). Homotopy perturbation method for solving partial differential equations. *Zeitschrift für Naturforschung A*, 64(3-4):157 – 170.

Mustapha, N., Amin, N., Chakravarty, S., and Mandal, P. K. (2009). Unsteady magnetohydrodynamic blood flow through irregular multi-stenosed arteries. *Computers in Biology and Medicine*, 39(10):896 – 906.

Muthucumaraswamy, R. (2002). Effects of a chemical reaction on a moving isothermal vertical surface with suction. *Acta Mechanica*, 155(1-2):65–70.

Muthucumaraswamy, R. and Ganesan, P. (2001). First-order chemical reaction on flow past an impulsively started vertical plate with uniform heat and mass flux. *Acta Mechanica*, 147(1-4):45–57.

Mythili, D., Sivaraj, R., Rashidi, M., and Yang, Z. (2015). Casson fluid flow over a vertical cone with non-uniform heat source/sink and high order chemical reaction. *Journal of Naval Architecture and Marine Engineering*, 12(2):125–136.

Nadeem, S. and Akbar, N. S. (2009). Effects of heat transfer on the peristaltic transport of mhd newtonian fluid with variable viscosity: Application of adomian decomposition method. *Communications in Nonlinear Science and Numerical Simulation*, 14(11):3844 – 3855.

Nadeem, S. and Akbar, N. S. (2010a). Effects of temperature dependent viscosity on peristaltic flow of a jeffrey-six constant fluid in a non-uniform vertical tube. *Communications in Nonlinear Science and Numerical Simulation*, 15(12):3950 – 3964.

Nadeem, S. and Akbar, N. S. (2010b). Influence of radially varying mhd on the peristaltic flow in an annulus with heat and mass transfer. *Journal of the Taiwan Institute of Chemical Engineers*, 41(3):286–294.

Nadeem, S., Akbar, N. S., Hayat, T., and Hendi, A. A. (2011). Influence of heat and mass transfer on newtonian biomagnetic fluid of blood flow through a tapered porous arteries with a stenosis. *Transport in Porous Media*, 91(1):81–100.

Nadeem, S., Hayat, T., Akbar, N. S., and Malik, M. (2009). On the influence of heat transfer in peristalsis with variable viscosity. *International Journal of Heat and Mass Transfer*, 52(21–22):4722 – 4730.

Navier, C. and Sur, M. (1827). Les lois du mouvement des fluides. *Mem Acad R Sci Inst Fr*, 6:389–44O.

Nishimoto, C., Ishiura, Y., Kuniyasu, K., and Koga, T. (2006). Effects of ultrasonic radiation on cutaneous blood flow in the paw of decerebrated rats. *Kawasaki journal of medical welfare*, 12(1):13–18.

Noreen Sher Akbar, Sohail Nadeem, M. E.-S. A. (2012). Influence of heat and chemical reactions on hyperbolic tangent fluid model for blood flow through a tapered artery with a stenosis. *Heat and Mass Transfer*, 43(1):69–94.

Noutchie, S. C. O. (2009). *Flow of a Newtonian fluid: The case of blood in large arteries.* PhD thesis.

Ogulu, A. and Abbey, T. (2005). Simulation of heat transfer on an oscillatory blood flow in an indented porous artery. *International communications in heat and mass transfer*, 32(7):983–989.

Ogulu, A. and Amos, E. (2007). Modeling pulsatile blood flow within a homogeneous porous bed in the presence of a uniform magnetic field and time-dependent suction. *International Communications in Heat and Mass Transfer*, 34(8):989–995.

Ollivier, R., Boulmier, D., Veillard, D., Leurent, G., Mock, S., Bedossa, M., and Breton, H. L. (2009). Frequency and predictors of renal artery stenosis in patients with coronary artery disease. *Cardiovascular Revascularization Medicine*, 10(1):23 – 29.

Olufsen, M. S., Peskin, C. S., Kim, W. Y., Pedersen, E. M., Nadim, A., and Larsen, J. (2000). Numerical simulation and experimental validation of blood flow in arteries with structured-tree outflow conditions. *Annals of biomedical engineering*, 28(11):1281–1299.

Ozgumus, T. and Mobedi, M. (2015). Effect of pore to throat size ratio on interfacial heat transfer coefficient of porous media. *Journal of Heat Transfer*, 137(1):012602–012611.

Pal, D. and Talukdar, B. (2011). Combined effects of joule heating and chemical reaction on unsteady magnetohydrodynamic mixed convection of a viscous dissipating fluid over

a vertical plate in porous media with thermal radiation. *Mathematical and Computer Modelling*, 54(11-12):3016–3036.

Pantokratoras, A. (2006). The falkner-skan flow with constant wall temperature and variable viscosity. *International Journal of Thermal Sciences*, 45(4):378 – 389.

Panton, R. L. (2006). *Incompressible flow*. John Wiley & Sons.

Pasceri, V. and Yeh, E. T. (1999). A tale of two diseases atherosclerosis and rheumatoid arthritis. *Circulation*, 100(21):2124–2126.

Petrofsky, J. S., Bains, G., Raju, C., Lohman, E., Berk, L., Prowse, M., Gunda, S., Madani, P., and Batt, J. (2009). The effect of the moisture content of a local heat source on the blood flow response of the skin. *Archives of Dermatological Research*, 301(8):581–585.

Pinto, F. and Meo, M. (2017). Design and manufacturing of a novel shear thickening fluid composite (stfc) with enhanced out-of-plane properties and damage suppression. *Applied Composite Materials*, 24(3):643–660.

Ponalagusamy, R. (2016). Two-fluid model for blood flow through a tapered arterial stenosis: Effect of non-zero couple stress boundary condition at the interface. *International Journal of Applied and Computational Mathematics*, 38(2):1–18.

Ponalagusamy, R. and Priyadharshini, S. (2018). Numerical investigation on two-fluid model (micropolar-newtonian) for pulsatile flow of blood in a tapered arterial stenosis with radially variable magnetic field and core fluid viscosity. *Computational and Applied Mathematics*, 37(1):719–743.

Ponalagusamy, R. and Selvi, R. T. (2011). A study on two-layered model (casson–newtonian) for blood flow through an arterial stenosis: Axially variable slip velocity at the wall. *Journal of the Franklin Institute*, 348(9):2308–2321.

Ponalagusamy, R. and Selvi, R. T. (2013). Blood flow in stenosed arteries with radially variable viscosity, peripheral plasma layer thickness and magnetic field. *Meccanica*, 48(10):2427–2438.

Ponalagusamy, R. and Selvi, R. T. (2015). Influence of magnetic field and heat transfer on two-phase fluid model for oscillatory blood flow in an arterial stenosis. *Meccanica*, 50(4):927–943.

Pop, I. and Ingham, D. B. (2001). *Convective heat transfer: mathematical and computational modelling of viscous fluids and porous media*. Elsevier.

Prabhakara, S. and Deshpande, M. (2004). The no-slip boundary condition in fluid mechanics. *Resonance*, 9(5):61–71.

Prakash, O., Singh, S., Kumar, D., and Dwivedi, Y. (2011). A study of effects of heat source on MHD blood flow through bifurcated arteries. *AIP Advances*, 1(4):042128–042135.

Pralhad, R. and Schultz, D. (2004). Modeling of arterial stenosis and its applications to blood diseases. *Mathematical biosciences*, 190(2):203–220.

Prasad, K., Abel, S., and Datti, P. (2003). Diffusion of chemically reactive species of a non-newtonian fluid immersed in a porous medium over a stretching sheet. *International Journal of Non-Linear Mechanics*, 38(5):651–657.

Preziosi, L. and Farina, A. (2002). On darcy's law for growing porous media. *International Journal of Non-Linear Mechanics*, 37(3):485–491.

Pries, A., Neuhaus, D., and Gaehtgens, P. (1992). Blood viscosity in tube flow: dependence on diameter and hematocrit. *American Journal of Physiology-Heart and Circulatory Physiology*, 263(6):1770–1778.

Pries, A., Secomb, T., Gessner, T., Sperandio, M., Gross, J., and Gaehtgens, P. (1994). Resistance to blood flow in microvessels in vivo. *Circulation research*, 75(5):904–915.

Pries, A. R., Secomb, T., Gaehtgens, P., and Gross, J. (1990). Blood flow in microvascular networks. experiments and simulation. *Circulation research*, 67(4):826–834.

Rabby, M. G., Razzak, A., and Molla, M. M. (2013). Pulsatile non-Newtonian blood flow through a model of arterial stenosis. *Procedia Engineering*, 56:225 – 231.

Rahbari, A., Fakour, M., Hamzehnezhad, A., Vakilabadi, M. A., and Ganji, D. (2017). Heat transfer and fluid flow of blood with nanoparticles through porous vessels in a magnetic field: A quasi-one dimensional analytical approach. *Mathematical Biosciences*, 283:38–47.

Ramesh, K. (2016). Influence of heat and mass transfer on peristaltic flow of a couple stress fluid through porous medium in the presence of inclined magnetic field in an inclined asymmetric channel. *Journal of Molecular Liquids*, 219:256–271.

Ramzan, M., Farooq, M., Alsaedi, A., and Hayat, T. (2013). Mhd three-dimensional flow of couple stress fluid with newtonian heating. *The European Physical Journal Plus*, 128(5):49.

Rao, A., Sivaiah, S., and Raju, R. S. (2012). Chemical reaction effects on an unsteady mhd free convection fluid flow past a semi-infinite vertical plate embedded in a porous medium with heat absorption. *Journal of Applied Fluid Mechanics*, 5(3):63–70.

Rashidi, M. M., Bhatti, M. M., Abbas, M. A., and Ali, M. E.-S. (2016). Entropy generation on mhd blood flow of nanofluid due to peristaltic waves. *Entropy*, 18(4):117.

Rashidi, M. M., Rostami, B., Freidoonimehr, N., and Abbasbandy, S. (2014). Free convective heat and mass transfer for mhd fluid flow over a permeable vertical stretching sheet in the presence of the radiation and buoyancy effects. *Ain Shams Engineering Journal*, 5(3):901 – 912.

Riahi, D. N. (2016). Modeling unsteady two-phase blood flow in catheterized elastic artery with stenosis. *Engineering Science and Technology, an International Journal*, 19(3):1233–1243.

Roozi, A., Alibeiki, E., Hosseini, S., Shafiof, S., and Ebrahimi, M. (2011). Homotopy perturbation method for special nonlinear partial differential equations. *Journal of King Saud University - Science*, 23(1):99 – 103.

Ross Jr, J. and Braunwald, E. (1968). Aortic stenosis. *Circulation*, 38(1s5):61–67.

Rott, N. (1990). Note on the history of the reynolds number. *Annual review of fluid mechanics*, 22(1):1–12.

Rubenstein, D., Yin, W., and Frame, M. D. (2015). *Biofluid mechanics: an introduction to fluid mechanics, macrocirculation, and microcirculation*. Academic Press.

Salomone, O. A., Elliott, P. M., Calviño, R., Holt, D., and Kaski, J. C. (1996). Plasma immunoreactive endothelin concentration correlates with severity of coronary artery disease in patients with stable angina pectoris and normal ventricular function. *Journal of the American College of Cardiology*, 28(1):14–19.

San, O. and Staples, A. E. (2012). Dynamics of pulsatile flows through elastic microtubes. *International Journal of Applied Mechanics*, 4(01):1250006.

Sankar, D. (2011). Two-phase non-linear model for blood flow in asymmetric and axisymmetric stenosed arteries. *International Journal of Non-Linear Mechanics*, 46(1):296–305.

Sankar, D. and Lee, U. (2007). Two-phase non-linear model for the flow through stenosed blood vessels. *Journal of Mechanical Science and Technology*, 21(4):678–689.

Sanyal, D., Das, K., and Debnath, S. (2007). Effect of magnetic field on pulsatile blood flow through an inclined circular tube with periodic body acceleration. *Journal of Physical Sciences*, 11:43–56.

Schneck, D. J. (2013). *Biofluid Mechanics· 2*. Springer Science & Business Media.

Sharan, M. and Popel, A. S. (2001). A two-phase model for flow of blood in narrow tubes with increased effective viscosity near the wall. *Biorheology*, 38(5, 6):415–428.

Sharan, M., Singh, B., and Kumar, P. (1997). A two-layer model for studying the effect of plasma layer on the delivery of oxygen to tissue using a finite element method. *Applied Mathematical Modelling*, 21(7):419–426.

Sharma, B., Mishra, A., and Gupta, S. (2013). Heat and mass transfer in magneto-biofluid flow through a non-darcian porous medium with joule effect. *Journal of Engineering Physics and Thermophysics*, 86(4):766–774.

Sharma, B., Sharma, M., Gaur, R., and Mishra, A. (2015a). Mathematical modeling of magneto pulsatile blood flow through a porous medium with a heat source. *International Journal of Applied Mechanics and Engineering*, 20(2):385–396.

Sharma, B. K., Agarwal, M., and Chaudhary, R. (2007). Radiation effect on temperature distribution in three-dimensional couette flow with suction or injection. *Applied Mathematics and Mechanics*, 28(3):309–316.

Sharma, M. K., Singh, K., and Bansal, S. (2014). Pulsatile mhd flow in an inclined catheterized stenosed artery with slip on the wall. *Journal of Biomedical Science and Engineering*, 7(04):194.

Sharma, S., Singh, U., and Katiyar, V. (2015b). Magnetic field effect on flow parameters of blood along with magnetic particles in a cylindrical tube. *Journal of Magnetism and Magnetic Materials*, 377:395–401.

Shit, G. and Majee, S. (2015). Pulsatile flow of blood and heat transfer with variable viscosity under magnetic and vibration environment. *Journal of Magnetism and Magnetic Materials*, 388:106 – 115.

Shit, G., Mondal, A., Sinha, A., and Kundu, P. (2016). Electro-osmotic flow of power-law fluid and heat transfer in a micro-channel with effects of joule heating and thermal radiation. *Physica A: Statistical Mechanics and its Applications*, 462:1040–1057.

Shit, G. and Roy, M. (2016). Effect of induced magnetic field on blood flow through a constricted channel: An analytical approach. *Journal of Mechanics in Medicine and Biology*, 16(3):1650030–1650049.

Shit, G., Roy, M., and Sinha, A. (2014). Mathematical modelling of blood flow through a tapered overlapping stenosed artery with variable viscosity. *Applied Bionics and Biomechanics*, 11(4):185–195.

Shukla, J., Parihar, R., and Rao, B. (1980). Effects of stenosis on non-newtonian flow of the blood in an artery. *Bulletin of Mathematical Biology*, 42(3):283–294.

Siddiqa, S., Begum, N., Safdar, S., Hossain, M., and Al-Rashed, A. A. (2017a). Influence of localized magnetic field and strong viscosity on the biomagnetic fluid flow in a rectangular channel. *International Journal of Mechanical Sciences*, 131:451–458.

Siddiqa, S., Naqvi, S., Begum, N., Awan, S., and Hossain, M. (2018). Thermal radiation therapy of biomagnetic fluid flow in the presence of localized magnetic field. *International Journal of Thermal Sciences*, 132:457–465.

Siddiqa, S., Naqvi, S., Hossain, M., Massarotti, N., and Mauro, A. (2017b). Strong temperature dependent viscosity effects on bio-magnetic fluid flow under the action of localized magnetic field and viscous dissipation. *Journal of Molecular Liquids*, 248:616–625.

Singel, D. J. and Stamler, J. S. (2005). Chemical physiology of blood flow regulation by red blood cells: the role of nitric oxide and s-nitrosohemoglobin. *Annu. Rev. Physiol.*, 67:99–145.

Sinha, A. and Misra, J. (2014). Mhd flow of blood through a dually stenosed artery: Effects of viscosity variation, variable hematocrit and velocity-slip. *The Canadian Journal of Chemical Engineering*, 92(1):23–31.

Srivastava, N. (2014a). Analysis of flow characteristics of the blood flowing through an inclined tapered porous artery with mild stenosis under the influence of an inclined magnetic field. *Journal of Biophysics*, 2014:1–9.

Srivastava, N. (2014b). The casson fluid model for blood flow through an inclined tapered artery of an accelerated body in the presence of magnetic field. *International Journal of Biomedical Engineering and Technology*, 15(3):198–210.

Srivastava, V. (1996). Two-phase model of blood flow through stenosed tubes in the presence of a peripheral layer: applications. *Journal of Biomechanics*, 29(10):1377–1382.

Srivastava, V. P. and Saxena, M. (1997). Suspension model for blood flow through stenotic arteries with a cell-free plasma layer. *Mathematical biosciences*, 139(2):79–102.

Stokes, V. K. (1966). Couple stresses in fluids. *The physics of fluids*, 9(9):1709–1715.

Swartz, R., Bhuta, S., Farb, R., Agid, R., Willinsky, R., Butany, J., Wasserman, B., Johnstone, D., Silver, F., Mikulis, D., et al. (2009). Intracranial arterial wall imaging using high-resolution 3-tesla contrast-enhanced mri. *Neurology*, 72(7):627–634.

Tashtoush, B. and Magableh, A. (2008). Magnetic field effect on heat transfer and fluid flow characteristics of blood flow in multi-stenosis arteries. *Heat and Mass Transfer*, 44(3):297–304.

Thompson, B. L., Gilbert, R. J., Mejia, M., Shukla, N., Haverstick, D. M., Garner, G. T., and Landers, J. P. (2016). Hematocrit analysis through the use of an inexpensive centrifugal polyester-toner device with finger-to-chip blood loading capability. *Analytica chimica acta*, 924:1–8.

Timmerman, R., Papiez, L., McGarry, R., Likes, L., DesRosiers, C., Frost, S., and Williams, M. (2003). Extracranial stereotactic radioablation*: results of a phase i study in medically inoperable stage i non-small cell lung cancer. *Chest*, 124(5):1946–1955.

Torrance, K. and Turcotte, D. (1971). Thermal convection with large viscosity variations. *Journal of Fluid Mechanics*, 47(1):113–125.

Tripathi, B. and Sharma, B. K. (2018a). Influence of heat and mass transfer on mhd two-phase blood flow with radiation. In *AIP Conference Proceedings*, volume 1975, pages 030009–030018. AIP Publishing.

Tripathi, B. and Sharma, B. K. (2018b). Influence of heat and mass transfer on two-phase blood flow with joule heating and variable viscosity in the presence of variable magnetic field. *International Journal of Computational Methods*.

Trivedi, R., U-King-Im, J., Graves, M., Horsley, J., Goddard, M., Kirkpatrick, P., and Gillard, J. (2004). Multi-sequence in vivo mri can quantify fibrous cap and lipid core

components in human carotid atherosclerotic plaques. *European journal of vascular and endovascular surgery*, 28(2):207–213.

Tzirtzilakis, E. (2005). A mathematical model for blood flow in magnetic field. *Physics of fluids*, 17(7):077103–077119.

Tzirtzilakis, E. (2008). Biomagnetic fluid flow in a channel with stenosis. *Physica D: Nonlinear Phenomena*, 237(1):66 – 81.

Umavathi, J., Sheremet, M., and Mohiuddin, S. (2016). Combined effect of variable viscosity and thermal conductivity on mixed convection flow of a viscous fluid in a vertical channel in the presence of first order chemical reaction. *European Journal of Mechanics-B/Fluids*, 58:98–108.

Verma, S. (2014). Analytical study of a two-phase model for steady flow of blood in a circular tube. *International Journal of engineering Research and Applications*, 1(4):1–10.

Vlachopoulos, C., O'Rourke, M., and Nichols, W. W. (2011). *McDonald's blood flow in arteries: theoretical, experimental and clinical principles*. CRC press.

Welty, J. R., Wicks, C. E., Rorrer, G., and Wilson, R. E. (2009). *Fundamentals of momentum, heat, and mass transfer*. John Wiley & Sons.

Womersley, J. R. (1955). Method for the calculation of velocity, rate of flow and viscous drag in arteries when the pressure gradient is known. *The Journal of physiology*, 127(3):553–563.

Wren, C., Oslizlok, P., and Bull, C. (1990). Natural history of supravalvular aortic stenosis and pulmonary artery stenosis. *Journal of the American College of Cardiology*, 15(7):1625–1630.

Young, D. (1968). Effect of a time-dependent stenosis on flow through a tube. *Journal of Engineering for Industry*, 90(2):248–254.

Zaman, A., Ali, N., Bég, O. A., and Sajid, M. (2016a). Heat and mass transfer to blood flowing through a tapered overlapping stenosed artery. *International Journal of Heat and Mass Transfer*, 95:1084 – 1095.

Zaman, A., Ali, N., and Sajid, M. (2016b). Slip effects on unsteady non-newtonian blood flow through an inclined catheterized overlapping stenotic artery. *AIP Advances*, 6(1):015118–015129.

Brief Biography of the Supervisor

Prof. Bhupendra Kumar Sharma is an Associate Professor & Head, Department of Mathematics, Birla Institute of Technology and Science, Pilani, (BITS Pilani) Pilani Campus, Rajasthan, India. He got his M.Sc. (1999), M. Phill (2000) and Ph. D. (2006) from Department of Mathematics, University of Rajasthan, Jaipur. He awarded NET-JRF (Junior Research Fellowship, CSIR) in 2001 and Senior Research Fellowship in 2003. His research interest includes Heat and Mass Transfer, Arterial Blood Flow, Magnetic Targeting Drug Delivery, Porous Medium, Boundary Layer Theory, Micro-polar Fluid, Differential Equations etc. He has published more than 60 international/national journals of repute and authored two books on Engineering Mathematics. He is an associate editor, member of editorial board, advisory board of a number of the journal of reputes. Prof Sharma is a member of various academic and management committees of many Institutes/Universities such as advisory committee, selection committee etc. He has also participated in many conferences and workshops.

Brief Biography of the Candidate

Ms. Bhavya Tripathi is a full-time research scholar in the Department of Mathematics, BITS Pilani, Pilani Campus, Rajasthan since January 2014. She did her graduation in science from C.S.J.M. University, Kanpur in the year 2010. She completed her Master's degree in Applied mathematics and Informatics from IIT Roorkee, Roorkee, Uttarakhand in the year 2013. After completing her Master's degree she joined BITS Pilani, Pilani Campus to pursue her Doctor of Philosophy (Ph.D.) in the area of Biomechanics under the guidance of Prof. Bhupendra Kumar Sharma. Till date, she has published 4 papers in international journals and 2 peer-reviewed proceedings of the international conferences.

Publications

Journal

[1] **Tripathi, Bhavya** and Sharma, Bhupendra K., Effect of heat transfer on MHD blood flow through an inclined stenosed porous artery with variable viscosity and heat source. *Romanian Journal of Biophysics*, 28(3):89-102, 2018.

[2] **Tripathi, Bhavya** and Sharma, Bhupendra K., Influence of heat and mass transfer on two-phase blood flow with Joule heating and variable viscosity In the presence of variable magnetic field. *International Journal of Computational Methods*,
DOI: `https://doi.org/10.1142/S021987621850139`.

[3] **Tripathi, Bhavya** and Sharma, Bhupendra K., Effect of Variable Viscosity on MHD Inclined Arterial Blood Flow with Chemical Reaction. *International Journal of Applied Mechanics and Engineering*,23(3):767–785, 2018,
DOI: `https://doi.org/10.2478/ijame-2018-0042`.

[4] Sharma, Madhu, Sharma, Bhupendra K., Gaur, R. K. and **Tripathi, Bhavya**, Soret and Dufour Effects in Biomagnetic Fluid of Blood Flow Through a Tapered Porous Stenosed Artery. *Journal of Nanofluids*, 8(2):327–336, 2019,
DOI: `https://doi.org/10.1166/jon.2019.1584`.

[5] **Tripathi, Bhavya**, Sharma, Bhupendra K. and Sharma, Madhu, MHD Pulsatile Two-Phase Blood Flow Through a Stenosed Artery with Heat and Mass Transfer, *International Journal of Thermal Sciences*, (Under Review).

[6] Sharma, Madhu, Sharma, Bhupendra K. and **Tripathi, Bhavya**, Radiation effect on MHD Copper Suspended Nanofluid flow through a Stenosed Artery with Temperature Dependent Viscosity, *International Journal of Heat and Technology*, (Under Review).

[7] **Tripathi, Bhavya**, Sharma, Bhupendra K. and Sharma, Madhu, Modeling and Analysis of MHD two-phase blood flow through a stenosed artery having temperature dependent viscosity, *The European Physical Journal Plus*, (Under Review).

Peer Reviewed International Conference Proceedings

[1] **Tripathi, Bhavya** and Sharma, Bhupendra K., Influence of heat and mass transfer on MHD two-phase blood flow with radiation. *AIP Conference Proceedings*, 1975(1): 030009–9, 2018, URL `https://doi.org/10.1063/1.5042179`.

[2] **Tripathi, Bhavya** and Sharma, Bhupendra K., Effects of Heat and Mass Transfer on MHD Flow of Blood through an Artery with Stenosis having Variable Viscosity. In *Sixth International Congress on Computational Mechanics and Simulation Proceedings*, July 2016.

Conferences/Workshop Attended

[1] International Conference on **Frontiers in Industrial and Applied Mathematics**, Department of Mathematics, NIT Hamirpur, Himachal Pradesh, India, April 26-27th, 2018.

[2] National Conference on **Mathematics "Googol 2017"**, Department of Mathematics, Birla Balika Vidyapeeth, Pilani, India, April 15-16th, 2017.

[3] Workshop on **Numerical Techniques for Partial Differential Equations**, Department of Mathematics, VNIT Nagpur, Nagpur, India, July 10-14th, 2017.

[4] One day Workshop for **Research Scholars on Teaching and Learning**, BITS Pilani, Pilani campus, India, September 10th, 2017.

[5] 6th International Congress on **Computational Mechanics and Simulation**, Department of Civil Engineering, IIT Bombay, Powai, Mumbai, India, 27th June- 1st July, 2016.

[6] Workshop for **Mathematical Modelling and Computational Techniques in Nanofluids**, Department of Mathematics, NIT Kurukshetra, India, September 21st-25th, 2015.

[7] Research School on **Mathematical Models in Biology and Medicine**, International Center for Pure and Applied Mathematics, Moka, Mauritius, December 5th-16th, 2015.

[8] National Congress on **Recent Trends and Developments in Operations Research**, Department of Mathematics, BITS Pilani, Pilani campus, India, February 22-23rd, 2014.

[9] National Workshop on **Latex and MATLAB for Beginners**, Department of Mathematics, BITS Pilani, Pilani Campus, India, December 24th-28th, 2014.